CRANFIELD UNIVERSITY
LIBRARY

CRANFIELD UNIVERSITY

School of Mechanical Engineering

PhD Thesis

Nicholas Michael Merriman

Simulation of Aero Engine Pre- and Post-Stall Transient Behaviour

Supervisor: Professor R L Elder

April 1994

© ROLLS-ROYCE plc 1994

The information in this document is the property of Rolls-Royce plc and may not be copied or communicated to a third party or used for any purpose other than that for which it is supplied without the express written authority of Rolls-Royce plc

While the information in this document is given in good faith based upon the latest knowledge available to Rolls-Royce plc, no warranty or representation is given concerning such information, which must not be taken as establishing any contractual or other commitment on the part of Rolls-Royce plc or any of its subsidiary or associated companies

ROLLS-ROYCE plc
PO BOX 3 FILTON BRISTOL BS12 7QE ENGLAND
Telephone: Bristol (0272) 791234 Telex 44185

ProQuest Number: 10820894

All rights reserved

INFORMATION TO ALL USERS
The quality of this reproduction is dependent upon the quality of the copy submitted.

In the unlikely event that the author did not send a complete manuscript
and there are missing pages, these will be noted. Also, if material had to be removed,
a note will indicate the deletion.

ProQuest 10820894

Published by ProQuest LLC (2019). Copyright of the Dissertation is held by Cranfield University.

All rights reserved.
This work is protected against unauthorized copying under Title 17, United States Code
Microform Edition © ProQuest LLC.

ProQuest LLC.
789 East Eisenhower Parkway
P.O. Box 1346
Ann Arbor, MI 48106 – 1346

ABSTRACT

The commercial and operational attractiveness of improving the specific thrust, whilst minimising the weight, of an aero gas turbine engine, has inevitably led to the compressor operating as near to stall as is considered safe. However, it is acknowledged that under extreme circumstances a compressor will stall, and so effecting a quick recovery is important with respect to safety and mechanical integrity. Because of these ever increasing demands made on the performance of civil and military aero engines alike, it has become increasingly clear that a means of simulating pre- and post-stall transient behaviour is now a computer modelling requirement of the major engine manufacturers. Computer modelling is essential because a thorough experimental evaluation of the pre- and post-stall transient behaviour of an engine during a development programme, is prohibitively expensive. Further, such a capability will find applications in the stability assessment and fault diagnosis of existing production engines.

Conventional transient performance computer codes operated within the aerospace industry, are limited to the simulation of engine performance during acceleration and deceleration. Performance prediction is good because the transient is predominately governed by spool inertia. However, account is not taken of the temporary accumulation of fluid mass, momentum and energy of flow disturbances as they pass through the engine; these effects become increasingly significant beyond frequencies of approximately 5 Hz. These codes are therefore incapable of predicting engine response, and in particular compressor stability, during high frequency flow transients such as a reheat mislight. Further, the

simulation of any subsequent post-stall flow transients which typically occur at frequencies up to 40 Hz, is similarly not possible. This thesis marks the introduction of a high frequency modelling capability into just such a performance code, the Rolls-Royce Aero Engine Performance system, **RRAP**; and the extension of this capability to the simulation of whole engine performance during post-stall events.

The high frequency response of an engine working fluid was achieved by splitting the engine into component volumes and solving time dependent equations conserving mass, momentum and energy across each. An extended version of the equations was used to predict radial flow, and hence further the modelling capability to multi-spool engines. The development of post-stall methods required extension of present compressor performance calculations as well as the introduction of post-stall performance characteristics. In addition, a whole new combustor model was developed to operate during low or reverse flow conditions commensurate with post-stall events. Together these modelling methods successfully simulated surge, cyclic surge and the 'descent' into rotating-stall. The simulations agreed favourably with test results.

Development of these methods using the RRAP system has ensured that the work marked the beginning of a truely generic pre- and post-stall engine modelling capability; and that the ultimate objective of creating a computer model sufficiently reliable and accurate so that it may be used in engine design and development, is one step nearer.

ACKNOWLEDGEMENTS

I am indebted to Rolls-Royce plc, Cranfield University and the Science and Engineering Research Council without whose support this work would not have been possible.

My thanks go to Mr Darrell Williams who instigated this work and to his successor as Chief of Powerplant Technology (Military), Rolls-Royce, Bristol, Dr Brian Lowrie for his continued support.

My thanks go also to my Group Leader, Mr Robert Hercock and to Mr Gordon Warnes, both of the Compatibility Group, Powerplant Technology Department, whose experience in compressor stability and transient engine modelling was invaluable to me.

The insight and constructive help provided by my supervising panel is acknowledged with thanks. The panel were,

Professor Robin Elder	Academic Supervisor - Cranfield University
Dr David Lambie	Industrial Supervisor - Rolls-Royce
Mr Kenneth Ramsden	Panel Chairman - Cranfield University
Mr Garth Ward	Project Management Supervisor - Cranfield School of Management

My thanks go to Mr Barry Curnock, Chief of Propulsion Systems Engineering Information Systems, Rolls-Royce, Bristol, whose comment and unrelenting enthusiasm for my work was a source of constant inspiration for me. My thanks go also to the members of the Performance Support Department whose patient help, and support, in using the 'Rolls-Royce Aero Engine Performance' computer system was invaluable.

It is stated that the contents of this thesis are the author's opinion and not a reflection of Rolls-Royce policy.

CONTENTS

NOTATION

a - Speed of sound

A - Area

Cd - Nozzle discharge coefficient

Cf - Skin friction coefficient

C_p - Specific heat capacity at constant pressure

C_v - Specific heat capacity at constant volume

D - Pipe diameter

e - Specific internal energy

E - Absolute energy, $= m(e + U^2/2)$

EP - Excess turbine power

FAR - Fuel-to-air ratio

FAR_a - Actual fuel-to-air ratio

FAR_e - Effective fuel-to-air ratio

F_{nr} - Internal force acting on component volume fluid in the radial direction - Component Performance Term (CPT)

F_{nx} - Internal force acting on component volume fluid in the x direction - Component Performance Term (CPT)

F_{tr} - Total force acting on component volume fluid in the radial direction - Component Performance Term (CPT)

F_{tx} - Total force acting on component volume fluid in the x direction - Component Performance Term (CPT)

h - Specific enthalpy

H - Specific total enthalpy

H_f - Specific heat of combustion of fuel

I - Spool inertia

K_1 - Mass fraction of oxygen gas consumed per unit mass of combusted fuel

K_2 - Mass fraction of unburnt fuel per unit mass of combustion products

K_3 - Mass fraction of oxygen gas consumed per unit mass of combustion products

K_4 - Mass fraction of oxygen is Standard Air

K_C - Combustor cold pressure loss factor

K_H - Combustor hot pressure loss factor

L - Component volume length dimension

m - Mass

m_{cp} - Mass of combustion products

m_{ox} - Mass of gaseous oxygen

M - Mach number

MOM - Momentum

N - Engine spool rotational speed (revolutions per minute, RPM)

p - Static pressure

P - Total pressure or power

Q - Flow function

Q* - Choked value of flow function

$\dot{Q}$ - Rate of heat transfer

r - Engine radial dimension

R - Gas constant for air and combustion products

Re - Reynolds number

s - Specific entropy

S - Absolute entropy

$\dot{S}_v$ - Rate of absolute entropy production in component volume fluid

$\bar{s}$ - Component volume averaged specific entropy

t - Time or static temperature

T - Total temperature

U - Fluid velocity

V - Volume

W - Mass flow rate

W_f - Fuel mass flow rate

W_B - Component volume bleed

$\bar{W}$ - Component volume averaged mass flow rate

x - Engine axial dimension

Greek letters

γ - Ratio of gas specific heats

δ^* - Boundary layer displacement thickness

Δ - Increment

η_c - Compressor isentropic efficiency

η_{cb} - Combustor burning efficiency

θ - Volume sector angle or combustor mixing constant

μ - Coefficient of viscosity

ρ - Static density

$\bar{\rho}$ - Component volume averaged static density

τ - Characteristic time

Subscripts

A - Volume A

B - Volume B

c - Pertaining to the compressor

cb - Pertaining to the combustor

i - Pertaining to volume surfaces perpendicular to engine axis

k - Pertaining to volume surfaces parallel to engine axis

m - Mean

o - Reference value

s - Pertaining to component volume surface

v - Pertaining to engine component volume

Superscripts

* - Steady-state value

r - Engine radial direction

x - Engine axial direction

FIGURES

TABLES

CHAPTER 1

Introduction

1.1 Background

Throughout the development of gas turbine engines, the detrimental effect on performance of compressor stall has remained a prevalent design consideration. Not only is engine performance significantly reduced during stall, but its operability is compromised, and the mechanical integrity of both compressor and turbine is invariably put at risk.

Prior to identifying some of the possible problems an engine can have during compressor stall it is necessary to describe the features of stall performance. This is best done by isolating the compressor from an engine and considering its performance on a rig.

Figure 1.1a is a schematic illustration of a multi-stage axial flow compressor driven by an electric motor and exhausting into a plenum chamber. Its speed is dictated by the motor and the mass flow rate by the throttle at the rear of the chamber. As the throttle is constricted at a given speed, the mass flow rate falls and the compressor pressure rise increases. This is shown by figure 1.1b. This trend will continue until the 'pumping' capability of the compressor begins to break down. This break down is termed stall inception.

Following stall inception the compressor will exhibit one of two forms of post-stall behaviour; rotating-stall or surge. Figure 1.2a shows a small deterioration in

compressor performance brought about by the formation of rotating-stall cells. This typically occurs at lower rotational speeds and is sometimes referred to as 'progressive' stall. Although not desirable because performance is reduced, it is usually possible to recover from it by simply opening the throttle.

What is considered to be a possible mechanism behind stall inception and the existence of rotating-stall cells was first put forward by Emmons et al, 1955. Here, the mechanism is for a single row of compressor blades and is summarised below.

For a given rotor speed, the demand for a greater pressure rise is met by an increase in aerodynamic incidence of the blades. As aerodynamic stall approaches a minor physical irregularity, or flow non-uniformity, can cause a momentary increase in flow incidence and so trip a blade into stall. This mechanism of stall inception is illustrated in figure 1.3a. The resulting blockage, due to flow separation, will cause on-coming flow to divert. Region A of figure 1.3a shows the resulting increase in blade flow incidence and Region B a decrease in incidence. Consequently the blades will tend to stall in region A and unstall in Region B. Figure 1.3b illustrates the resulting developed stall 'cell' which, owing to the continual stalling and unstalling of the blades, will propagate around the circumference of the compressor. It is this circumferential motion of the stall cell that gives rise to its name 'rotating-stall'. Although the stall cell depicted by figure 1.3b moves from right to left relative to the rotor, its motion relative to a stationary observer will be with the rotor, but moving at a fraction of the rotor speed.

The progressive stall of figure 1.2a is the result of one, or a number of separate rotating-stall cells, usually existing in the inner or outer part span portion of a single blade row. The cells, which are illustrated in figure 1.4a, will typically rotate at about half the rotor speed. If a compressor is further throttled then the behaviour depicted by figure 1.2b leads to a significant drop in pressure rise and mass flow rate. As the compressor stalls the operating point moves transiently to a new steady operating point commensurate with the throttle line. Here, it is usually just one, full span rotating-stall cell extending to the rear of the compressor, that will have formed. If the compressor is further throttled then the reduction in flow rate is accomplished by the cell growing to occupy a larger sector. The cell, which is illustrated in figure 1.4b, will typically rotate at below half the rotor speed. Note that the progressive stall is not usually sustainable but is more often than not, part of the transitory development of the single celled rotating-stall.

A significant feature of rotating-stall is recovery hysteresis. Here, before recovery from rotating-stall can be effected, the flow rate has to be increased significantly. As a compressor recovers, its operating point moves to a point on the pre-stall performance characteristic commensurate with the new throttle line, see figure 1.2b. It is recovery hysteresis that can make recovery from rotating-stall in an engine very troublesome.

Experimental work conducted by Wilson and Freeman, 1993, indicates that the nature of stall inception is independent of speed. The compressor was a high speed and high pressure ratio design, and operated as part of a

complete single shaft turbojet engine, the Rolls-Royce Viper. Stall development was always found to begin with isolated rotating-stall cells combining to form one spanwise cell extending to the rear of the compressor. However, at higher compressor speeds this single stall cell was found to grow and occupy the entire circumference at the rear of the compressor. This always led to what is known as compressor surge.

Surge is markedly different from rotating-stall and is depicted by figure 1.2c. It is thought that the development of a circumferential stall cell at the rear of the compressor leads to what is commonly regarded as a near planar breakdown of the flow structure. The axial force exerted by the blades can no longer support the static pressure at the compressor exit. The break down in flow structure thus moves upstream causing the rapid reduction in overall pressure rise and mass flow rate depicted by figure 1.2c. As the pressure within the plenum chamber falls, and the impetus for the flow breakdown diminishes, there comes a point where recovery will begin. Both compressor exit pressure and mass flow rate will rise and return to its original steady-state operating point provided whatever caused the initial instability is removed.

If the cause of the initial instability is not removed then repeated surges, or 'cyclic' surge, will occur. Here, the surge process is repeated resulting in a periodic rise and fall of pressure ratio and mass flow rate. In engine applications the surge cycle frequency is typically between 5 and 15 Hz.

The occurrence of rotating-stall and surge in an engine compressor have profoundly different effects on engine

operability. If rotating-stall occurs, the consequent low flow and pressure ratio causes damaging turbine temperatures and a dramatic loss in thrust. Recovery can usually be initiated by reducing the compressor throttling. For instance, the fuel rate can be reduced, thereby allowing the compressor mass flow rate to increase to the point of recovery. This is a typical recovery procedure which takes no longer than a few seconds. However, some compressors are known to have a large rotating-stall hysteresis loop, which can make recovery impossible under normal operating conditions. This situation is often referred to as 'hung', 'stagnation' or 'locked-in' rotating-stall. In operation, recovery can only be achieved by extinguishing the combustor and starting the engine afresh.

In the case of surge, and provided the cause of the surge is temporary, the compressor will complete one surge cycle and recover of its own accord with only a momentary loss in engine performance. On the surface this may appear to be the more desirable post-stall behaviour. However, large aerodynamic loads are exerted on the compressor blading, casing and inlet duct, and integrity can be threatened, see Mazzawy, 1980. Should cyclic surge occur, the threat of mechanical damage is not only repeated, but due to the net reduction in turbine power, the spool speed will fall and thus increase the likelihood of surge cycles degenerating into rotating-stall.

Surge and, up to a point, rotating-stall generate unsteady combustion phenomena which strongly influence the nature of whole engine post-stall behaviour. For example, if a compressor surge is sufficiently strong, flow may be expelled forwards from the compressor - it has been known for flames to be seen at a compressor face. Such extreme

combustor conditions tend to exceed combustion stability limits and so 'blow-out' may occur, and spool 'run-down' ensue.

The development of rotating-stall results in low flow rates which, assuming no change in fuel flow rate, will cause a rapid rise in fuel-to-air ratio. Combined with the commensurate fall in combustion pressure (or combustor loading) it is not unusual for the combustor to blow-out. Ironically, blow-out will encourage the compressor to recover. This is because the fall in entry temperature will allow the turbine to pass a greater mass flow and so help the compressor to 'escape' stall hysteresis. Conversely, if blow-out does not occur the mass flow rate will be kept low and locked-in rotating-stall will be all the more likely.

Engine operability during compressor stall is not solely dictated by the nature of the stall and combustor flame stability, but is also dependent on the interaction between the engine as a whole and the stalling compressor. This is highlighted by the early in-service experience of the Pratt and Whitney Aircraft JTF22 engine which revealed a serious engine and compressor stall interaction problem, see Aircraft Engineering, 1979.

Although the engine powered the Grumman F-14B and the General Dynamics F-16, the stall problem was found to be particularly acute in the McDonnell Douglas F-15 for which the JTF22 core was fitted with a re-heat system and a smaller fan. It was discovered that when reheat was selected at high altitudes and low flight speeds, the compressor was likely to surge and on occasion, very quickly degenerate into locked-in rotating-stall. Characteristically the engine would not respond to

throttle movements, produced markedly less thrust and the turbines over-heated. Return to normal operating conditions could only be achieved by shutting the engine down and starting it afresh. Despite an appreciation of compressor aerodynamic performance during rotating-stall and surge, their interaction with the engine as a whole was not understood.

Pratt and Whitney Aircraft, McDonnell Douglas and the United States Air Force conducted extensive engine and flight tests to deduce the cause of what, at first, were sporadic surge cycles but on occasion would settle into locked-in rotating-stall.

The cause of surge turned out to be inadequate re-heat control. At high altitudes and low speeds re-heat flame stability was poor and on occasion unburnt fuel would accumulate. Ignition of the fuel by hot turbine gases generated an over-pressure which travelled up the by-pass duct and on reaching the rear face of the fan caused it to stall. This in turn led to a compressor surge due to the falling fan delivery pressure. The increasing engine pressures and temperatures which accompanied recovery from surge, ignited fuel which had again accumulated in the jet pipe and so caused the process to repeat. This process repeated sporadically until the pilot managed to establish stable reheat combustion.

The occurrence of locked-in rotating stall was found to be a product of 'whole engine dynamic response'; and more specifically the length of by-pass duct and surge cycle frequency.

It was found that the over-pressure generated by the ignition of unburnt re-heat fuel, which reflected from the

rear of the fan, reflected again from the end of the by-pass duct and returned to the rear of the fan as an under pressure. The length of by-pass duct and frequency of compressor surge cycle was such that the under pressure was 'felt' by the compressor just as it was recovering. This caused the compressor to settle into a locked-in rotating-stall.

The occurrence of locked-in rotating stall was finally prevented by introducing two modifications. The first concerned the engine control system. If the engine surged after a re-heat mislight, the control system would automatically increase the nozzle area and decrease the re-heat fuel flow rate. This reduced the intensity of any subsequent pressure pulses passing up the by-pass duct. The second modification was an extension to the compressor inlet and by-pass flow duct 'splitter'. This served to partially shield the compressor face from the pressure pulses in the by-pass duct.

To cure the JTF22 of its in-stall problems was a very expensive and time consuming process. It served to illustrate the potential, post-stall operational problems that can remain latent during the design and development of an engine. Although compressor stall has been the subject of much theoretical and experimental research over a number of decades, work primarily concentrated on compressors operating in isolation on rigs. The transient effect of compressor stall on gas turbine performance has remained a qualitative understanding based on limited experimental and in-service data. Thorough rig testing of pre- and post-stall transient behaviour during engine design and development, was, and still is prohibitively expensive. However, due to the computing power now available to gas turbine manufacturers and academia, the theoretical prediction of both pre- and post-stall

transient gas turbine performance is now becoming possible. The objective is to create computer models sufficiently reliable and accurate that they may be used as part of the design and development process.

At present, typical engine performance computer codes used by gas turbine manufacturers can predict steady-state performance and spool speed during acceleration and deceleration. However, the time dependent behaviour of the engine working fluid during high frequency transients such as cyclic surge, cannot be predicted by a steady-state model. This is because account is not taken of the temporary accumulation of fluid mass, momentum and energy as flow disturbances pass through the engine. A steady-state model lacks what is often referred to as a high frequency, gas dynamic response capability.

A high frequency response, Computational Fluid Dynamics (CFD) model of a complete engine is not possible at present. Apart from which, such a model would be extremely complex and peculiar to a single engine geometry and could not be quickly, or cheaply, applied to another. This approach therefore, does not lend itself to inclusion into a generic computer performance code of the ilk cited above. However, high frequency response of an engine working fluid can be predicted by discretising an engine into component volumes and solving time dependent equations conserving mass, momentum and energy across each. Not only is numerical complexity greatly reduced, but the modelling approach is generic, and therefore compatible with typical engine performance codes. Such a generic modelling capability could then be cheaply introduced to the gas turbine design and development process.

Rolls-Royce has recently developed a High Frequency Transient Compression System Model in conjunction with Cranfield University. It is capable of simulating the pre-stall, high frequency gas dynamic response (up to approximately 40Hz) for a one and two spool compression system. The compression system is discretised into component volumes and time dependent equations conserving mass, momentum and energy solved across each. The model is a 'stand alone' computer code and serves as a methods demonstrator.

Part of the work presented in this thesis built on the above by introducing the high frequency response capability into the Rolls-Royce Aero Engine Performance computer code, RRAP. The remainder of the thesis concentrates on the creation and verification of post-stall modelling methods including the simulation of cyclic surge and the 'descent' into rotating-stall. Development using the RRAP system ensured that the work marked the beginning of a truely generic, pre- and post-stall engine modelling capability.

1.2 **Project Justification**

The commercial and operational attractiveness of improving the specific thrust, whilst minimising the weight of an aero engine, has inevitably led to the compressor operating as near to stall as is considered safe. However, it is acknowledged that under extreme circumstances a compressor will stall, and so a quick recovery is important with respect to safety and mechanical integrity. Because of these ever increasing demands made on the performance of civil and military aero engines alike, it has become increasingly clear that a means of simulating pre- and post-stall transient

behaviour is now a computer modelling requirement of the major engine manufacturers. Computer modelling is essential because a thorough experimental evaluation of the pre- and post-stall transient behaviour of an engine during a development programme is prohibitively expensive. Further, such a capability will find applications in the stability assessment and fault diagnosis of existing production engines.

Some applications of pre- and post-stall computer simulation as seen by Rolls-Royce are detailed below.

i) **Application to engine design and development**

a) Application of a whole engine model during design and development would provide an insight into the post-stall behaviour and so enable potential problems to be designed out. If such a model had been used during the initial sizing and performance evaluation of the JTF22 its costly problems may have been avoided, see section 1.1.

b) It is accepted that under certain, usually extreme, combinations of circumstances, a compressor will stall. However, recovery from stall may be affected by, for example, appropriate and possibly simultaneous control of fuel flow rate, final nozzle area (if possible) and compressor bleeds. Application of a whole engine model would enable a quick parametric development of an engine control recovery strategy.

c) During engine development, transient control tests are carried out which occasionally generate engine behaviour which cannot be readily explained.

Application of a whole engine model will provide a problem solving capability; and if an insight is gained, will enable extensive parametric studies to be conducted quickly. This application can also be used on in-service production engines.

d) Future vertical and short take-off military aircraft will require engines to change their operating mode by redirecting flow through the use of valves. With a computer model, the stability of the compression system may be assessed during the shift from one mode of operation to another.

e) Parametric studies of engine performance parameters leading up to compressor stall could enable the 'paper' development of what are termed 'semi-smart surge control strategies'. 'Semi-smart surge control' operates by continuously assessing the relevant performance parameters. If it concludes that stall is approaching, it instigates avoiding action by appropriate engine control. The complete process could be designed using a whole engine model.

f) Simulation of stall events and in particular surge, will enable prediction of the aerodynamic loads exerted on the compressor blading and intake ducting. Such information may influence design with respect to mechanical integrity.

ii) **Application to production engine compressor stability assessment**

Engine compression stability could be assessed by subjecting a whole engine model to various scenarios of time dependent,

a) inlet planar wave distortion
b) nozzle area
c) fuel flow rate

a) Engine inlet planar wave distortion can simulate, for example, engine response and stability to,

- hot-gas-reingestion (vertical take-off and landing aircraft)
- ingestion of missile effluent
- extreme aircraft manoeuvres

b) Nozzle transients can simulate engine response to,

- high speed nozzle area actuation systems
- variable cycle engine mode shifts

c) Fuel control schedules can simulate engine response to,

- reheat lights
- pre-armament-firing-fuel-dip (The destabilising effect of the ingestion of armament effluent on the compressor is negated by a momentary drop in fuel flow rate)
- pilot induced engine acceleration/deceleration
- rapid landing engine decelerations

Much of the above can also be applied to engines in design and development.

1.3 Objective

The computer modelling capability required to satisfy the applications described above was summarised in the following objective.

To develop and verify a generic computer based modelling method, capable of simulating the high frequency transient response to one-dimensional flow disturbances in the pre- and post-stall domains of single and multi-spool gas turbine engines.

1.4 Project Specification

To provide the greatest chance of completing a successful project, project management techniques were used to define the project specification and scope, and subsequently plan and control the progress and quality of work.

The specification was defined using an iterative procedure which took into account the project justification, objective, literature search and an estimate of time and resource required. The procedure is detailed in chapter 3, Project Management.

The resulting project specification is detailed in appendix 1.1. Note that the specification includes PhD course requisites and as it was a statement of intent, is written in the future tense.

1.5 Overview of Thesis Contents

The work presented herein is the product of three years of work based in industry at Rolls-Royce plc, Bristol. The academic supervisory body was Cranfield University which, for an industrially based PhD study, stipulates that the work be project managed and the thesis written to reflect its Company oriented objective and working practices.

Accordingly, following the Introduction and Review of Previous work, chapter 3 details how the project work was organised and launched, and its progress monitored, by using project management techniques. An appraisal of the techniques used is also presented.

Chapter 4 details the theoretical approach taken to simulate the response of rapid time dependent changes in flow properties of an engine working fluid. A one-dimensional high frequency gas dynamic equation set, is derived and the method of application to an engine model detailed. An equation set extended to predict radial flow is also described. Its application to the prediction of radial flow within the fan, and before the flow 'splitter', of a two-spool engine is detailed.

Chapter 5 details the introduction of the high frequency gas dynamic equation set, to the Rolls-Royce Aero Engine Performance computer system, RRAP. The equation set is verified against rig test data of high frequency flow transients in a simple duct pipe. The performance of the equation set extended to predict radial flow, is also discussed - verification work is not presented due to lack of appropriate test data.

Chapter 6 details the development of a whole engine model using the RRAP system, which is capable of simulating high frequency flow transients of the working fluid. Examples of the transient movement of the compressor operating point during rapid changes in entry flow properties and fuel flow rate are presented. Although test data was not available for comparison, the results are discussed.

Chapter 7 builds on the engine models of chapter 6 by developing a post-stall modelling capability. Simulation of surge, cyclic surge and the 'descent' into rotating-stall, are each demonstrated with a whole engine single spool model. Results are shown to compare favourably with test data.

Chapter 8 presents the technical conclusions.

Chapter 9 describes recommended future work items for further technical development and verification of the modelling methods.

1.6 **Contributions made by this work**

Although the format of a time dependent equation set conserving mass momentum and energy is common place in the open literature, the problems and ultimate advantages of successfully applying it to a generic whole engine performance code utilising an implicit numerical scheme, have not been addressed. A number of models using time marching explicit schemes are described in the open literature. However, their application to conventional engine performance codes typical of those used by engine manufacturers, is fundamentally inappropriate. Their ultimate versatility with respect to the design and development of engines is therefore limited. Known to the

author, there is only one example of what is referred to as 'a conventional deck using an implicit numerical scheme' which is used to simulate whole engine high frequency transient behaviour. The reference is made by Hosny et al, 1985, but fails to release any numerical scheme details. This thesis contributes a complete description of the problems and ultimate advantages, of introducing time dependent conservation equations into an implicit engine performance code. The code used was the Rolls-Royce Aero Engine Performance system, RRAP. Prediction of high frequency flow disturbances using the RRAP system were also verified against test data.

The conventional approach to post-stall modelling predicts performance from a post-stall characteristic with a modification to account for the finite time required for the development of stall cells. This modification is either omitted from the literature, or if it is included, typically takes the form of a first order time lag applied to the net force exerted by the compressor blading on the fluid. This thesis describes how the approach has been furthered by applying the lag to both the net force and the rate of entropy production of the compressor. By doing so changes in compressor efficiency, as well as pressure ratio, during stall transients were represented. Compressor exit temperatures were therefore more physically representative and so in turn combustor, and engine performance overall, more representative.

To the author's knowledge the open literature does not describe an attempt to model combustor performance during conditions of low or reverse flow at entry - such conditions occur during more severe post-stall events. Conventional 'steady' or 'through flow' calculation methods break down under these flow conditions. This thesis details the development of a new model that

actually accounts for the quantity of air and combustion products contained by the combustor at any given time. By doing so performance could be predicted during conditions of low or even reverse flow at combustor entry.

Simulation of whole engine response to compressor surge, cyclic surge and rotating-stall was successfully achieved using the RRAP performance system. Predictions were shown to compare favourably with rig test results. This thesis therefore contributes the first step in achieving a truely generic, pre- and post-stall engine modelling capability; and is the first step in achieving the ultimate objective which is to generate a computer model sufficiently accurate and reliable that it may be used as part the engine design and development process.

CHAPTER 2

Review of Previous Work

2.1 Introduction

Research into pre- and post-stall compressor performance has evolved into three distinct, fundamental areas of work. These are,

i) experimental and theoretical derivation of both overall and stage compressor rotating-stall and reverse flow aerodynamic performance characteristics

ii) experimental and theoretical study of stall inception

iii) experimental and theoretical study of pre- and post-stall compressor high-frequency-transient behaviour and its dependence on the compressor operating environment

Each of the above are relevant to the achievement of the project objective, see section 1.3. However, section 1.1 highlighted the need to predict the interaction of whole engine performance with compressor post-stall performance. The literature search therefore concentrates on the simulation of compression system, or whole engine response, to stall.

To create a generic, whole engine pre- and post-stall model, as cited by the project objective, requires the combination of four distinct modelling capabilities. These are,

a) High frequency gas dynamic response
b) Compressor post-stall performance
c) Combustor post-stall performance
d) Whole engine steady-state performance prediction

The prediction of whole engine steady-state performance using a computer synthesis code, is now common place amongst aero engine manufacturers and academic institutions. Prediction methods are well established and described in academic texts, see Cohen et al, 1987, consequently a review of the relevant literature is not presented here. The review of previous work is set out below and describes some of the approaches used in the modelling the remaining three.

2.2 **Review of Previous Work**

a) High frequency gas dynamic response (> 5 Hz)

The purpose of this section is to describe the mathematical approaches adopted in the literature for the modelling of high frequency gas dynamic response. Attention is paid to its application to engine geometry and the boundary conditions and numerical solution techniques used. Any reverse flow capability, which is required to model 'deep' or 'violent' compressor surge, is also highlighted.

For flow disturbances in gas turbines of greater than approximately 5 Hz, the time dependence of flow behaviour,

due to temporary accumulation of mass, momentum and energy, becomes significant. The inclusion of what is often referred to as 'high frequency gas dynamic response' is therefore necessary if the simulation of engine response during rapid pre- and post-stall transients is to be representative. For convenience, the method of predicting 'high frequency gas dynamic response' will from here on be referred to as **'Gas Dynamic Methods' (GDM)**, and engine time dependent transients greater than 5 Hz as **'high-frequency-transients'**. The use of the term 'high-frequency-transient' is used to distinguish it from the time dependent modelling of engine spool speed which is conventionally known as 'transient' performance prediction.

Almost without exception the literature describes how time dependent equations conserving mass, momentum and energy are applied to each component volume of a compression system or engine model in order to simulate high-frequency-transient response. Each of the three governing equations express a time dependent flow variable (first order derivative) as a function of volume entry and exit flow conditions. A typical one-dimensional equation set is,

conservation of mass

$$\frac{d\bar{\rho}}{dt} = \frac{1}{V}\left[W_i - W_{i+1} - W_B \right]$$

conservation of momentum

$$\frac{d\bar{W}}{dt} = \frac{1}{L}\left[(WU)_i - (WU)_{i+1} + (pA)_i - (pA)_{i+1} + F_{nx} \right]$$

conservation of energy

$$\frac{d(\overline{\rho e})}{dt} = \frac{1}{V}\left[W_i H_i - W_{i+1} H_{i+1} + E_v \right]$$

Engine component performance is represented by evaluating the volume bleed W_B, net force applied to the fluid F_{nx}, and the rate of energy production E_v. The three terms are often referred to as the Component Performance Terms (CPTs). The 'barred' time dependent variables represent the volume averaged quantities of flow density, mass flow rate and enthalpy. Each have to be estimated from their respective volume entry and exit values by using an interpolation or averaging scheme of some kind. The governing equations can then be solved element by element, or for all elements simultaneously at a time step, using either explicit or implicit integration schemes. With updated values of each time dependent variable for each of the model elements, corresponding updated element entry and exit flow variables are calculated. Thus the calculation sequence can proceed to the next time step.

Tesch, Moszee and Steenken, 1976, and Tesch and Steenken, 1976 (a) and (b), describe the application of Gas Dynamic Methods to a compression system model of the J85-13 turbojet. The model consists of 29 volumes representing the intake, compressor and combustor. The equation set is identical to the above except that the energy equation is expressed with respect to entropy, rather than enthalpy, thereby ensuring that the 2nd law of thermodynamics is obeyed.

$$\frac{d(\overline{\rho s})}{dt} = \frac{1}{V}\left[(Ws)_i - (Ws)_{i+1} + \dot{S}_v \right]$$

The time dependent, volume averaged quantities, are approximated by a Taylor series expansion and evaluated using an unspecified, explicit time marching technique. The boundary conditions are upstream total pressure and temperature, and combustor 'nozzle' flow function.

Each of the eight compressor stages are split into a blade and stator volume thereby increasing frequency response. The shorter the volume length the higher the frequency response. Thus a compressor model with each stage represented by a volume and a performance characteristic, will have a higher attainable frequency response than a compressor represented by a single element and an overall characteristic. Stage performance characteristics are derived computationally from overall characteristics and applied across the blade volumes only. The combustor is represented by volumes similar in size to the blade and stator volumes, and so frequency response is not compromised. Combustor heat addition is not modelled.

The model is used to simulate compressor stability during time variant inlet circumferential distortion; circumferential capability is achieved by introducing 'parallel compressor theory'. Potential post-stall capability is not addressed in the reports.

A compression system model of the General Electric TF34 high by-pass ratio turbofan, marks the extension of the Gas Dynamic Methods used in the J85-13 model, from an axial, to an axial and radial flow capability. Hosny and Steenken, 1979, extend the above equation set to allow for flow between adjoining volumes placed in both a radial and circumferential sense. Again the energy equation is expressed with respect to entropy. By allowing radial flow between volumes, variation in by-pass ratio or more

specifically, the radial migration of the annular stream surface separating the core and by-pass flow, is accommodated without including variable volume geometry.

The intake, fan, by-pass duct, swan neck duct, compressor and combustor is represented by 60 volumes. However, the model does not include volumes positioned circumferentially.

The equation set requires five boundary conditions, three at the intake front and one each at the combustor and by-pass duct exit. Radial flow at intake entry is assumed zero, and combined with total pressure and temperature comprise the three upstream boundary conditions. Exit static pressure at the by-pass duct exit and flow function at the combustor exit are defined as the final two boundary conditions. The equation set is solved using the same unspecified numerical technique as the J85-13 model.

The model is used to predict both fan and compressor stability, and the variation in by-pass ratio, during time dependent throttling of the core and by-pass flows. By comparison with test results, the predicted fan and compressor transient interaction is representative and the prediction of radial flow valid. The potential post-stall capability of the model is not addressed in the report.

Extension of the TF34 model to allow circumferential flow is described by Steenken, 1982. The model is identical to the above, except that circumferential flow is allowed in volumes upstream and downstream of a compression component, and in volumes within a compression component that are 'large'.

Circumferentially the flow annulus is split into no more than twelve sectors. It is assumed that a distorted region must occupy, approximately, a 30° sector before aerodynamic stability of the compressor/fan is affected.

Stability of solution of the Gas Dynamic Methods is referenced for the first time, and attributed to,

i) expressing the energy equation with respect to entropy rather than enthalpy

ii) second-order Taylor series time marching solution technique

iii) the interpolation scheme used to evaluate the volume averaged time dependent variables

The interpolation scheme is termed the 'Transmittal of Properties' technique, and is illustrated below with respect to a one-dimensional schematic volume.

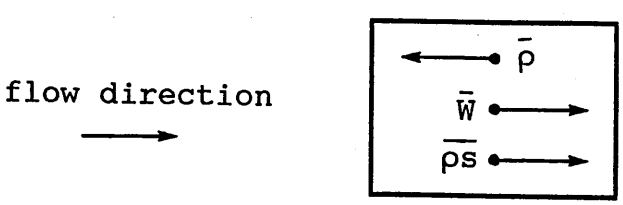

Here, the volume averaged density $\bar{\rho}$, is set equal to the entry value of flow density and the average mass flow rate $\bar{W}$, set equal to the exit value of mass flow rate. The volume averaged quantity $\overline{\rho s}$, is set equal to the product of the entry flow density and the exit entropy.

The model is used to simulate the propagating characteristics of a pressure pulse generated by a 'hard'

reheat light, such as that described in section 1.1. Investigation of the effect of 'splitter' position is also possible. Combined with 'parallel compressor' theory, investigation of compression system stability is also investigated subject to time variant circumferential total pressure distortion.

Chung, Leamy and Collins, 1985, describe a simplified whole engine model of the TF34, which marks one of the first attempts to simulate whole engine high-frequency-transient response to compressor stall. The model does not allow circumferential flow and has far fewer volumes. The compressor is represented by three volumes, the combustor by two, and each turbine by one. The equation set and boundary conditions are as above but the equations are solved using an explicit, second-order Runge-Kutta method.

This paper is significant because it provides evidence that the frequency response is sufficient for the simulation of post-stall transients despite the use of larger component volumes. Secondly, simulation of compressor surge reveals a reverse flow capability of the equation set. The fan, however, does not exhibit reverse flow and so the boundary conditions are not compromised. No mention is made of accounting for the possibility of reverse flow occurring at entry to the combustor during surge.

Hosny, Bitter and Steenken, 1985, describe a whole engine model of the F101X represented by volumes of similar coarseness to the above TF34. The model is based on a conventional steady state and transient performance prediction computer deck. Any reverse flow capability is not clear, the boundary conditions are not described and

the Gas Dynamic Methods, although the same as above, are solved by an unspecified, implicit numerical scheme. However, it is clear that the 'transmittal of properties' scheme is different to the above, with the volume averaged quantities represented by one half of the sum of their inlet and exit values.

Sugiyama, Tabakoff and Hamed, 1976, developed a whole engine model of the J85 turbojet capable of simulating high-frequency-transient response to surge and rotating-stall. It is the only model known to the author to demonstrate the existence of reverse flow at the intake entry as a consequence of compressor surge.

The compressor is represented by stage volumes with all other engine component volumes of a similar length, again maximising frequency response. Unlike the above models, engine component performance is represented by using actuator disc theory.

The Gas Dynamic Methods are of the above form, with the energy equation expressed in terms of enthalpy rather than entropy. The volume averaged quantities are evaluated from entry and exit values using an unspecified interpolation scheme and the equation set solved using a fourth-order Hammings predictor-corrector explicit integration method. The boundary conditions are total pressure and temperature at intake entry, and nozzle exit static pressure. During reverse flow, it is stated that boundary conditions at intake entry are swopped to those commensurate with a nozzle. The consequent 'loss' of a boundary condition and its replacement is not acknowledged. However, it is mentioned that there is a link between the boundary conditions and the volume averaged quantities of the adjoining volumes using again, an unspecified inter- and extrapolation method.

Reports by Davis et al 1980, Davis, 1982 and 1987, and Davis and Hale, 1992, describe the evolution of a stage compression system model, with an intake but without heat addition in the combustor, using Gas Dynamic Methods of the above form. The methods are extended to predict radial and circumferential flow between adjoining volumes, and the energy equation is expressed with respect to enthalpy and not entropy. However, the evaluation of the volume averaged quantities or 'transmittal of properties' scheme is not discussed.

The method of solving the governing equations changed from model to model,

- 1980, explicit, fourth-order Runge-Kutta scheme
- 1982 and 1987, explicit, second-order predictor/corrector MacCormack scheme
- 1992, equations expressed in matrix form and solved using an unspecified explicit scheme

The choice of boundary conditions also changed,

- 1980, intake entry total pressure and temperature, and final nozzle exit static pressure
- 1982, 1987 and 1992, method of characteristics applied to intake entry total pressure and temperature, and final nozzle exit static pressure

The models of 1980 and 1982 are each used to simulate pre-stall high-frequency-transients but both models of 1987 and 1992 are capable of simulating compression system response to stall. Although reverse flow is shown to occur at the compressor face during surge, it is not clear whether reverse flow is present at the intake entry and therefore compromising the boundary conditions used.

O'Brien and Davis, 1987, O'Brien and Boyer, 1989, and O'Brien, 1992, describe the development of a stage compressor model with an intake and combustor but without combustor heat addition. The model is used specifically for high-frequency-transient post-stall simulation. The equation set used is identical to Davis et al, 1980, but again, the evaluation of the volume averaged quantities or 'transmittal of properties' scheme is not discussed. The solution technique and boundary conditions remained unchanged during the model development and are, respectively,

- explicit, second-order predictor/corrector MacCormack scheme
- method of characteristics applied to intake entry total pressure and temperature, and final nozzle exit static pressure

Again, although reverse flow is shown to occur at the compressor face during surge, it is not clear whether reverse flow is present at the intake entry and therefore compromising the boundary conditions used.

Rolls-Royce and Cranfield University have jointly developed a two spool High-Frequency-Transient Compression System model. It includes a simple combustor model exhausting through a choked nozzle, see Gill, 1987, (1988, (a), (b) and (c)) and 1989, Gill and Haynes, 1990, and Gill et al, 1991. The turbines are not represented and so spool rotational speed is constant but compressor corrected speed can vary with inlet temperature.

The Gas Dynamic Methods are the same as those described above, except the energy equation is expressed with respect to entropy, rather than enthalpy. The equation set is also extended to allow for radial flow. Radial

flow is allowed, both in front of, and behind the fan, and so variation in by-pass ratio is therefore accommodated. Although to cater for radial flow within the fan is computationally possible, it is rare that fan inner and outer performance characteristics are available as a function of by-pass ratio. The equation set is solved using a 4th and 6th order predictor corrector, explicit time marching technique. Greatest numerical stability is achieved by using the entropy form of the energy equation and the 'transmittal of properties' scheme used by Steenken, 1982. The boundary conditions are upstream total pressure and temperature, and combustor 'nozzle' exit area; two spool compression systems are the same, but with intake entry radial velocity set to zero, and by-pass duct exit area defined.

The model represents the compressor with a single volume, and the fan by an inner and outer volume. Its frequency response is approximately 40 Hz and suitable for compression stability prediction. Although the modelling approach is compatible with stage-by-stage compressor representation, it is not included because of the poor availability of stage characteristics, particularly for low hub/tip ratio fans and compressors.

b) Compressor post-stall performance

Experimental or theoretical determination of true high-frequency-transient component performance characteristics is not practical. This is because a characteristic so derived, would be unique to a particular engine transient and so inappropriate for use in a model. A practical compromise is to assume that component high-frequency-transient performance can be represented by a steady-state performance characteristic.

This approach is adopted by all the engine models referenced in this review. The assumption states that the high-frequency-transient performance of any engine component is equal to its instantaneous steady-state performance, see section 4.3.3. Consequently, in the case of a compressor, it is the steady-state post-stall performance characteristics that are required.

Detailed compressor post-stall performance characteristics in the open literature are very rare. This is due to the expense in generating them and the possible additional expense in repairing any damage that may have occurred to the compressor.

The literature search revealed just one complete high speed compressor pre- and post-stall characteristic. Small and Lewis, 1985, describe the experimental determination of both the steady-state rotating-stall and reverse flow performance characteristics of what is referred to as a three stage High Speed Research (HSR) compressor. This compressor is believed to be the final three stages of the JT9 compressor. Steady-state reverse flow performance was measured by forcing air from a remote supply backwards through the compressor whilst the blades rotated in the normal sense.

The performance characteristic presented is for one, undefined, speed and the nature of the characteristic in the zero flow region is omitted, see figure 2.1a.

However, there are detailed, low speed, compressor post-stall data in the literature. A notable example is the work presented by Gamache, 1985. The compressor used is the final three stages of the Pratt and Whitney JT9 compressor, believed to be identical to the one used by Small and Lewis, 1985. Although the compressor is a high

speed design it was only run at low speeds generating at most, a pressure ratio of 1.08. The variation of both pressure and torque coefficient with flow coefficient for both rotating-stall and reverse flow are presented for three different speeds, see figure 2.1b. Steady-state reverse flow was achieved by using a 'bigger' compressor to blow air backwards through the test compressor.

Turner and Sparkes, 1964, present both steady-state rotating-stall and reverse flow characteristics for a low speed, single stage fan of unspecified origin. Both pressure and temperature coefficient vs flow coefficient are given for three different speeds.

O'Brien, 1992, describes a mathematical technique for predicting rotating-stall and reverse flow stage compressor performance characteristics. The method is a modified version of standard axial flow compressor mean line analysis. However, the predicted characteristics are adjusted with what are unspecified empirical data in order to match experimental data.

The characteristics of Turner and Sparkes, 1964, and O'Brien, 1992, are similar in trend to those of Small and Lewis, 1985, and Gamache, 1986.

c) Combustor post-stall performance

Surge and, up to a point, rotating-stall generate unsteady combustion phenomena which strongly influence the nature of whole engine post-stall behaviour, see section 1.1.

A combustor model suitable for inclusion into a whole engine pre- and post-stall model must have the following capabilities.

i) prediction of combustion flame stability
ii) prediction of re-ignition
iii) operation during low and reverse flow at combustor entry
iv) compatibility with Gas Dynamic Methods

There are two notable combustor models in the open literature. The first is described by Steenken et al, 1985. It is a two volume combustor model which includes flame stability criteria and re-ignition capability. The two volumes are positioned in series and represent the 'cold' outer combustor volume and the 'hot' inner flame tube volume. Like each of other engine volumes Gas Dynamic Methods are applied across the two combustor volumes.

Combustion stability is assessed by a computer graphical 'look-up' with respect to the combustor loading and fuel-to-air ratio. Although re-ignition limits typically lie outside of extinction limits, the two are assumed coincident for modelling purposes. At the point of extinction the combustion efficiency is assumed to fall to zero exponentially, and at the point of re-light, to rise exponentially.

Combustion calculations are traditionally based on a steady through flow and so cannot be used in cases of reverse or low flow at entry. The difficulty in performing combustion calculations at such flow conditions is not acknowledged, nor is the ability demonstrated in the simulation results given. It is suspected that this capability is not present and the combustor hot volume was

kept sufficiently 'far away' from the compressor exit to avoid such problems.

Steele et al, 1987, describe a combustor model which is very similar in approach to Steenken et al, 1985. The model consists of a 'cold' and 'hot' volume in series but unlike Steenken, the respective volume performance is represented by an actuator disc at entry. The model is run in isolation and its performance compared to the results of a specifically designed transient combustion test rig. The rig is capable of simulating the effect of compressor rotating-stall and surge, however, very few experimental and model simulation results are given.

Przybylko, 1985, describes the introduction of the above combustor model to a whole engine model with post-stall capability. However, very few results are given. Again, the difficulty in performing combustion calculations at very low, or reverse flow conditions at combustor entry is not acknowledged or the ability demonstrated in the simulation results given.

CHAPTER 3

Project Management

3.1 Introduction

To provide the greatest chance of completing a successful project, project management techniques were used to define the specification and scope, and subsequently plan and control the progress and quality of work.

The project management of the work was split into two; the **Project Organisation and Launch,** and the **Project Execution.** Each are described below and the chapter concluded with an appraisal of their effectiveness.

The Project Organisation and Launch was an iterative procedure which was developed specifically for technology research projects. It resulted in three 'working' documents which were the,

i) **Project Specification**
ii) **Estimate of Time and Resource**
iii) **Work Plan and Strategy**

Together the documents provided the information necessary to direct and control the work during the three year course period. The Project Organisation and Launch is detailed in section 3.2.

Despite a detailed approach, and even with the benefit of some experience, it was expected that the time schedules estimated during the Project Organisation and Launch phase would, to a degree, fall prey to unforeseen problems.

Thus, there was a need for a thorough but simple means of assessing the progress of work completed such that if problems occurred they could be dealt with as early as possible. A simple method of progress assessment and an approach to be adopted in overcoming unforeseen technical problems, were developed and are detailed in section 3.3, Project Execution.

3.2 **Project Organisation and Launch**

The Project Justification, section 1.2, and Review of Previous of Work, chapter 2, provided the necessary base work to launch the project. The iterative procedure used for the Project Organisation and Launch is shown in figure 3.1. The procedure was developed as a generic method suitable for project managing complex research projects subject to the constraints of cost, quality and time. The procedure resulted in a detailed and definitive statement of the,

i) Project Specification
ii) Estimate of Time and Resource
iii) Work Plan and Strategy

The process began by condensing the needs of the Project Justification, section 1.2, into a formal technical statement which was the Objective, section 1.3. A literature search was then completed, and combined with research into the then present applicable Rolls-Royce technology, an **Outstanding Need** was derived, figure 3.1. Based on the Outstanding Need, a Specification was written which in turn provided the necessary information to determine the Estimate of Time and Resource. Evaluation of the Estimate of Time and Resource is detailed in

section 3.2.1. At this point the benefits identified in the Project Justification in completing the work, were weighed up against the estimate of time and resource required - Decision Point 1, figure 3.1. This decision was somewhat subjective due to the difficulty in predicting the full potential of the developed modelling methods.

The first iteration illustrated that the Specification was too ambitious, suggesting a work period of greater than the three year course period, and so had to be amended. But at Decision Point 2 the subsequent Estimate of Time and Resource proved suitable. With a converged Specification, and Estimate of Time and Resource, the Work Plan and Strategy was derived. If it was discovered in finalising the Work Plan and Strategy that a significant incursion in time or cost was likely, then a further iteration would of had to of been done. Here again the Specification would have to be amended and the Estimate of Time and Resource made again, figure 3.1.

The final Specification derived by the Project Organisation and Launch is detailed in appendix 1.1. The method used to generate an Estimate of Time and Resource based on the Specification is described in section 3.2.1, and the derived Work Plan and and Strategy is detailed in section 3.2.2.

3.2.1 **Estimate of Time and Resource**

An estimate of the time required to complete a project must be made from a statement of the **Scope of Work.** The Scope of Work is a definitive statement of the work that will be done and perhaps more importantly, of the work

that will not be done. The Scope of Work is in turn based on the Project Specification - the Scope of Work must contain all the items of work required to fulfil the specification.

The Scope of Work was determined from a **Work Breakdown Structure (WBS)**. It is a formal means of defining exactly, to a 'hands on level', the items of work that have to be completed to meet the specification. It was the WBS which provided a basis for estimating the total time required to complete the project.

For this project it was necessary to split the WBS into four levels. These were,

Level 1 - A statement of the '**Final Deliverable**' which in this case was the PhD thesis itself.

Level 2 - A list of each distinct **Area of Work** required to achieve the Specification.

Level 3 - A list of **Work Packages** within each Area of Work identified in Level 2.

Level 4 - Where necessary, a list of **Work Items** that together formed a Work Package.

Figure 3.2 is a schematic illustration of the WBS and complete details are presented in appendix 3.1.

Against each Level 3 and Level 4 activity of the WBS, an estimate was made of the number of working hours required to complete it. Working hours were categorised as either industrially based or 'own'. Where 'own' hours applied to the completion of additional PhD studies. Appendix 3.1

states the **Estimated Hours** for each WBS Level 3 and 4 work item and a total Estimated Hours for each Area of Work. A contingency was also included by assessing the risk of each Level 3 and 4 work item - the extent of contingency was set according to the scale shown in table 3.1. Note that appendix 3.1 also identifies the risk assessment for each work item.

The Estimated Hours and **Total Hours** (including contingency) for each Area of Work of the WBS are summarised in table 3.2. Note that the Areas of Work include the **Alternative Courses of Work** identified in the Technical Specification, Part vi) appendix 1.1. In fact, the Work Plan and Strategy, section 3.2.2, identifies four possible Alternative Courses of Work, where each is composed from the appropriate Areas of Work, see table 3.3. The Estimated Hours and Total Hours for each Alternative Course of Work are given in table 3.4.

'Hands-On' resource was one man for three years. The total number of industrially based hours available during the three year period was predicted from the Rolls-Royce Man Hour Utilisation Rates listed in table 3.5. Note that the number of hours made available is greater than those required to complete any of the four Alternative Courses of Work, table 3.4, and therefore represents a converged solution to the Project Organisation and Launch procedure.

3.2.2 Work Plan and Strategy

The Work Breakdown Structure conventionally provides the necessary information with which to complete a **Network Analysis**. A Network Analysis results in a statement of the interdependence of each work item, i.e it ensures that

before any given item of work is started all requisite items of work have been completed. Consequently the project **Critical Path**, or minimum time to completion given unlimited resource, is also defined. Although this is a powerful technique, where the results would obviously of been desirous, it was deemed inappropriate for this project. This was because, like most research projects, items of work often rely on a cross fertilisation of ideas and so their completion in a defined order is rarely possible. Use of Network Analysis would have lead to an unwieldy project work plan.

The alternative to a Network Analysis is illustrated in figure 3.3, the Work Plan and Strategy. Note that the research work can take one of four alternative courses - the Four Alternative Courses of work. This was necessary due to two items of work that were identified as being possibly insurmountable, given the chosen technical approach, during the Project Organisation and Launch phase.

The Work Plan and Strategy is detailed in appendix 3.2. The strategy was a statement of intent and is therefore written in the future tense. Table 3.6 summarises the anticipated modelling capability of each of the four Alternative Courses of Work - note that Course of Work No. 4 was the most desirous as it completely satisfied the Project Specification.

3.3 Project Execution

3.3.1 Progress Assessment

Progress was assessed at the end of each calendar quarter by evaluating the technical progress achieved against what should have been accomplished in the cumulative time spent. This provided a regular revision of the estimate of time required to complete the project; and so provided an early warning system of project over-run.

Cumulative time spent per quarter was calculated from a weekly log of hours spent on each Work Package/Work Item (Level 3 and 4 of the Work Breakdown Structure). The new estimate of time required to complete the project was then calculated using the following ratios.

If A_i = Total Hours (including contingency) of Work Package/Work Item

B_i = Cumulative hours spent on Work Package/Work Item

C_i = Percentage estimate of Work Package/Work Item completed

i = Work Package/Work Item number

then at the end of a quarter a Work Package/Work Item should be so many percent complete.

$$\left[\frac{B_i}{A_i} \right] 100\%$$

However, if the work is predicted to be C_i % complete, then the revised value of A_i (Total Hours) is

$$\left[\frac{B_i}{A_i}\right]\left[A_i - C_i\right]$$

The revised estimate of Total Hours to complete the whole project is then

$$\sum_{i}^{N}\left[B_i - C_i\right]$$

Where i = 1, total number of Work Packages/Work Items (N).

The project progress data was stored and manipulated by computer. At the end of each quarter a graph of project Total Hours vs the then quarter, was obtained to assess progress for the current Course of Work. Figure 3.4 illustrates each revised time for project completion, at each quarter, for the 3 year project period. Note that the graph in figure 3.4 is with respect to Course of Work No. 4, which was the actual model development route taken.

Figure 3.4 highlights an apparent excessive time consumed in overcoming what was an anticipated technical difficulty. This was prior to Decision Point 1 of the Project Work Plan and Strategy, figure 3.3. The problem was strongly pursued and eventually solved. Had it not been, the generic capability of the pre- and post-stall modelling methods would have been lost.

At the end of the three year period the project was approximately six weeks behind, see figure 3.4. This was due to unforeseen technical difficulties.

3.3.2 Back-Up Strategy in case of a major technical problem

The Work Plan and Strategy, section 3.2.2, highlighted the inclusion of two Decision Points designed to provide for what were called the Alternative Courses of Work, in the event of encountering an insoluble problem. Of course events may uncover other unforeseen technical difficulties for which the strategy illustrated in figure 3.5 was created.

Prior to Decision Point 2, of the Project Work plan and Strategy, figure 3.3, a feasibility study was made on the inclusion of reverse flow capability. The study was favourable and so the response to Decision point 2 was 'yes'. However, the ensuing development of reverse flow capability, WBS Level 1.10, revealed a difficulty that was in fact impractical to overcome. At this point in time, to complete the alternative Course of Work No. 3, within the three year period, was not possible.

It was decided that the optimum way forward was to adopt the strategy route no. 1 of figure 3.5. In this case, route 2 would have resulted in not knowing why the capability could not be achieved, and route 3 would have resulted in an intolerable project over-run.

With the remainder of the time left allocated for the development of reverse flow capability, WBS Level 1.10, a study into understanding the problem and suggesting

possible ways that the capability could be achieved, was done. This led in turn to the identification of a future work item, see chapter 9.

3.4 Appraisal of the Project Management techniques used

Completion of the 'Project Organisation and Launch', which produced a detailed Specification, Estimate of Time and Resource, and a Work Plan and Strategy proved invaluable. Because it was an iterative procedure and based on the Project Justification and the Review of Previous Work, it ensured that the technical background to a work item, and the reasons for doing it, were methodically questioned. This inevitably led to a more realistic definition of the Scope of Work and Estimate of Time and Resource.

Creation of the Work Plan and Strategy provided a reassuring platform from which to launch the project. Concentration on the work in hand benefited from the knowledge that the 'what if' questions had already been asked and answered. The decision not to use Network Analysis in the creation of the Work Plan and Strategy was shown to be correct. As anticipated the cross fertilisation of ideas and results between work items was prevalent; and therefore incompatible with the sequential completion of work items that is required by Network Analysis.

Assessment of project progress at each calendar quarter, was again invaluable as it ensured an early warning of any project over-run. However, despite the contingency included in the original Estimate of Time and Resource, the project did over-run by almost six weeks due to unforeseen technical difficulties. Although the over-run was predicted in good time, the nature of the difficulties

were such that the time could not be made up - the over-run was therefore caused by the inherent nature of research work rather than of any lacking in the project management techniques used.

3.5 **Course Summary**

The course specification which is detailed in appendix 1.1 stated that both technical and project progress had to be presented to a Supervisory Panel at least three times a year. Appendix 3.3 gives details on the members of the Supervisory Panel and lists all the 'panel meetings' held. Further to the panel meetings, individual academic and project management supervision meetings were also held on a regular basis. Each meeting is also listed in appendix 3.3.

A further course requirement was attendance of relevant technical and project management courses. Each course is listed in appendix 3.3. In addition, a conference attended, a paper presented and further presentations made on project progress, are listed.

Chapter 4

Development of a high frequency response Gas Dynamic Equation Set

4.1 Introduction

For flow disturbances in gas turbines of greater than approximately 5 Hz, the time dependence of flow behaviour, due to temporary accumulation of mass, momentum and energy, becomes significant. The prediction of what is often referred to as 'high frequency gas dynamic response' is therefore necessary if the simulation of engine response during high frequency pre- and post-stall transients is to be representative. The prediction of high frequency gas dynamic response is achieved by using a high frequency gas dynamic equation set.

The equation set is derived by conserving mass, momentum and energy across a volume through which the engine working fluid passes. The high frequency gas dynamic response of the fluid flow for a whole engine, can then be predicted by combining volumes of appropriate geometry. Figure 4.1 is a schematic illustration of how a two-spool turbofan engine may be split into component volumes.

The equation set is one-dimensional but is extended to predict radial flow between volumes. This option is particularly useful for simulating the transient behaviour of flows in high by-pass ratio turbofan engines, in which the fan characteristics vary significantly across the blade radius. The equation set may also be extended to predict flow between volumes positioned circumferentially, but the development of this capability was beyond the scope of the work presented here.

As previously stated in chapter 2, the method of predicting 'high frequency gas dynamic response' will from here on be referred to as 'Gas Dynamic Methods' (GDM), and engine time dependent transients greater than 5 Hz as 'high-frequency-transients'. The use of the term 'high-frequency-transient' is used to distinguish it from the time dependent modelling of engine spool speed which is conventionally known as 'transient' performance prediction.

4.2 Derivation of the Gas Dynamic Equation set

The complete set of non-linear partial differential equations which describe the transfer and accumulation of mass, momentum and energy within a fluid are derived below and with respect to the component volume illustrated in figure 4.2. Note that the derivation allows volume K planes to be set at an angle to the engine axis but insists that i planes be perpendicular.

The engine working fluid is considered compressible and assumed to be a calorically perfect gas obeying the ideal gas equation of state. The gas is also assumed inviscid, although account can be taken of viscous pressure loss by including user defined data. Heat transfer between the working fluid and engine casings is a secondary effect during high-frequency-transients and so the flow process is assumed adiabatic.

(a) Time dependent conservation of mass equation

Without the inclusion of circumferential flow the mass flow rate into the volume shown in figure 4.2 is given by

$$W_i + W_K$$

and similarly the mass flow rate out of the volume is given by

$$W_{i+1} + W_{K+1}$$

If the rate of accumulation of mass within the volume is denoted by,

$$\frac{dm}{dt}_V$$

then by conserving mass, the time dependent conservation of mass equation becomes,

$$\frac{dm_V}{dt} = W_i + W_K - W_{i+1} - W_{K+1}$$

If a volume is representing an engine component where mass flow is removed from, or introduced to, the working fluid, such as compressor bleed or cooling air, then account can be taken by including a 'bleed' term.

$$\frac{dm_V}{dt} = W_i + W_K - W_{i+1} - W_{K+1} - W_B$$

The above equation can be made more amenable to solution by approximating,

$$\frac{dm}{dt}_V$$

in terms of the volume averaged density, $\bar{\rho}$. The mass within the volume may be expressed as

$$\int_V \rho dV$$

and so

$$\frac{dm_V}{dt} = \frac{d}{dt}\int_V \rho dV$$

Now if $\bar{\rho}$ is the volume averaged density then,

$$\bar{\rho}V = \int_v \rho dV$$

and so the time dependent conservation of mass equation takes the final form,

$$\frac{d\bar{\rho}}{dt} = \frac{1}{V}\left[W_i + W_K - W_{i+1} - W_{K+1} - W_B\right]$$

It is this equation that takes account of the accumulation of mass within a volume during high-frequency-transients. The rate of change of contained mass is expressed in terms of volume averaged density and calculated from the instantaneous rate of mass flow into and out of the volume. The volume averaged density $\bar{\rho}$, is in turn approximated from the flow density at the point of entering and leaving the volume - this is described in section 4.3.1

(b) **Time dependent conservation of energy equation**

Energy flowing into, and out of the component volume is expressed in terms of entropy, thereby, in addition to conserving energy, the second law of thermodynamics is obeyed.

Without the inclusion of circumferential flow the rate of entropy entering the volume in figure 4.2 is given by,

$$W_i s_i + W_K s_K$$

and similarly the rate of entropy leaving the volume is given by

$$W_{i+1}s_{i+1} + W_{K+1}s_{K+1}$$

where specific entropy takes the form

$$s - s_o = C_p \ln \left[\frac{t}{T_o} \right] - R \ln \left[\frac{p}{p_o} \right]$$

If the rate of accumulation of entropy within the volume is denoted by

$$\frac{dS}{dt}_v$$

then by obeying the second law of thermodynamics, the time dependent conservation of energy equation becomes,

$$\frac{dS_v}{dt} + W_{i+1}s_{i+1} + W_{K+1}s_{K+1} - W_i s_i - W_K s_K - \frac{\dot{Q}_v}{T_v} \geq 0$$

or

$$\frac{dS_v}{dt} + W_{i+1}s_{i+1} + W_{K+1}s_{K+1} - W_i s_i - W_K s_K - \frac{\dot{Q}_v}{T_v} = \dot{S}_v$$

where $\dot{S}_v$ is the rate of entropy production within the volume due to irreversible processes such as flow compression (compressor), heat addition (combustor) and viscous pressure loss (ducts and jet pipes).

The above equation can be made more amenable to solution by approximating,

$$\frac{dS}{dt}_v$$

in terms of the volume averaged product of density and entropy, $\bar{\rho}\bar{s}$.

The entropy within the volume may be expressed as

$$S_v = \int_v \rho s dV$$

Now if $\bar{s}$ is defined as the volume averaged value of specific entropy then,

$$\bar{\rho}\ \bar{s}\ V = \int_v \rho s dV$$

and so the time dependent conservation of energy equation becomes,

$$\frac{d(\bar{\rho}\bar{s})}{dt} = \frac{1}{V}\left[W_i s_i + W_K s_K - W_{i+1} s_{i+1} - W_{K+1} s_{K+1} + \frac{\dot{Q}_v}{T_v} + \dot{S}_v\right]$$

Heat transfer between the working fluid and the engine casings is a secondary effect during high-frequency-transients and so the flow process is assumed adiabatic. The rate of heat transfer $\dot{Q}$ is therefore zero and so the final form of the time dependent conservation of energy equation is

$$\frac{d(\bar{\rho}\bar{s})}{dt} = \frac{1}{V}\left[W_i s_i + W_K s_K - W_{i+1} s_{i+1} - W_{K+1} s_{K+1} + \dot{S}_v\right]$$

It is this equation that accounts for the accumulation of energy within a volume during high-frequency-transients. The rate of change of contained energy is expressed by volume averaged entropy, and calculated from the instantaneous rate of entropy production within the volume, and the entropy flowing into and out of the volume. Like volume averaged density, $\bar{\rho}$, volume averaged

entropy, $\bar{s}$, is approximated from the entropy of the flow entering and leaving the volume - this is described in section 4.3.1.

(c) **Time dependent conservation of momentum equation**

As momentum is a vector quantity it must be conserved in both the radial and axial directions. This results in two time dependent conservation of momentum equations.

(i) Time dependent conservation of momentum equation - **axial direction.**

The rate of momentum entering the volume of figure 4.2 is given by

$$W_i U_i^x + W_k U_k^x$$

and similarly the rate of momentum leaving the volume is given by

$$W_{i+1} U_{i+1}^x + W_{K+1} U_{k+1}^x$$

If the rate of accumulation of axial momentum within the volume is denoted by

$$\frac{d}{dt}(MOM)_v^x$$

then by Newton's second law of motion the time dependent conservation of momentum equation becomes,

$$\frac{d(MOM)_v^x}{dt} + W_{i+1} U_{i+1}^x - W_i U_i^x + W_{K+1} U_{k+1}^x - W_k U_k^x = F_{tx}$$

where F_{tx} is the total force acting on the fluid in the axial direction.

The above equation can be made more amenable to solution by approximating,

$$\frac{d(MOM)_v^x}{dt}$$

in terms of the volume averaged mass flow rate in the axial direction, $\bar{w}^x$.

Now by evaluating the component volume momentum in the x direction,

$$\frac{d(MOM)_v^x}{dt} = \frac{d}{dt}\int_v \rho U^x dV = \frac{d}{dt}\int_x \rho\, U^x A dx$$

and defining $\bar{w}^x$ as the volume averaged mass flow rate in the x direction, then

$$L^x \frac{d\bar{W}^x}{dt} = \frac{d}{dt}\int_x \rho U^x A dx$$

The time dependent conservation of momentum equation in the axial direction therefore becomes

$$\frac{d\bar{W}^x}{dt} = \frac{1}{L^x}\left[W_i U_i^x - W_{i+1}U_{i+1}^x + W_K U_K^x - W_{K+1}U_{K+1}^x + F_{tx}\right]$$

The force F_{tx} represents the total force acting on the component volume fluid in the axial direction, see figure 4.2. It can be calculated by evaluating the following

$$F_{tx} = (pA)_i - (pA)_{i+1} + \int p dA^x + F_{nx}$$

Where F_{nx} is the net axial force exerted on the fluid, such as that by compressor and turbine blades, and the drag produced by combustion inner casings; and the integral

$$\int pdA^x$$

represents the mean axial force exerted on the fluid by virtue of the surfaces K and K+1. The pressures p_K and p_{K+1} are the respective mean pressures and can be calculated by integrating pressure over the K and K+1 surfaces.

$$p_K = \int pdA^x \; / \; \int dA^x$$

$$\text{and} \quad p_{K+1} = \int pdA^x \; / \; \int dA^x$$

With the evaluation of F_{tx} the time dependent conservation of momentum equation in the axial direction becomes,

$$\frac{d\bar{W}^x}{dt} = \frac{1}{L^x}\left[W_i U_i^x - W_{i+1}U_{i+1}^x + W_K U_K^x - W_{K+1}U_{K+1}^x + (pA)_i - (pA)_{i+1} + \frac{1}{2}(p_K + p_{K+1})(A_{i+1} - A_i) + F_{nx}\right]$$

It is this equation that accounts for the accumulation of momentum in the axial direction within the volume during high-frequency-transients. The rate of change of accumulated momentum is calculated from the rate of momentum flowing into, and out of the volume, and the internal and external forces acting on the volume fluid. Again the volume averaged quantity, $\bar{W}^x$, is approximated from the mass flow rate entering and leaving the volume - this is described in section 4.3.1.

(ii) Time dependent conservation of momentum equation - **radial direction.**

The basic form of the radial momentum equation can be derived by using the same approach as above.

$$\frac{d(MOM)^r_v}{dt} + W_{K+1}U^r_{K+1} - W_KU^r_K + W_{i+1}U^r_{i+1} - W_iU^r_i = F_{tr}$$

As before the rate of change of momentum can be approximated in terms of the volume averaged radial mass flow rate and volume geometry.

$$\frac{d(MOM)^r_v}{dt} = L^r \frac{d\bar{W}^r}{dt}$$

The time dependent conservation of momentum equation therefore becomes,

$$\frac{d\bar{W}^r}{dt} = \frac{1}{L^r}\left[W_KU^r_K - W_{K+1}U^r_{K+1} + W_iU^r_i - W_{i+1}U^r_{i+1} + F_{tr} \right]$$

where $L^r = r_{K+1} - r_K$ and is a mean value.

The force F_{tr} represents the total force acting on the component volume fluid in the radial direction, see figure 4.2. It can be evaluated by resolving forces in the vertical direction. No circumferential flow is assumed and so the centripetal force is not included.

$$dF_{tr} = p_Kr_KL^x\Delta\theta - p_{K+1}r_{K+1}L^x\Delta\theta + 2(r_{K+1} - r_K)L^xp_\theta Sin\left[\frac{\Delta\theta}{2}\right] + dF_{nr}$$

Where F_{nr} is of the same origin as F_{nx}, but acts in the radial direction. Note that the radial dimensions and pressure at planes K and K+1 are mean values.

By making the approximations

$$\text{Sin}\left[\frac{\Delta\theta}{2}\right] \simeq \frac{\Delta\theta}{2} \quad \text{and} \quad p_\theta = \frac{1}{2}(p_K + p_{K+1}), \text{ then}$$

$$dF_{tr} = \frac{\Delta\theta}{2} L^x (p_K - p_{K+1})(r_K + r_{K+1}) + dF_{nr}$$

The total radial force F_{tr} is evaluated by integrating round the circumference.

$$F_{tr} = \pi L^x (p_k - p_{k+1})(r_k + r_{k+1}) + F_{nr}$$

The time dependent conservation of momentum equation therefore becomes,

$$\frac{d\bar{W}^r}{dt} = \frac{1}{L_r}\left[W_K U_K^r - W_{K+1}U_{K+1}^r + W_i U_i^r - W_{i+1}U_{i+1}^r + \right.$$
$$\left. + \pi L^x (p_k - p_{k+1})(r_k + r_{k+1}) + F_{nr} \right]$$

It is this momentum equation that accounts for the accumulation of momentum in the radial direction within the volume during high-frequency-transients. The rate of change of accumulated momentum is calculated from the rate of momentum flowing into, and out of the volume, and the internal and external forces acting on the volume fluid. Unlike $\bar{W}^x$, the volume averaged mass flow rate in the radial direction $\bar{W}^r$, is calculated directly - see section 4.3.1.

4.3 Application of the Gas Dynamic Equation Set

Figure 4.1 is a schematic illustration of a typical two-spool turbofan showing how it can be represented by component volumes. The inclusion of Gas Dynamic Methods is achieved by applying the gas dynamic equation set across each volume.

The one-dimensional equation set

For components other than the fan and intermediate casing where radial flow can occur, the one-dimensional form of the equation set is used.

Conservation of mass

$$\frac{d\bar{\rho}}{dt} = \frac{1}{V}\left[W_i - W_{i+1} - W_B \right]_{t+\Delta t}$$

Conservation of momentum

$$\frac{d\bar{W}}{dt} = \frac{1}{L}\left[(WU)_i - (WU)_{i+1} + (pA)_i - (pA)_{i+1} + F_{nx} \right]_{t+\Delta t}$$

Note that the term representing the mean axial force exerted by the volume planes K and K+1 is omitted.

$$\frac{1}{2}(p_K + p_{K+1})(A_{i+1} - A_i)$$

This is because, for engine model applications, not only is the term computationally difficult to calculate, but its value is significantly smaller than the pressure force term,

$$(pA)_i - (pA)_{i+1}$$

Conservation of energy

$$\frac{d(\bar{\rho}\bar{s})}{dt} = \frac{1}{V}\left[(Ws)_i - (Ws)_{i+1} + \dot{S}_v\right]_{t+\Delta t}$$

Note that the equation set is expressed in implicit form. This is because it is applied to models using the Rolls-Royce Aero Engine Performance computer system (RRAP) which solves the governing performance equations with an implicit numerical scheme - this is described in section 5.2.2.

The one-dimensional equation set extended to predict radial flow

The gas dynamic equation set extended to predict radial flow, is used, for example, to simulate radial migration of the fan 'splitter' streamline by predicting radial flow within the fan and intermediate casing volumes. Note that again the momentum equation does not include the mean axial force exerted by planes K and K+1.

Conservation of mass

$$\frac{d\bar{\rho}}{dt} = \frac{1}{V}\left[W_i + W_K - W_{i+1} - W_{K+1} - W_B\right]_{t+\Delta t}$$

Conservation of momentum - axial

$$\frac{d\bar{W}_x}{dt} = \frac{1}{L^x}\left[W_i U_i^x - W_{i+1}U_{i+1}^x + W_K U_K^x - W_{K+1}U_{K+1}^x + (pA)_i - (pA)_{i+1} + F_{nx}\right]_{t+\Delta t}$$

Conservation of momentum - radial

$$\frac{d\bar{W}^r}{dt} = \frac{1}{L^r}\left[W_K U_K^r - W_{K+1}U_{K+1}^r + W_i U_i^r - W_{i+1}U_{i+1}^r + \right.$$
$$\left. + \pi L^x (p_K - p_{K+1})(r_K + r_{K+1}) + F_{nr}\right]_{t+\Delta t}$$

Conservation of energy

$$\frac{d(\bar{\rho}\bar{s})}{dt} = \frac{1}{V}\left[W_i s_i + W_K s_K - W_{i+1}s_{i+1} - W_{K+1}s_{K+1} + \dot{S}_v\right]_{t+\Delta t}$$

Note again that the equation set is expressed in implicit form.

Solution of the gas dynamic equation set requires the following to be calculated.

1) calculation of the volume averaged quantities $\bar{\rho}$, $\bar{W}^x$ and $\bar{\rho}\bar{s}$

2) calculation of the time dependent derivatives

3) evaluation of W_B, F_{nr}, F_{nx} and $\dot{S}_v$ - these are called the Component Performance Terms

4) specification of appropriate boundary conditions

Each of the above are detailed below in sections 4.3.1 to 4.3.4 respectively.

4.3.1 Calculation of the volume averaged quantities

Component volume averaged quantities are approximated by linear interpolation between the volume entry and exit stations.

$$\bar{\rho} \simeq \frac{1}{2} \rho_i + \frac{1}{2} \rho_{i+1}$$

$$\bar{W}^x \simeq \frac{1}{2} W_i + \frac{1}{2} W_{i+1}$$

$$\bar{s} \simeq \frac{1}{2} s_i + \frac{1}{2} s_{i+1}$$

$$\overline{\rho s} \simeq \bar{\rho}.\bar{s}$$

Whilst the above approximations enable solution of the one-dimensional equation set further approximations must be made to solve for radial flow. Figure 4.3 illustrates how the geometry of a fan or intermediate casing is represented. Note that the radii and lengths are mean values. The volume averaged radial mass flow rate $\bar{W}^r_A$, and $\bar{W}^r_B$ are calculated at their respective volume average radii, $r_{k+\frac{1}{2}}$ and $r_{k-\frac{1}{2}}$. The radial mass flow rate at the plane k, between the inner and outer volume, is approximated by taking the mean of the inner and outer volume averaged radial mass flow rates.

$$W_k = \frac{1}{2} \left[\bar{W}^r_A + \bar{W}^r_B \right]$$

Appendices 4.1a and 4.1b detail the remaining approximations necessary to calculate radial flow.

4.3.2 Calculation of time dependent derivatives

Each of the three time dependent derivates are approximated to first order accuracy by backward finite deferencing.

$$\left.\frac{d\bar{\rho}}{dt}\right|_{t+\Delta t} \simeq \frac{\bar{\rho}_{t+\Delta t} - \bar{\rho}_t}{\Delta t}$$

$$\left.\frac{d\bar{W}}{dt}\right|_{t+\Delta t} \simeq \frac{\bar{W}_{t+\Delta t} - \bar{W}_t}{\Delta t}$$

$$\left.\frac{d\overline{\rho s}}{dt}\right|_{t+\Delta t} \simeq \frac{(\overline{\rho s})_{t+\Delta t} - (\overline{\rho s})_t}{\Delta t}$$

4.3.3 Evaluation of Component Performance Terms

Engine component performance is represented in the above gas dynamic equation set by evaluating its volume bleed W_B, net force applied to the fluid F_{nx} and F_{nr}, and rate of entropy production $\dot{S}_v$. The three terms are called the Component Performance Terms (CPT's).

Because each engine component is represented by a volume across which the equation set is applied, the calculation of the Component Performance Terms must be done using volume entry, and/or exit flow conditions. The CPT's are therefore calculated from a component performance characteristic.

Experimental or theoretical determination of true high-frequency-transient characteristics is not practical. This is because a characteristic so derived, would be unique to a particular engine transient and so

inappropriate for use in a generic model. A practical alternative is to assume that component performance can be represented by a steady-state performance characteristic.

This assumption states that the transient performance of any engine component is equal to its instantaneous steady-state performance. For example, in the case of a compressor, it is the steady-state performance characteristics that are used to calculate the Component Performance Terms.

4.3.4 **Boundary conditions**

Assuming a given fuel flow, three boundary conditions are required for a single-spool engine model. Here, provision for radial flow is not required and so transient response for each volume is calculated using the one-dimensional equation set.

Upstream boundary conditions are total temperature and pressure. The remaining condition is the final nozzle area.

For a two-spool engine model where the occurrence of radial flow is predicted by the extended gas dynamic equation set, a further two boundary conditions are required. These are zero upstream radial velocity and a second downstream final nozzle area.

Engine high-frequency-transient behaviour is induced by any one, or a combination, of the boundary conditions and fuel flow rate being varied as a function of time.

CHAPTER 5

Introduction of the gas dynamic equation set into the Rolls-Royce Aeroengine Performance computer deck - RRAP

5.1 Introduction

A whole engine model capable of predicting performance during pre- and post-stall high-frequency-transients was generated by extending the capability of the Rolls-Royce Aero Engine Performance computer system (RRAP). By doing so, the modelling methods were made generic, satisfying the project objective, section 1.3, and therefore applicable to all RRAP engine models both present and future.

Existing RRAP transient capability enabled prediction of engine performance during acceleration and deceleration. At each time step a steady-state performance calculation is done which includes a prediction of the compressor/turbine power imbalance. Knowing the spool inertia, the acceleration and hence the rotational speed at the next time step, is calculated. Performance prediction is good because the transient is predominantly governed by spool inertia. The performance calculations used are described in section 5.2. However, for flow disturbances greater than approximately 5 Hz the time dependency of flow properties become increasingly significant and the steady-state performance calculations made by the RRAP system, progressively more inadequate. The RRAP system did not include GDMs and was therefore unable to faithfully simulate high-frequency-transients.

This chapter describes the first step in reaching the project objective. This was to enable RRAP to simulate

high-frequency-transients by introducing the gas dynamic equation set detailed in chapter 4. However, a numerical instability caused by the interaction of the RRAP system with the gas dynamic equation set, was discovered; the nature and removal of this instability is described in section 5.3. Verification was achieved by comparing simulation results to experimental data taken during the passage of high frequency pressure pulses along a plane open ended pipe. Verification is described in section 5.4. Note that these data were taken from Boroomand, 1992. Also described is the application of the gas dynamic equation set extended to predict radial flow, to a simple two nozzle duct system. Although verification was not possible its performance is discussed.

Chapter 5 concludes with section 5.5 which discusses the numerical approach used to solve the gas dynamic equation set within RRAP.

5.2 An overview of the RRAP modelling philosophy

The Rolls-Royce Aero Engine Performance computer deck (RRAP) is a Company wide computer package primarily used to predict gas turbine performance. It enables the engineer/programer to construct an engine model using selected 'component performance calculations'. For example, a single spool turbojet model would comprise a 'performance calculation' representing each of the intake, compressor, combustor, turbine, jet pipe and nozzle components. Each calculation is of a Company 'performance standard' and only becomes peculiar to a particular engine when used with the appropriate performance characteristics. By simply including additional 'performance calculations', a two or three spool engine

model is easily constructed. Additionally, engine 'bleeds', power 'off-takes', intake performance and reheat etc are easily included. Automatic reference is also made to the International Standard Atmosphere (ISA) and so engine performance prediction throughout its operating envelope is possible.

In addition to engine modelling, any one of the engine component performance calculations can be executed in isolation. Similarly, a suite of thermodynamic and gas property calculations are available which again can be executed in isolation.

RRAP is thus a multi-purpose and versatile performance prediction tool, conforming to recognised and documented standards, which is available company wide.

5.2.1 The computer format of a RRAP model

A performance model is constructed by piecing together the required engine 'component performance calculations'. Each calculation is a stand alone computer subroutine. The subroutines are called from a user written computer file called the 'Engine Routine'. All engine component performance data are contained in an 'Engine Data' set, and details of each performance calculation required are specified in a 'Permutation' data set. Figure 5.1 is a schematic illustration of the RRAP system where, for example, the Engine Routine represents a single spool turbojet model.

Numerical solution of a performance model invariably requires the simultaneous solution of non-linear equations. The RRAP system solves these equations by using what is called the Implicit Matching Method. The

Matching Method also exists as a subroutine and is called from within the Engine Routine, see figure 5.1.

5.2.2 The RRAP Implicit Matching Method

The Implicit Matching Method is a Newton-Raphson numerical scheme capable of solving up to ninety-eight non-linear simultaneous equations. The equation error functions are known as **Matching Quantities** and the unknowns as **Variables**. Predicted or updated values of Variables are calculated by matrix inversion of a governing 'influence matrix'. The influence matrix relates the change in each Matching Quantity with respect to a defined **Increment** in each of the Variables. Solution is achieved when, for a given set of Variables, each Matching Quantity pair is equal to within a defined tolerance. When a solution is found the Engine Routine is said to be '**Matched**'. Figure 5.2 illustrates the lines of communication between the Implicit Matching Method and the RRAP system, and appendix 5.1 details the numerical scheme itself.

5.3 Solution of the Gas Dynamic Equation set

The RRAP system executes the component performance subroutines listed in the Engine Routine one by one and in descending order, see figures 5.1 and 5.2. Chapter 4 described how the gas dynamic equation set is applied across each component volume of an engine model. Therefore, the logical approach to introducing the gas dynamic equation set, was to execute the solution of the equation set within a subroutine which is called immediately after each component performance subroutine. Figures 5.4 and 5.5 illustrate the calculation sequence.

5.3.1 Conversion of Gas Dynamic equation set into a RRAP compatible form

Solution of the gas dynamic equation set requires calculation of the Component Performance Terms W_B, F_{nx}, F_{nr} and $\dot{S}_v$. These terms were assumed to be a steady-state value and calculated from steady-state component performance characteristics, see section 4.3.3. Although a bleed may be specified, the RRAP system does not calculate values of F_{nx}, F_{nr} or $\dot{S}_v$. This is because it is unconventional to represent component performance characteristics in terms of F_{nx}, F_{nr} and $\dot{S}_v$. This definition is not supported by the RRAP system. To overcome what was a computationally awkward problem, the format of the gas dynamic equation set was changed such that the Component Performance Terms were indirectly calculated via the component steady-state performance calculation.

For example, the steady-state value of the W_B, term can be calculated from the time dependent conservation of mass equation by setting the derivative equal to zero. Note that the bleed is assumed to be a function of flow conditions at the i plane only and so,

$$0 = \frac{1}{V}\left[W_i - W^*_{i+1} - W_B \right]$$

Note that the exit mass flow rate is a steady-state value and is denoted by the superscript '*'.

By substituting the above expression into the original time dependent conservation equation the bleed term is eliminated.

$$\frac{d\bar{\rho}}{dt} = \frac{1}{V}\left[W^{*}_{i+1} - W_{i+1} + W_k - W_{k+1} \right]$$

Similarly the F_{nx} and $\dot{S}_v$ terms were removed from the time dependent equations conserving momentum and energy. Note again that both F_{nx} and $\dot{S}_v$ were assumed to be a function of inlet flow conditions only.

$$\frac{d\bar{W}^{x}}{dt} = \frac{1}{L_x}\left[(WU + pA)^{*}_{i+1} - (WU + pA)_{i+1} - W_{k+1}U^{x}_{k+1} + W_k U^{x}_{k} \right]$$

$$\frac{d\overline{\rho s}}{dt} = \frac{1}{V}\left[(Ws)^{*}_{i+1} - (Ws)_{i+1} + W_k S_k - W_{k+1} S_{k+1} \right]$$

The RRAP system did not include a dedicated performance subroutine for the prediction of radial flow. There was therefore no benefit in terms of computational complexity in replacing the F_{nr} term in the radial momentum equation with steady-state terms. The F_{nr}, was calculated directly according to the theory presented in section 4.2.

Solution of the gas dynamic equation set was thus made possible without having to directly calculate the W_B, F_{nx} and $\dot{S}_v$ terms. Inclusion into RRAP was then simply achieved by introducing a call to a subroutine which solved the gas dynamic equation set after each call to a component performance subroutine, see figure 5.5.

5.3.2 Solution of the gas dynamic equation set

A self convergent iterative scheme based on Successive Back Substitution (SBS) was developed to solve for the three unknowns of the one-dimensional gas dynamic equation set. An 'off the shelf', non-linear, simultaneous equation solver was not used because its possible inclusion in future Rolls-Royce customer performance codes would infringe copyright law.

Appendix 5.2 gives the complete gas dynamic equation set in terms of the three chosen unknowns - these were volume exit pressure, temperature and density. Note that the equation set is in the RRAP compatible form as derived in section 5.3.1 above. Investigation into the nature of the three equations revealed a possible self convergent Successive Back Substitution iterative method. Figure 5.6a is a schematic illustration of the linear relationship between exit mass flow rate and exit density of the conservation of mass equation. This equation was used to calculate the exit mass flow rate from a guessed value of exit density and marks the first step of the SBS method.

For a given exit mass flow rate the conservation of momentum and energy equations reduced to two simultaneous equations with two unknowns - exit pressure and temperature. Figure 5.6b is schematic illustration of the two equations in the exit pressure and temperature plane. The equations were solved by first 'guessing' a pressure, and from the conservation of energy equation, predicting a value of temperature. This temperature was then used to calculate an improved value of pressure from the conservation of momentum equation. The value of pressure was improved because of the inherent shape of the momentum

and energy curves in the pressure and temperature plane, see figure 5.6b. Simultaneous solution of the momentum and energy curves was therefore self convergent.

Together the values of pressure and temperature provide a new value of flow density. This value of exit flow density was improved, and marked the completion of an iteration of the SBS method. The value of density was improved because of the inherent shape of the 'solution curve' of the momentum and energy equations and the conservation of mass curve, in the exit mass flow rate and density plane, see figure 5.6a. The complete SBS iteration was therefore self convergent.

A 'gas dynamic subroutine' was written to solve the gas dynamic equation set using the above SBS iteration method. The subroutine was 'called' immediately after each 'call' to a component performance subroutine. The gas dynamic subroutine therefore corrected the component exit steady-state flow variables for any gas dynamic effects. The SBS calculation procedure used by the gas dynamic subroutine is detailed in appendix 5.3.

5.3.3 The origin and correction of a gas dynamic solution failure

5.3.3.1 Identification of the cause of failure

Application of the Gas Dynamic Methods to a single spool, RRAP engine model, revealed a limiting numerical instability problem. The boundary conditions were as described in section 4.3.4 - for a given fuel flow, upstream total pressure and temperature, and final nozzle throat area. Regardless of which boundary condition was

perturbed sinusoidally with time, prediction of engine gas dynamic response was only possible at low perturbation amplitudes and frequencies. The Gas Dynamic Methods were found to fail at perturbations with amplitudes and frequencies significantly smaller than those expected of compressor stall transients. Initial investigation attempted to reduce the magnitude of the change in flow variables from time-step to time-step, by reducing the size of time-step. This improved stability, but was limited by computation precision errors. The smallest time step possible was 1 milli-second (mS), which did not reap the required numerical stability.

The instability was studied in isolation by applying the equation set to each of ten identical volumes that together formed a simple duct. The duct, shown in figure 5.7, represents an example length of an infinitely long duct conveying air at ISA sea level temperature and pressure, and at a mass flow rate of 25 Kg/s. The cross section area was 0.14 m^2 giving a flow Mach number of near 0.5. This is typical of the intake flow, at 100 % speed, of a small turbojet.

Each of mass flow rate, total pressure and temperature were perturbed in turn, for a single time-step only, at entry to the first duct volume, see figure 5.7. The Implicit Matching Method was not invoked because the objective was to study the behaviour of the Gas Dynamic Methods alone. The time-step used was 2 mS to ensure that computation precision errors did not influence numerical stability. Figure 5.8a shows the prediction made by the gas dynamic equation set subject to six individual, increasing perturbations (each done for the same time-step) in mass flow rate. In each case the gas dynamic equation set was solved for each of the ten

duct volumes. Note that perturbation of either temperature or pressure produced similar trends. Figure 5.8b illustrates a failure of the gas dynamic equation set in volumes 8, 9 and 10. Here the magnitude of the increasing perturbations stretched to beyond those illustrated in figure 5.8a.

On progressing downstream, figures 5.8a and b, illustrate an accumulative, or divergent change, in the flow variables, mass flow rate, temperature and pressure. The greater the perturbation, the greater the rate of divergence, and consequently, the nearer a failure to the source of perturbation. The rate of change of perturbation with respect to time, was found to be a controlling factor. For example, halving the magnitude of perturbation or the size of time-step, gave a comparable result. The length of each duct element was not found to influence stability. For example, the same length of duct was split into 50 and 90 volumes without influence. Note again, near identical results were achieved by perturbing either of temperature or pressure.

The instability or failure was found to be caused by the absence of a physical solution to the gas dynamic equation set. Figure 5.6b shows the conservation of momentum and energy solution curves for a successful solution of the equation set; and figure 5.9a, which illustrates the absence of a physical solution, a failure case. Further investigation revealed that the limiting point of stability was a sonic condition at volume exit, see figure 5.9b.

5.3.3.2 Correction of the failure

A possible solution might of been to modify the operation of the RRAP Implicit Matching Method. The matching method is summarised in section 5.2.2 and detailed in appendix 5.1. For example, a reduction in the magnitude of the Variable Increments, which are used to determine the influence matrix, and of the change in updated solution Variables, would enable a smaller time-step to be used. Although this would reduce the divergence of the solutions of the gas dynamic equation set, the approach is limited due to computational precision errors. Apart from which, to simply increase the precision would have a been a palliative measure for two reasons,

(i) A major advantage of using an implicit numerical scheme such as RRAP, rather than an explicit scheme, is its ability to predict 'large' changes in the solution Variables and so reach a solution in the minimum of computational time. Alternatively, in the case of time dependent modelling, the use of larger time-steps is made possible. The introduction of greater computer precision simply to use a smaller time-step is therefore inappropriate.

(ii) The cumulative, or divergent, nature of successive solutions of the gas dynamic equation set will always lead to failure, no matter how small the originating perturbation, provided the physical length of the model is sufficiently long. The use of smaller time-steps is therefore no guarantee of stability.

An alternative approach was to 'capture' a failure of the gas dynamic equation set. Three alternative ideas were proposed to replace the equation set should a physical solution not exist,

(i) The first method, at the point of failure, simply calculated the steady-state performance instead. This approach was partly successful but computationally time consuming. This was because the influence of the steady-state 'solutions' resulted in a poor influence matrix calculated by the Implicit Matching Method.

(ii) An improvement on the above idea was, at the point of failure, to solve the conservation of mass equation alone. This maintained a pseudo gas dynamic solution trend and consequently produced a more accurate influence matrix. Although computation time was reduced, the diverging nature of mass flow rate remained resulting in choking problems.

(iii) The third approach was, at the point of failure, to increase the volume exit area temporarily such that the Mach number was set at unity or just below. This ensured a physical solution to the gas dynamic equation set. However, the divergent nature of the flow variables was now greater and led to difficulty in calculating engine component performance.

Each method, though partly successful, was hindered by its inconsistent influence on the operation of the Implicit Matching Method. For example, because the above 'fixes' were invoked solely at the occurrence of a non-physical solution, they were likely to occur in different volumes

during the calculation of the influence matrix. Thus the predicted solution Variables were poor. Avoidance of these problems would have required comprehensive 'communication' between the model volumes (gas dynamic equation sets) and the Implicit Matching Method. To realise this would have been computationally complex and an unwelcome intervention into the workings of an already long standing, refined and 'stand-alone' computer routine - the Implicit Matching Method. Apart from which, there was no guarantee of stability for models of 'long' physical length.

Individually, the gas dynamic equation set can invariably find a solution subject to flow perturbations of comparable rate of change (with respect to time) to those expected during compressor stall transients. The true cause of the instability was the divergent nature of consecutive solutions of the gas dynamic equation set leading to choking, sooner or later, in the duct. Stability was finally achieved by preventing this divergence from volume to volume. This was done by specifying the mass flow rate and total pressure at entry to each volume, as Implicit Matching Method Variables. The required extra two Matching Quantities were the mass flow rate and total pressure between the same adjoining volumes, see figure 5.10. No discernible improvement in stability was gained by doing the same to total temperature and so in the interests of keeping model complexity to a minimum, an extra Matching Quantity and Variable in temperature was not included.

Stability for the duct models described below and the engine models of chapters 6 and 7 was achieved by the above method. In the case of the engine models, prudent choice of volume station positions led to improved

stability. For example, volume stations, if possible, were kept away from high Mach number flow such as that at turbine and nozzle entry.

5.4 Verification of the gas dynamic equation set

5.4.1 Introduction

Two simple duct models were written using the RRAP system. The first was used to verify the one-dimensional gas dynamic equation set; and the second to develop and assess the prediction of the equation set extended to predict radial flow.

The one-dimensional duct model was of an experimental rig based at Cranfield University. Some years ago the rig was used to measure the progression of high frequency pressure waves in low Mach number flow (less than 0.1). The objective was to compare the experimental results with predictions made by computer codes developed by Boroomand, 1992. The same experimental results were made available to this project to verify the gas dynamic equation set.

A literature search did not reveal any suitable experimental data with which to verify the equation set extended to predict radial flow. However, its performance was developed and assessed using a simple twin duct model. It comprised a single volume capable of predicting radial flow which exhausted into two one-dimensional ducts. Although not verified, its performance was considered physically representative.

5.4.2 Verification of the one-dimensional gas dynamic equation set

5.4.2.1 Rig and duct model details

The duct rig constructed by Cranfield University is schematically illustrated in Figure 5.11. It comprised a plenum chamber containing air at a pressure of approximately 8 KPa (gauge) exhausting into a plane cylindrical duct - the duct in turn exhausted to the atmosphere. The duct was 2.9m long, 0.1m in diameter and had a plane open end nozzle. Between the chamber and entrance to the duct was a 'pressure pulse generator'. Pressure pulses were generated by rotating a disc with four slots relative to a second identical, but stationary disc. The rotating disc was driven by an electric motor and introduced four pressure pulses with each revolution. The pulse frequency was therefore determined directly by the motor speed. A gauze was positioned just downstream of the pulse generator and served to maintain a near planar (one-dimensional) variation in flow properties.

The amplitude of pressure pulse was set by the plenum pressure and the time averaged total temperature of the duct flow set by the plenum temperature. Tests were completed with a pressure pulse amplitude of approximately 3% of atmospheric pressure, and over a range of frequencies between 14 and 200Hz. For each test the following measurements were taken,

- time averaged plenum temperature and pressure
- time averaged mass flow rate
- transient total and static pressure at duct station 1
- transient flow velocity and static pressure at duct stations 2,3,4 and 5

It is these data that were provided to this project for the verification of the Gas Dynamic Methods introduced into the RRAP system.

The RRAP model of the duct rig is shown in figure 5.12. The model boundary conditions were upstream total pressure and temperature and duct exit flow area. The plenum chamber and pulse generator were not modelled but replaced by the upstream boundary conditions total temperature and pressure. The model was perturbed by varying the upstream total pressure (boundary condition) in accordance with the time dependent total pressure measured at rig station 1, see figure 5.11. The upstream total temperature was set equal to the measured plenum temperature. (Work done on the flow by disc windage was assumed negligible.) The predicted flow velocity and static pressure were output to be commensurate with the experimental data taken at stations 2, 3, 4 and 5.

For a simple duct model only one Implicit Matching Method, Variable and Matching Quantity was required. In this case the entry mass flow rate was set equal to the Variable, and the duct exit, and 'nozzle' entry pressure, as the Matching Quantity, see figure 5.12. However, with the inclusion of Gas Dynamic Methods extra Matching Quantities and Variables were required to maintain numerical stability. A Matching Quantity and Variable in both mass flow rate and total pressure were introduced between each volume, see section 5.3.3.2. The duct could be represented by 10, 20, 30 or 40 volumes. This was done to enable investigation of the effect of model discretisation on the quality of high frequency simulation.

Pressure loss due to viscous drag is not directly predicted by the Gas Dynamic Methods, see section 4.2,

and so had to be defined for each volume. This was done by assuming a linear drop in pressure with duct length commensurate with a single value of skin friction coefficient. The value of friction coefficient was set according to experimental data presented by Boroomand, 1992. Skin friction coefficient was presented with respect to Reynolds Number for steady-state flow along with a correction factor for unsteady flow. The coefficient was found to increase with the pressure pulse frequency and thought to be due to unsteady boundary layer behaviour.

The pressure drop for each model duct element was calculated from,

$$\Delta P = \frac{2\Delta x}{D^3 \rho} \mu^2 C_f Re^2 \qquad \text{see Boroomand, 1992}$$

where the Reynolds Number was given by,

$$Re = \frac{\rho U D}{\mu}$$

The flow density ρ, and velocity U, were time averaged values, and the flow viscosity defined by the ISA at sea level.

Flow at the duct exit was not choked and was predicted by the actuator disc theory detailed in appendix 6.1e. However, the geometric flow area at duct exit was modified to take into account the reduction in flow area due to the boundary layer. This was done by introducing a nozzle

discharge coefficient which was calculated from an estimate of the boundary layer displacement thickness at duct exit. The layer thickness within the duct was predicted from so called 'flat plate theory' and used as a first approximation. The boundary layer was also assumed turbulent along the entire length of the duct because the Reynolds Number (approx 130,000) was greater than the typical transition value of 2000 for pipe flow, see Miller, 1978.

$$\delta^* = 0.0479x(Re_x)^{-0.2}$$

This prediction of displacement thickness was taken from Houghton and Corruthers, 1982 and is applicable to turbulent layer growth on a flat plate.

The nozzle discharge coefficient was calculated from,

$$Cd = \left[1 - \frac{4\delta^*}{D} \right]$$

The coefficient was estimated to be 0.74 which was found to give a mean mass flow rate/velocity comparable with test rig results.

5.4.2.2 **Gas dynamic simulation results and verification**

Prior to direct comparison with rig test results the duct model was used to check that fundamental characteristics of the propagation of flow disturbances were faithfully modelled.

The first check was to ensure that the propagation of small pressure disturbances travelled downstream at a speed equal to the sum of the mean flow velocity plus the acoustic velocity. Model steady-state flow conditions were set to be comparable to the steady-state flow conditions of the Cranfield rig. Upstream total temperature was set at 293K, time averaged upstream total pressure at 1Kpa above atmospheric, and the flow was allowed to exhaust to atmospheric pressure which gave a mass flow rate of 0.27Kg/S. A half sinusoid variation in total pressure (amplitude of 2%) with an equivalent frequency of 60 Hz was set as an upstream boundary condition. The time step was set at 1 mS and the simulation time halted after 8 mS. The simulation was halted to ensure that the pressure disturbance did not reach the nozzle, reflect, and alter the shape of the wave form. The progression of the pressure disturbance could then be faithfully tracked. Figure 5.13 shows the progression of the pressure pulse along the duct and illustrates that the propagation speed was equal to the sum of the mean flow velocity and the acoustic velocity. The propagation speed was also confirmed for lower and higher frequencies. However, at frequencies beyond approximately 120 Hz, the definition of the pressure pulse using a 1 mS time-step was too poor to calculate propagation speed with any degree of accuracy.

A change in flow temperature should be carried downstream at the average flow velocity. This was confirmed by introducing a temperature/time ramp in the upstream total temperature boundary of the above duct model. Progression of the 'ramp' profile downstream is shown in figure 5.13.

Comparison with rig test data was done to assess attenuation and superposition of wave forms predicted by the Gas Dynamic Methods. Although wave superposition was found to be faithfully predicted, wave attenuation was found to limit the frequency response.

Measured time dependent total pressure at rig station 1 was used as the perturbing function for the duct model. The pressure pulses were sinusoid in form and at an amplitude of approximately 1 KPa above atmospheric. Frequencies used for comparison were 14, 20, 40 and 80 Hz. Although test data was available at 160 and 200 Hz the time-step of 1 mS would not have provided sufficient wave form definition to make results representative. The test data of static pressure and flow velocity were compared to those predicted by the model.

Figures 5.14a and b show a direct comparison of predicted and rig test data of the flow velocity and static pressure at four stations along the duct. The frequency of the perturbing pressure function was 14Hz. The data was studied and checked against the following criteria,

i) Frequency corruption

The predicted frequency remained constant throughout the length of the duct.

ii) Wave superposition

The total simulation time was 0.6 S which is equivalent to approximately 70 acoustic traverses of the duct. The alignment in wave form therefore illustrated that superposition was faithfully

predicted and that the downstream nozzle condition reflected incident waves correctly.

iii) Pressure losses

The loss in mean pressure on progression downstream was in good agreement. This indicated that the prediction of pressure loss from a skin friction coefficient (or an alternative pressure loss definition) can be successfully included in the Gas Dynamic Methods.

iv) Magnitude of mean flow velocity

The amplitude of velocity oscillation was rightly predicted to remain constant on progression downstream. Further, the predicted value of nozzle discharge coefficient of 0.74, see section 5.4.2.1, was found to cause the correct mean flow velocity.

v) Wave attenuation

Wave attenuation was negligible and was not noticeably reduced by increasing the number of duct model elements from 10 to 40.

Comparison of the 20 Hz rig test case with model predictions was identical with respect to quality of simulation and again attenuation was negligible and not reduced by increasing the number of duct volumes. Note that the quality of both the 14 and 20 Hz simulations was good with the duct model split into just 10 volumes and the time-step set to 2 mS.

Figures 5.15a and b show a direct comparison of model results with the 40 Hz rig test data. Simulation was good with respect to the above criteria i) through iv). However, the simulation was run with a smaller time-step of 1 mS because wave attenuation had become noticeable. Curiously, wave attenuation was not noticeably reduced by increasing the number of duct volumes from 10 to 40.

Figure 5.16 shows a direct comparison of model results with the 80 Hz rig test data. The simulation is poor, particularly with respect to wave attenuation. Increasing the number of duct volumes from 10 to 40 volumes reduced the attenuation, but not sufficiently for the simulation to be physically representative.

The frequency response of the Gas Dynamic Methods thus, for this particular application, had a limit of between 40 and 80 Hz. The wave attenuation was found to be the limiting factor and the size of time-step the most influential in reducing attenuation. Compared to the size of time-step the influence of the length of volumes was found to be weak.

5.4.3 **Simulation of radial flow**

A literature search did not reveal any suitable experimental data with which to verify the equation set extended to predict radial flow. However, its performance was developed and assessed using a simple twin duct model.

5.4.3.1 **Duct model details**

Figure 5.17 illustrates the twin duct model. The front volume comprises an inner and outer volume which represent the inner and outer, concentric, annulus volumes of say the 'intermediate casing' or fan volume of a two-spool engine. Radial flow between the concentric volumes was predicted by the gas dynamic equation set extended to predict radial flow. The inner and outer volume exhausted into identical ducts. Each duct was represented by three volumes where the one-dimensional gas dynamic equation set was solved across each.

Unlike the one-dimensional equation set, the equation set extended to predict radial flow, was not solved using a SBS iterative method. This was because a future work item, section 9.1, identified the possibility of removing the need for the SBS method. The SBS method can be replaced by the equivalent of three Matching Quantities and Variables whilst also maintaining numerical stability. In principal the same can be done for the equation set extended to predict radial flow. Effort was therefore not wasted in developing another SBS method and so an 'off the shelf' non-linear equation solver was used instead. The method was an IMSL computer algorithm based on a Levenberg-Marquard finite difference method, see reference IMSL, 1987.

The model required five boundary conditions, see section 4.3.4. Total temperature and pressure, and zero radial velocity were the upstream conditions and the remaining two were the final nozzle area for each of the two ducts. For a twin duct model two Implicit Matching Method, Variables and Matching Quantities were required. The entry mass flow rate for the inner and outer volumes were defined as Variables, and at each duct exit, the pressure

at 'nozzle' entry was defined as a Matching Quantity pair. However, with the inclusion of Gas Dynamic Methods extra Matching Quantities and Variables were required to maintain numerical stability. A Matching Quantity and Variable in both mass flow rate and total pressure were introduced between each volume, see section 5.3.3.2.

5.4.3.2 **Simulation results**

The purpose of the gas dynamic equation set extended to cater for radial flow, was to allow for the transient change in by-pass ratio during, for example, compressor stall and rapid final nozzle throat area change. Such flow behaviour was approximated by transient control of just one of the model final nozzle throat areas. Prediction of radial mass flow rate was done for both a steady-state and a high-frequency-transient case. The resulting static pressure distribution and commensurate mass flow rates within the concentric volumes, were found to be what was considered as physically representative.

Entry conditions were chosen to be comparable to a large turbofan operating at sea level static conditions. Steady-state total mass flow rate was 84 kg/s and was split equally between the two downstream ducts. Flow Mach number was approximately 0.4 and each final nozzle exhausted to a static pressure of 50 kPa to ensure each were choked, see figure 5.17.

Figure 5.18 shows the static pressure and mass flow rate distribution in the concentric volumes during a 20 % 'smoothed' ramped decrease in the 'outer' nozzle throat area. The ramp was for a period of 50 mS and to allow steady-state flow conditions to prevail, the total simulation time was set at 0.1 S.

Because the 'inner' duct nozzle throat area and the upstream boundary conditions remained unchanged, the mass flow rate through the inner duct nozzle must also remain unchanged. The model predicted this to be the case. However, because the mass flow rate in the outer duct must fall and with it the static pressure in the outer concentric volume rise, there should exist a static radial pressure gradient. This was also predicted, see figure 5.18. The static pressure gradient lead to a radial mass flow rate from the outer to the inner of the concentric volumes, see figure 5.18.

Figure 5.19a shows the static pressure and mass flow rate distribution in the concentric volumes during a sinusoidal variation in the outer nozzle throat area - the amplitude was 10 % and the frequency, 20 Hz. Here, the sinusoidal variation in nozzle throat area generated an expected, commensurate variation in mass flow rate and static pressure in the outer duct. Again the mass flow rate through the inner duct nozzle was shown to remain constant. The radial static pressure gradient therefore varied in sympathy with the static pressure in the outer duct. Variation in radial mass flow rate was therefore shown to be sinusoid in form.

In each of the above test cases the greater proportion of the total change in mass flow rate at entry to the concentric volumes, was accommodated by the outer volume. This was the predicted result because the inner and outer flow areas were set equal; and the steady-state entry mass flow rate of each set equal by using equal nozzle throat areas. However, this was only found to be the case provided the flow area between the concentric volumes was smaller than the volume entry areas. By making the area

between the volumes greater than the entry volumes (this was done by elongating the concentric volumes), the radial static pressure gradient resulted in a higher radial mass flow rate. This in turn resulted in a near equal mass flow rate at entry to the concentric volumes - see figure 5.19b and compare with figure 5.19a. Although it was not possible to verify these predictions they appeared physically representative.

5.5 Summary and discussion of the numerical methods

The gas dynamic equation set is expressed in an implicit form and so solution of a multi-volume model using the RRAP Implicit Matching Method meant that the overall numerical scheme was wholly implicit. However, the frequency response of a numerical scheme is generally thought to be primarily dependent upon the time-step and the maximum length of component volume. The smaller the time-step and length of volume, the less the attenuation of a wave form. Use of 'long' volumes comparable to engine components, and the use of 'large' time-steps by implicit schemes therefore appears to be a drawback. However, it was shown in section 5.4.2.2, for what is an implicit scheme (the RRAP Implicit Matching Method), that of the two, it was the size of time-step that was the most influential in reducing wave attenuation. This is encouraging, because it suggests that a frequency response of even greater than 40 Hz, could be achieved by using a time-step smaller than 1 mS whilst allowing volume lengths comparable to actual engine components. It was not possible to use smaller time-steps due to precision errors, it is recommended that the RRAP system be upgraded to a higher precision capability, see section 9.1.

Simulation of flow disturbances using the gas dynamic equation set was verified for frequencies of at least 40 Hz. There was no apparent frequency corruption, pressure loss and wave superposition prediction was good, and wave propagation velocities were accurate. Wave attenuation was found to be the limiting factor for frequency response and the size of time-step the most influential in reducing attenuation. Compared to the size of time-step the influence of the length of volumes was found to be weak.

The stage was thus set for the development of a whole engine model capable of simulating flow disturbances with frequencies of up to 40 Hz using volume lengths comparable to engine components. However, it must be born in mind that the gas dynamic equation set was only verified for small amplitude pressure disturbances. Although engine performance response during surge and the 'descent' into rotating-stall typically exhibit frequencies of less than 40 Hz, the pressure disturbances are far from small. Further, the occurrence of what are commonly regarded as pressure shock waves cannot be modelled as such, using 'large' volumes. The 'capture' of shock waves requires the size of volume typically adopted by Computational Fluid Dynamic methods - approximately 100 volume lengths per blade chord.

CHAPTER 6

Development of Gas Turbine Pre-Stall High Frequency Simulation Methods using RRAP

6.1 Introduction

Chapter 5 described the inclusion and verification of the gas dynamic equation set into the RRAP system. This chapter describes the application of the equation set to the modelling of pre-stall high-frequency-transients in single and two spool engine models.

The single spool engine model was of the Rolls-Royce Viper Mk 522 turbojet. It was an ideal development vehicle because the Viper is a simple engine and therefore easy to model. The two spool model was typical of a military turbofan. Application to a turbofan was done to further investigate the behaviour of the gas dynamic equation set extended to predict radial flow.

Unfortunately, although there was a prospect of pre-stall verification data becoming available during the project period, it did not materialise. However, pre-stall simulation results are presented and discussed.

6.2 Pre-stall gas turbine simulation methods development

Chapter 5 described how the steady-state performance predicted by a component subroutine was corrected by the gas dynamic subroutine for any high frequency time dependent changes in the flow variables. The inclusion of Gas Dynamic Methods therefore required nothing more than a

call to the gas dynamic subroutine after each call to an engine component performance subroutine, see figure 5.5.

The calculations used by the RRAP system to predict time dependent spool speed and engine component steady-state performance, are summarised below.

6.2.1 Steady-state gas turbine component performance and time dependent spool speed prediction

At each time step, spool speed is predicted before the engine performance calculations are Matched. Once Matched, spool speed is predicted for the next time step and again engine performance Matched. Updated spool speed is the only performance parameter, other than fuel mass flow rate, which is passed forward from one time step to the next.

6.2.1.1 Time dependent spool speed prediction

At each time step the excess power generated by the turbine is calculated. Based on the spool inertia and the rotational speed at the previous time step, the spool speed is then predicted at the end of the next time step. The calculation used is detailed in appendix 6.1a.

6.2.1.2 Intake performance

Although the RRAP system can provide an intake performance subroutine each of the two engine models were run uninstalled and at sea level static conditions. The equivalent of a bell mouth intake was therefore assumed and the total pressure loss assumed negligible.

6.2.1.3 Compressor performance

The compressor operating point is defined by the compressor corrected speed $N/\sqrt{T}$ and a parameter called the compressor 'beta', or β, value. The corrected speed is calculated from the predicted spool speed and the inlet total temperature. The compressor β value is not a performance measure and has no dimension but exists as a range of lines running approximately perpendicular to the corrected speed lines as illustrated by figure 6.1. Defining a compressor operating point in this way ensures a single value of pressure ratio regardless of whether or not the compressor is choked.

A compressor performance characteristic is represented by three graphs. The graphs can be defined in a number of ways but here flow function, enthalpy rise and ideal enthalpy rise are each tabulated with respect to corrected speed and compressor β value, see figure 6.1.

Compressor exit temperature and pressure, and mass flow rate are calculated from the upstream temperature and pressure, and a definition of the operating point using the calculations detailed in appendix 6.1b. Note that the compressor β value is defined as an Implicit Matching Method Variable.

6.2.1.4 Combustor performance

Combustor exit temperature is calculated from an enthalpy balance and the fundamental pressure loss due to heating, by conserving momentum. The pressure loss due to viscous drag is predicted from a user defined factor. The combustion calculation is detailed in appendix 6.1c.

6.2.1.5 **Turbine performance**

Like the compressor β value, the excess power generated by the turbine is an Implicit Matching Method Variable. The power produced by the turbine is then calculated from a compressor/turbine power balance. The enthalpy drop across the turbine and hence the exit temperature are thus defined. The exit pressure is then calculated from a performance characteristic relating the efficiency and enthalpy drop to the corrected speed. The calculations are detailed in appendix 6.1d.

The turbine entry flow function is defined by a performance characteristic relating the flow function to the enthalpy drop and corrected speed. For a Matched performance point, this flow function, and the flow function at exit from the combustor, must be equal. The two flow functions are thus used by the Implicit Matching Method as a Matching Quantity Pair, see appendix 6.1d.

6.2.1.6 **Nozzle performance**

The nozzle is represented by an actuator disc. The nozzle throat area is also specified as a boundary condition and so only a further two flow parameters are required to specify the flow. The chosen two are mass flow rate and temperature at nozzle entry, which together are used to calculate what should be the pressure at entry to the nozzle. For a Matched performance point, the pressure at exit from the jet pipe must equal the pressure calculated at entry to the nozzle. The two pressures are therefore used as a Matching Quantity pair by the Implicit Matching Method. The nozzle performance calculation is detailed in appendix 6.1e.

6.3 Single spool gas turbine model details

The Viper engine is a simple single shaft engine of civil and military application. The compressor is an eight stage axial flow design delivering a design pressure ratio of approximately 5.5 at 13,760 RPM.

In the interests of keeping engine model complexity to a minimum, heat transfer between the working fluid and engine casing was not accounted for, and the secondary air cooling system was not modelled. Also excluded were duct pressure losses and any 'customer' air bleed.

Figure 6.2 is a schematic illustration of the engine model. The three boundary conditions were upstream total pressure and temperature and the final nozzle throat area. The Implicit Matching Method Variables were the compressor β, value and the turbine excess power. The Matching Quantity Pairs were the flow function at entry to the turbine and the total pressure at entry to the nozzle.

Simulation of gas dynamic behaviour of the engine working fluid was done by calling the gas dynamic subroutine after each call to an engine component performance subroutine. The compressor, combustor, and turbine were therefore each represented by a single volume. The geometric dimensions of the volumes were based on actual engine dimensions. The jet pipe duct was split into three volumes to ensure that the length of each was comparable to the other volumes. This was done to ensure that the high frequency response of the model was not compromised. Numerical stability was achieved by including a Variable and Matching Quantity Pair in mass flow rate and pressure between each adjoining component volume, see section 5.3.3.2.

6.4 Single spool gas turbine simulation results

Two examples of high-frequency-transient behaviour are presented below to illustrate the pre-stall whole engine modelling capability. The RRAP Viper model illustrated in figure 6.2 was used for each example. The engine steady-state running condition was 100 % speed at sea level static conditions.

1) The behaviour of the compressor operating point subject to time variant planar waves in pressure and temperature at engine inlet was simulated. Such inlet distortion is typical of that due to hot-gas-reingestion, armament firing and extreme aircraft manoeuvres etc.

A time variant, planar, sinusoidal variation in inlet total pressure accompanied by a corresponding isentropic change in total temperature was set as an upstream boundary condition. The total pressure variation had an amplitude of 9 % and a frequency of 20 Hz. Figure 6.3 illustrates the behaviour of the compressor operating point. Trajectory A was generated without the Gas Dynamic Methods and therefore represents nothing more than a series of steady-state performance solutions. Trajectory B shows the compressor operating point generated by including the Gas Dynamic Methods. This example served to illustrate how the dramatic loss in surge margin caused by a rapid drop in inlet total pressure can be simulated by the inclusion of the Gas Dynamic Methods.

The change in corrected speed for each trajectory was comparable because the variation in mechanical spool speed was negligible, and therefore was essentially governed by inlet total temperature. However, the contrast in the

prediction of pressure ratio was marked. This was due to the Gas Dynamic Methods correcting for the temporary accumulation of mass, momentum and energy within the compressor volume.

When a compressor experiences an increase in pressure at its face the instantaneous pressure ratio will drop because the rear of the compressor will not 'see' the equivalent rise before a finite time. This is due to the temporary accumulation of mass, momentum and energy within the compressor volume. Thus, if a compressor face is subject to a sinusoidal variation in inlet total pressure, the pressure ratio will rise and fall in sympathy.

The trajectory of the compressor operating point in figure 6.3 was looped due to the superposition of the pressure ratio and corrected speed excursions.

2) The high-frequency-transient response of the engine to a rapid over-fuelling was simulated.

A simulation of the transient behaviour influenced by both the Gas Dynamic Methods and spool inertia was done by subjecting the Viper model to a 35 % increase in fuel flow rate. The fuel flow increase followed a linear ramp of duration 0.1 S. Figure 6.4 illustrates the resulting compressor operating point trajectory.

Trajectory A was generated without the Gas Dynamic Methods and therefore represents nothing more than a series of steady-state performance solutions. Trajectory B, generated by including the Gas Dynamic Methods, illustrated an apparent lag in the compressor delivery pressure for a given rotor speed. This in turn, resulted

in a greater surge margin, for a given rotor speed, during the over-fuel phase of the transient. Note that the inlet planar wave transient simulation above, where the inclusion of the Gas Dynamic Methods predicted a greater loss in surge margin during the transient, was contrary to the over-fuel case.

The difference in the two trajectories of figure 6.4 can be explained by considering engine performance during an over-fuelling transient. During over-fuelling the combustor exit temperature initially rises in unison with the the fuel flow rate and, with the air flow at entry to the turbine choked, causes a corresponding increase in total pressure and decrease in mass flow rate at turbine entry. It is this increase in flow pressure, combined with the sluggish response of the spool speed, that causes the compressor pressure ratio to rise rapidly with a consequent loss in surge margin. It is here that the simulations with, and without, the Gas Dynamic Methods differ. For the steady-state calculation, an increase in pressure at the turbine entry would necessarily cause an instantaneous increase in the compressor delivery pressure. However, with the inclusion of the Gas Dynamic Methods, the rise in compressor delivery pressure lagged, with respect to time, that at turbine entry. Thus, for a given spool speed during the over-fuel phase of the transient, the Gas Dynamic Methods predicted a lower pressure ratio and consequently a larger surge margin.

Following the fuel transient the spool continues to accelerate for some time. Due to the high inertia of the spool, the acceleration is too slow for the Gas Dynamic Methods to influence the performance of the engine, see figure 6.4.

6.5 Two spool gas turbine model details

In the interests of keeping model complexity to a minimum, heat transfer between the working fluid and engine casing was not accounted for, and the secondary air cooling system was not modelled. Also excluded were duct pressure losses and any 'customer' air bleed.

Figure 6.5 is a schematic illustration of the two spool engine model. Again, in the interests of keeping model complexity to a minimum the core and by-pass flows were not mixed nor was the reheat system included. The core and by-pass flows exhausted through separate nozzles.

Fan performance was split into an inner and an outer performance characteristic, each defined with respect to the total inlet flow and not as a function of by-pass ratio. The fan was therefore represented by an inner and outer volume between which flow could not move radially. Radial movement of the 'splitter streamline' due to variation in by-pass ratio, was therefore approximated by allowing radial flow within the intermediate casing only. Inner and outer fan performance was thus assumed to be independent of the radial position of the 'splitter streamline'.

The boundary conditions were the same as the Viper, but two extra were required to enable the calculation of radial flow. These were zero upstream radial velocity and by-pass duct exit throat area.

The Implicit Matching Method Variables were the fan and compressor β values and the low and high pressure turbine excess powers. The Matching Quantity pairs were the turbine entry flow functions and the total pressure at each nozzle entry.

Again, inclusion of Gas Dynamic Methods was achieved by calling the gas dynamic subroutine after each call to an engine component performance subroutine. The inner and outer fan, compressor, combustor, and turbines were therefore each represented by a single volume. The geometric dimensions of the volumes were based on actual engine dimensions. The jet pipe and by-pass duct were each split into five volumes to ensure that the length of each was comparable to the other volumes. This was done to ensure that the high frequency response of the model was not compromised. Numerical stability was achieved by including a Variable and Matching Quantity Pair in mass flow rate and pressure between each adjoining component volume, see section 5.3.3.2.

6.6 Two spool gas turbine simulation results

The turbofan model was written to exercise and assess the gas dynamic equation set extended to predict radial flow. Radial flow was predicted in the intermediate casing only and not in the fan. This was because the fan performance characteristic was only available as a function of total inlet flow and not with respect to by-pass ratio, and so prediction of radial flow within the fan would have compromised its use.

The prediction of transient radial flow was assessed by studying engine response to a simulated reheat mislight. This was done by momentarily reducing the throat areas of the by-pass and jet pipe nozzles simultaneously. This had the effect of introducing an over pressure 'blip'. The throat areas were reduced by 15 %, and returned to their original value over a period of 20 mS. The throat

area/time profile was a 'smoothed' half sinusoid and the engine steady-state running condition was 100 % speed at sea level static conditions.

Figures 6.6a and b, show a rise in pressure at exit to the outer concentric volume commensurate with the reduction in by-pass nozzle throat area. The pressure rise within the jet pipe volume due to the reduction in its nozzle throat area, was not felt upstream due to the choked turbine entry planes. However, because the equation set extended to predict radial flow, allowed pressure communication between the inner and outer volumes, the high pressure compressor inlet face 'felt' a rise in pressure in sympathy with that at entry to the by-pass duct. The compressor pressure ratio, therefore momentarily fell. Because any spool speed change was insignificant and the compressor was operating on a near vertical portion of its performance characteristic, its mass flow rate rose with the falling pressure ratio, see figure 6.6b. It was this momentary rise in mass flow rate in the engine core that necessarily caused the jet pipe volume pressure to rise proportionately more than that in the by-pass duct, see figure 6.6a.

The pressure at the by-pass duct entry, was therefore alone in its influence on the pressure ratio of the inner and outer fan. Both were correctly predicted to rise, again illustrating that the equation set allowed pressure communication between the inner and outer volumes, figure 6.6a. The momentary radial static pressure gradient between the concentric volumes caused flow to move into the inner concentric volume. The by-pass ratio was therefore correctly predicted to fall, see figure 6.6b, thereby simulating a momentary outward movement of the 'splitter streamline'.

6.7 Discussion of results

Application of the one-dimensional gas dynamic equation set to the prediction of pre-stall high-frequency-transients, although not verified, generated what were considered as physically representative results. Prediction of compressor operating point excursions, during inlet planar wave distortion, served to illustrate the dramatic loss in stall margin that can be caused by the temporary accumulation of mass, momentum and energy within the compressor volume. Even during relatively slow transients such as an over-fuelling, the accumulation of flow mass etc, within the engine volumes, lead to a distinguishable change in stall margin prediction.

Application of the equation set extended to predict radial flow, to the prediction of radial flow in the intermediate casing of the turbofan model, although not verified, again generated what were considered as physically representative results. Prediction of the pressure distribution and mass flow rates within the concentric volumes were shown to be representative. However, the predicted rise in fan inner and outer pressure ratio during the simulated reheat mislight, had to be regarded with care, especially with respect to the loss in stall margin. This was because the fan inner and outer mass flow rates were calculated assuming no radial flow within the fan volume. Thus the predicted change in the inner and outer mass flow rates was probably too great as some flow would have undoubtedly moved radially within the fan. The predicted fan operating point excursions and therefore stall margin loss, may not have been representative.

Although the equation set can be readily applied to a fan volume, performance characteristics are conventionally generated with respect to total inlet flow and not inner and outer flows (or by-pass ratio); the characteristics were therefore incompatible with the equation set. Prediction of fan operating point excursions has therefore been identified as an area of future work. Both test data and appropriate fan performance characteristics will be required before modelling progress can be made, see chapter 9.2.

CHAPTER 7

Development of Gas Turbine Post-Stall High Frequency Simulation Methods Development within RRAP

7.1 Introduction

The surge cycle of a compressor in a gas turbine engine has a frequency of approximately 15 Hz and the engine performance response during descent into rotating-stall, can exhibit frequencies of up to approximately 40 Hz. Whole engine post-stall simulation therefore required the inclusion of Gas Dynamic Methods. The Post-stall simulation methods were developed by extending the above pre-stall simulation methods described in chapter 6, see also Merriman, 1993.

Post-stall simulation required the inclusion of post-stall compressor and combustor performance modelling methods. Like pre-stall, post-stall performance characteristics were used to predict compressor performance. A complete post-stall compressor characteristic was used to define performance during rotating-stall and reverse flow. A definition of the reverse flow characteristic was required to cater for the possible occurrence of compressor reverse flow during a 'deep' or 'violent' surge. Like pre-stall, the post-stall characteristics were also in a steady-state form. Again, the generation of true transient characteristics would be peculiar to a particular stall incident and therefore inappropriate for use in a generic model. However, unlike pre-stall, compressor post-stall performance could not be predicted directly from the characteristic but had to be modified to take into account the finite time required for the development of rotating-stall cells.

Surge and, up to a point, rotating-stall each generate unsteady combustion phenomena which strongly influence the nature of gas turbine post-stall behaviour. Post-stall transients can cause extremely low, and even reverse flow at combustor entry. Such conditions can influence flame stability and therefore engine operability. It was therefore essential to model combustor performance and flame stability at these extreme flow conditions if post-stall engine operability was to be predicted.

Section 7.2 details the compressor and combustor post-stall performance modelling methods. The methods were developed using the RRAP Viper engine model described in chapter 6. Again, like the development of pre-stall high-frequency-transient modelling, the Viper was chosen for its simplicity. Secondly, Rolls-Royce has recently completed some post-stall engine testing using the Viper. These test data, which included surge and descent into rotating-stall, were made available for verification. Section 7.3 details the post-stall simulation results and illustrates that they compared favourably with the test data. The post-stall modelling methods are discussed in section 7.4.

7.2 Post-Stall Simulation Methods Development

Section 7.2 is split into four subsections. The first two describe the generation of post-stall compressor performance characteristics and how compressor performance was predicted from them. The third section describes the changes in model boundary conditions required during conditions of reverse flow at the engine intake entry plane; and the final subsection details the development of

an all new combustor model which was capable of simulating combustor performance during post-stall events.

7.2.1 Compressor Post-Stall Performance Characteristics

Like pre-stall simulation, the compressor post-stall Component Performance Terms F_{nx}, and $\dot{S}_v$, were indirectly calculated from a steady-state performance characteristic. This was in keeping with the assumption described in section 4.3.3 which states that the high-frequency-transient performance of any engine component is equal to its instantaneous steady-state performance. Compressor post-stall performance was therefore based on steady-state rotating-stall and reverse flow performance characteristics.

7.2.1.1 Rotating-stall

Rotating-stall performance was predicted from an overall steady-state characteristic. Although the overall performance of the compressor can be regarded as steady, the internal rotating-stall flow structure is far from steady. The characteristic therefore represents the time averaged annulus flow conditions. Theoretical prediction of what is a complex three dimensional flow structure was beyond the scope of this work and so rotating-stall performance characteristics were based on a collection of experimental data.

Gamache, 1985, presents detailed performance characteristics of the rotating-stall performance of a three stage axial flow compressor. Although the compressor was the final three stages of the Pratt and Whitney JT9 compressor it was operating at low speed

producing a maximum pre-stall pressure ratio of approximately 1.08. Experimental data was presented as pressure and torque coefficient against flow coefficient at three different speeds.

The data were converted to compressible form in order to deduce performance trends that could be applied to a high speed compressor. Figure 7.1a shows the pressure ratio and isentropic efficiency plotted against entry flow function for each speed. Figure 7.1b illustrates the corresponding performance characteristic in terms of ideal and actual enthalpy rise. The following observations were made,

i) For a given speed, Figure 7.1a illustrates that an increase in flow is accompanied by an increase in pressure ratio. Apart from the small dependency of the ratio of specific heats of air on temperature, the ideal enthalpy is seen to vary with the pressure ratio, see figure 7.1b. This trend is thought to be due to the stall cell reducing in both axial and circumferential extent because of the increasing flow. The number of blades operating in normal conditions therefore increases and so a higher pressure ratio is generated. Commensurate with the decreasing stall cell size is a decrease in exit temperature and enthalpy rise, see figure 7.1b. Predictably the efficiency is seen to rise with the decreasing size of stall cell commensurate with increasing flow, see figure 7.1a.

ii) If flow is kept constant the pressure ratio rises with increasing rotational speed. This is thought to be because, although the stall cell will grow in order to maintain the same flow, the fewer blades that operate under normal conditions manage to

generate a greater pressure rise due to their increased speed. Commensurate with the increasing stall cell size is increasing enthalpy rise and decreasing efficiency, see figure 7.1b.

iii) At zero flow conditions the enthalpy rise shown in figure 7.1b shows a marked peak. This is due to the compressor continually doing work on the same mass of air. The magnitude of the enthalpy rise is not compressor performance dependent but dictated by the rate of steady-state heat flow from the compressor rig.

iv) Figures 7.1a and 7.1b also illustrate what has long been recognised as a performance discontinuity between the rotating-stall flow structure and the essentially axisymmetric flow structure of reverse flow. However, Gamache, 1985, discovered that a rotating-stall flow structure could actually accommodate a net reverse flow. Further, hysteresis was not exhibited by the flow at the discontinuity point.

Small and Lewis, 1985, presented a rotating-stall and reverse flow performance characteristic of the same compressor used by Gamache, 1985. Unlike Gamache, the compressor was run at high speed generating a maximum pressure ratio of approximately 1.7. Unfortunately the characteristic is of only one, unspecified, speed but it did allow the comparison of performance trends at low and higher speeds. Performance data at near zero flow was also omitted. Figures 7.2 a and b, show the variation in efficiency, pressure ratio and enthalpy rise, respectively with entry flow function.

Comparison of the experimental results of Gamache, 1985, and Small and Lewis, 1985, illustrated that the steady-state rotating-stall performance trends for what was a three stage compressor, were consistent across the speed range. Further the rotating-stall performance characteristics presented by Turner and Sparkes, 1964, for a single stage fan were not inconsistent.

Steady-state rotating-stall performance characteristics were derived by scaling data from the above analysis.

7.2.1.2 **Reverse Flow**

Both Gamache, 1985, and Small and Lewis, 1985, measured the steady-state reverse flow performance characteristic as well as the rotating-stall characteristic. In each case the data were generated by blowing air backwards through the test compressor while the blades rotated in the normal sense. The published data were converted into enthalpy and ideal enthalpy rise; and like forward flow, the flow function and the temperature used to calculate the corrected speed, were taken at compressor entry. The data was analysed in this format to ensure subsequent compatibility with the RRAP system. The calculation procedure used to convert the performance data is presented in appendix 7.1 and the characteristics produced shown in figures 7.1 and 7.2. Note that under reverse flow conditions the conventional definition of efficiency is inappropriate and so an alternative 'reverse flow performance parameter', θ, was created - this is also defined in appendix 7.1.

Gamache, 1985, deduced by inter-blade measurement that the flow structure during overall steady-state flow conditions

was essentially axisymmetric. Stall cells were not found; and like Small and Lewis, 1985, and Turner and Sparkes, 1964, the compressor was found to perform in a similar way to an aerodynamic throttle. Figure 7.1a shows the characteristic in the pressure ratio and flow function plane as near parabolic. Predictably, for a given flow function, the resistance to the flow can be seen to be greater the higher the rotational speed.

Like forward flow, the compressor will absorb power during reverse flow conditions. The temperature at compressor entry is therefore higher than at exit and contrary to forward flow conditions. Note that the enthalpy change is still defined as positive as illustrated by figure 7.1b. Also shown is that the enthalpy rise, and therefore the power absorbed, increases with rotational speed at a given flow. This is due to the increasing heating effect of blade windage.

Comparison of the experimental results of Gamache, 1985, and Small and Lewis, 1985, illustrated that the steady-state reverse flow performance trends for what was a three stage compressor, were consistent across the speed range. Further the reverse flow performance characteristics presented by Turner and Sparkes, 1964, for a single stage fan were not inconsistent.

Steady-state reverse flow performance characteristics were derived by scaling data from the above analysis.

7.2.2 Compressor Performance Prediction

7.2.2.1 Stall Line

The point of irretrievable breakdown of the compressor flow structure was not theoretically calculated but

determined by superimposing an experimentally derived stall-line over the pre-stall characteristic. Such a stall-line is steady-state because it is generated on a rig by steadily increasing pressure ratio, at a given speed, until inception occurs and stall ensues. However, up to a point the stall inception process is retrievable. In the operating environment, it is possible that the destabilising influence can diminish sufficiently quickly that, although the stall inception process may have begun, it may not have reached the point of no return and so the compressor will not stall. The transient stall-line is therefore not coincident with the steady-state line. However, the difference between the two is very small and so it was assumed that the transient stall-line was coincident with the steady-state line. At each calculation step a check was performed to see whether the stability margin (or surge margin) had fallen below zero, and if so, the post-stall performance characteristic was used for the subsequent calculation step.

7.2.2.2 **Forward Flow**

Like pre-stall, the post-stall characteristic, described above in section 7.2.1, was steady-state and therefore consistent with the calculation of the Component Performance Terms described in section 4.3.3. However, direct use of the characteristic will lead to poor post-stall transient simulation because account must be taken of the finite time required for stall cell development. This is defined as the time taken from the point of no return to the time for the initial stall cells to have grown and merged to form a single cell at the rear of the compressor.

Davis, 1987, Greitzer, 1975 (a) and O'Brien, 1992, each account for the time taken for the full development of rotating-stall by introducing a first order lag. The lag was applied to the net axial force F_{nx}, exerted by the compressor which was determined from the post-stall characteristic. Steenken, 1986, and other papers produced by General Electric do not allude to the inclusion of a lag or of an alternative method.

Here, the time required for stall cell development was taken into account by introducing a first order lag to the calculation of both of the compressor Component Performance Terms F_{nx}, and $\dot{S}_v$. Application of a lag to the production of entropy term $\dot{S}_v$, which the above models did not include, accounted for the time dependent drop in compressor efficiency. In the interests of keeping model complexity to a minimum compressor bleeds were not included. However, if an engine model included a control system, a bleed lag might well be appropriate.

The first order lags applied to the net axial force F_{nx}, and entropy production term $\dot{S}_v$, took the form,

$$F^*_{nx,t+\Delta t}\ (\text{Lagged}) = F^*_{nx,t+\Delta t} + (F_{nx,t} - F^*_{nx,t+\Delta t})\ e^{-\left[\frac{\Delta t}{\tau}\right]}$$

$$\dot{S}^*_{v,t+\Delta t}\ (\text{Lagged}) = \dot{S}^*_{v,t+\Delta t} + (\dot{S}_{v,t} - \dot{S}^*_{v,t+\Delta t})\ e^{-\left[\frac{\Delta t}{\tau}\right]}$$

where * denotes a steady-state value determined from the post-stall characteristic.

Note that experimental data presented by Freeman and Wilson, 1993, show that regardless of whether rotating-stall or surge develop they each begin with the merging of stall cells to form a single cell at the rear of the compressor. The inclusion of the first order lag where the time constant τ, is representative of the stall cell development time is therefore common to the modelling of each. For a given time constant, it is the influence of the Gas Dynamic Methods and the geometry of the compression system and combustor, that dictate whether cyclic surge or rotating-stall occur.

Greitzer, 1975 (a), references experimental rotating-stall data produced by a Pratt and Whitney Aircraft three stage compressor. The results show that regardless of compressor speed, it took approximately eight rotor revolutions to reach fully developed rotating-stall from the first noted occurrence of stall cells. However, this is not an indication of the stall cell development time but actually comprises the following,

1) the onset of stall cell development up to the point of irretrievable flow breakdown - this is regarded as stall inception

2) the development and merging of stall cells to form one cell at the rear of the compressor - this is regarded as the stall cell development time

3) the sudden drop in flow and pressure rise brought about by the development of rotating-stall causes unsteady flow inertia effects which take time to settle - this is regarded as the settling time which runs concurrently with, but outlasts the cell development time

Freeman and Wilson, 1993, present experimental data of stall cell growth in the eight stage axial flow compressor of a single spool military turbojet, the Rolls-Royce Viper. Axial development of rotating-stall cells and their merging to form a single cell at the rear of the compressor is illustrated at 60, 78, 82 and 100% engine speed. From the results presented it is possible to deduce that the stall cell development time at each speed was approximately one rotor revolution. This experimental evidence was used as a basis for determining the representative stall cell development time τ, in the above first order lag equations.

7.2.2.3 **Reverse Flow**

During a deep surge a compressor may spend part of the cycle in a state of reverse flow. Here, there are no rotating-stall cells and the flow is essentially axisymmetric. During reverse flow there was therefore no need to model stall cell development time and so the above first order lags were omitted from the calculation.

The steady-state compressor performance calculation, described in appendix 6.1b, which precedes the Gas Dynamic Methods calculation, is not valid during reverse flow. The calculation procedure had to be modified and is detailed in appendix 7.2.

7.2.2.4 **Stall Recovery**

The point of compressor recovery form post-stall operation was defined by a 'recovery line' superimposed over the rotating-stall characteristic. Like the rotating-stall characteristic it was derived by scaling experimental rig data.

At each calculation step a check was performed to see whether the operating point had crossed the recovery line, and if so, the pre-stall performance characteristic was used for the subsequent calculation step.

7.2.3 **Reverse Flow Boundary Conditions**

The boundary conditions used for normal flow conditions were described in sections 4.3.4 and 6.3 and are, for a single-spool engine, upstream total temperature and pressure and final nozzle area. However, during deep surge compressor flow can reverse in direction which poses a model boundary condition problem. Although the reversing flow can be considered to exhaust to ambient static pressure, the upstream total temperature condition was no longer valid.

An alternative boundary condition appropriate to reverse flow, was the combustion temperature. To a first approximation under reverse flow conditions, flow can be considered to emanate from the flame tube volume both forwards through the turbine and rearwards through the compressor. The combustion temperature could therefore be used as a boundary condition.

At each post-stall Matched point a prediction was made of the combustion temperature at the end of the next time step. If reverse flow occurred at the next time step the already calculated combustion temperature was used as a boundary condition. The method used to predict the combustion temperature is described below in section 7.2.4.1. Final nozzle area and reversed flow exhausting to compressor inlet ambient static pressure, were the remaining boundary conditions.

Under conditions of reverse flow the Engine Routine matching scheme was changed to allow the compressor entry temperature to rise accordingly. The compressor entry temperature was defined as an Implicit Matching Method Variable and the calculated combustor exit temperature set as a Matching Quantity. The required value, or other half of the Matching Quantity, was set equal to the predicted combustor temperature described above.

7.2.4 **Combustor Performance Prediction**

During surge, and sometimes rotating-stall, the combustion steady-state performance calculation described in appendix 6.1c breaks down. This is because the mass flow rate of air entering the combustor can be very low or even reverse in direction. These severe flow conditions cannot be accounted for in the steady-state energy balance, nor in the calculation of the fundamental pressure loss due to heating. Also, the conventional definition of fuel-to-air ratio becomes ill defined.

An alternative approach was to break away from steady flow calculations and evaluate instead the instantaneous mass of 'burnt' and 'unburnt' air contained in the combustor at the end of each calculation time step. This allowed the fuel-to-air ratio (FAR), and combustion temperature to be calculated regardless of the combustor entry flow condition.

7.2.4.1 **Prediction of Combustion Temperature**

Figure 7.3a is a schematic section view of a conventional annular combustion chamber illustrating the 'hot' flame

tube volume and the surrounding 'cold' volume. The combustor model which is shown in Figure 7.3b, was represented by a 'cold' and a 'hot' volume in series. This was necessary because the Gas Dynamic Methods cannot model the complex internal flows that exist along the length of the hot volume casing.

The combustion temperature was calculated from an enthalpy balance based on the mass of fuel burnt, and on the mass of flow that entered and left the combustor hot volume during a time step.

The value of absolute enthalpy entering the volume during a single time step was given by,

$$\Delta t W_i H_i$$

similarly the the absolute value of enthalpy leaving the combustor volume was given by,

$$\Delta t W_{i+1} H_{i+1}$$

and the absolute enthalpy added to the combustor gases by the combustion of fuel was given by,

$$\Delta t W_f \eta_{cb} H_f$$

It was assumed that the combustor gases within the hot volume were fully mixed at the beginning and end of each time step and so T_{i+1} was set equal to the combustion

temperature. The enthalpy balance thus took the form,

$$\Delta t(W_i H_i)_{t+\Delta t} - \Delta t(W_{i+1} H_{i+1})_{t+\Delta t} + \Delta t H_f (W_f \eta_{cb})_{t+\Delta t}$$

$$+ (me)_{v,t} = (me)_{v,t+\Delta t}$$

where e, is the specific internal energy of the gases.

The exit mass flow rate was a steady-state value and calculated from,

$$W_{i+1,t+\Delta t} = W_{i,t+\Delta t} + W_{f,t+\Delta t}$$

This ensured that the combustor temperature was also a steady-state value and therefore compatible with the Gas Dynamic Methods. Similarly the mass of gas contained by the hot volume at time t + Δt, was also a steady-state value.

$$m_{v,t+\Delta t} = m_{v,t}$$

The enthalpy balance was made more amenable to solution by relating the specific internal energy e, to enthalpy by using the thermodynamic relationship,

$$C_p - C_v = R$$

Again by assuming the combustion temperature to be equal

to T_{i+1}, the internal energy of the combustor gases was given by,

$$e_v = H_{i+1} - T_{i+1}R$$

The enthalpy balance thus took the final form,

$$H_{i+1,t+\Delta t}(\Delta t W_{i+1,t+\Delta t} + m_{v,t}) - Rm_{v,t}T_{i+1,t+\Delta t} = \Delta t(W_i H_i)_{t+\Delta t}$$

$$+ \Delta t(W_f \eta_{cb})_{t+\Delta t} H_f - Rm_{v,t}T_{i+1,t} + m_{v,t}H_{i+1,t}$$

The occurrence of reverse flow at combustor entry was catered for by assuming the entry temperature to be equal to the combustion temperature. The enthalpy balance thus took the form,

$$H_{i+1,t+\Delta t}(m_{v,t} + \Delta t(W_{i+1} - W_i)_{t+\Delta t}) - m_{v,t}RT_{i+1,t+\Delta t} =$$

$$\Delta t(W_f \eta_{cb})_{t+\Delta t} H_f + H_{i+1,t}m_{v,t} - m_{v,t}RT_{i+1,t}$$

For a given FAR and combustion burning efficiency η_{cb}, the combustion temperature T_{i+1} was calculated by an iterative procedure. This was necessary because Cp was evaluated as a function of both temperature and FAR. The specific total enthalpy was given by,

$$H = C_p T$$

The combustion temperature at time t + 2Δt was predicted at time t + Δt in case its value had to be used as a boundary condition during compressor reverse flow, see section 7.2.3. For forward flow at combustor entry the combustor temperature at time t + 2Δt was predicted from the the following enthalpy balance,

$$H_{i+1,t+2\Delta t}(\Delta t W_{i+1,t+\Delta t} + m_{v,t+\Delta t}) - Rm_{v,t+\Delta t} T_{i+1,t+2\Delta t} =$$

$$\Delta t(W_i H_i)_{t+\Delta t} + \Delta t H_f(\eta_{cb})_{t+\Delta t} W_{f,t+2\Delta t} - Rm_{v,t+\Delta t} T_{i,t+\Delta t}$$

$$+ m_{v,t+\Delta t} H_{i+1,t+\Delta t}$$

and for reverse flow at combustor entry the combustion temperature was predicted from the following enthalpy balance,

$$H_{i+1,t+2\Delta t}(m_{v,t+\Delta t} + \Delta t(W_{i+1} + W_i)_{t+\Delta t}$$

$$- m_{v,t+\Delta t} RT_{i+1,t+2\Delta t} = \Delta t \eta_{cb,t+\Delta t} H_f W_{f,t+2\Delta t}$$

$$+ H_{i+1,t+\Delta t}\, m_{v,t+\Delta t} - m_{v,t+\Delta t}\, RT_{i+1,t+\Delta t}$$

7.2.4.2 Prediction of fuel-to-air ratio (FAR)

The conventional definition of FAR is ill defined during the low mass flow rates which can occur at combustor entry during post-stall transients. Two different FAR's were required and are defined below,

i) The effective fuel-to-air ratio, FAR_e,

At a given point in time, the effective FAR_e, was the ratio of the mass of fuel required to generate the combustion products present, to the mass of air contained in the combustor volume. The mass of air does not include the 'excess' nitrogen left by the combustion of oxygen. This approximation was necessary to calculate the specific heat Cp, of the combusted mixture. Specific heat was only defined for a air and combustion product mixture only, where account was not taken for the presence of any unburnt fuel. The effective FAR was given by,

$$FAR_e = \left[\frac{\text{mass of fuel required to generate the combustion products present at time t}}{\text{mass of 'unburnt' air present at time t}} \right]$$

ii) The actual fuel-to-air ratio, FAR_a,

At a given point in time the actual fuel air ratio was defined to take into account the presence of any

unburnt fuel by specifying the combustion burning efficiency. The actual FAR was related to the effective FAR by,

$$FAR_a = \frac{FAR_e}{\eta_{cb}}$$

Where η_{cb}, is the combustor burning efficiency. Here the conventional definition was used which is given by the ratio of the ideal quantity of fuel, to actual quantity of fuel, required to generate a given temperature rise.

$$\eta_{cb} = \frac{\text{ideal fuel flow rate}}{\text{actual fuel flow rate}}$$

In order to calculate the effective FAR an assumption had to be made relating the quantity of combustion products with the fuel burnt and oxygen consumed. The chemical process was taken to be the complete oxidation of kerosene fuel giving carbon dioxide and water. This chemical reaction was used to calculate the relative proportions by mass, of the combustion products with the fuel burnt. The relative proportions are defined and evaluated in appendix 7.3.

The mass of fuel required to generate the combustion products present at a given time was given by,

$$K_2 m_{cp}$$

Where K_2, is the mass fraction of fuel per unit mass of combustion products, and m_{cp}, is the mass of combustion products. Note that the mass of any unburnt fuel is therefore not included.

The mass of 'unburnt' air was given by,

$$\frac{m_{ox}}{K_4}$$

Where K_4, is the mass fraction of oxygen gas in standard air, see appendix 7.4, and m_{ox}, is the mass of oxygen gas.

The effective FAR was thus given by,

$$FAR_e = K_2 K_4 \left[\frac{m_{cp}}{m_{ox}} \right]$$

and the actual FAR given by,

$$FAR_a = \frac{K_2 K_4}{\eta_{cb}} \left[\frac{m_{cp}}{m_{ox}} \right]$$

The calculation of FAR was thus reduced to predicting the mass of combustion products and gaseous oxygen. These two unknowns were reduced to one by expressing each in terms of a known quantity which was the total mass of gas in the combustor. This relationship was derived by conserving

mass and invoking the chemical mass fractions evaluated in appendix 7.3. The relationship is derived in appendix 7.5 and takes the form,

$$m_{cp} = \frac{m_v - \left[\frac{m_{ox}}{K_4}\right]}{\left[\frac{K_3(1-K_4) + 1}{K_4}\right]}$$

The total mass of gases in the combustor was predicted from the volume averaged density approximated by the Gas Dynamic Methods; and so knowing the combustor volume the mass of contained gas was calculated.

$$m_v = \bar{\rho}_v \, V_{cb}$$

It therefore remained to predict the mass of oxygen to calculate the effective FAR and also the burning efficiency η_{cb}, to calculate the actual FAR.

For each time step the mass of oxygen was approximated by conserving the mass of oxygen consumed by the combustion of fuel, and the mass of oxygen entering and leaving the combustor. The mass of oxygen entering the combustor during a time step was given by,

$$A = K_4 W_{i,t+\Delta t} \cdot \Delta t$$

The mass of oxygen leaving the combustor was assumed proportional to the mass flow rate of gas leaving, and on the mass fraction of gaseous oxygen contained in the combustor. The constant of proportionality was termed the 'mixing constant' and assumed constant regardless of the combustor operating condition. The mass of oxygen leaving the combustor was given by,

$$B = \Delta t \frac{\theta}{2} \left[\frac{m_{ox,t}}{m_{v,t}} + \frac{m_{ox,t+\Delta t}}{m_{v,t+\Delta t}} \right] W_{i+1,t+\Delta t}$$

where θ, is the mixing constant. Note that numerical stability was improved by averaging the mass fraction of oxygen with respect to time.

Note also that here the exit mass flow rate was the transient value predicted by the Gas Dynamic Methods at time $t + \Delta t$. This was found to give more realistic results during rapid changes in flow conditions.

If reverse flow occurred at combustor entry the mass of oxygen leaving from the front of the combustor was taken to be,

$$\Delta t \frac{\theta}{2} \left[\frac{m_{ox,t}}{m_{v,t}} + \frac{m_{ox,t+\Delta t}}{m_{v,t+\Delta t}} \right] W_{i,t+\Delta t}$$

The mass of oxygen consumed by the combustion of fuel was given by,

$$C = \Delta t K_1 (W_f \eta_{cb})_{t+\Delta t}$$

where K_1, is the mass fraction of oxygen consumed per unit mass of fuel combusted.

By conserving the mass of oxygen, the mass of oxygen present at the end of a time step was approximated from,

$$m_{ox,t+\Delta t} = m_{ox,t} + A - B - C$$

and by rearranging, the mass of oxygen, $m_{ox,t+\Delta t}$, under forward flow conditions was approximated by,

$$m_{ox,t+\Delta t} =$$

$$\frac{m_{ox,t} + \Delta t K_4 W_{i,t+\Delta t} - \left[\dfrac{\theta \Delta t m_{ox,t} W_{i+1,t+\Delta t}}{2m_{v,t}} \right] - \Delta t K_1 (W_f \eta_{cb})_{t+\Delta t}}{\left[1 + \dfrac{\theta \Delta t W_{i+1,t\Delta t}}{2m_{v,t+\Delta t}} \right]}$$

Similarly, the mass of oxygen, $m_{ox,t+\Delta t}$, under reverse flow conditions was approximated by,

$$m_{ox,t+\Delta t} =$$

$$\frac{m_{ox,t} + \left[\frac{\theta \Delta t \, m_{ox,t+\Delta t}[W_i - W_{i+1}]_{t+\Delta t}}{2m_{v,t}} \right] - \Delta t K_1 (W_f \eta_{cb})_{t+\Delta t}}{\left[1 - \frac{\theta \Delta t [W_i - W_{i+1}]_{t+\Delta t}}{2m_{v,t+\Delta t}} \right]}$$

The mixing constant θ, and an initial value of the mass of oxygen were calculated by calibration against the combustor performance model of section 6.2.1.4.

7.2.4.3 **Combustor 'blow-out' and re-ignition**

For a given combustion chamber and flow condition there is a rich and weak limit of the FAR beyond which the flame is unstable and will extinguish. However, flame stability is also dependent on air flow rate, temperature and pressure.

Flame stability will deteriorate as flow velocity local to the flame becomes comparable with the flame propagation speed; and the rate of chemical reaction during combustion decreases with decreasing flow temperature and pressure, and hence stability again deteriorates. These parameters

are conventionally combined in an empirical expression known as the combustor 'loading' parameter.

$$\frac{W_{i-1}\,10^{9}}{P_{i-1}^{1.8}\; e^{\left[\frac{T_{i-1}}{300}\right]}\; V_{cb}}$$

Note that the station i-1 was set at entry to the combustor 'cold' volume, see figure 7.3b. Figure 7.4 shows a typical stability curve as a function of combustor loading and FAR. Note that combustor re-ignition is also dependent on the combustor loading and FAR but the re-ignition curve typically lies inside the stability curve.

At each calculation point and if the combustor was lit, the stability was assessed by reference to a graph of the form shown in figure 7.4. If the stability limit was exceeded the combustion burning efficiency was assumed to fall to zero exponentially.

$$\eta_{cb}(NEW) = \eta_{cb}\; \rho^{\left[\frac{-\Delta t}{\tau}\right]}$$

Similarly, at each calculation point and if the combustor was extinct, the occurrence of re-ignition was checked for. If conditions were suitable the combustion burning

efficiency was assumed to rise exponentially to its appropriate operating value.

$$\eta_{cb}(NEW) = \eta_{cb}(1 - \rho^{\left[\frac{-\Delta t}{\tau}\right]})$$

Where τ, is the characteristic time constant.

7.2.4.4 Calculation of combustion burning efficiency

The combustor burning efficiency was defined graphically as a function of FAR and combustor loading. Figure 7.5 illustrates a typical variation of combustor burning efficiency with FAR and loading.

The curve representing efficiency at the stoichometric FAR is commonly available and determined experimentally. For a given loading, the efficiency is assumed unchanged at FAR's below stoichometric. However, at FAR's greater than stoichometric the efficiency was assumed to fall linearly with the amount of excess fuel according to,

$$\eta_{cb} = \left[\frac{\text{Stoichometric FAR}}{\text{FAR}}\right] \eta_{cb(stoichometric)}$$

where FAR is greater than the stoichometric FAR.

7.2.4.5 Calculation of combustor pressure loss

Combustor pressure loss is the sum of the loss due to the aerodynamic drag of the internal structure and the

fundamental loss due to heat addition. The loss due to aerodynamic drag was assumed to occur across the cold volume and the fundamental loss due to heating across the hot volume. Appendix 7.6 states the formulae used to calculate the pressure losses. Note that under conditions of reverse flow at combustor entry the pressure losses were assumed zero due to the negligible flow velocities.

7.2.4.6 **Solution of equations**

The combustion temperature, burning efficiency, FAR and the Gas Dynamic Methods are each interdependent and so their calculation had to be iterative. Figure 7.6 is a schematic illustration of the calculation procedure used in the iteration.

7.3 **Single spool gas turbine simulation and verification**

Post-stall test data for the purpose of methods verification was taken from results presented by Freeman and Wilson, 1993. An instrumented Viper Mk 522 engine was run in a test bed and deliberately stalled. Compressor stall was induced at lower speeds by over-fuelling, but at higher speeds, high pressure air was injected into the combustion chamber from a remote reservoir. Post-stall events were presented at 100, 82, 78 and 60 % engine speed. Tests at 82 and 78 % speed, marked the transition between the completion of a complete surge cycle and the descent into rotating-stall. It is these data that were used to verify the simulation results of the above post-stall methods.

7.3.1 Model data input

The RRAP Viper model described in chapter 6 was used as the simulation test vehicle - the simulation time-step was set at 1 mS. The compressor, combustor, turbine and nozzle performance characteristics remained unchanged. The component volume geometry also remained unchanged save for the combustor. The combustor was no longer represented by a single volume but by a 'cold' and a 'hot', or 'flame tube', volume in series, as dictated by the modelling method described in section 7.2.4.

The post-stall compressor performance characteristic was based on rotating-stall data provided by Wilson and Freeman, 1993. The data was insufficient to define a complete characteristic and so performance trends were scaled from the experimentally derived characteristics of Small and Lewis, 1985, and Gamache, 1985, see section 7.2.1. Figure 7.7a illustrates the pre- and post-stall compressor performance characteristic in the pressure ratio and flow function plane - the flow function was defined at compressor entry. The stall line was defined by test data presented by Freeman and Wilson, 1993, and the stall recovery line scaled from the data of Small and Lewis, 1985, and Gamache, 1985. Figure 7.7b completes the definition of the post-stall performance characteristic - note that the performance trends are faithful to those of Small and Lewis, 1985, and Gamache, 1985, see figures 7.1a and b.

Section 7.2.2.2 described the need to take into account the finite time required for the development of rotating-stall cells if a simulation was to be physically representative. The 'time required' was represented by a time constant in a first order lag relating actual performance, to the steady-state performance given by the

post-stall characteristic. The time constant was termed the 'stall cell development time' and was deduced from the test evidence of Freeman and Wilson, 1993, to be approximately equivalent to one rotor revolution. For example at 100 % speed the rotor RPM was near 13,800 which equates to a time of approximately 4.4 mS per rotor revolution.

7.3.2 **Simulation results**

The RRAP viper model was stalled at 100, 82, 78 and 60 % speeds, and the simulation results compared to the test data. In each case the model was stalled by subjecting the compressor inlet face to a momentary drop in pressure. Under these conditions the change in corrected spool speed was negligible and so the compressor operating point moved from its steady state position towards the stall line along a line of constant corrected spool speed. At each engine speed the magnitude of the fall in inlet pressure was set to be just sufficient to stall the compressor. The pressure/time profile was a 'smoothed' half sinusoid of 20 mS duration. The duration was made sufficiently short to ensure minimum influence on the ensuing post-stall behaviour and on the final operating point of the engine.

i) - Stall performance at 60 % engine speed

Figure 7.8a illustrates the simulated compressor operating point trajectory during the stall event. Note that only a small portion of the pre- and post-stall compressor performance characteristics are shown - compare with the complete characteristic of figure 7.7.

Figure 7.8a also shows the pressure/time profile 'felt' by the the compressor face. The onset of stall occurred at approximately the point of minimum pressure at the compressor face, and corresponded to a simulation time of approximately 15 mS. From this point on, the compressor performance was predicted from the steady-state rotating-stall characteristic. The performance was however, lagged to account for the finite time required for the development of stall cells - see section 7.2.2.2. The stall cell development time was set at 7.3 mS - equivalent to one rotor revolution.

The compressor operating point trajectory oscillated in both mass flow rate and pressure ratio as the compressor performance degenerated into deeper and deeper rotating-stall. The oscillations were due to fluid inertia effects which can be seen to progressively degenerate with time. At a simulation time of approximately 50 mS the oscillations had all but disappeared. Note that during the descent into rotating-stall the trajectory did not cross the recovery line and so recovery from stall was not predicted to have occurred.

Figure 7.8b illustrates the prediction of the dramatic deterioration in engine performance commonly associated with the descent into rotating-stall.

a) Due to the loss of pressure ratio and reduction in mass flow rate, the gross thrust was shown to markedly fall.

b) The fuel flow rate was not altered during the simulation, and so with the fall in engine flow, led to a significant rise in both turbine entry temperature and fuel-to-air ratio, FAR. The rise in FAR was insufficient to threaten flame extinction.

c) Once in rotating-stall the compressor efficiency was too low to sustain engine operation and so the engine progressively ran down.

The above simulation agreed favourably with the results presented by Freeman and Wilson, 1993. The simulation correctly predicted that the compressor would not recover and further, the compressor operating point after the transitory oscillations, was found to be very near that of test, see figure 7.8a. Like the simulation, the test engine combustor remained lit and the compressor operated at too low an efficiency to sustain engine operation.

ii) - Stall performance at 78 % engine speed

Figure 7.9 illustrates the simulated compressor operating point trajectory during the stall event. The data input was identical to the above simulation save for the fuel flow rate. The stall cell development time was again set to one rotor revolution which equated to 5.6 mS.

Again the above simulation agreed favourably with the results presented by Freeman and Wilson, 1993. The simulation correctly predicted that the compressor would not recover and further, the compressor operating point after the transitory oscillations, was found to be very near that of test, see figure 7.9. Like the simulation, the test engine combustor remained lit and the compressor operated at too low an efficiency to sustain engine operation.

iii) - Stall performance at 82 % engine speed

Figure 7.10 illustrates the simulated compressor operating point trajectory during the stall event. The data input was identical to the above simulations save for the fuel

flow rate. The stall cell development time was again set to one rotor revolution which equated to 5.5 mS.

The compressor was predicted to surge and for a portion of the cycle operate under reverse flow conditions. The compressor was also predicted to recover because the operating point trajectory crossed the stall recovery line, see figure 7.10. Further, the combustor was predicted to remain lit. Although these predictions were born out in the results of Freeman and Wilson, 1993, the test engine was found to enter cyclic surge rather than complete just one cycle.

At 82 % speed the test engine was stalled by injecting high pressure into the combustor from a remote reservoir. However, the delivery of air from the reservoir could not be stopped at the moment of compressor stall. The compressor therefore completed a number of surge cycles before finally recovering. This scenario was simulated by temporarily restricting the flow swallowing capacity of the turbine. Figure 7.11 illustrates the resulting cyclic surge simulation. Note that because the turbine repeatedly operated off design, the spool speed was shown to steadily fall. The 'size' of the surge cycle loop therefore reduced with each cycle. The surge cycle frequency was predicted to be 15 Hz which compared favourably to the frequency measured by Freeman and Wilson, 1993, of 14 Hz.

iv) - Stall performance at 100 % engine speed

Like the 82 % speed case, Wilson and Freeman, 1993, injected high pressure air into the combustor to initiate stall. This time surge cycles did not ensue but instead

the initial surge was sufficiently strong that the combustor flame was extinguished. The engine subsequently 'ran down'.

Figure 7.12a illustrates the simulation of this stall event. The data input was identical to the above simulations save for the fuel flow rate. The stall cell development time was again set to one rotor revolution which equated to 4.4 mS.

The model correctly predicted the extinction of the combustor flame and the subsequent compressor recovery and spool 'run down'. The maximum FAR, beyond which flame extinction was assumed to occur, was a data input value, and set at 0.09. This value was estimated from the Rolls-Royce combustor performance data base.

This stall event also served to illustrate that the combustor model detailed in section 7.2.4, was capable of operating under what were severe flow conditions. Figure 7.12b illustrates the combustor performance during the 100 % speed stall. Note that during the simulation the flow at the combustor entry plane was predicted to reverse in direction. The 'effective' FAR which relates to the amount of fuel actually burnt, was shown not to rise above the maximum stoichometric FAR of 0.066. The value of the stoichometric FAR was not an input data item but indirectly born out by the combustor model 'K' constants. These constants relate to the ideal combustion process defined in appendix 7.3. However the 'actual' FAR_a which accounted for the burnt and unburnt fuel was seen to rise above the imposed extinction limit. Following extinction the 'effective' FAR_e fell to a default zero and the 'actual' FAR_a fell steadily in line with the increasing engine flow commensurate with compressor recovery.

The combustion temperature can be seen to vary in accordance with the burning efficiency which was in turn defined as a function of the combustor loading parameter and the actual, FAR_a. At extinction the burning efficiency fell to a default zero which left the 'combustion temperature' to fall in line with the compressor exit temperature.

The simulation of the 82 and 100 % speed, stall events each showed an unexpected loop in the compressor operating point trajectory, see figures 7.10, 7.11 and 7.12a. The frequency response of the instrumentation used by Freeman and Wilson, 1993, to measure compressor flow was insufficient to define the transient compressor operating point. It was therefore impossible to say for sure whether the prediction of the trajectory 'loops' were physical or not. However, the loops were thought to be similar in origin to the Helmholtz resonance. The compressor and combustor were considered as the duct and plenum volume of a Helmholtz system respectively, and the resonant frequency calculated from,

$$f = \frac{a}{2\pi}\sqrt{\left[\frac{A_c}{V_p L_c}\right]}$$

Where A_c = compressor mean cross section flow area
L_c = compressor length
V_p = combustor volume

The predicted resonate frequency was 92 Hz which was to within 10 Hz of the frequency of oscillation of the trajectory loops. Although this result was encouraging,

it must be noted that the calculation of the Helmholtz resonance was at best approximate. Further, the frequency of the loops themselves is strictly beyond that which can modelled by the Gas Dynamic Methods with the time-step and size of component volumes used, see section 5.5. Consequently further investigation of the trajectory loops had to be cited as a future work item, see chapter 9.

The simulation of the 82 and 100 % speed, stall events was thought to highlight a further restriction imposed by the minimum size of time-step - smaller time-steps were found to generate computer precision errors, see section 5.3.3. Strictly the post-stall performance characteristic should have had a discontinuity between the reverse flow and rotating stall portions of the characteristic as shown by Small and Lewis, 1985, figure 7.2, and Gamache, 1985, figure 7.1. However, the minimum size of time-step, set at 1 mS, was found to be too large for the RRAP Implicit Matching Method to find successive Matches on passing across such a discontinuity. The post-stall performance characteristic was therefore made continuous, see figure 7.7.

The simulation of the stall events at 82 and 100 % speeds correctly predicted the occurrence of compressor reverse flow. However, the calculations actually used during reverse flow were not those described in section 7.2.3. When these calculation methods were used a numerical instability was uncovered.

At the point of compressor reverse flow the calculation method necessarily switched from the forward flow method detailed in appendix 6.1b, to the reverse flow method detailed in appendix 7.2. However, subsequent solution of the gas dynamic equation set was found to be illusive.

The steady-state reverse flow calculation correctly predicted a compressor inlet temperature that was significantly higher than at exit. During reverse flow, blade windage raises the enthalpy of the air and so the temperature at entry is greater than at exit. The compressor volume averaged flow density, therefore fell significantly compared to its value under forward flow conditions. This is because the volume averaged density was assumed to be the average of the volume entry and exit values, see section 4.3.1. What was in effect a step jump in density could not be absorbed into the gas dynamic equation set. With respect to the conservation of mass equation of the equation set, it can be seen that a significant drop in volume averaged density leads to an inappropriately large prediction of the time corrected volume exit mass flow rate. Invariably, with just such a prediction of volume exit mass flow rate, there was no physical solution to the gas dynamic equation set.

The reverse flow predictions were finally done by using the steady-state 'forward flow' calculation instead. The upstream total temperature boundary condition, although inappropriate, was therefore kept in place - however the reverse flow was exhausted to a constant ambient static pressure rather than imposing a constant upstream total pressure. Further, compressor efficiency during reverse flow had to be defined in the conventional form and not with respect to the performance parameter defined in appendix 7.1.

Possible methods of successfully passing from forward to reverse flow with an appropriate change in boundary conditions, hinge on the ability to predict physically representative changes in the compressor volume averaged density. The use of a smaller time-step would probably

help but it is thought that the greatest chance of success would be achieved by representing the compressor with stage-by-stage volumes. During the transition from forward to reverse flow, the step change in volume averaged density would then be necessarily smaller. Subsequent solution of the gas dynamic set might then be possible. Research into this problem was cited as future work item, see chapter 9.

7.4 **Discussion of results**

The post-stall modelling methods have demonstrated the ability to distinguish between surge and rotating-stall. This illustrated that, for a given engine geometry and post-stall compressor characteristic, the rate of 'pump down' of the combustor volume was correctly predicted by setting the stall cell development time to be equivalent to one rotor revolution. The quicker the 'pump down' the greater the likelihood that the compressor surged rather than descended into rotating-stall.

Although it was not possible to compare simulated compressor operating point trajectories with test trajectories, the following characteristics commonly associated with surge and rotating-stall were correctly predicted.

i) In the case of surge, the model correctly predicted that the compressor would complete one surge cycle and recover of its own accord provided the cause of the initial compressor instability was removed. The engine then correctly settled back to its former performance condition. Conversely, if the cause of the initial stability remained, the compressor was

correctly predicted to enter cyclic surge. Further, the surge cycle frequency was also correctly predicted. Commensurate with cyclic surge, the spool was seen to run down and with it the engine performance steadily deteriorate.

ii) In the case of the descent into rotating-stall the gross thrust was correctly predicted to markedly fall and the turbine entry temperature to rise significantly. Once in rotating-stall the compressor efficiency was too low to sustain engine operation and so the engine progressively ran down - this is not an uncommon occurrence but some engines can remain in steady operation with the compressor in rotating-stall.

The stall simulations also indicated that compressor recovery can be predicted with reasonable accuracy by superimposing a steady-state recovery line over the post-stall performance characteristic.

Although detailed performance of the combustor during post-stall events could not be verified due to lack of test data, its performance was found to be physically representative. Predictions of FAR, burning efficiency and combustion temperature were all deemed sensible even under conditions of low and reverse flow at entry to the combustor. Further, during surge at 100 % speed, the Viper combustor was correctly predicted to extinguish.

CHAPTER 8

Conclusions

Literature describes how the simulation of high-frequency-transients is achieved by splitting a flow path into a number of component volumes, and for each, predicting the rate of change of three volume averaged flow quantities. The rate of change of these averaged quantities, is predicted by solving time dependent equations conserving flow mass, momentum and energy - the gas dynamic equation set. The smaller the volume, the less the error in 'volume averaging', and therefore the more accurate is the final simulation. This has been the conventional approach leading to models with short volumes and in the case of the compressor, stage-by-stage representation - further, due to computational ease the governing equations are invariably solved using explicit numerical schemes. However, their ultimate versatility with respect to the design and development of engines is limited because typical codes used by industry and academia predict the performance of each engine component as a whole and use an implicit numerical scheme - implicit schemes are invariably more robust and versatile than explicit schemes. It was therefore feared that introduction of a gas dynamic equation set into an implicit code such as the Rolls-Royce Aero Engine Performance code, RRAP, would compromise accuracy due to the large component volumes and the typically large time-steps used.

Introduction of the gas dynamic equation set into the RRAP code, has revealed that these fears were unfounded. Prediction of high-frequency-transients has been verified using volumes of significantly greater length than those

used in the explicit models of Tesch et al, 1976, and Tesch and Steenken, 1976 (a) and (b), Davis et al, 1980 and O'Brien, 1992, for example. In fact volume sizes comparable to typical engine component volumes can represent flow transients of at least 40 Hz. Further, the length of volume has very little influence on reducing any wave attenuation compared to the influence of the size of time-step. The smaller the time-step the less the wave attenuation. In the case of RRAP, computation precision errors limited the smallest time-step to 1 mS, which in turn limited the maximum frequency response to between 40 and 80 Hz.

Inclusion of Gas Dynamic Methods using volumes of comparable size to engine component volumes is therefore possible using an implicit numerical scheme to solve the governing equations. Simulation of flow transients in engines is thus possible in conventional performance decks like RRAP, without having to split components such as the compressor into stage-by-stage volumes.

Application of the gas dynamic equation set to the simulation of engine high-frequency-transients using the RRAP deck, produced physically representative results. Prediction of the effect on stall margin due to the temporary accumulation of flow mass, momentum and energy within the the compressor volume were as expected. However, prediction of excursions in the fan operating point of two spool engines, were considered limited. At present fan characteristics are typically defined as a function of overall inlet flow and not seperate inner and outer flows (or by-pass ratio) - calculation of radial flow in the fan volume by the equation set would have therefore compromised their use. A representative prediction will require definition of fan characteristics

with respect to both the inner and outer flow. This inadequacy must be overcome before post-stall development of a turbofan engine can be extended further.

The post-stall modelling methods developed are capable of distinguishing between surge and rotating-stall. This illustrated that, for a given engine geometry and a steady-state post-stall compressor characteristic, the rate of 'pump down' of the combustor volume was correctly predicted by setting the stall cell development time to be proportional to the rotor speed. In the case of surge, the methods correctly predict that a compressor will complete one surge cycle and recover of its own accord provided the cause of the initial compressor instability is removed. Conversely, if the cause of the initial instability remains, the methods will simulate cyclic surge. Further, the prediction of surge cycle frequency has been verified. In the case of rotating-stall, the methods correctly predict a marked fall in thrust and a significant rise in turbine entry temperature. Simulations also indicated that recovery from surge or rotating-stall can be predicted with reasonable accuracy by superimposing a steady-state recovery line over the post-stall performance characteristic.

Prediction of combustor performance based on calculating the mass of air and combustion products within the combustor volume, was shown to be physically representative. This approach was necessary because conventional performance which is based on mass flow rate through the combustor, fails under the low and reverse flow conditions that can occur during compressor stall. Prediction of fuel-to-air ratio FAR, from the mass of air and combustion products, was shown to be representative and capable of correctly predicting flame extiction in the

case of the Viper surge at 100 % speed. Although not verified, the prediction of FAR, burning efficiency and combustion temperature under conditions of reverse flow at combustor entry, were shown to be representative. The combustor model is therefore deserving of application to whole engine post-stall simulation.

CHAPTER 9

Future Work

9.1 Methods development

At present the smallest time-step that may be used by the RRAP system (including the Gas Dynamic Methods) before precision errors take effect is 1 mS. Chapter 5 concluded that the frequency response with volumes comparable in size to engine components and with a 1 mS time step, is between 40 and 80 Hz. Although, this frequency response is in excess of typical engine response to surge and the descent into rotating-stall, simulation of the recovery from surge has revealed a possible Helmholtz resonance, see section 7.3.2. The resonance had a frequency of approximately 90 Hz which is beyond the present response capability. With a view to further research it is therefore recommended that the computation precision of the RRAP system be improved in order to at least half the present minimum time-step. Further, the prediction of post-stall compressor operating point trajectories will be 'smoother' if a smaller time step is used. The transition from compressor forward to reverse flow and vice versa during deep surge; and the transition from pre-stall to post-stall performance characteristics and vice versa, will also be computationally more stable by using smaller time-steps.

Chapter 5 concluded that to maintain numercial stability of the gas dynamic equation set within RRAP, an Implicit Matching Method Variable and Matching Quantity in both flow mass flow rate and total pressure, had to be

introduced between each adjoining model volume. It is therefore recommended that in the interests of reducing computational complexity and time, that an extra Variable and Matching Quantity in total temperature between each volume be introduced. Not only should numerical stability be further improved, but the Successive Back Substition (SBS) iterative method, see section 5.3.2, developed to solve the gas dynaminc equation set, would be made redundant. Similarly appropraite use of Variables and Matching Quantities would enable solution of the gas dynamic equation set extened for radial flow, to be solved without the use of the IMSL 'off the shelf' equation solver.

Introduction of Variables and Matching Quantities in mass flow rate, temperature and pressure between each volume, and the removel of the SBS and IMSL solvers, will produce a very stable and a computationally simpler numerical scheme. Combined with improved computation precision, the resulting numerical scheme would provide a surer 'footing' for the continued development of pre- and post-stall high frequency flow transients.

Comparison of simulation with post-stall test data has shown that representing the compressor with a single volume is a good approximation. Stage-by-stage compressor modelling was avoided because of calculation complexity and the need for stage performance characteristics which are rarely available. However, it is thought that a stage model will be necessary for the 'correct' modelling of compressor reverse flow during deep surge, see section 7.3.2. Further, a stage model will be necessary if stall prevention or recovery using inter-stage bleed, is to be modelled. Research into stage modelling must therefore depend on the anticipated use of the modelling methods.

Simulation of post-stall compressor behaviour is dependent on the nature of the post-stall performance characteristic. It is therefore recommended that research is done into theoretically predicting post-stall characteristics from basic compressor geometry. Such a capability will result a truely predictive modelling method once verified.

Further research into the application of fan performance characteristics and their compatibility with the gas dynamic equation set extended to predict radial flow, is required. At present fan characteristics are typically defined as a function of overall inlet flow and not seperate inner and outer flows (or bypass ratio) - calculation of radial flow in the fan volume by the equation set would therefore compromise their use. Prediction of fan operating point excursions during flow transients is therefore, at present, limited. This inadequacy must be overcome before post-stall development of a turbofan engine can begin proper.

9.2 **Verification**

Despite the verification of the Gas Dynamic Methods at low Mach Number using the duct test data, see section 5.4, application to the higher flow Mach Numbers found in gas turbine engines remains to be verified. It therefore remains unknown whether or not the Gas Dynamic Methods can be legitimately applied to engine components - without a doubt pre-stall high frequency engine test data are required to verify the methods developed. However, it is expected that the pre-stall methods will be successfully verified. This because, not only were the simulation results physically representative, see section 6.4, but

the post-stall methods, which are an extension of the pre-stall methods, produced simulation results that agreed favourably with test data.

The post-stall verification done, see section 7.3, is encouraging but further test data is required, particularly of time accurate compressor operating point trajectory definition. Verification of this transient phase of stall will add credance to the prediction of stall recovery, combustion stability and to the estimation of aerodynamic loads exerted by the flow on engine internal structures and blading.

REFERENCES

Aircraft Engineering, November **1979.**

J S **Alford** and I W Victor
Dynamic measurements of forward gas expulsion during high speed stall of jet engines
Flight Propulsion Division, General Electric Company
National Aeronautic and Space Engineering and Manufacturing meeting, October **1965.**

M **Boroomand**
Simulation and measurement of transients in pipes and compressors
Cranfield University, School of Mechanical Engineering, PhD Thesis **1992.**

K **Chung**, K R Leamy and T P Collins
A turbine engine aerodynamic model for in-stall transient simulation
AIAA/SAE/ASME/ASEE, 21st Joint Propulsion Conference, **1985.**

H **Cohen**, G F C Rogers and H I H Saravanamuttoo
Gas Turbine Theory 3rd Edition
Published by Longman Group UK Ltd, **1987**
ISBN 0-582-30539-X

M W **Davis**, C E Chamblee and W F Kimzey
A multi-stage axial flow compressor mathematical modelling technique with application to two current turbofan compression systems
AIAA-80-0054, **1980.**

M W **Davis**
A stage-by-stage dual-spool compression system modelling technique
ASME 82-GT-189, **1982.**

M W **Davis**
A post-stall compression system modelling technique
Arnold Engineering Development Centre
AEDC-TR-86-34, **1987.**

M W **Davis** and A A Hale
DYNamic Turbine Engine Compressor Code DYNTECC - Theory and capabilities
AIAA-92-3190, **1992.**

S D **Dvorak**, W M Hosny and W G Steenken
E3 10C Compressor test analysis of high speed post-stall data
Prepared for NASA Lewis Research Centre, CR-179521, **1986**.

S D **Dvorak**, W M Hosny and W G Steenken
Dynamic data acquisition, reduction, and analysis for the identification of high speed compressor component post-stability characteristics
AIAA/SAE/ASME/ASEE 23rd Joint Propulsion Conference
AIAA-87-2089, **1987**.

H W **Emmons**, C F Pearson and H P Grant
Compressor Surge and Stall Propagation
Transactions of ASME, Vol. 79, **1955**.

J V **French**
Modelling post-stall operation of aircraft gas turbines
AIAA-85-1431, **1985**.

R N **Gamache**
Axial Compressor Reverse Flow Performance
PhD Thesis, Dept. of Aeronautics and Astronautics
Massachusetts Institute of Technology, **1985**.

R N **Gamache** and E M Greitzer
Reverse flow in multistage axial compressors
Arnold Engineering Development Centre and
Massachusetts Institute of Technology.
AIAA-86-1747, **1986**.

M E **Gill**
Engine high frequency aerodynamic model - interim report phase 1
Cranfield University TR/87/3, **1987**, not published.

M E **Gill (a)**
Engine high frequency aerodynamic model Interim report phases 2 and 3
Cranfield University Report TR/88/1, **1988**, not published.

M E **Gill (b)**
Engine high frequency aerodynamic model phase 4 report
Cranfield University, TR/88/5, **1988**, not published.

M E **Gill (c)**
HIFEM - Engine high frequency aerodynamic model - summary report
Cranfield University TR/86/6, **1988**, not published.

M E **Gill**
HIFEM - Engine high frequency aerodynamic model - entropy model development (HIFEM3) - phase 1
Cranfield University TR/89/2, **1989**, not published.

M E **Gill** and J R Haynes
HIFEM - Engine high frequency aerodynamic model - entropy model (HIFEM 3) phase 2
Cranfield University TR/90/2, **1990** not published.

M E **Gill**, J R Haynes and R L Elder
HIFEM - Engine high frequency aerodynamic model - entropy model (HIFEM 3) - final report
Cranfield University TR/90/6, **1991** not published.

E M **Greitzer** (a)
Surge and Rotating Stall in Axial Flow Compressors Part I: Theoretical Compression System Model
ASME 75-GT-9, **1975.**

E M **Greitzer** (b)
Surge and rotating-stall in axial flow compressors Part II: Experimental results and comparison with theory, ASME 75-GT-10, **1975.**

W R **Hopf** and W G Steenken
Stall recovery and control strategy methodology and results
AIAA-85-1433, **1985.**

W M **Hosny**, S J Bitter and W G Steenken
Turbofan engine non-recoverable stall computer-simulation development and validation
AIAA/SAE/ASME/ASEE 21st Joint Propulsion Conference, **1985.**

W M **Hosny** and W G Steenken
TF34 Engine compression system computer study
Prepared for NASA-Lewis Research Centre
NA53 - 20599, **1979.**

W M **Hosny** and W G Steenken
Aerodynamic instability performance of advanced high pressure ratio compression component
AIAA/ASME/SAE/ASEE 22nd joint Propulsion Conference
AIAA-86-1619, **1986.**

E L **Houghton** and N B Carruthers
Aerodynamics for engineering students 3rd edition
Edward Arnold (Publishers) Ltd, **1982**
ISBN 0-7131-3433-X.

IMSL, Inc. Math Library - NEQNF/DNEQNF
Version 2.0, **1987.**

R S **Mazzawy**
Surge-induced structural loads in gas turbines
ASME Volume 102, **1980.**

N M **Merriman**
Simulation of aero engine transient behaviour including the effects of volume dynamics
IMechE Seminar Paper 'Turbo compressor and fan stability', **1993.**
Published by Mechanical Engineering Publications Ltd. ISBN 0 85298 864 8

D S **Miller**
Internal Flow Systems
Vol 5 BHRA Fluid Engineering Series
Published by BHRA Fluid Engineering Series, **1978**
ISBN 0 900983 78 7

W F **O'Brien** and M W Davis
A stage-by-stage post-stall compression system modelling technique
AIAA-87-2088, **1987.**

W F **O'Brien** and K Boyer
Model predictions for improved recoverability of a multistage axial flow compressor
AIAA-89-2687, **1989.**

W F **O'Brien**
Dynamic simulation of compressor and gas turbine performance
AGARD-LS-183, Paper no. 5, **1992.**

S J **Przybylko**
Application of system identification techniques to post-stall combustor dynamics
AIAA/SAE/ASME/ASEE 21st Joint Propulsion Conference
AIAA-85-1353, **1985.**

C J **Small** and J T Lewis
High speed compressor rig as a stall recovery research tool
Pratt and Whitney Engineering Division
AIAA/SAE/ASME/ASEE Propulsion Conference
AIAA-85-1428, **1985.**

L L **Steele**, J R Grant, D P Harrold and J J Erhat
Application of system identification techniques to combustor post-stall dynamics
Wright-Patterson Air Force Base
AFWAL-TR-86-2105, **1987.**

W G **Steenken**
Modelling compression component stability characteristics
AGARD (Marathon **1982**) CPP 324, Paper 24.

W G **Steenken**
Turbofan post-instability behaviour - computer simulations, test validation and application of simulations AGARD CP 400, session 3, **1986.**

Y **Sugiyama**, W Tabakoff and A Hamed
J85 Surge Transient simulation
ISABE 87-7076, **1976.**

W A **Tesch**, R H Moszee and W G Steenken
Linearized blade row compression component model - stability and frequency response analysis of a J85-13 compressor
NASA CR-135162, **1976.**

W A **Tesch** and W G Steenken (a)
Blade row dynamic digital compressor program Volume 1 - J85 clean inlet flow and parallel compressor models
Prepared for NASA-Lewis Research Centre NASA - CR-134978, **1976.**

W A **Tesch** and W G Steenken (b)
Dynamic blade row compression component model for stability studies
AIAA paper No 76-203, **1976.**

R C **Turner** and D W Sparkes
Complete characteristics for a single stage axial flow fan
Thermodynamics and Fluid Mechanics Convention
IMechE, Paper 29, **1964.**

A G **Wilson** and C Freeman
Stall Inception and Development in an Axial Flow Aeroengine
ASME 93-GT-2, **1993.**

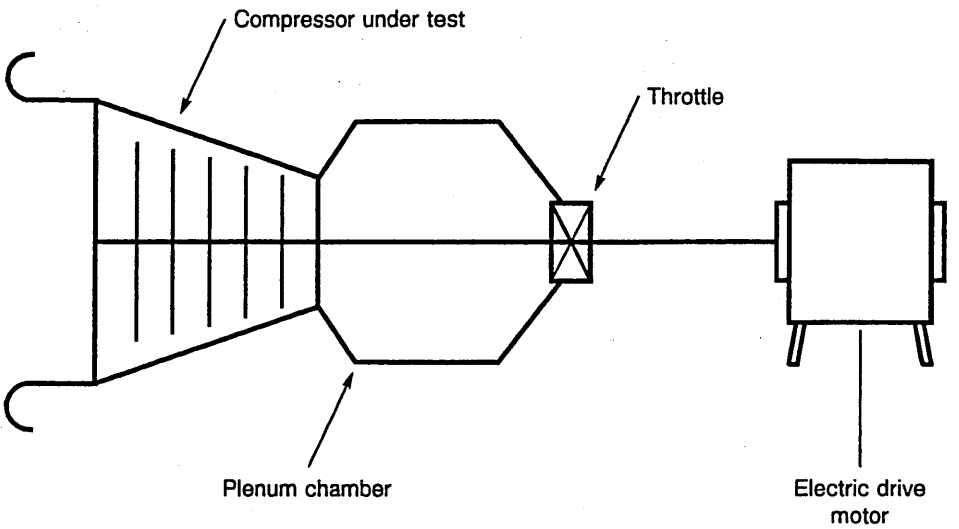

Figure 1.1a Compressor in a test rig

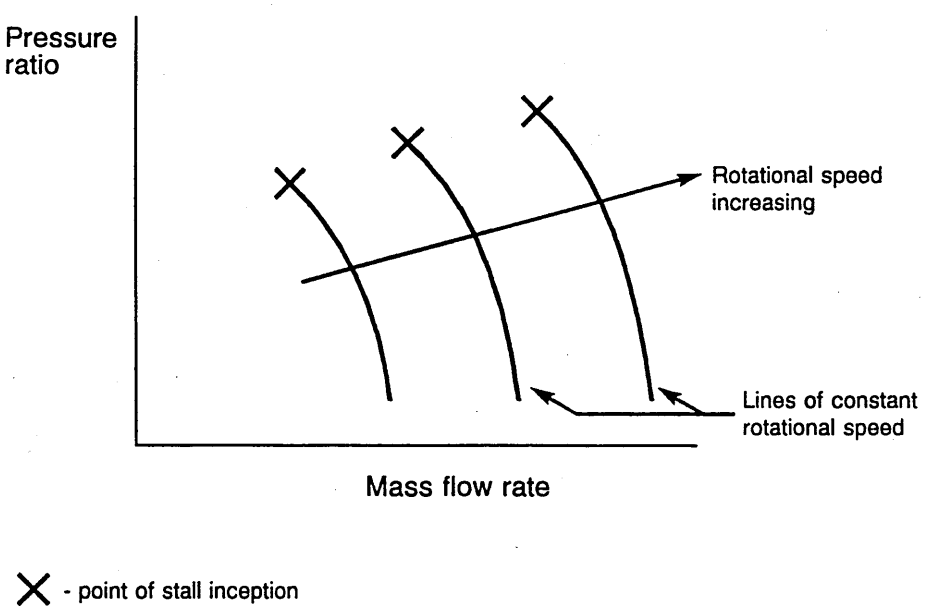

Figure 1.1b Compressor performance characteristic

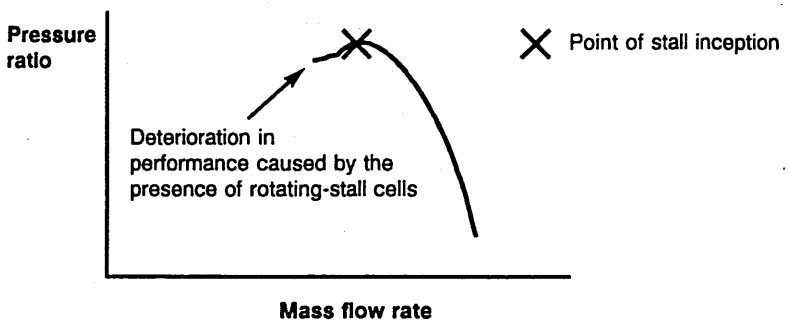

Figure 1.2a - Progressive stall

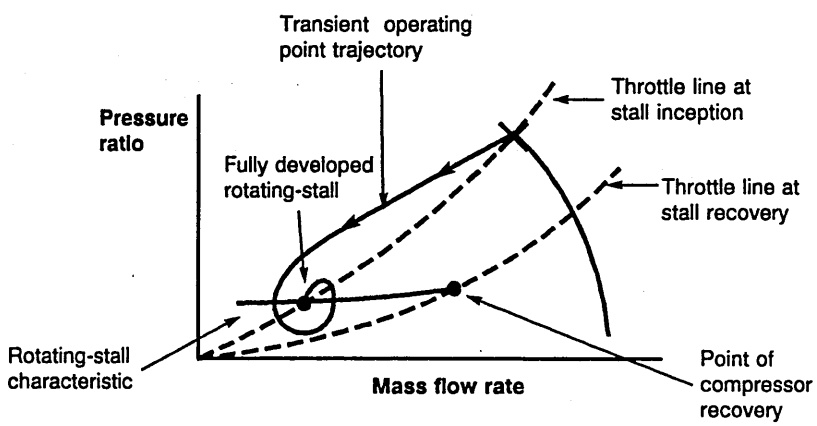

Figure 1.2b - Rotating-stall

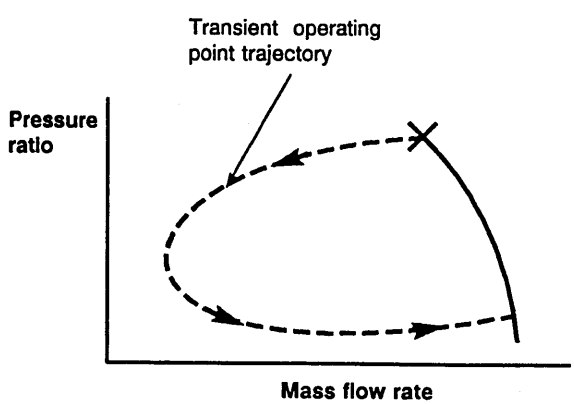

Figure 1.2c - A surge cycle

Figure 1.2 Compressor post-stall performance

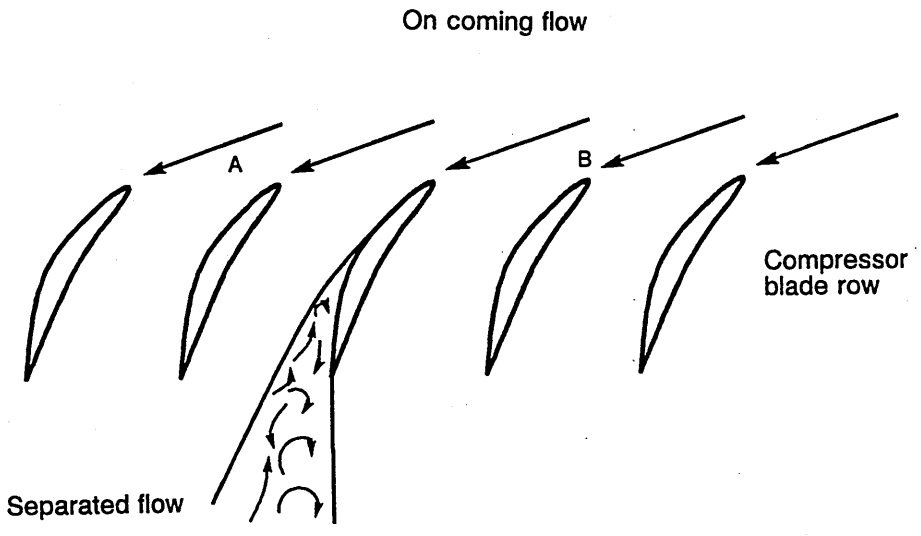

Figure 1.3a Stall cell inception

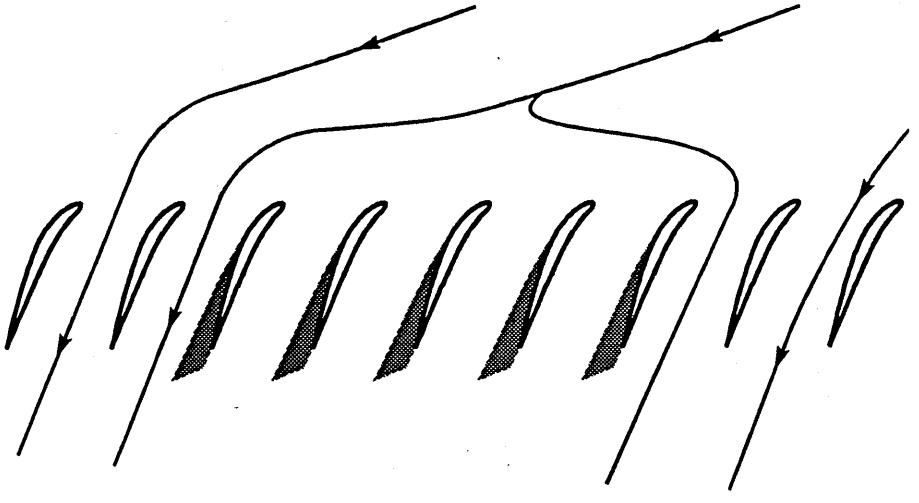

Stall cell propagates from right to left relative to the blades

Figure 1.3b Rotating - stall cell development

Figure 1.3 Schematic illustration of the Emmons et al mechanism of stall inception and rotating - stall cell development

Figure 1.4a - View of compressor face

Figure 1.4b - View of compressor face

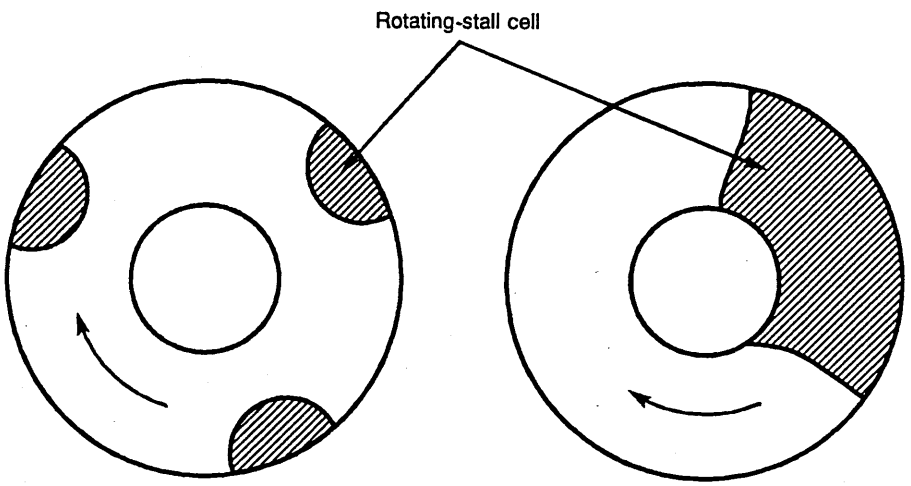

Figure 1.4 Developed rotating - stall cells

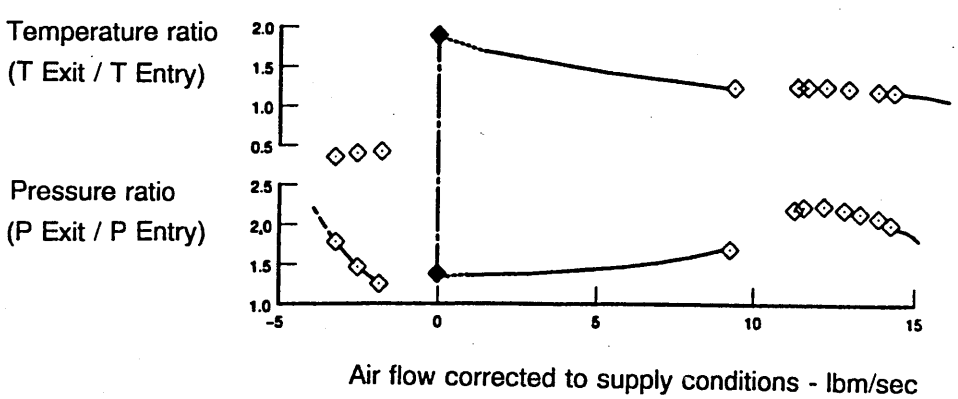

taken from small and Lewis, 1985

Figure 2.1a Compressor post-stall performance characteristic - Small and Lewis, 1985

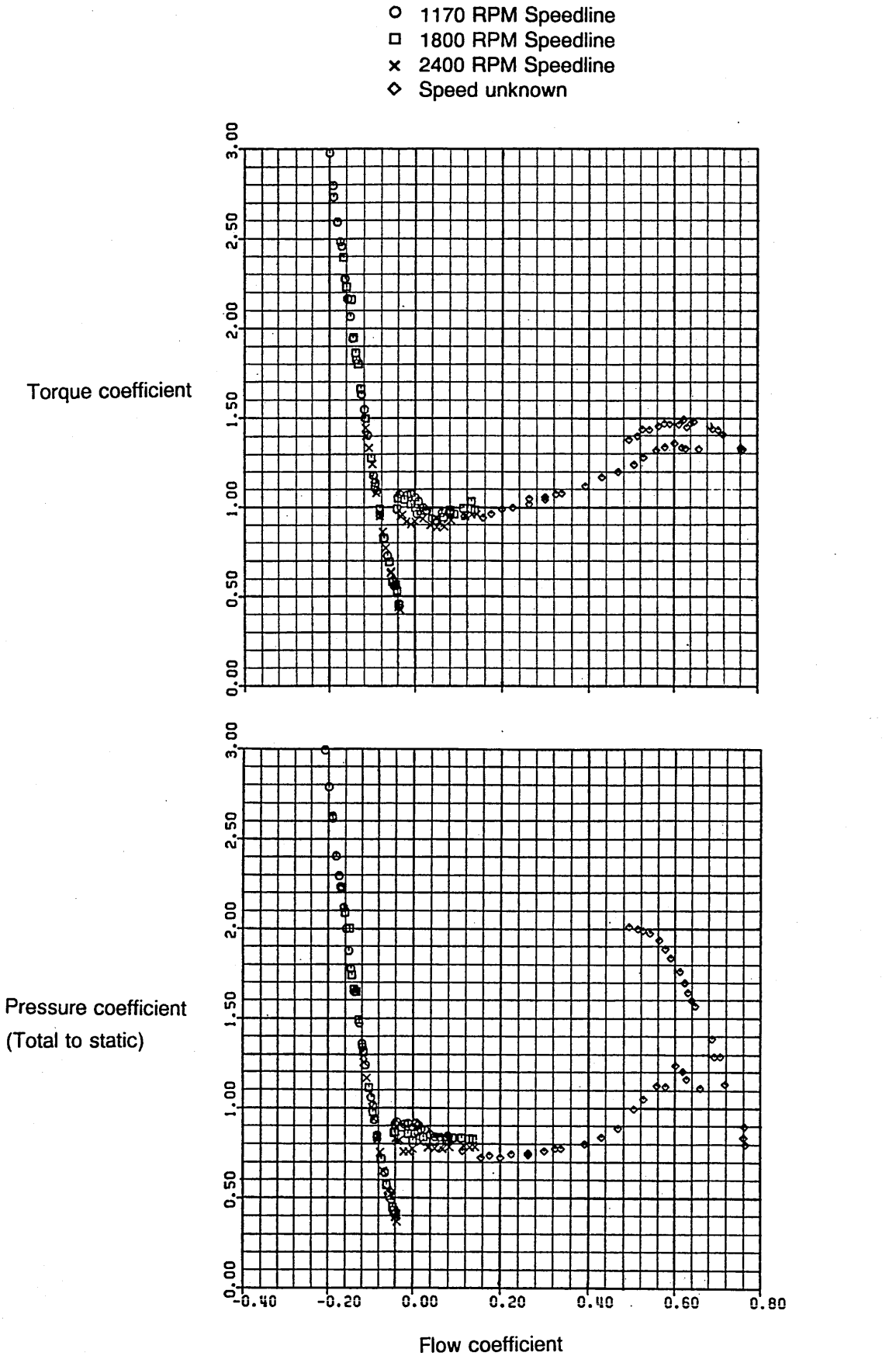

taken from Gamache, 1985

Figure 2.1b Compressor post-stall performance characteristic - Gamache, 1985

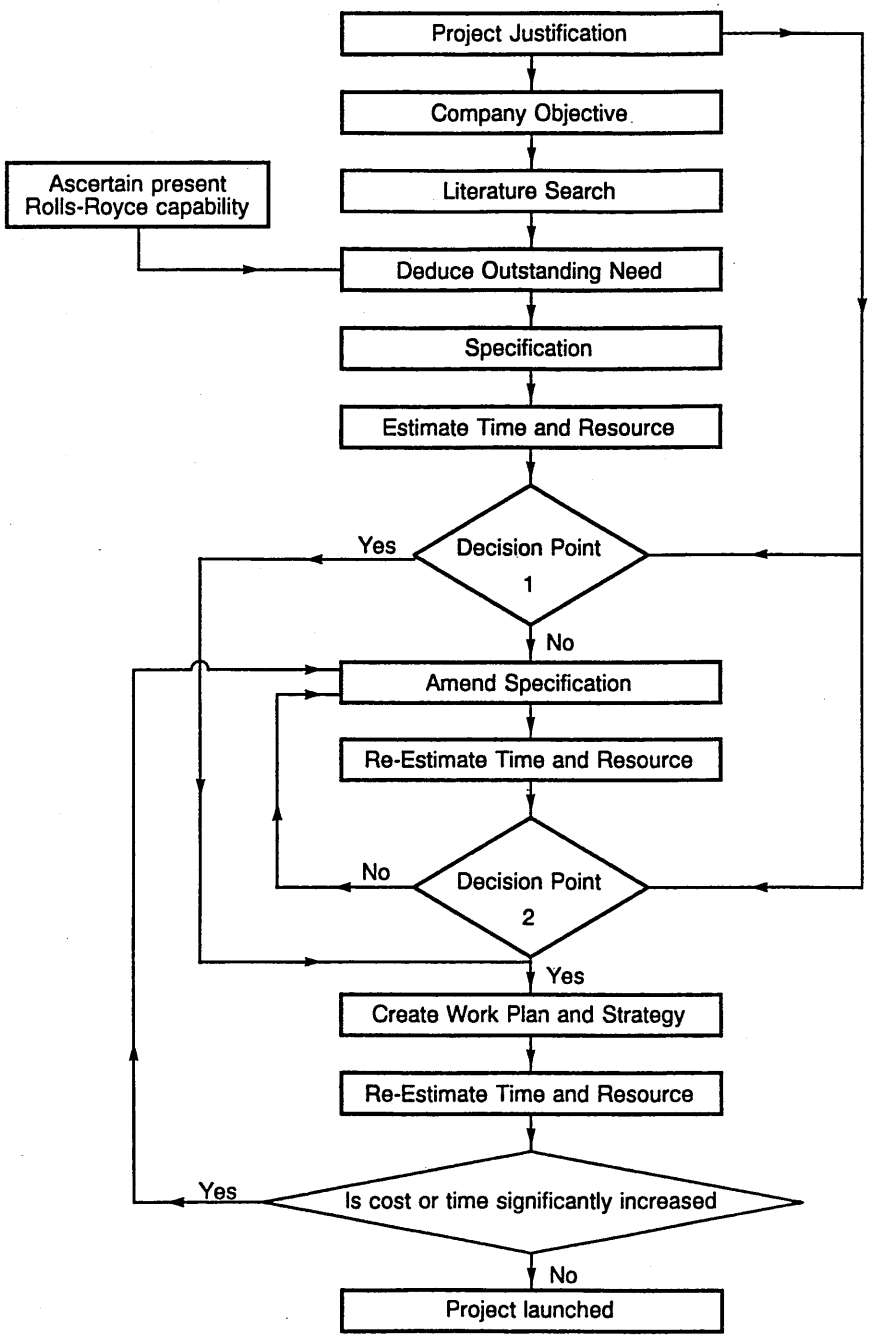

Figure 3.1 Project Organisation and Launch

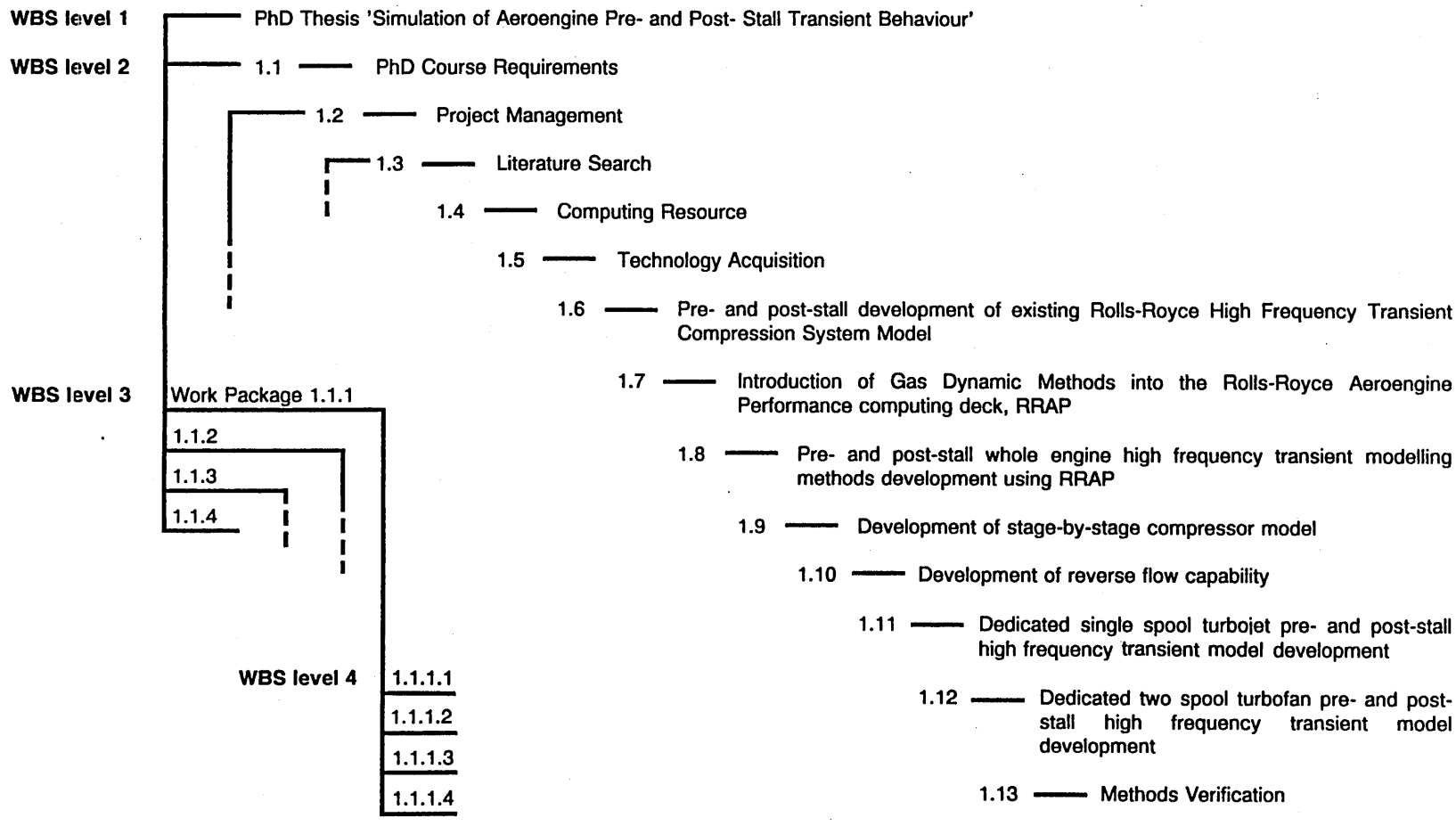

Figure 3.2 - Schematic illustration of the Work Breakdown Structure (WBS)

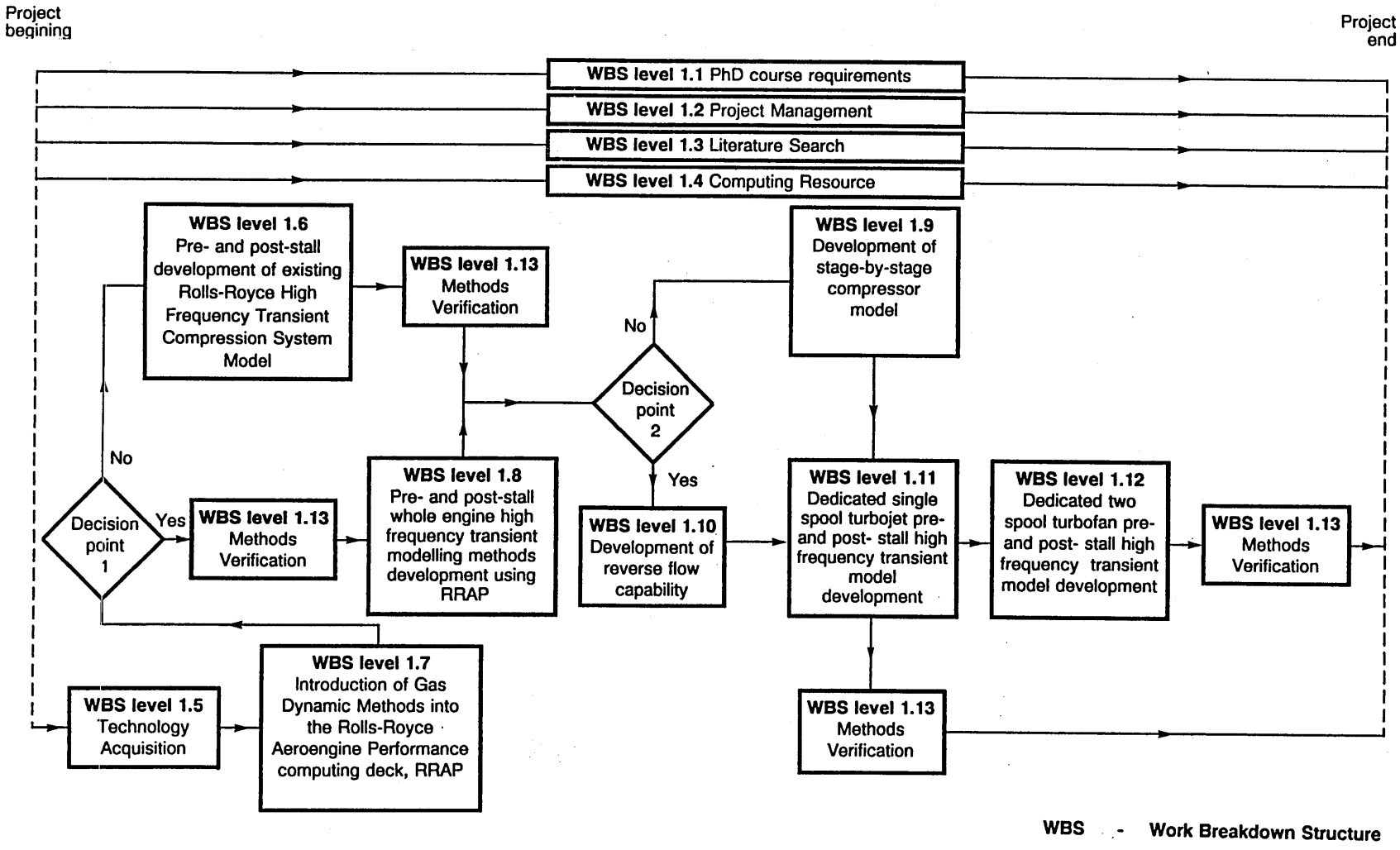

Figure 3.3 - Project Work Plan and Strategy

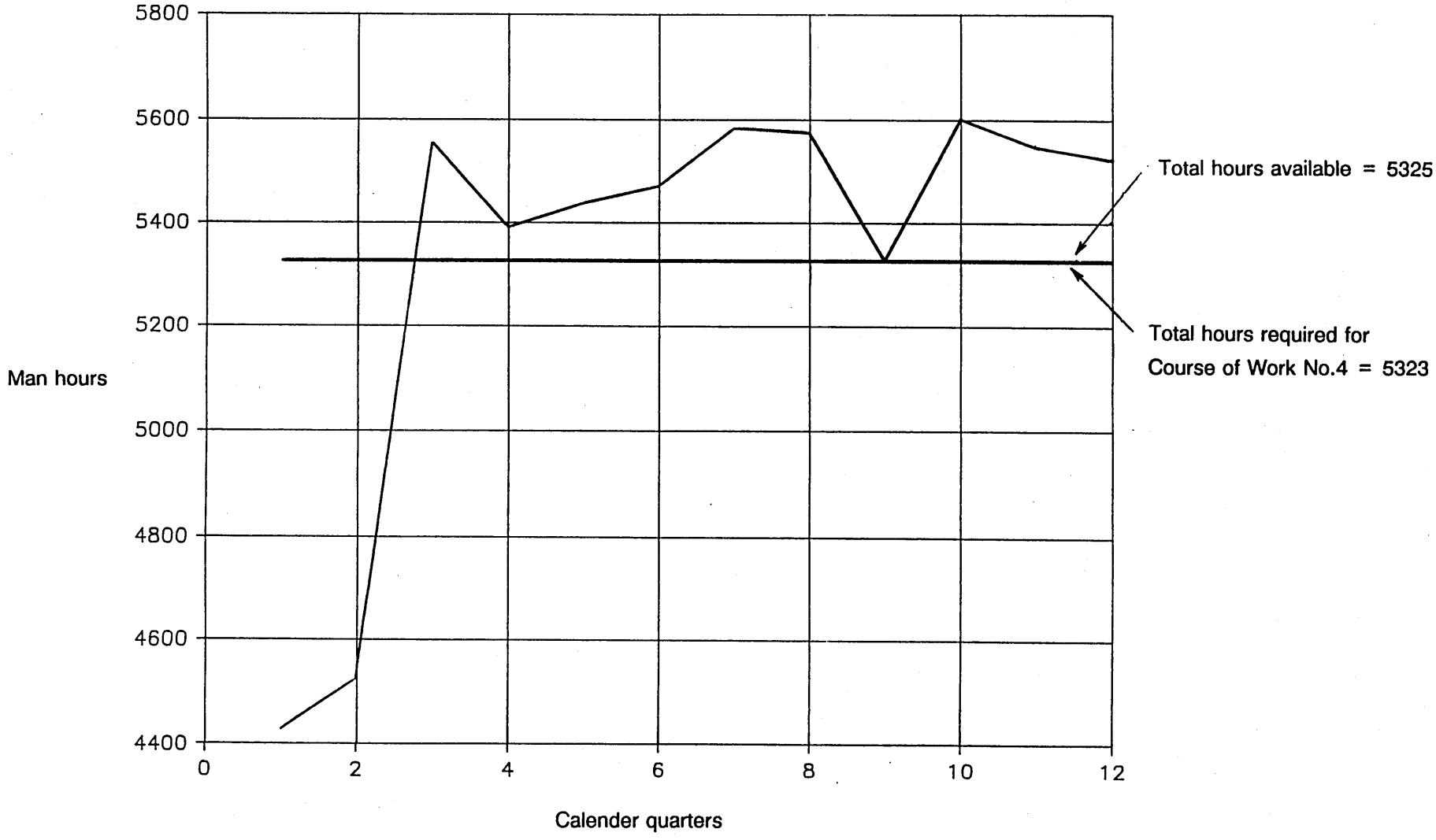

Figure 3.4 Project Progress

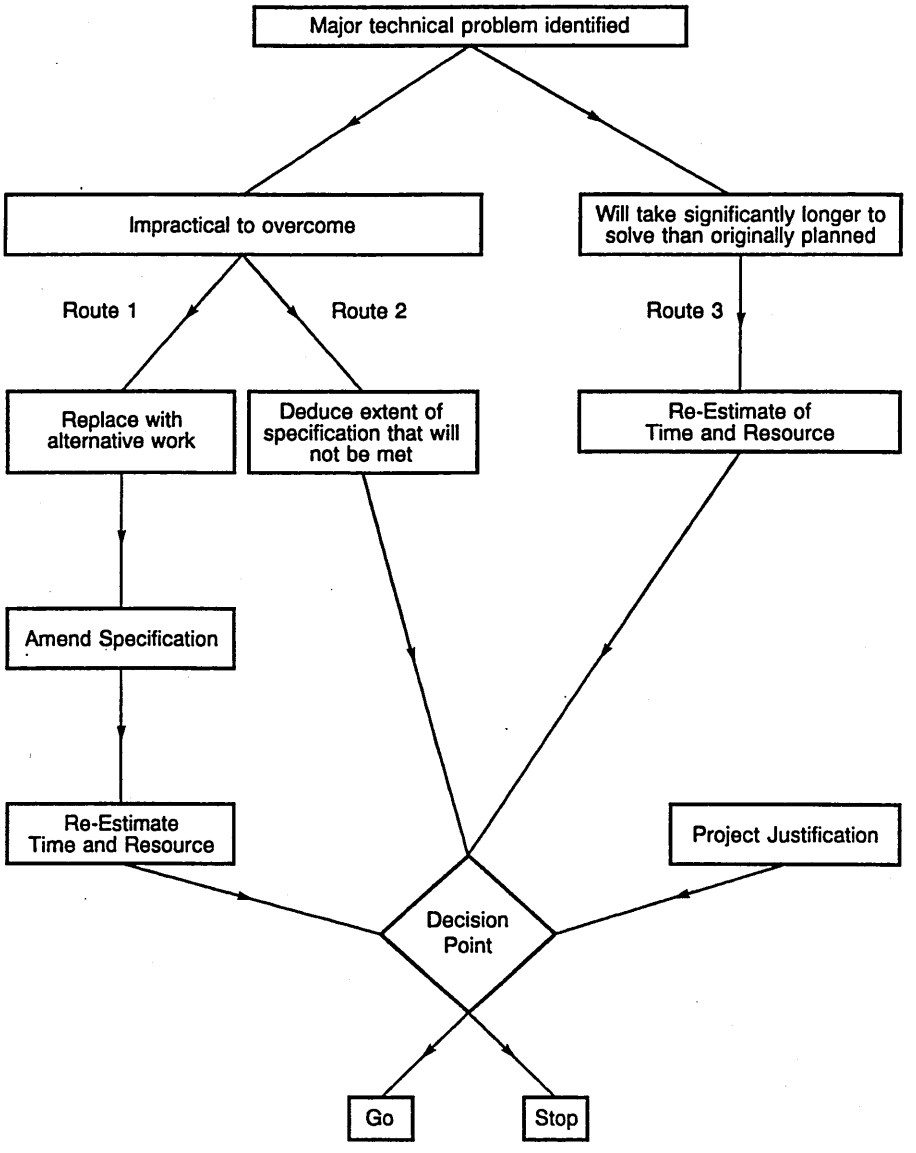

Figure 3.5 Back up strategy in case of a major technical problem

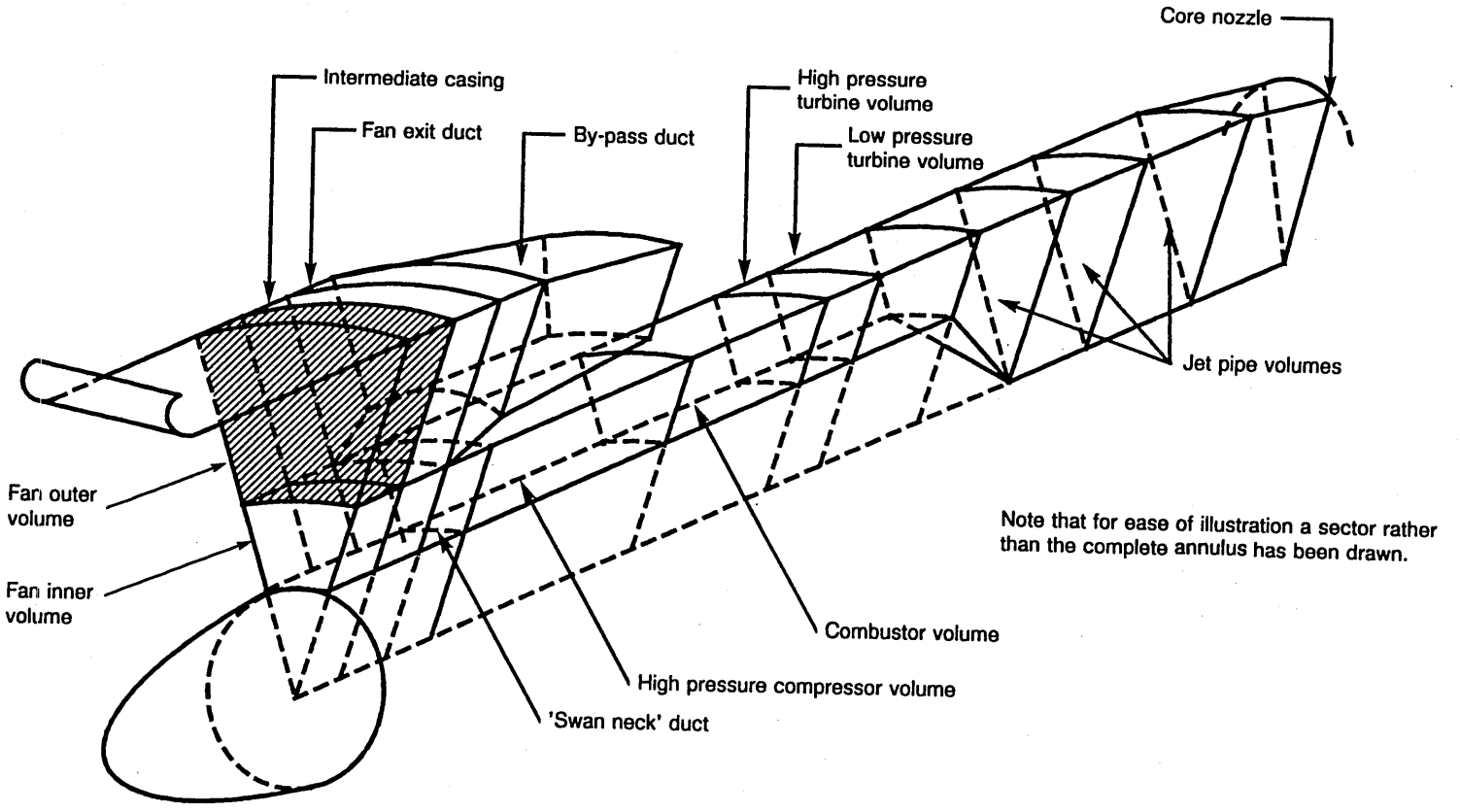

Figure 4.1 - Schematic illustration of a two-spool turbofan showing component volumes

Note that for ease of illustration a sector rather than the complete annulus has been drawn. The K planes are therefore cylindrical and the i planes annuli.

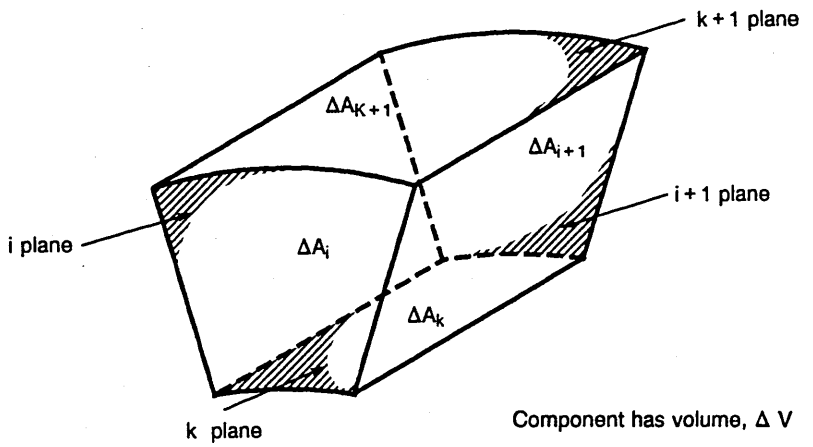

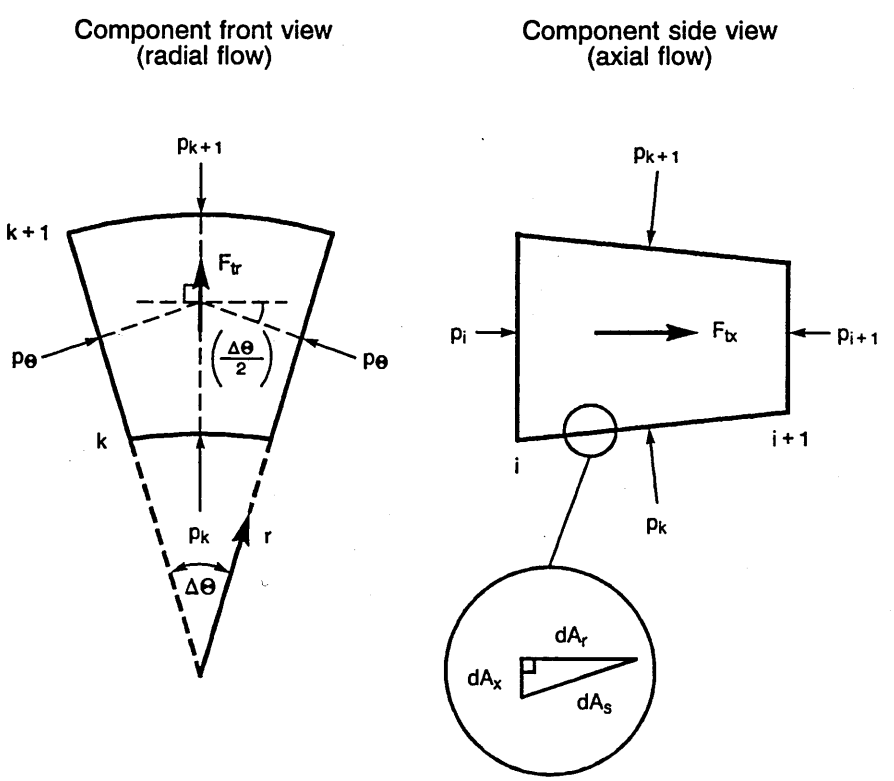

Note - all forces have positive direction as drawn

Figure 4.2 Component volume Geometry

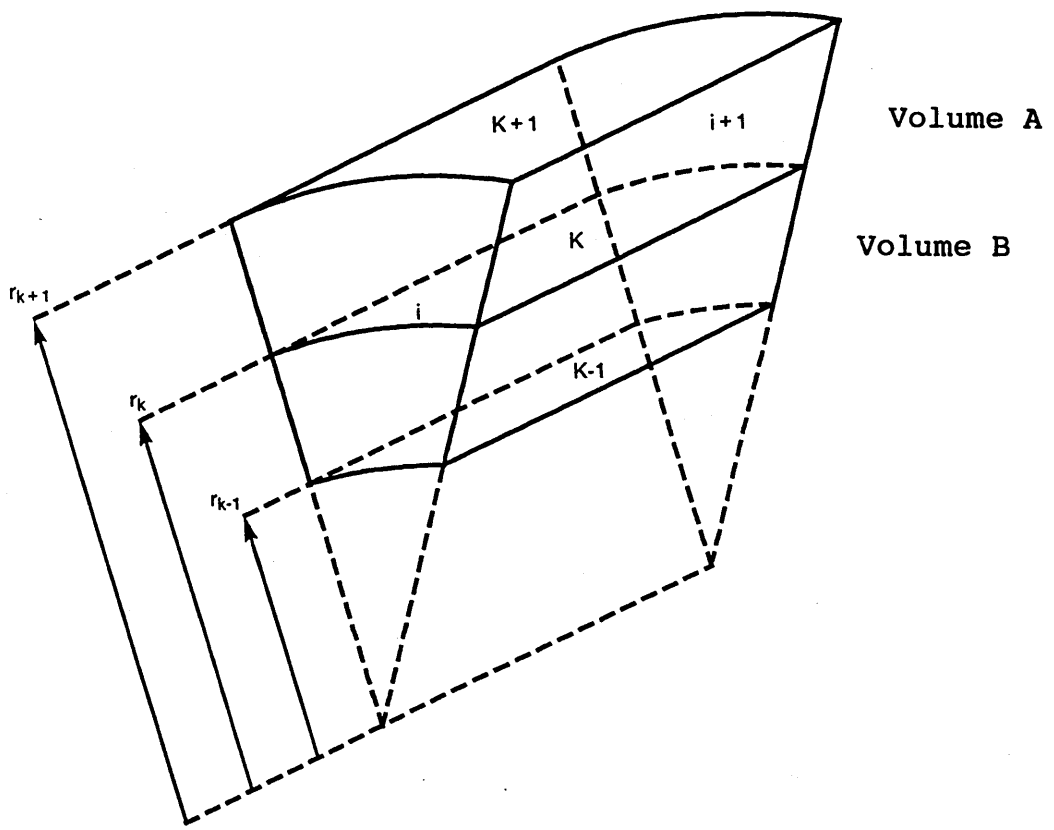

$$A_{K+\frac{1}{2}} = 2\pi\frac{1}{2}(r_{K+1} + r_K)L_A = L_A\pi(r_{K+1} + r_K)$$

$$A_{K-\frac{1}{2}} = 2\pi\frac{1}{2}(r_K + r_{K-1})L_B = L_B\pi(r_K + r_{K-1})$$

Figure 4.3 Component volume geometry with radial flow

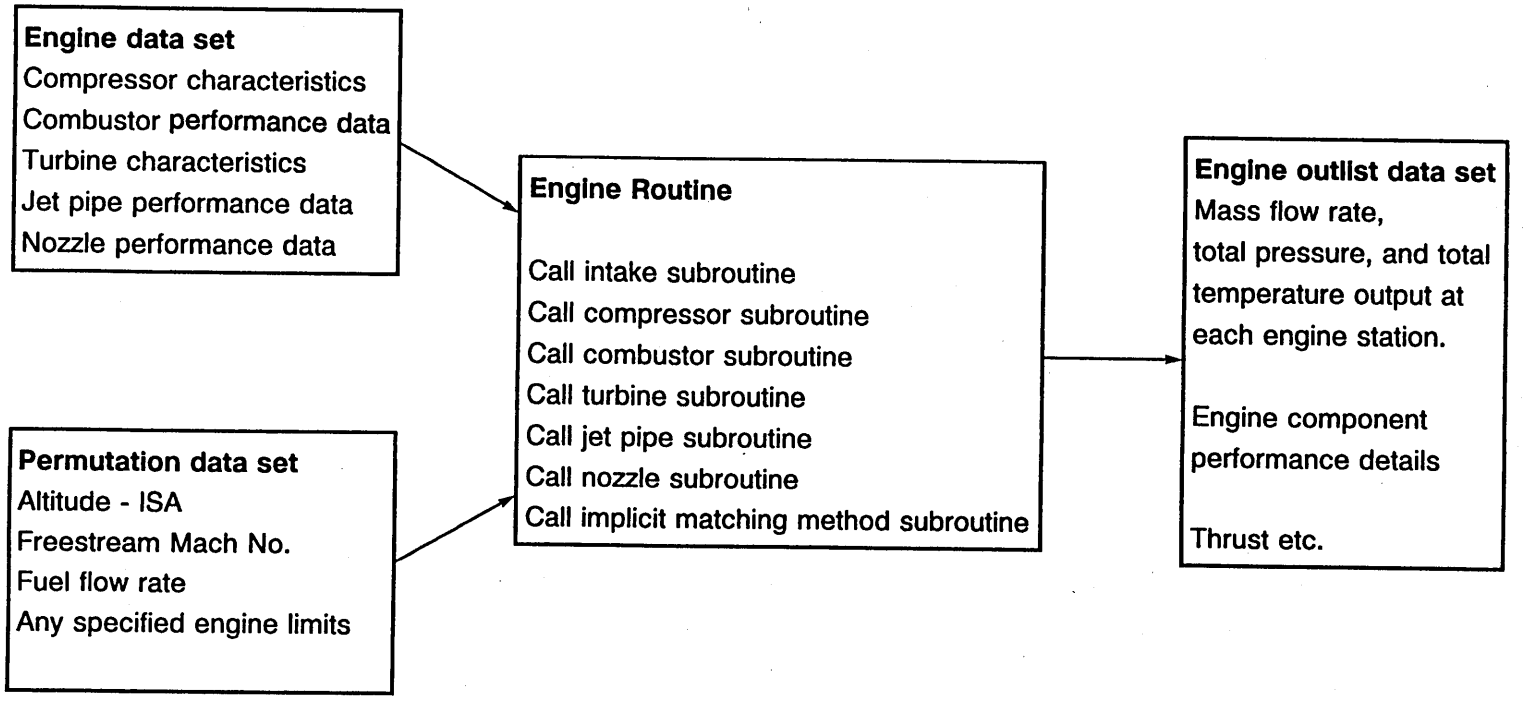

Figure 5.1 The RRAP System

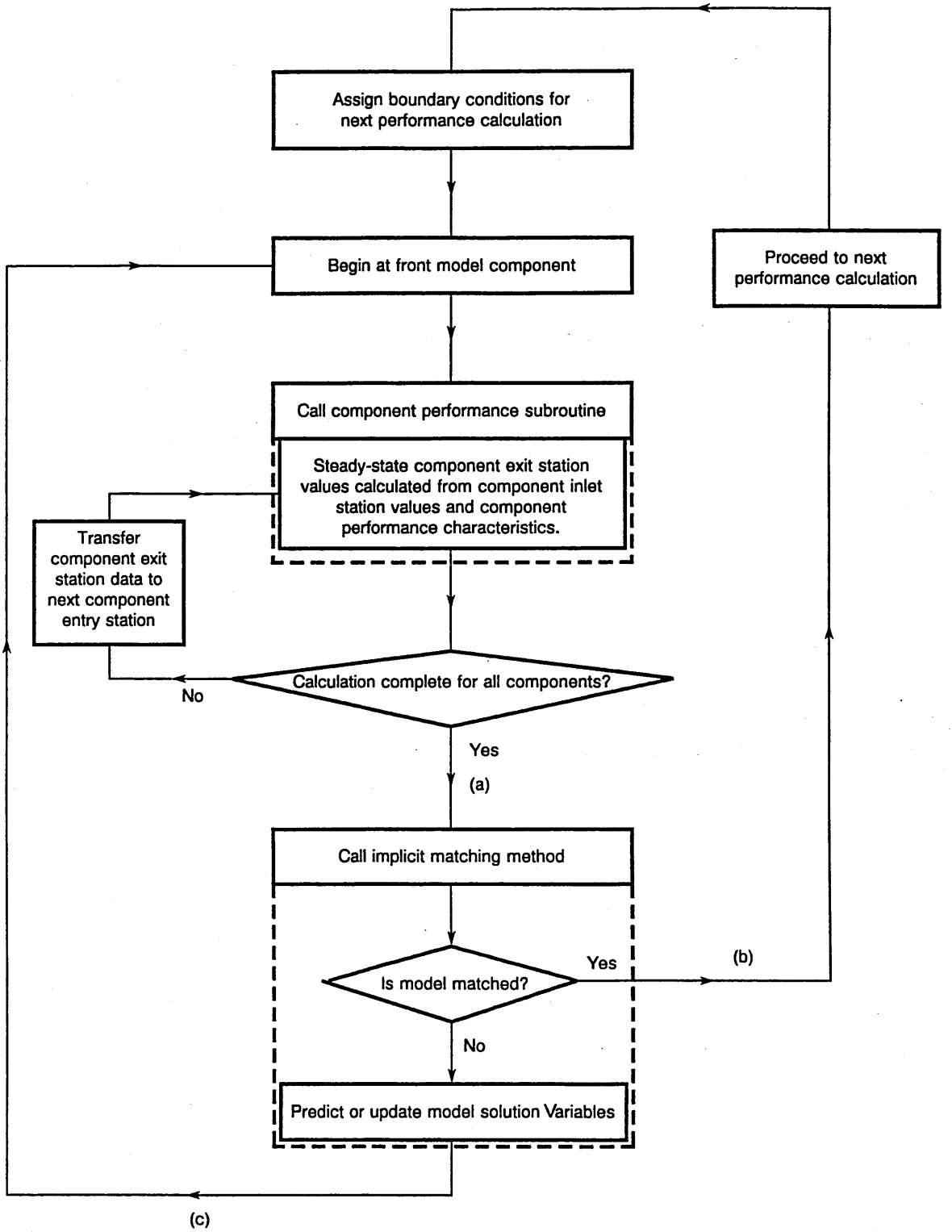

Figure 5.2 The RRAP system calculation sequence

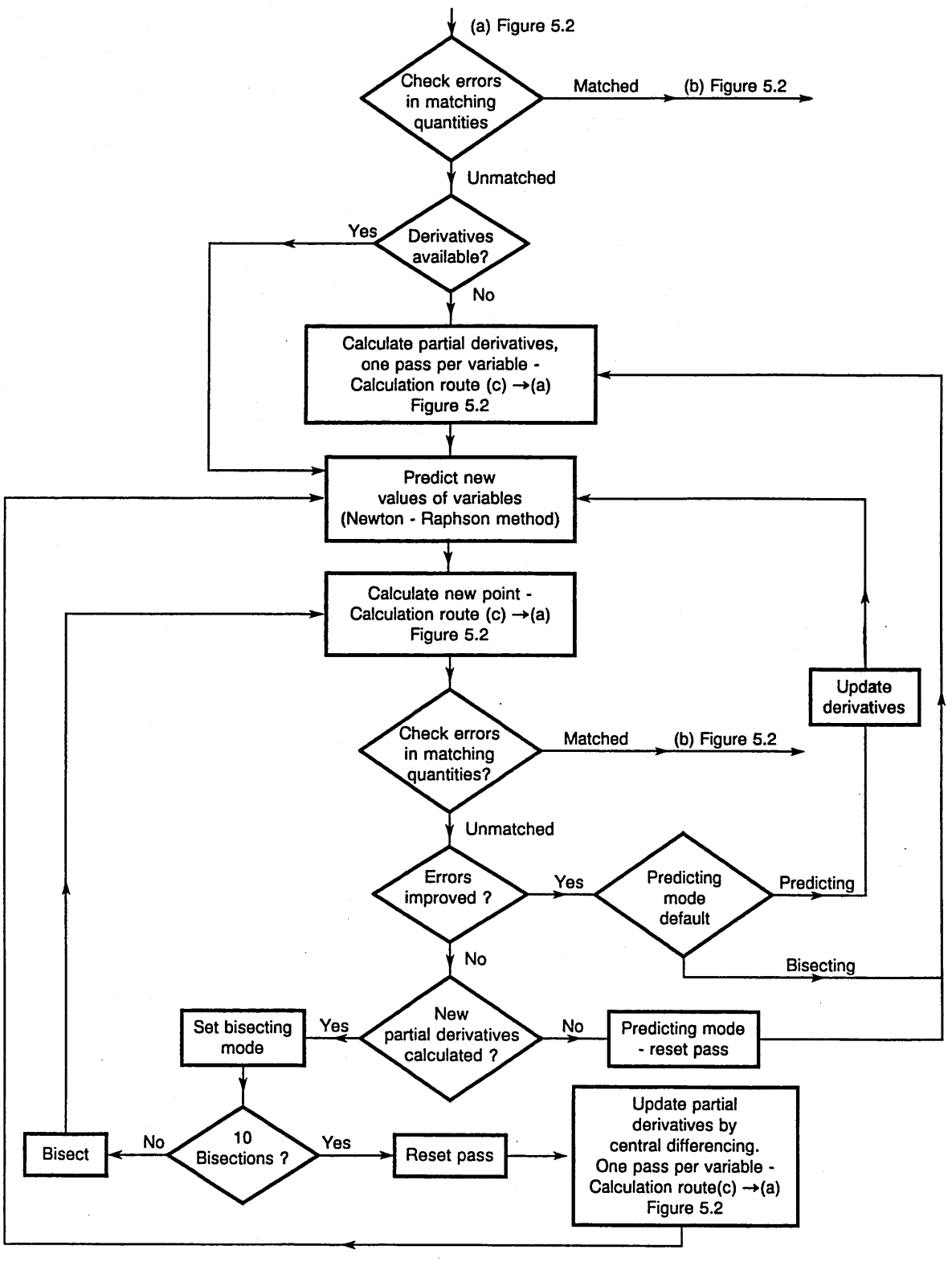

Figure 5.3 The logic sequence of the RRAP Implicit Matching Method

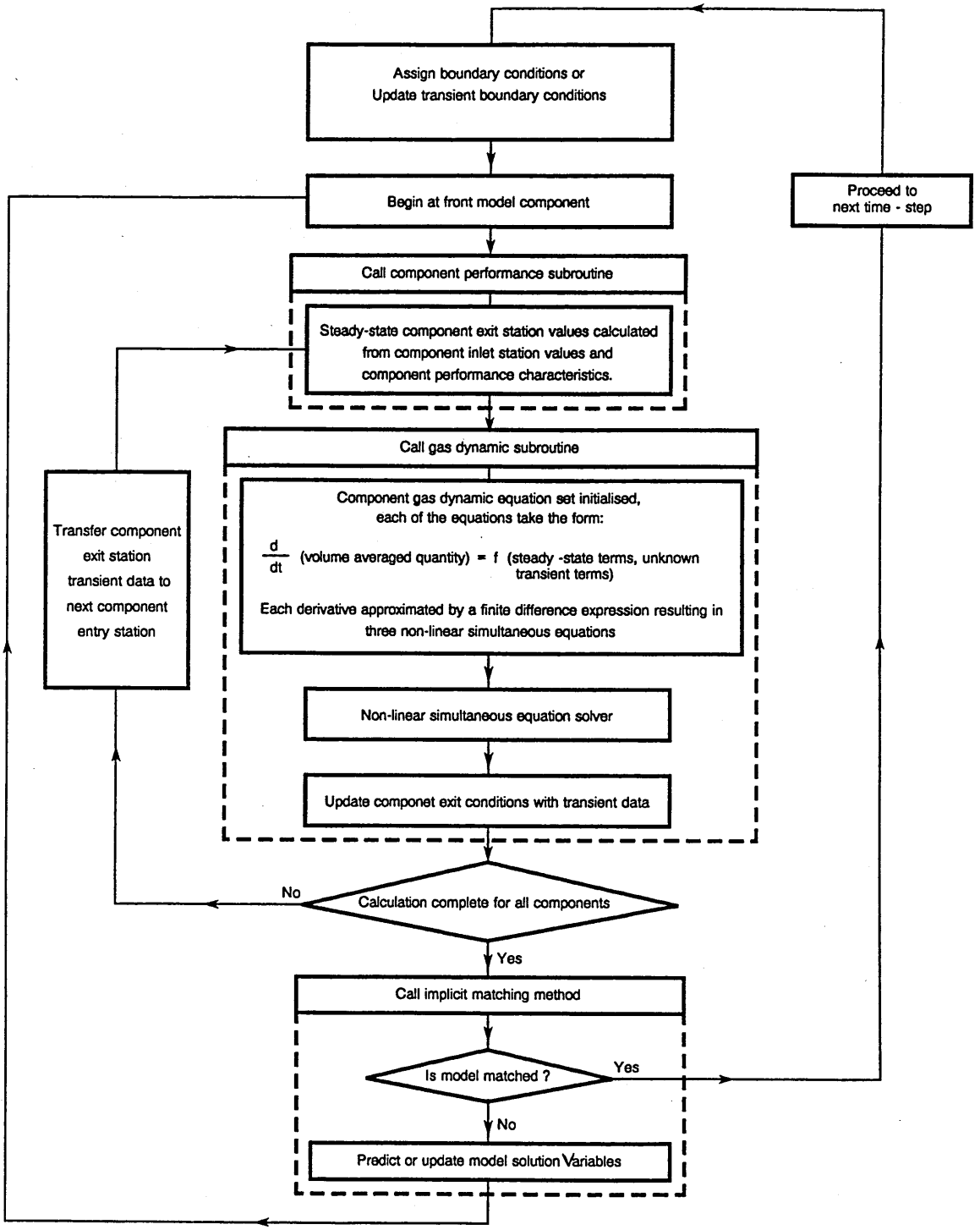

Figure 5.4 The RRAP system calculation sequence including the gas dynamic equation set

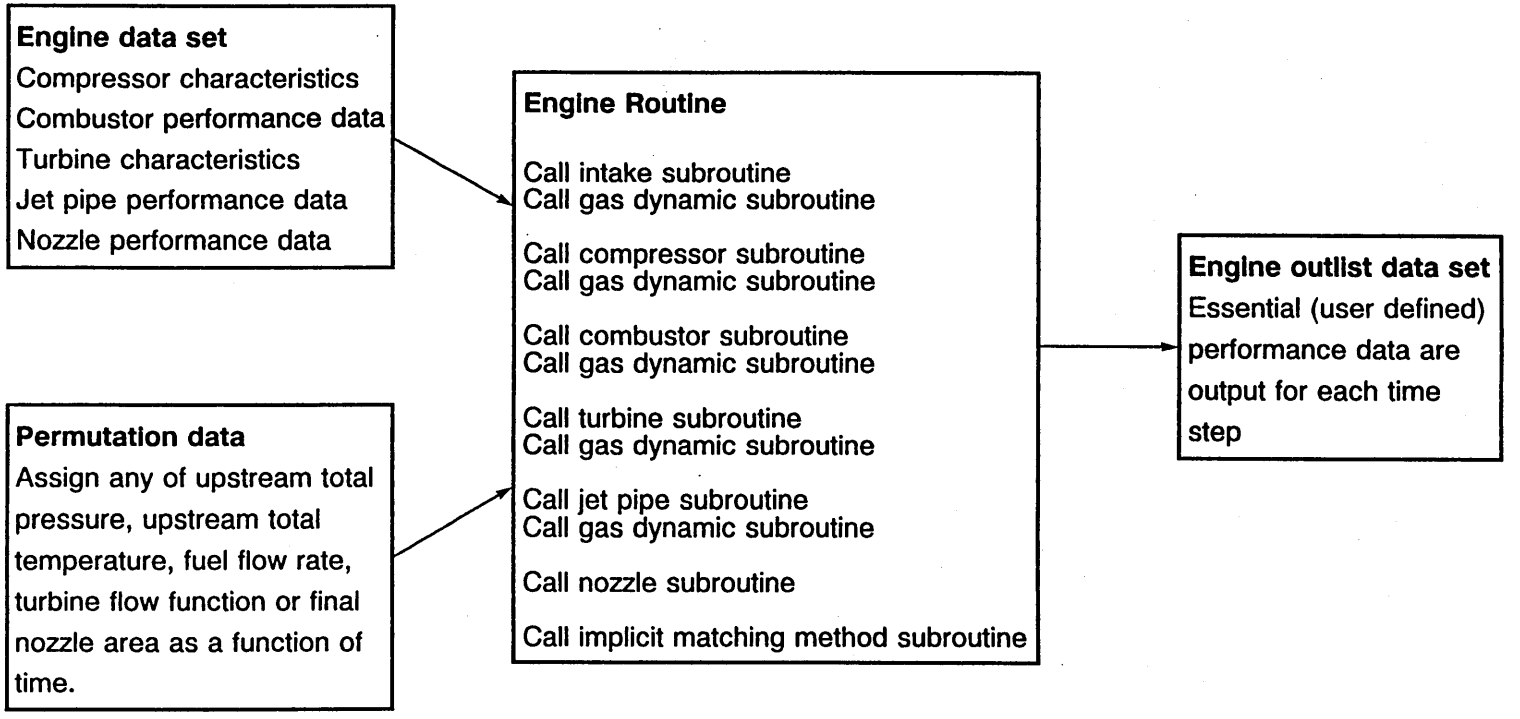

Figure 5.5 The RRAP System including gas dynamic prediction capability

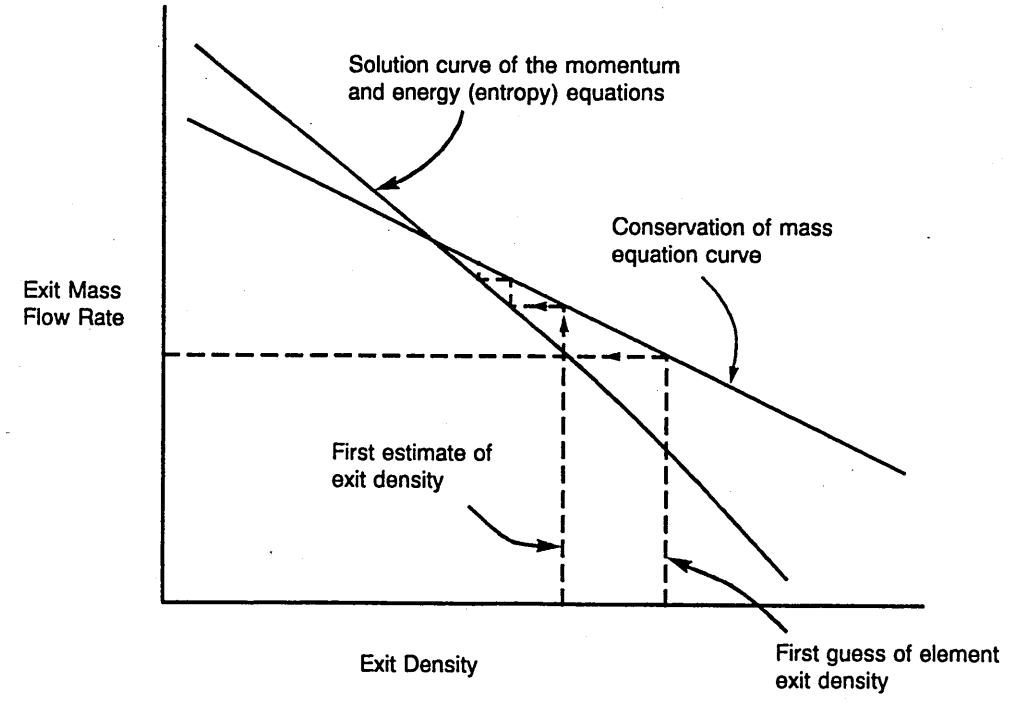

Figure 5.6a Gas dynamic equation set solution curves

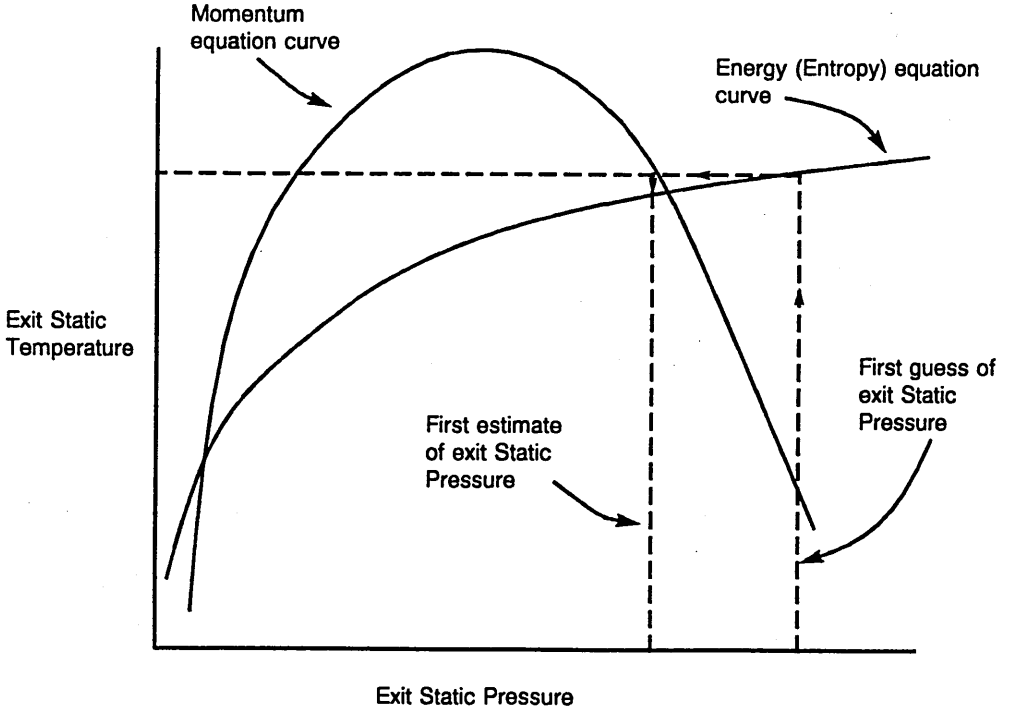

Figure 5.6b Gas dynamic equation set solution curves

Flow conditions throughout length of duct at time t

P = 101.325KPa

T = 288.15K

W = 25.0 Kg/s

M ≈ 0.5

Flow perturbed at time $t + \Delta t$ at station 1

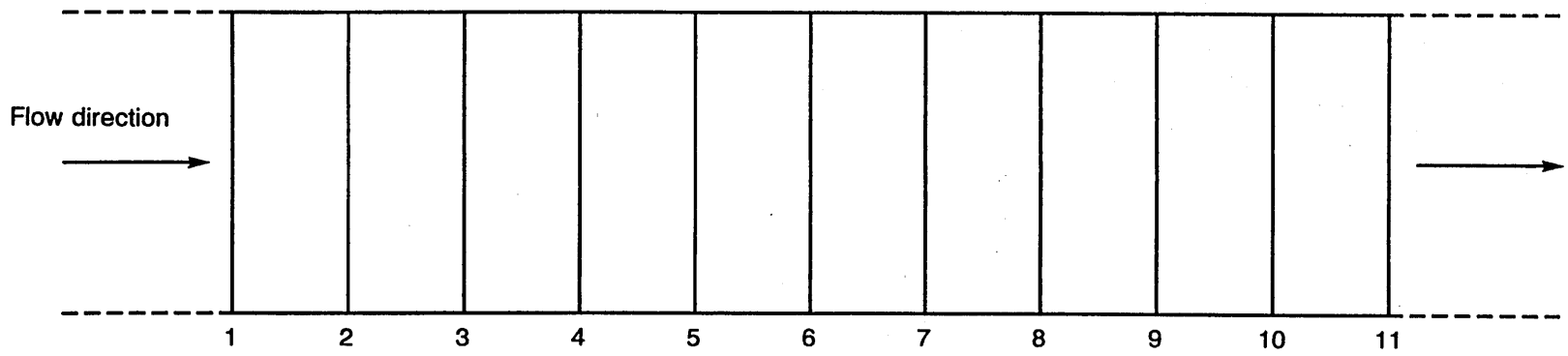

Duct cross section area = $0.14m^2$

Individual volume length = 0.2m

Figure 5.7 Simple duct model of infinite length

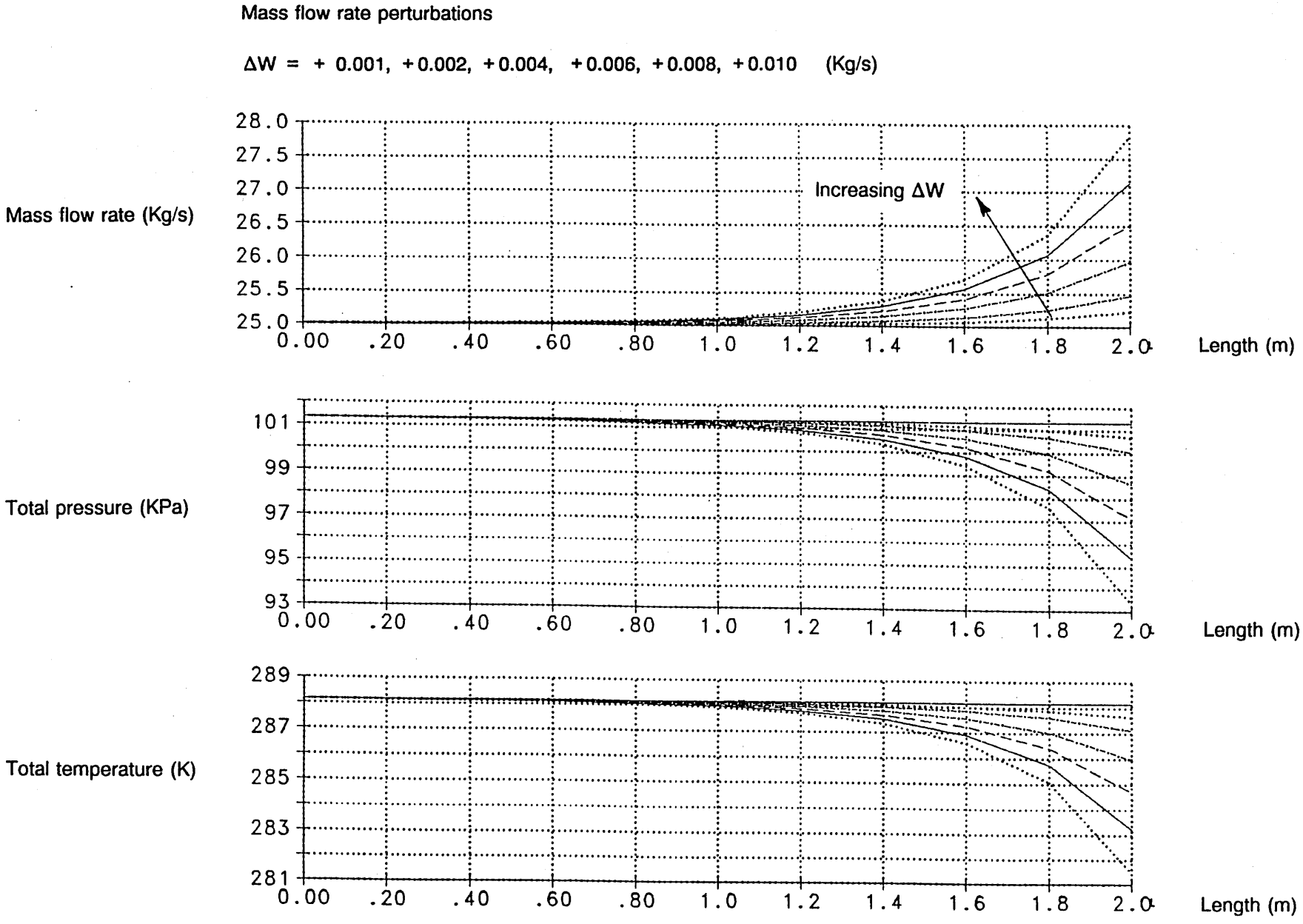

Figure 5.8a Gas dynamic equation set solutions

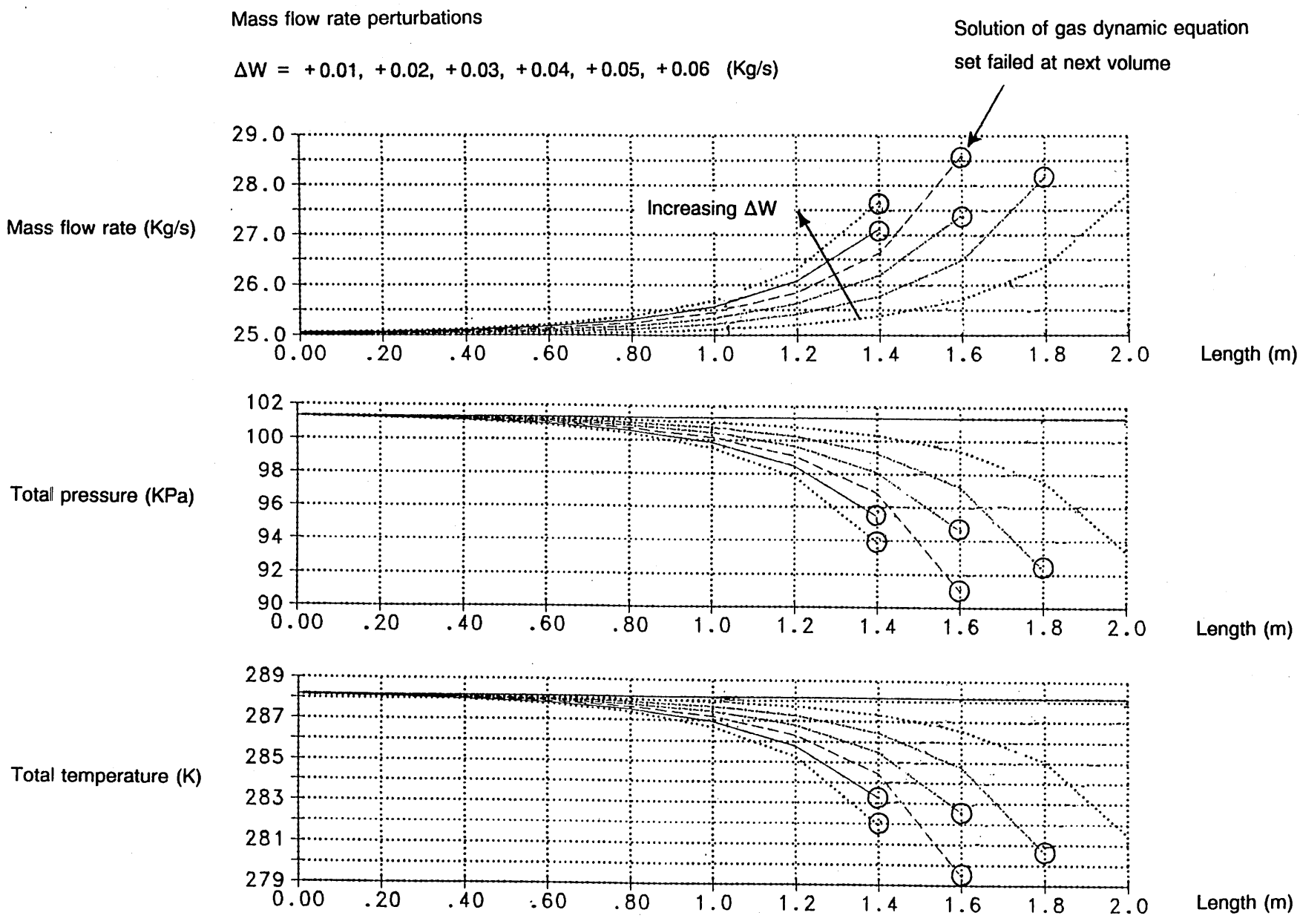

Figure 5.8b Gas dynamic equation set solution failure

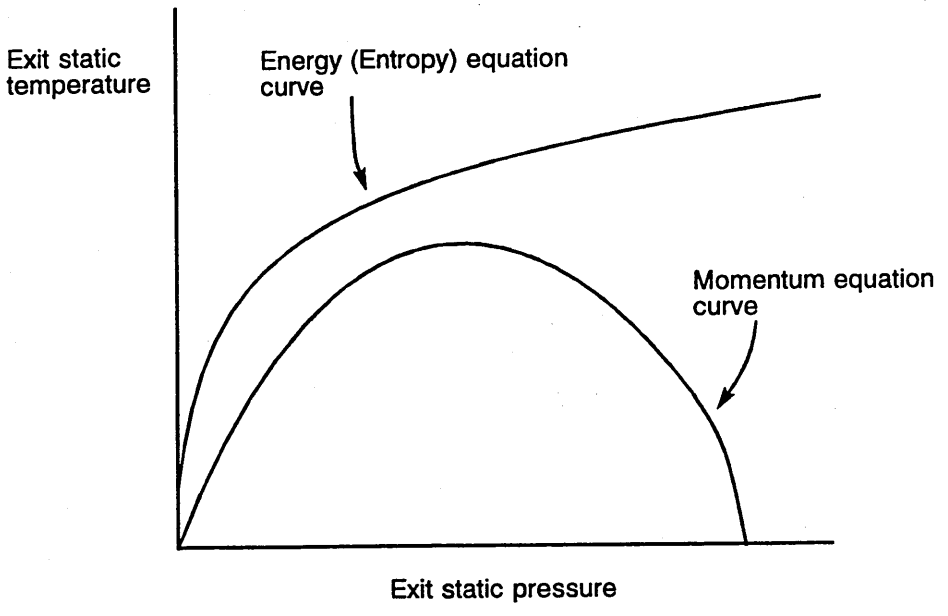

Figure 5.9a Gas dynamic equation set solution failure

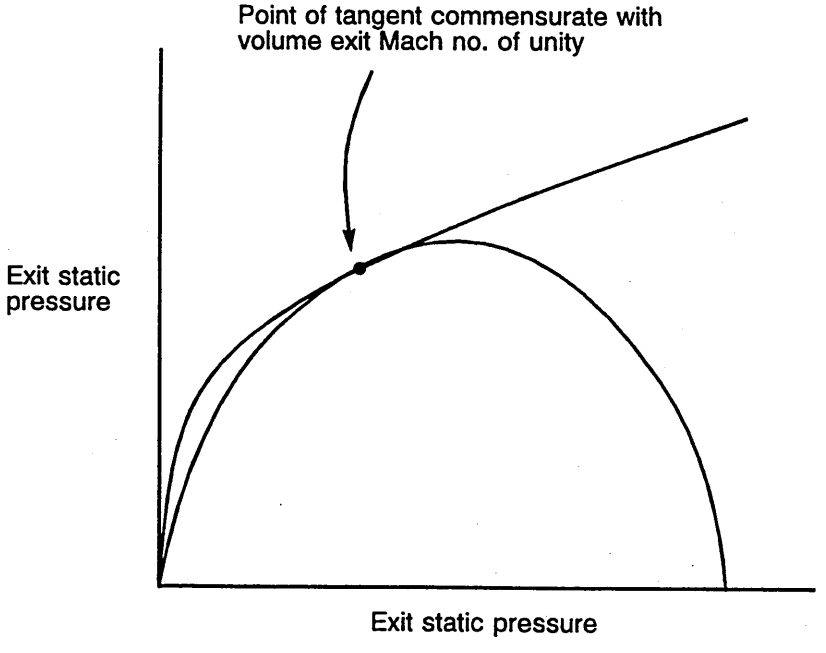

Figure 5.9b Gas dynamic equation set limit of solution

Below are two adjoining component volumes drawn apart to illustrate the application of the extra Matching Quantities and Variables required to maintain numerical stability.

Note that the value of mass flow rate W, and pressure P, at entry to volume 2 is set by their respective variable values and not by the exit values of volume 1. Divergence in successive solutions of the gas dynamic equation set is therefore prevented.

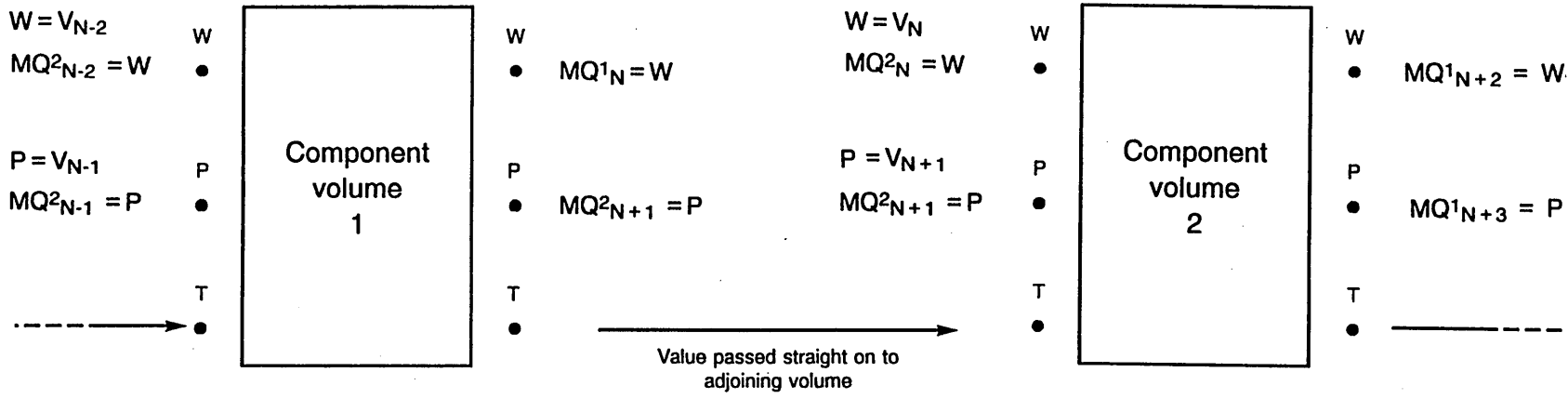

The system of equations is matched when

$MQ^1_N = MQ^2_N = V_N$

$MQ^1_{N+1} = MQ^2_{N+1} = V_{N+1}$

etc for all Matching Quantity pairs

MQ^1 and MQ^2 = Matching Quantity pair

V = Variable

Figure 5.10 Gas dynamic equation set stability control

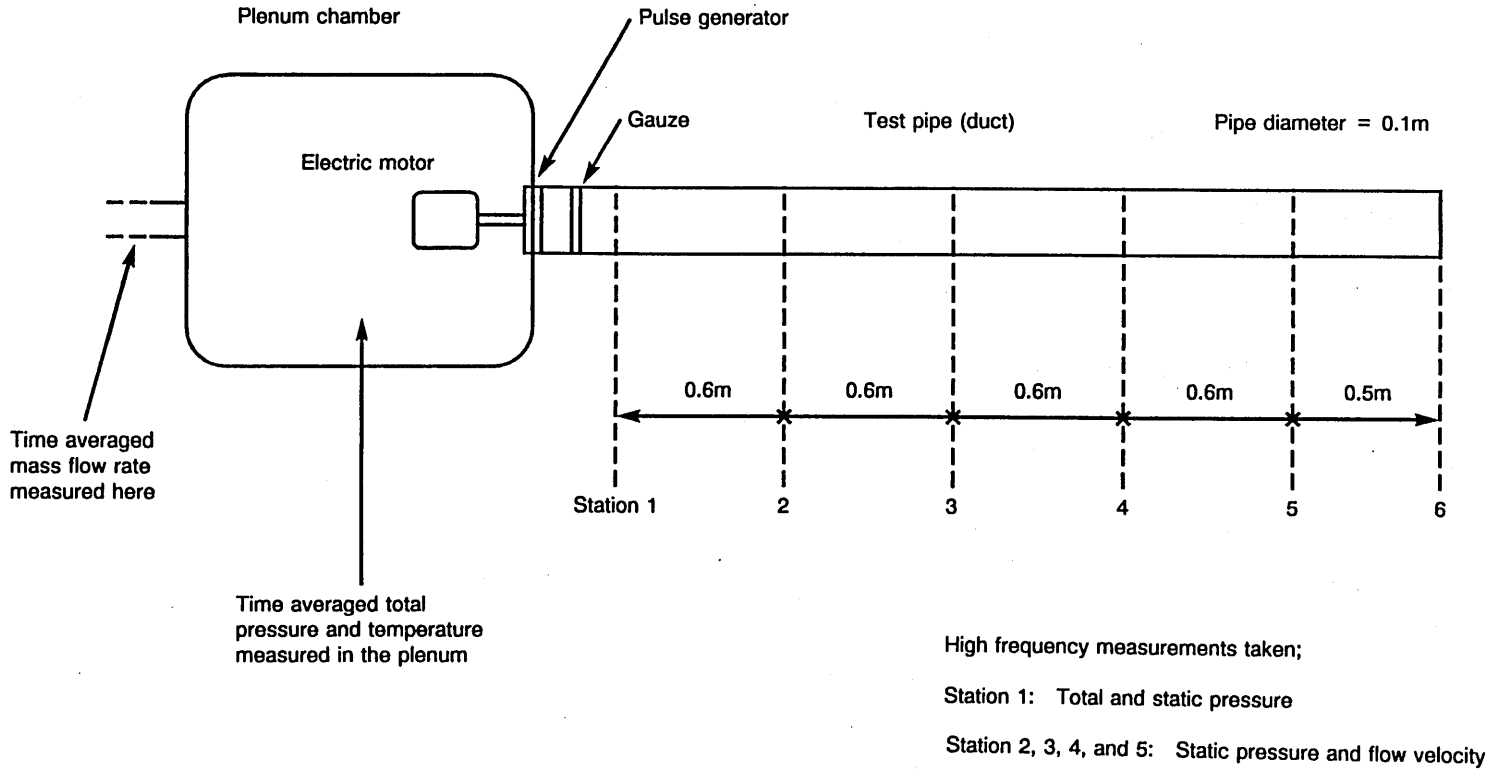

Figure 5.11 Schematic illustration of duct rig

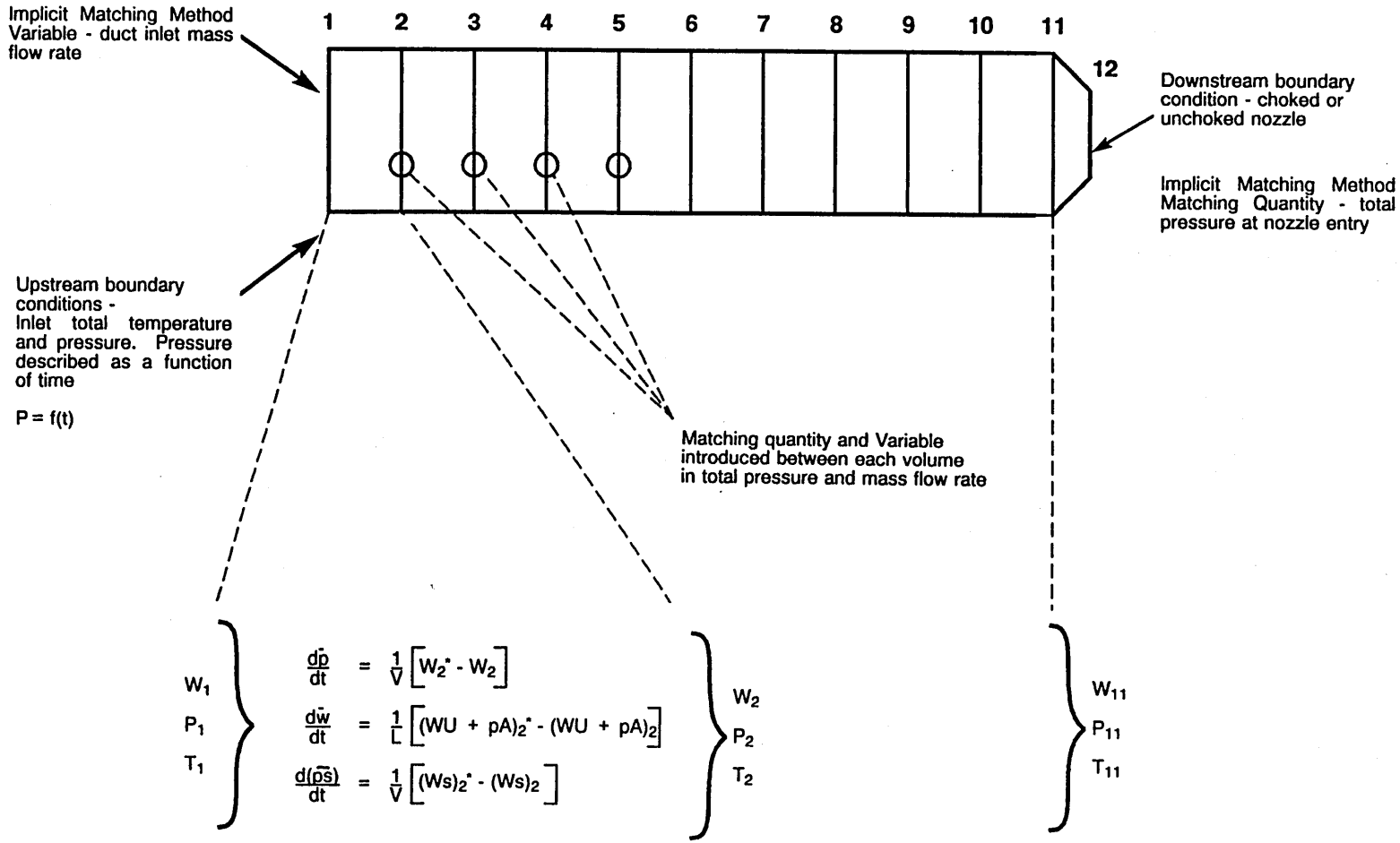

Figure 5.12 RRAP duct Model

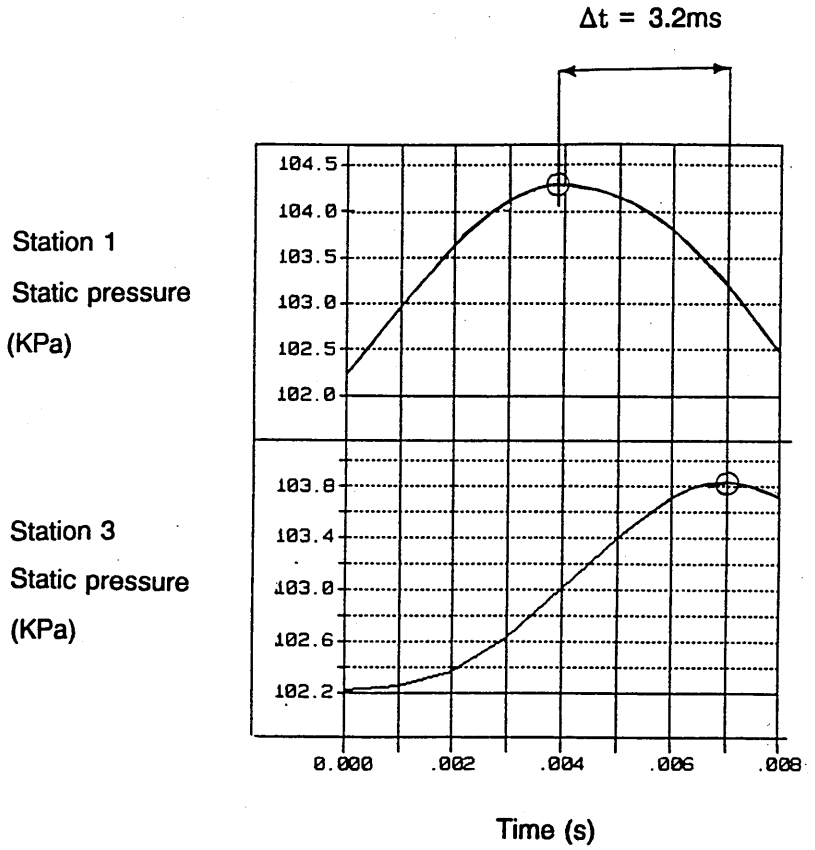

Wave speed ≈ $\frac{1.2}{0.0032}$ = 375ms^{-1}

Average flow velocity = 29ms^{-1}

Acoustic speed = $(\gamma R\, t)^{1/2}$

= 342 ms^{-1}

Therefore, acoustic speed ≈

Wave speed - Average flow velocity

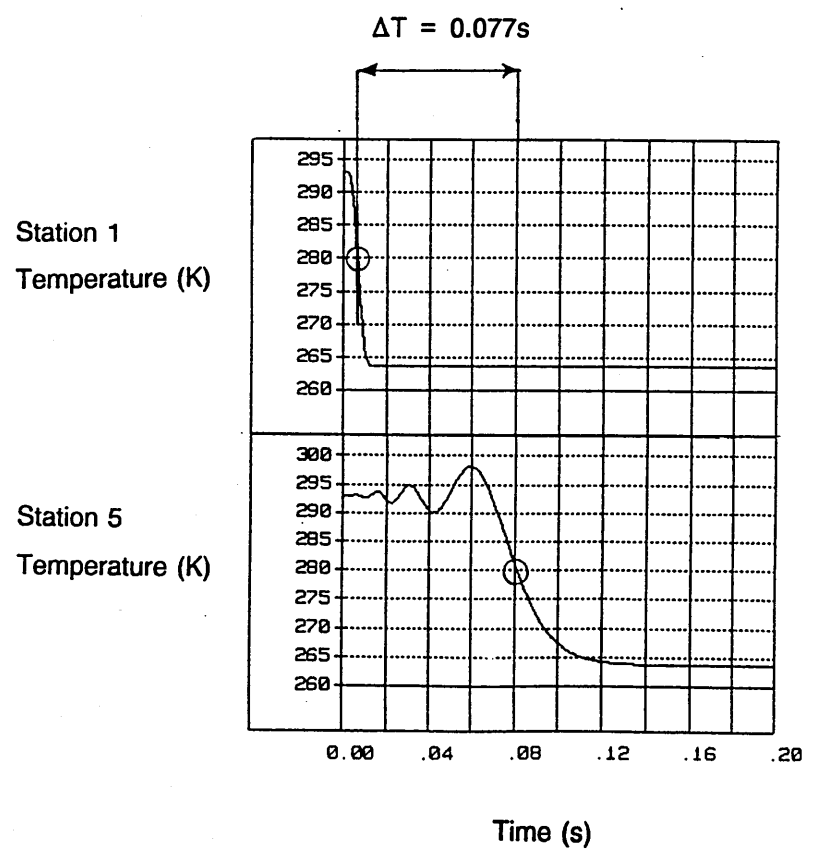

Propagation speed ≈ $\frac{2.4}{0.078}$

=31 ms^{-1}

Figure 5.13 Simulation of propagation of flow disturbances

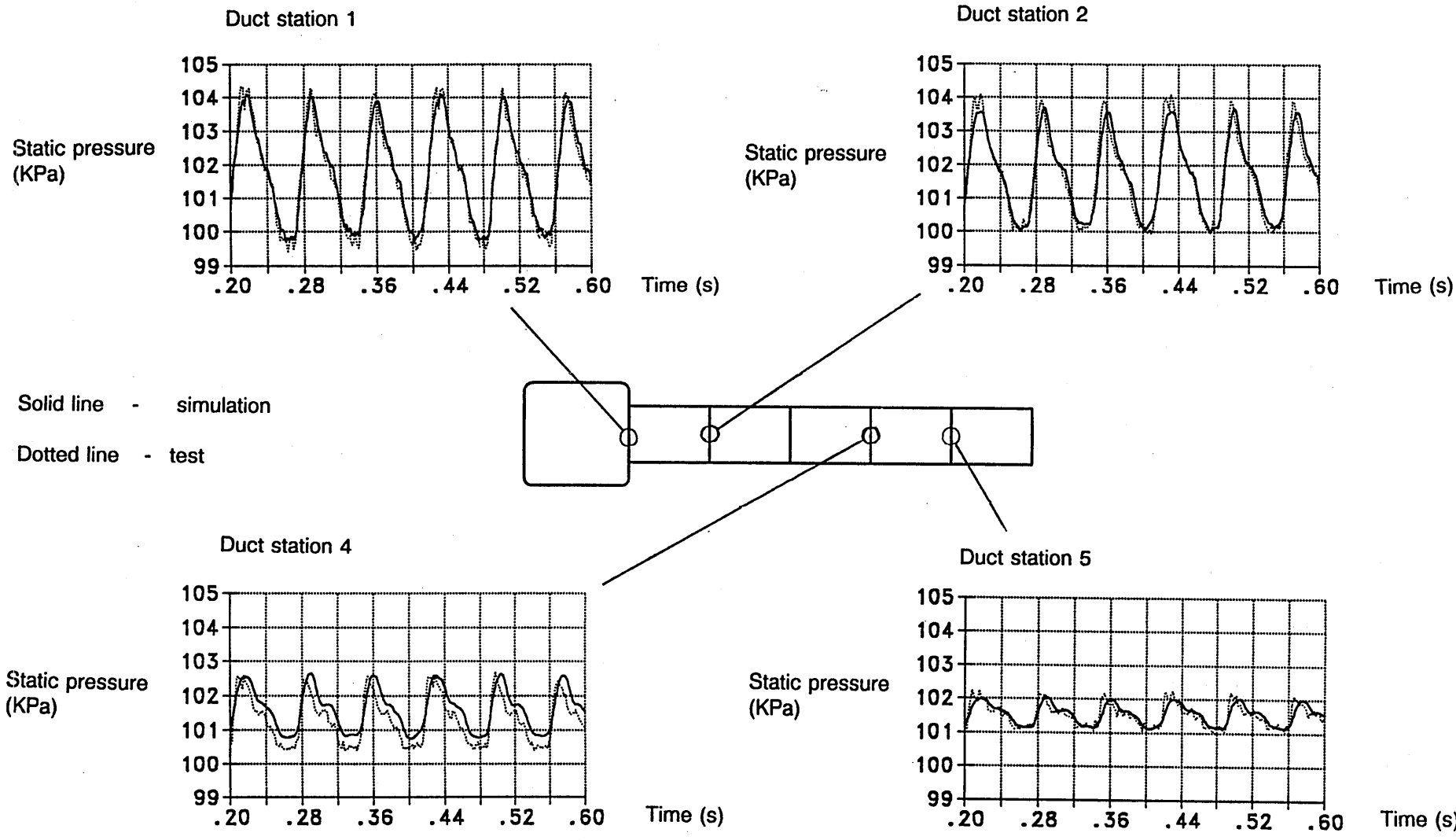

Figure 5.14a Comparison of test and simulated high-frequency - transient duct flow - 14Hz

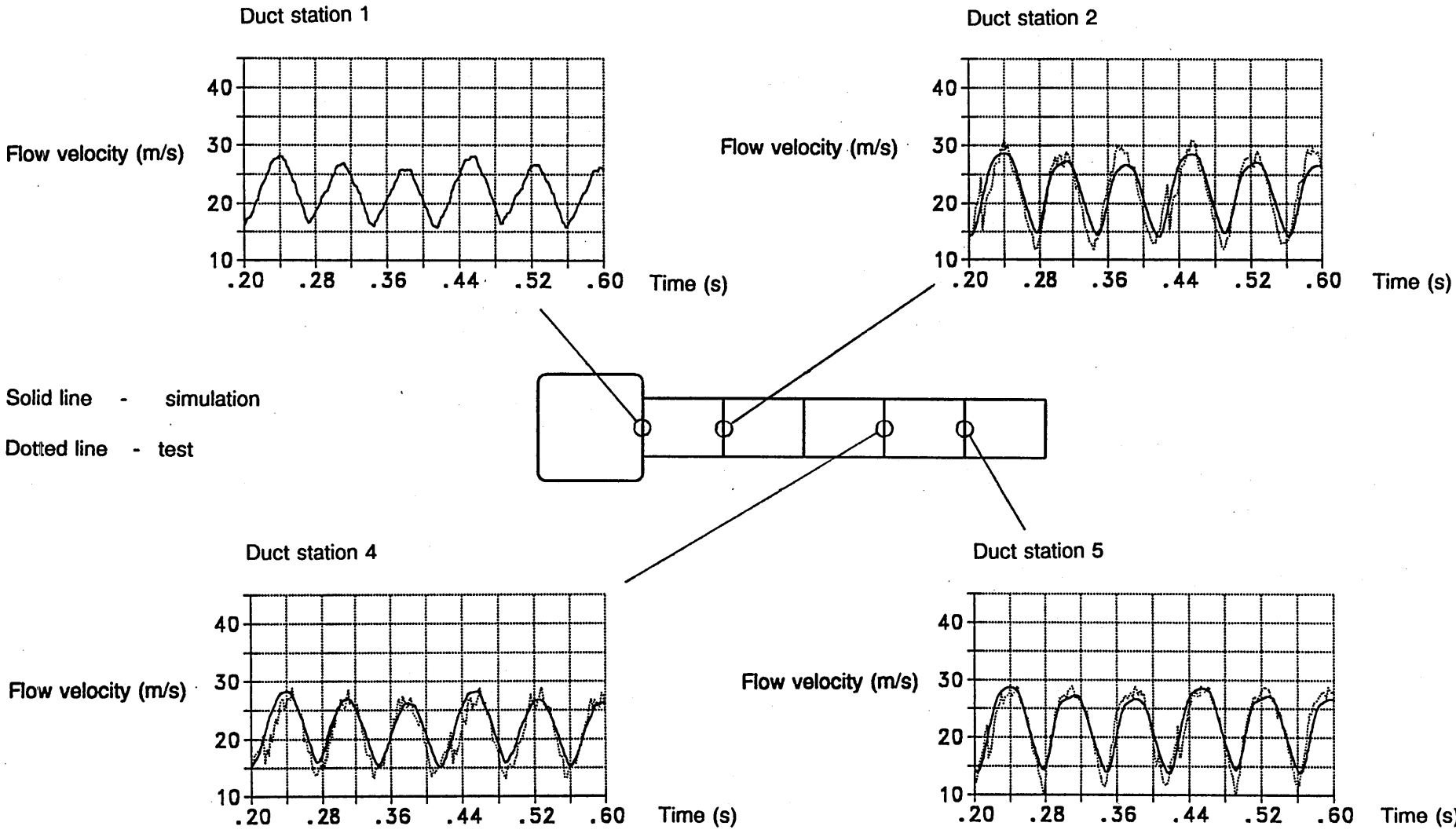

Figure 5.14b Comparison of test and simulated high-frequency - transient duct flow - 14Hz

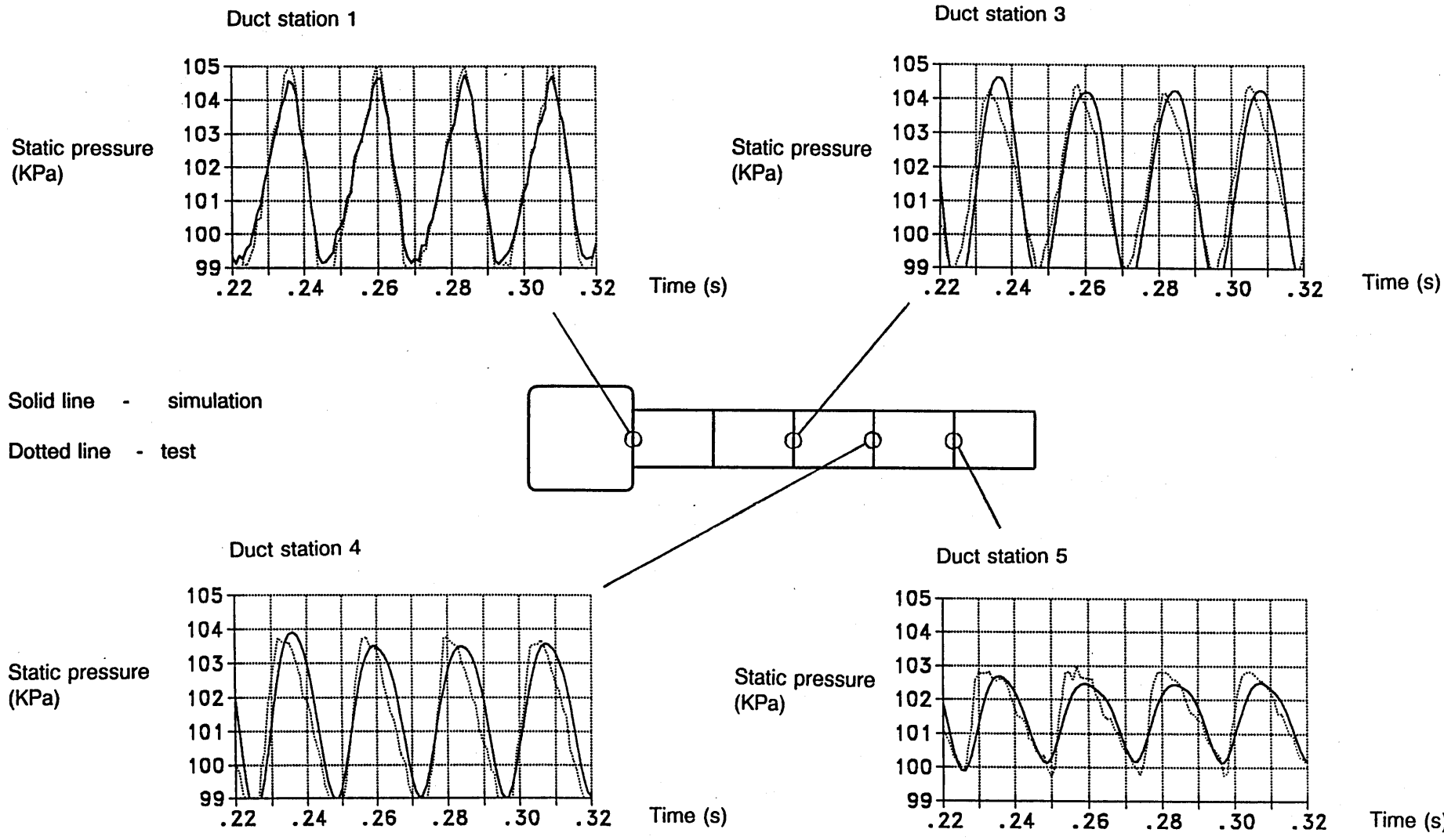

Figure 5.15a Comparison of test and simulated high-frequency - transient duct flow - 40Hz

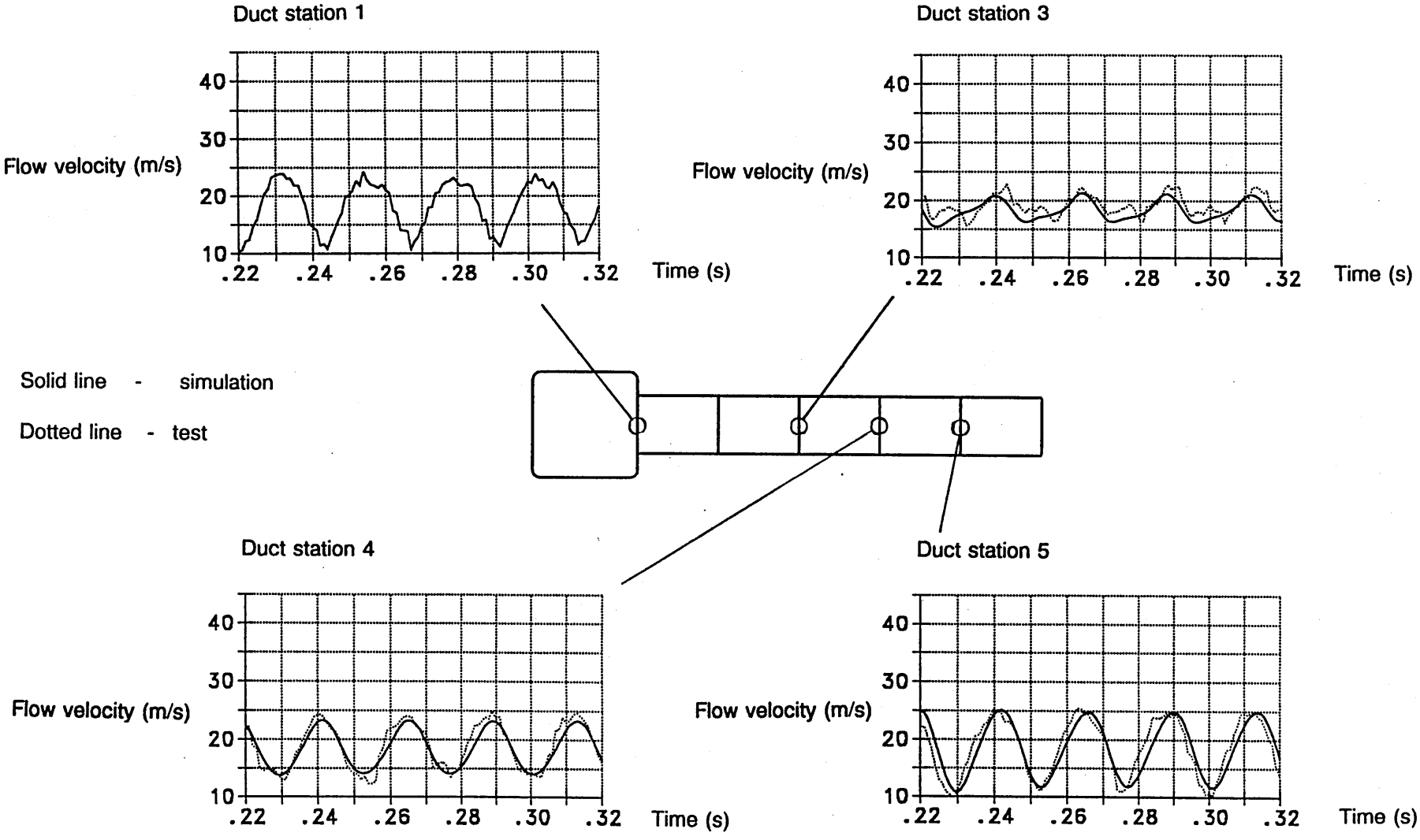

Figure 5.15b Comparison of test and simulated high-frequency - transient duct flow - 40Hz

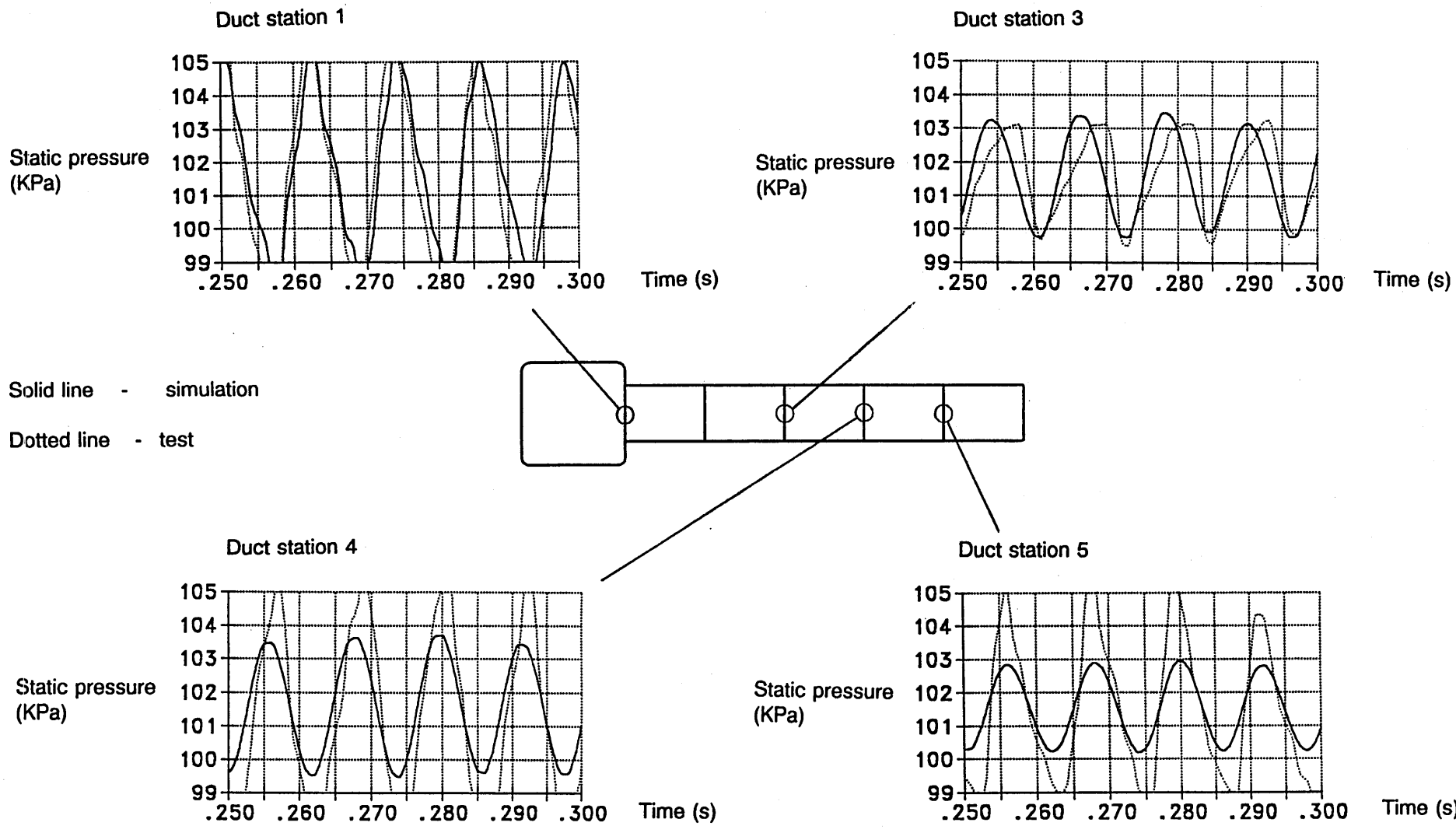

Figure 5.16 Comparison of test and simulated high-frequency - transient duct flow - 80Hz

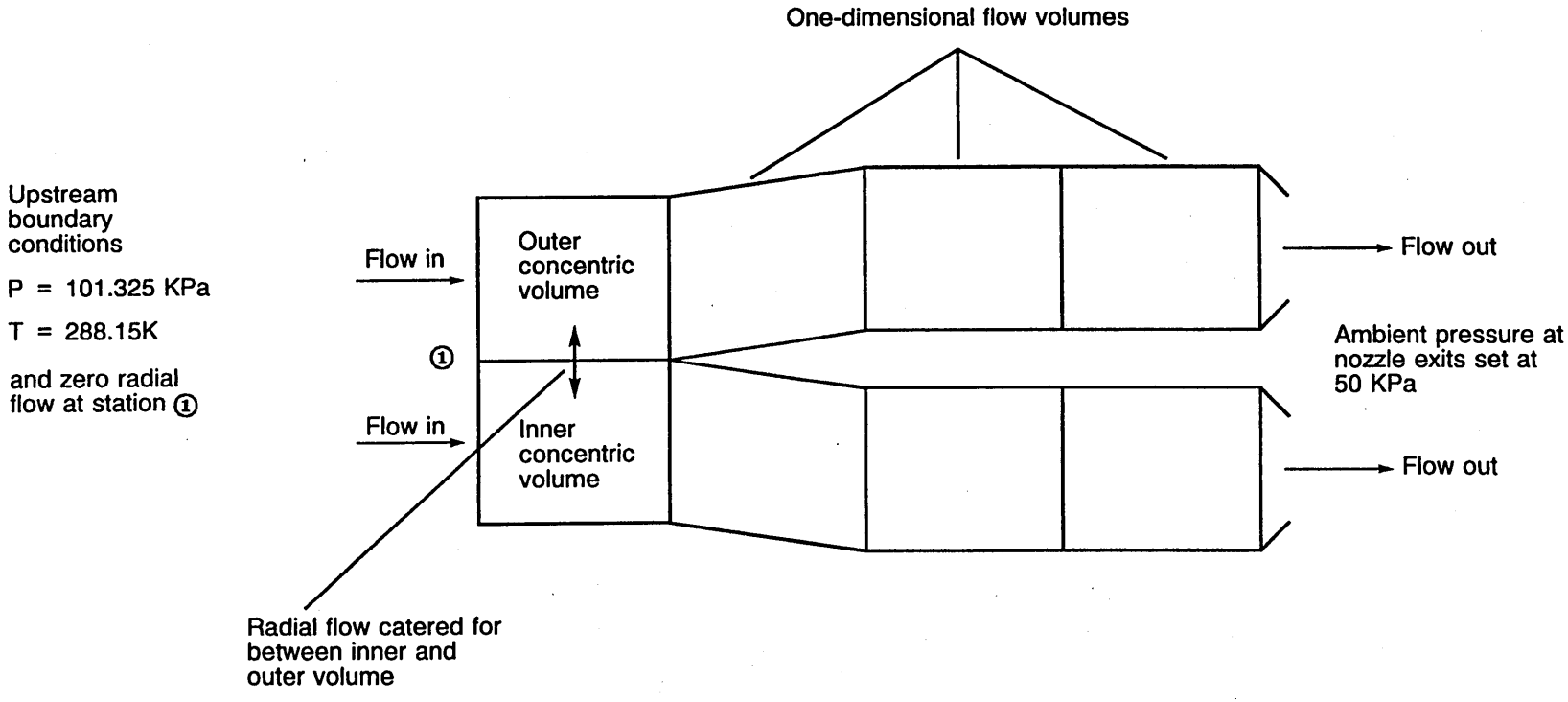

Figure 5.17 RRAP twin duct model

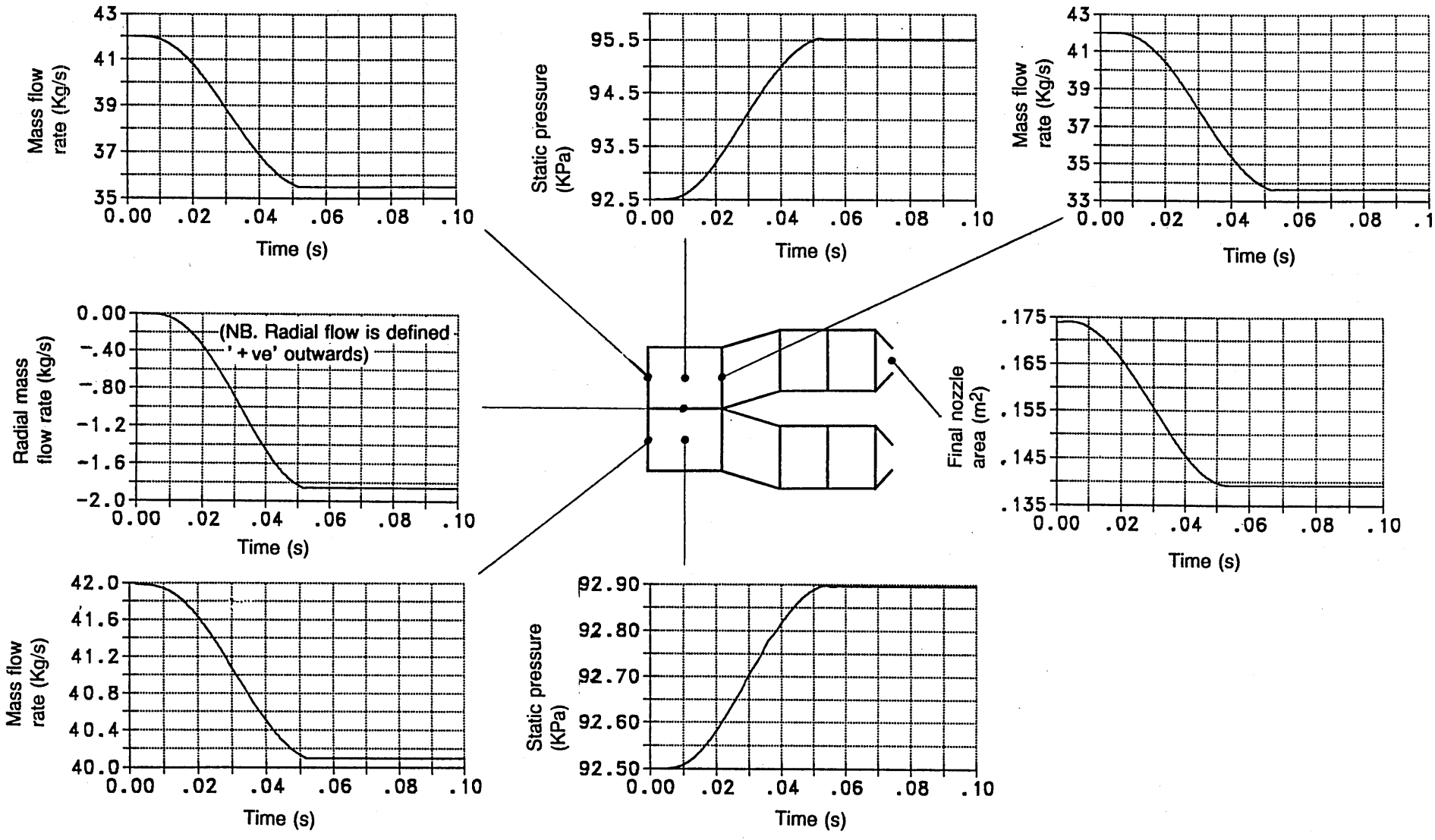

Figure 5.18 RRAP twin duct model steady-state radial flow simulation

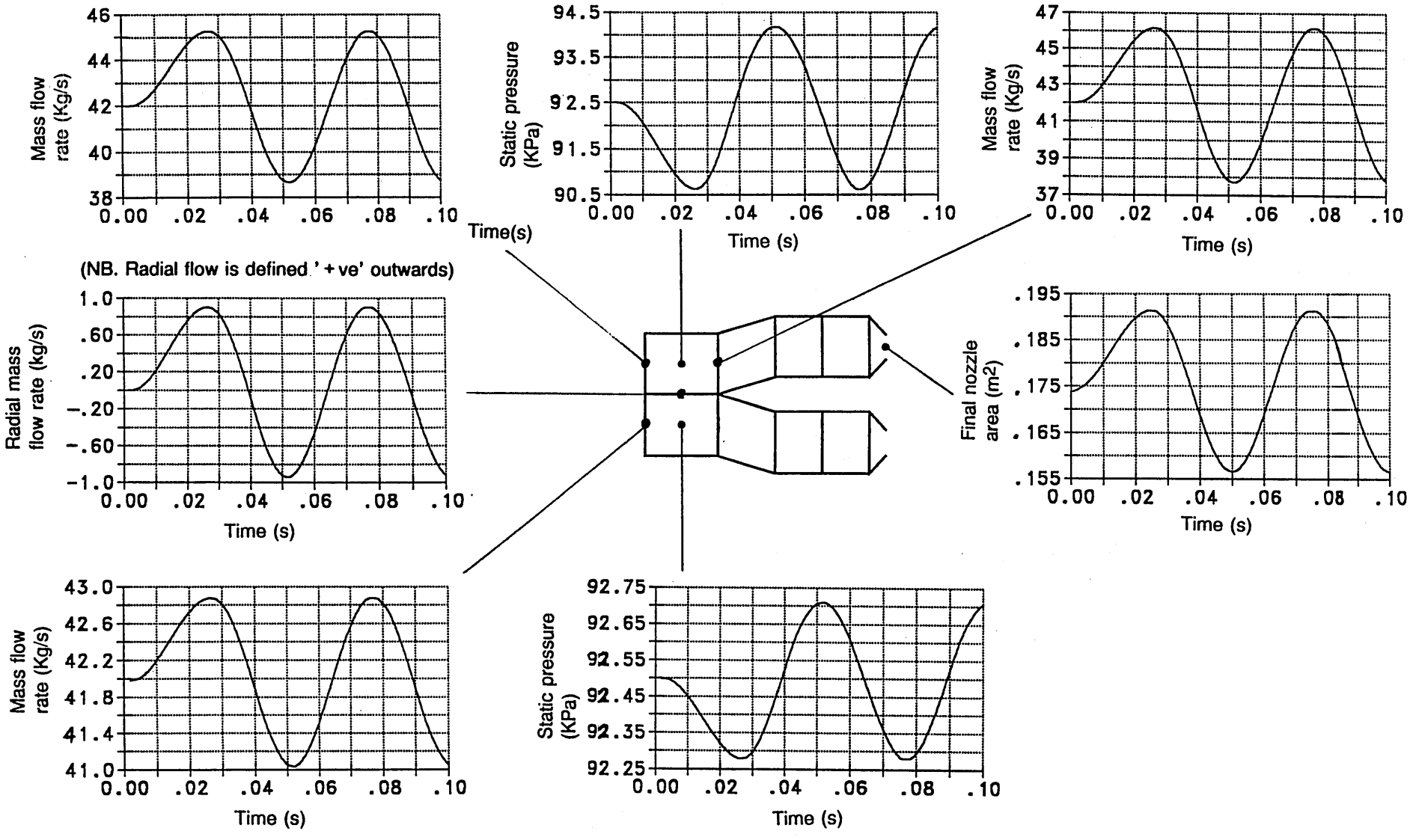

Figure 5.19a RRAP twin duct model transient radial flow simulation

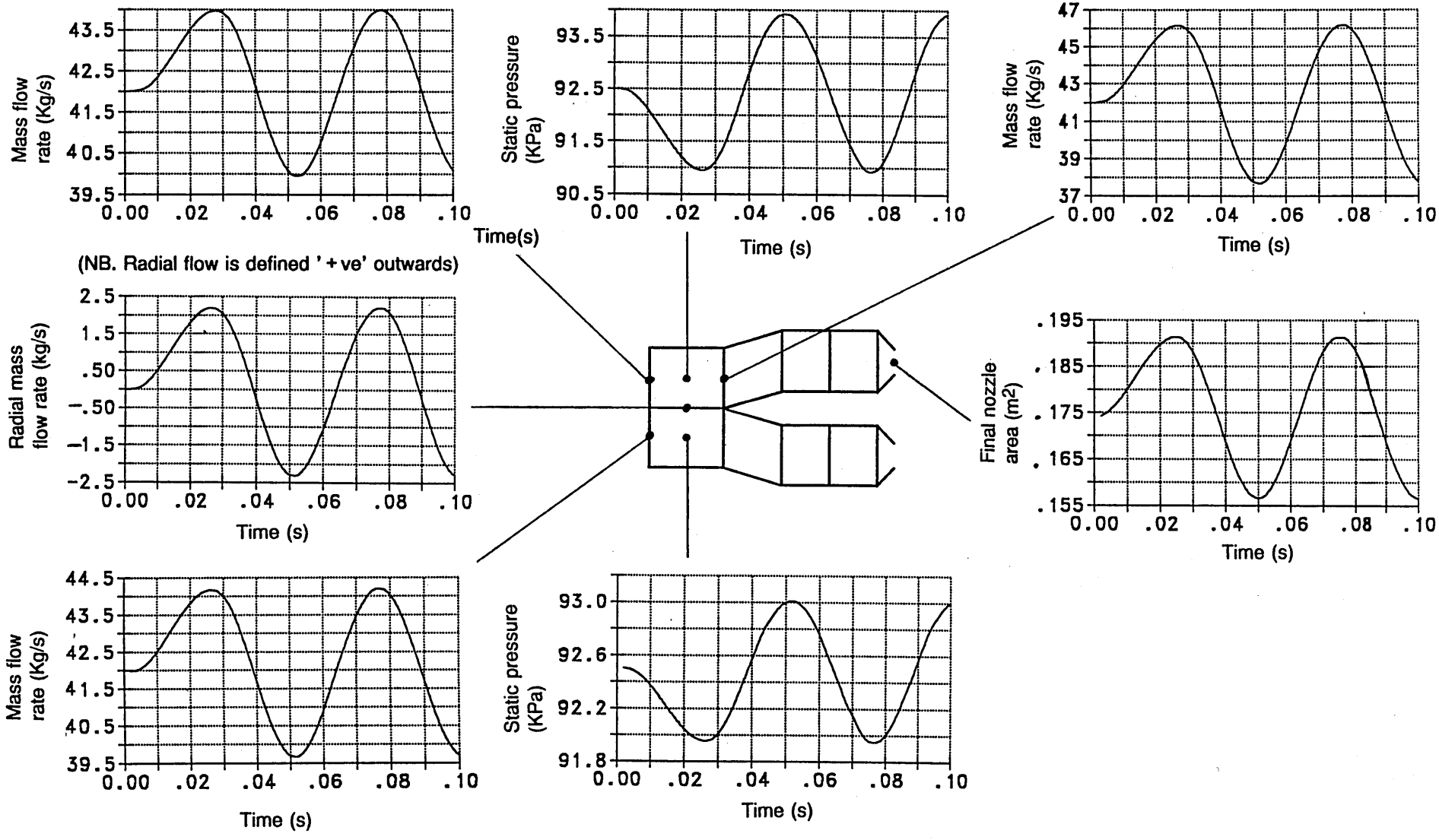

Figure 5.19b RRAP twin duct model transient radial flow simulation

Compressor beta lines drawn on a typical compressor characteristic

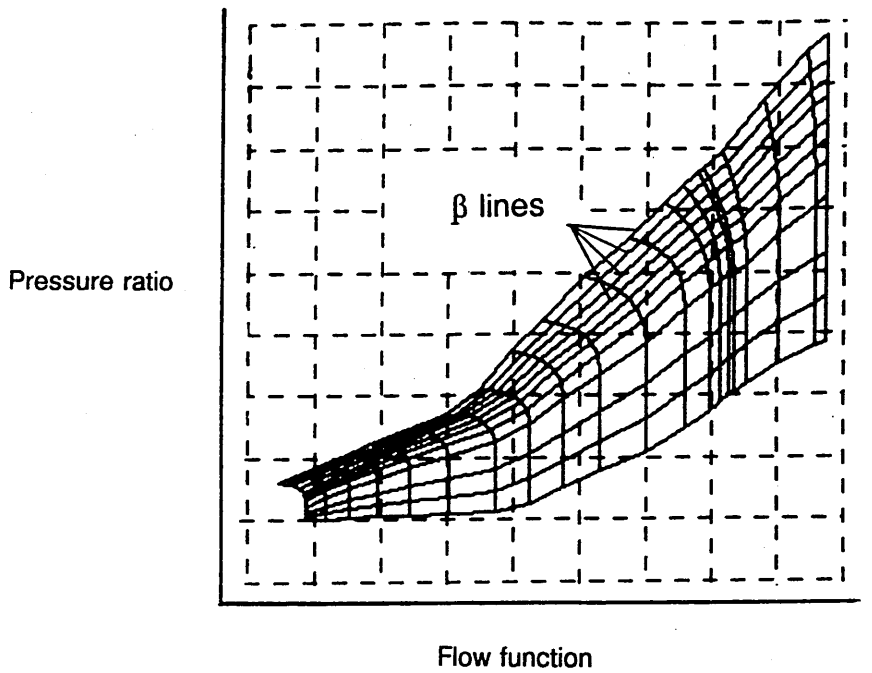

Complete RRAP compressor characteristic expressed with respect to a beta value and corrected speed

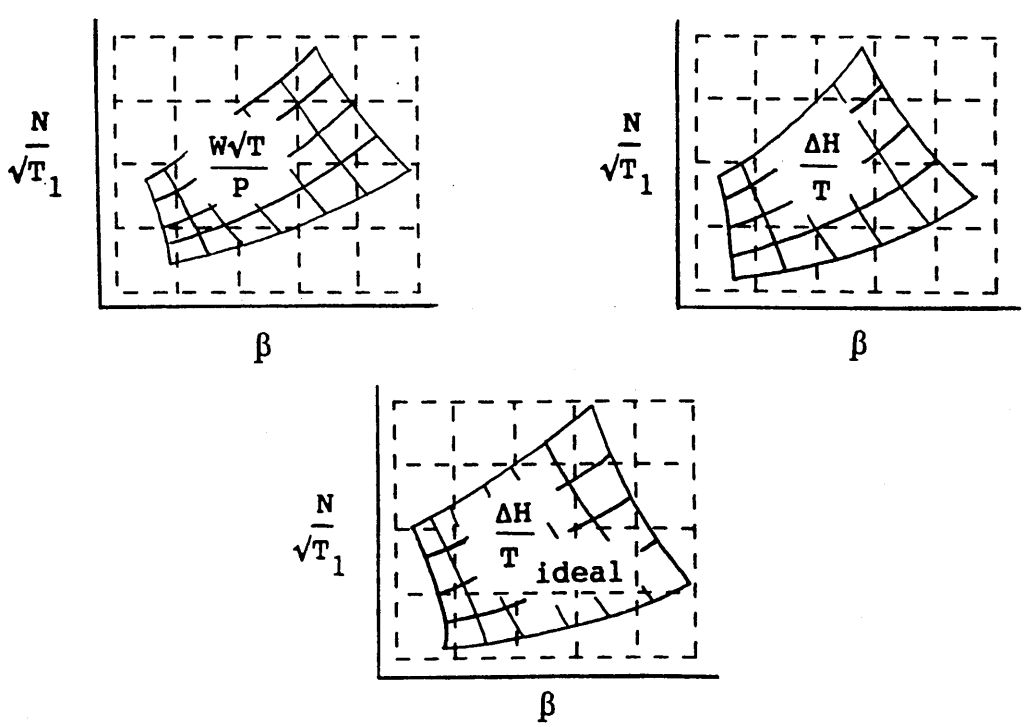

Figure 6.1 Definition of compressor operating point

Model Matching Scheme

Variables	Matching quantities
Turbine excess power EP	Turbine entry flow function
Compressor β value	Final nozzle entry pressure

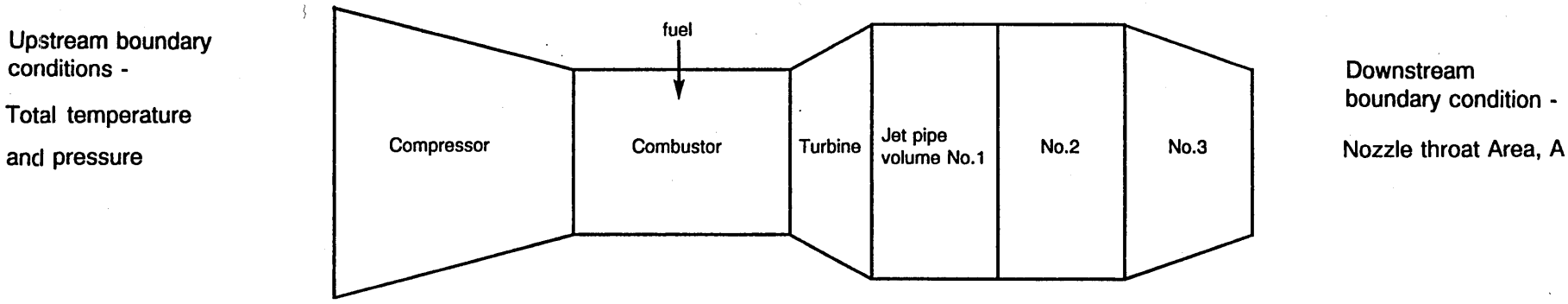

Figure 6.2 Schematic illustration of the RRAP Viper engine model

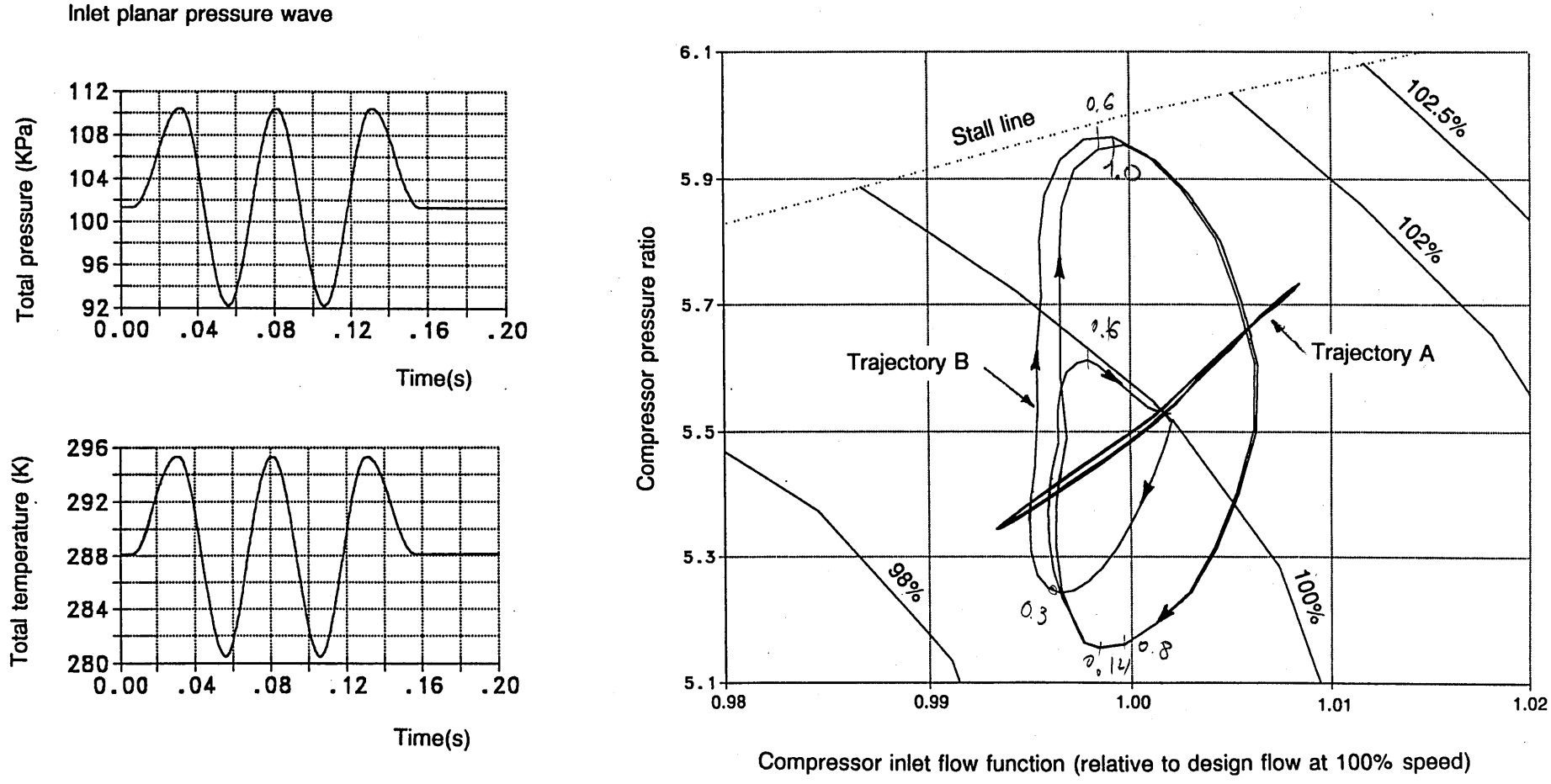

Figure 6.3 Compressor operating point excursion due to engine inlet planar pressure Waves

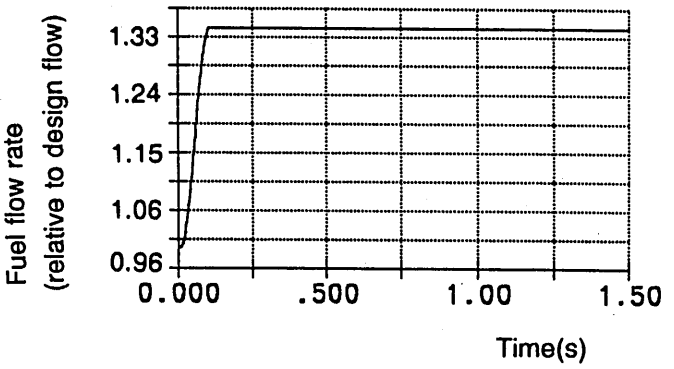

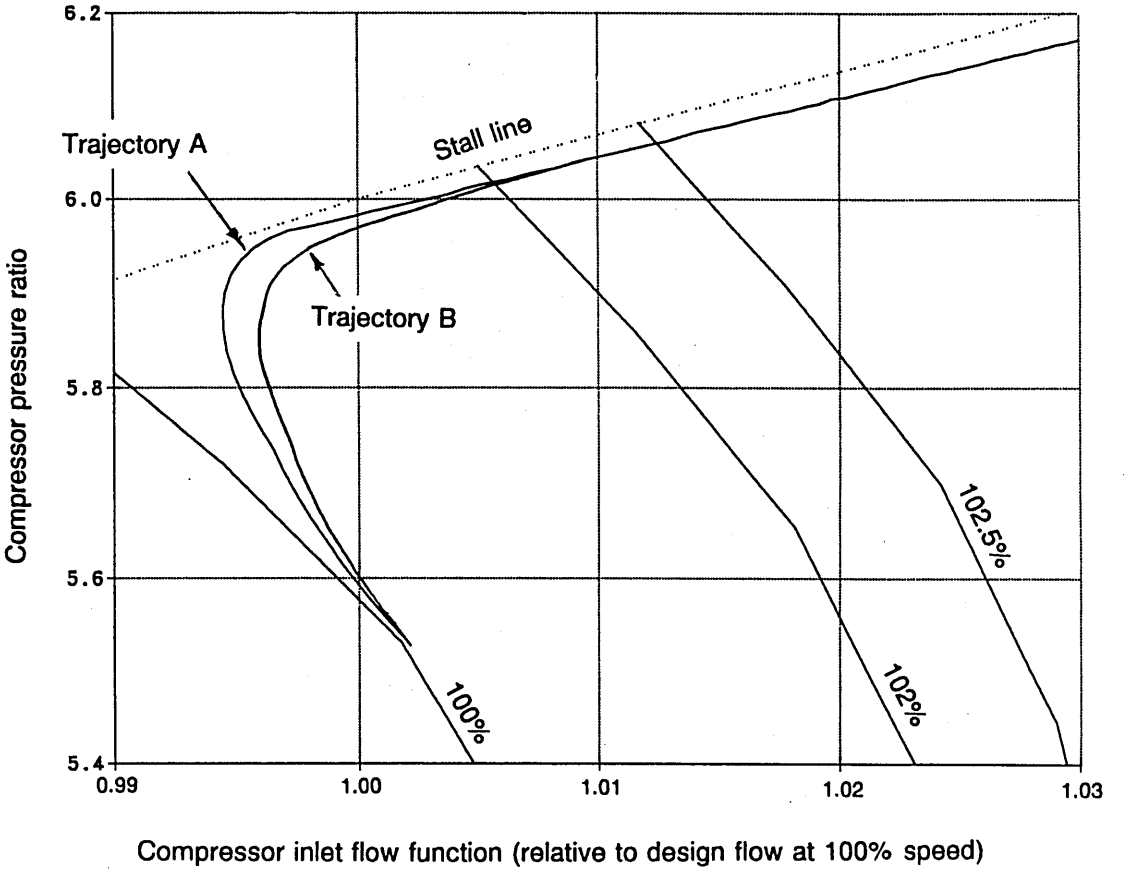

Figure 6.4 Engine high-frequency-transient response to overfuelling

Model Matching Scheme

Matching quantities	**Variables**
Entry pressure at each nozzle	Fan and compressor β value
High and low pressure turbine inlet flow functions	High and low pressure turbine excess powers

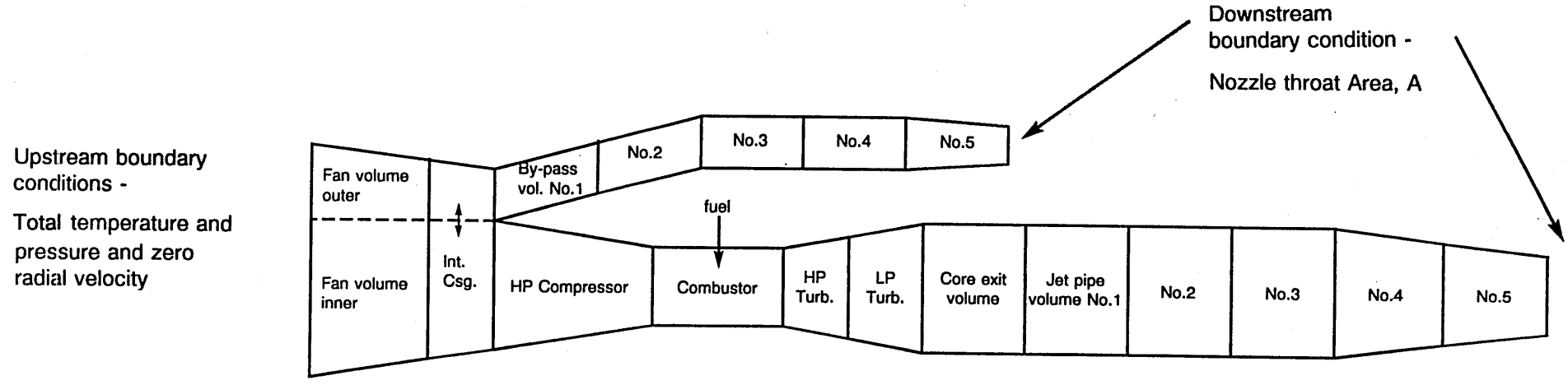

Figure 6.5 Schematic illustration of the turbofan engine model

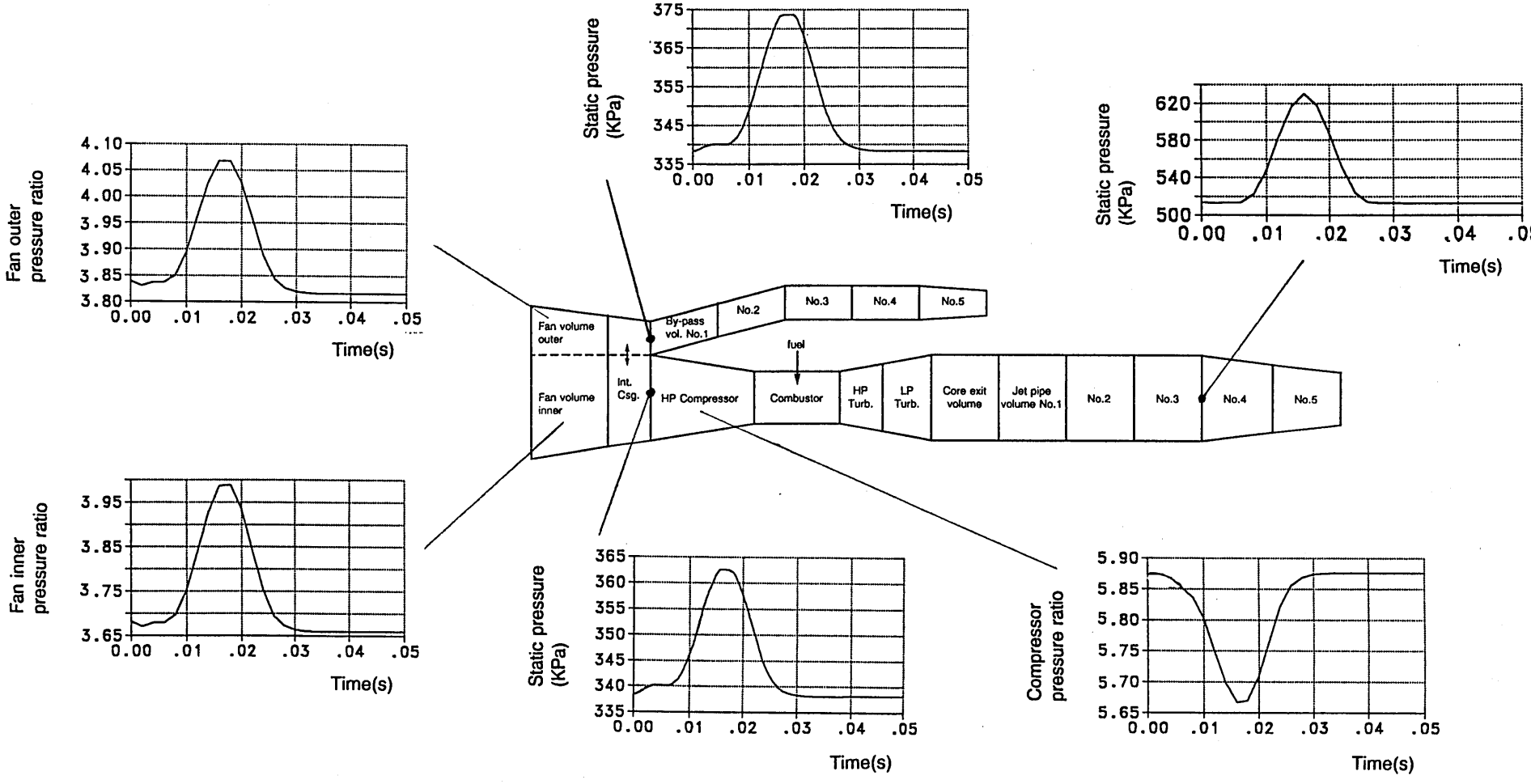

Figure 6.6a Prediction of radial flow in the intermediate casing of the turbofan engine

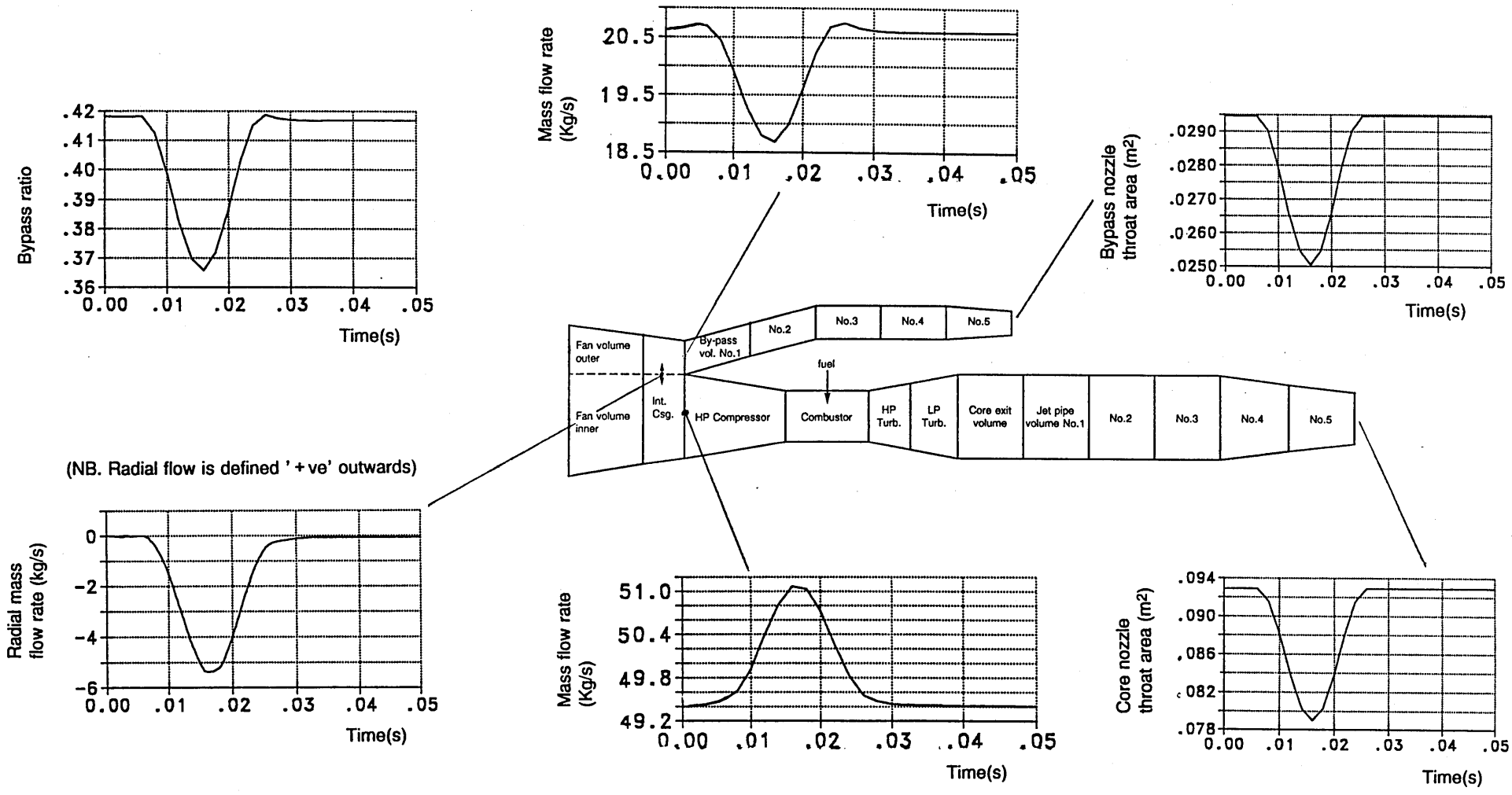

Figure 6.6b Prediction of radial flow in the intermediate casing of the turbofan engine

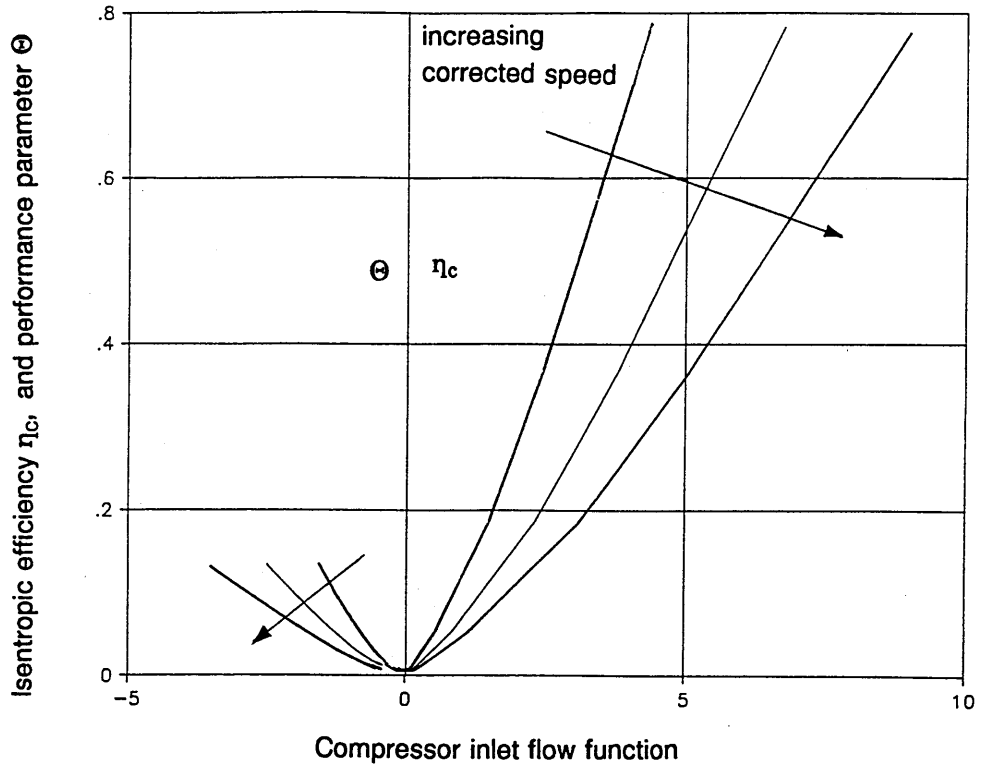

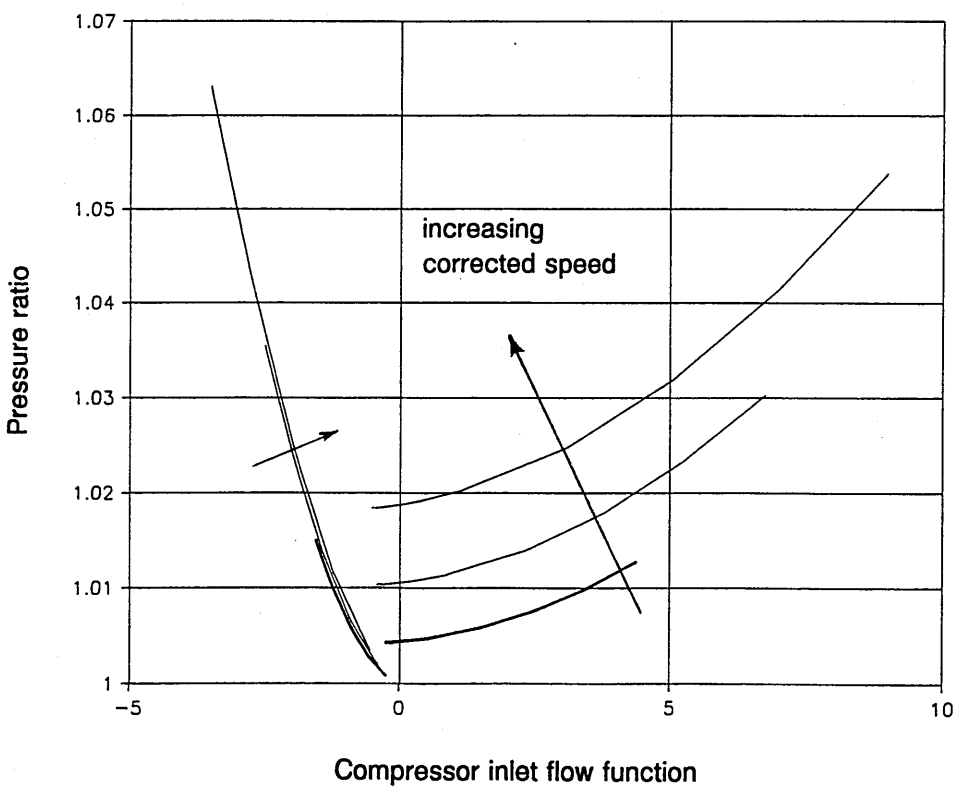

Figure 7.1a Compressor low speed post-stall performance characteristic

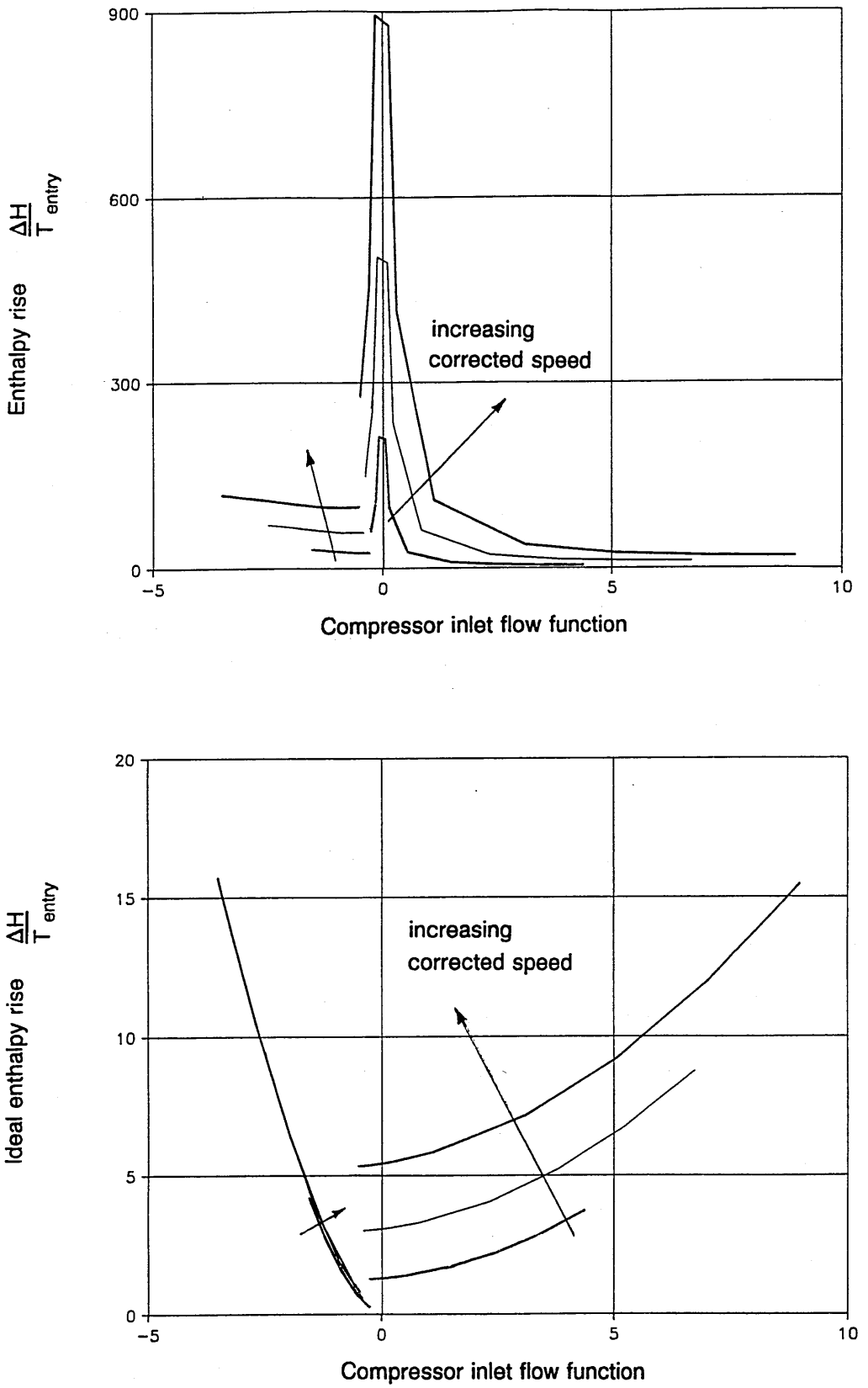

Figure 7.1b Compressor low speed post-stall performance characteristic

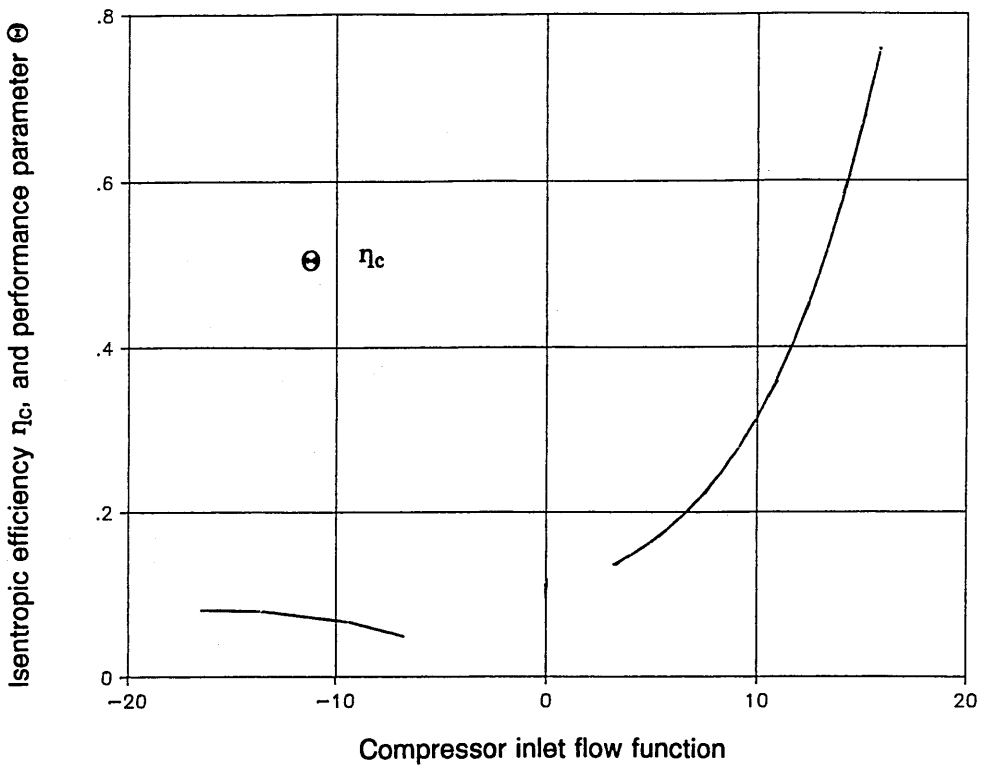

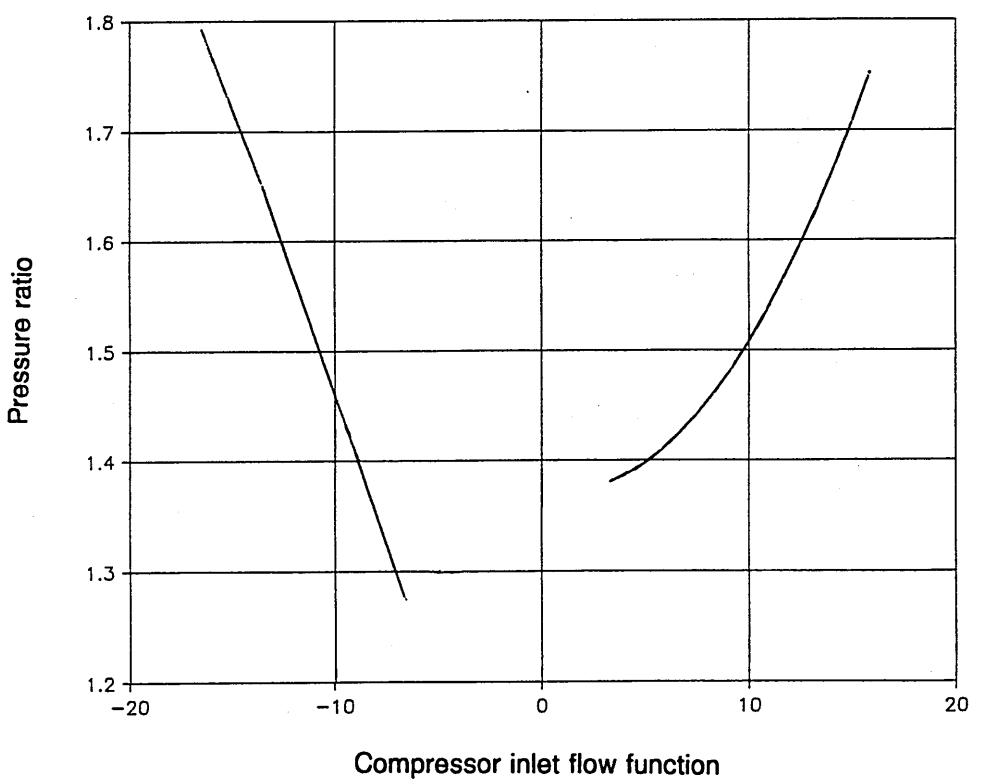

Figure 7.2a Compressor high speed post-stall performance characteristic

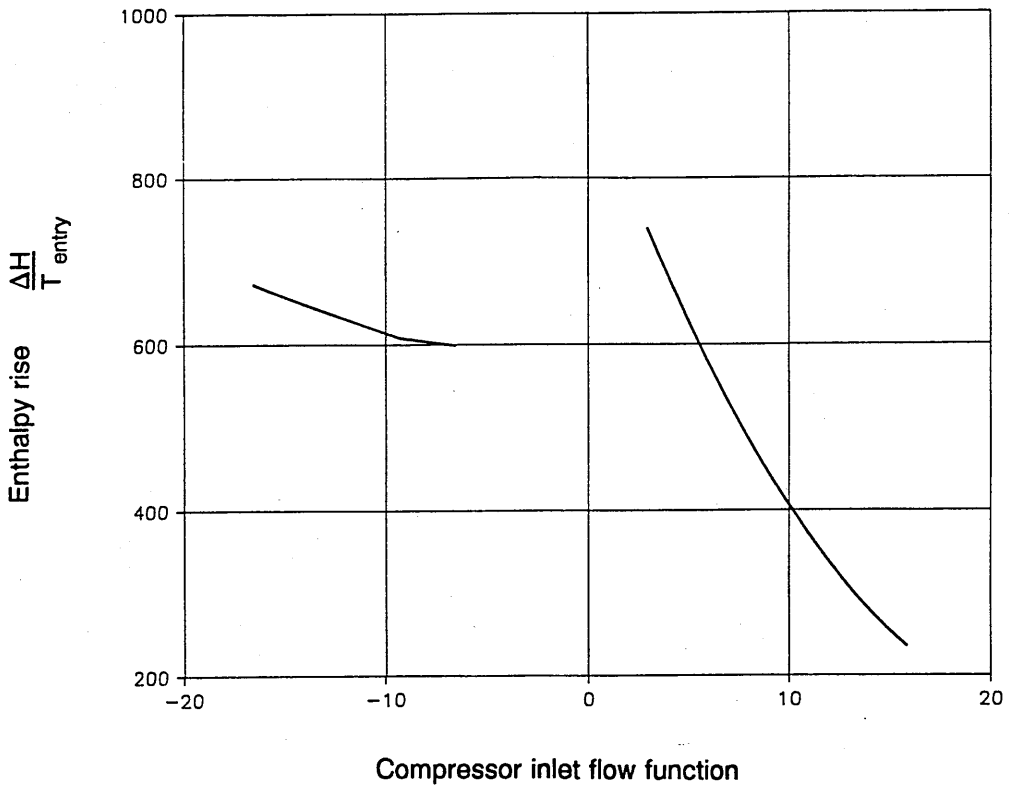

Figure 7.2b Compressor high speed post-stall performance characteristic

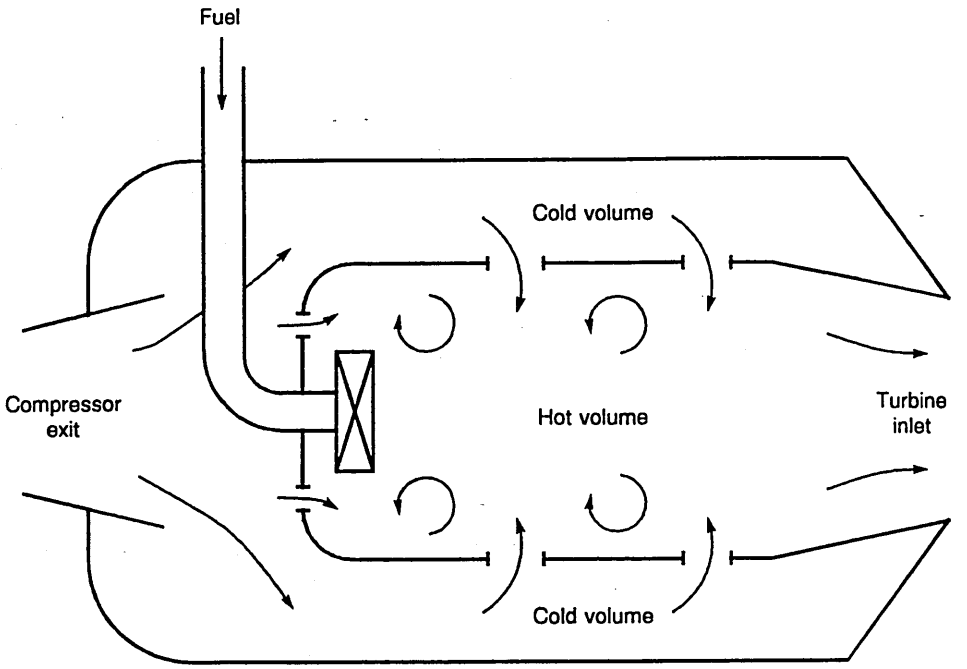

Figure 7.3a Schematic illustration of a typical annular combustion chamber

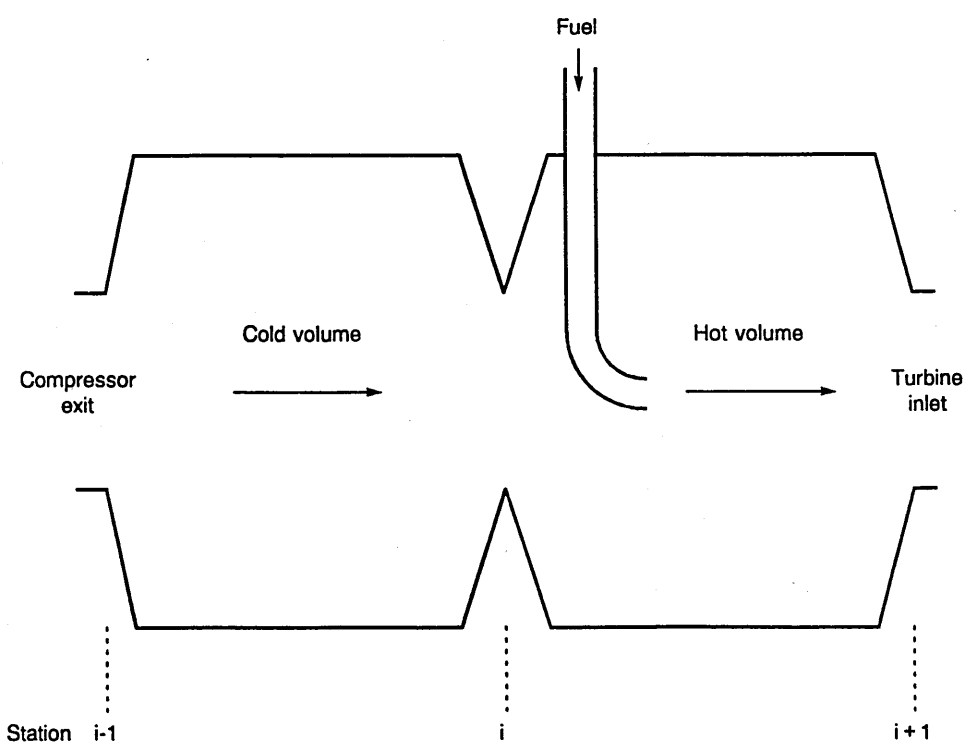

Figure 7.3b The combustor model

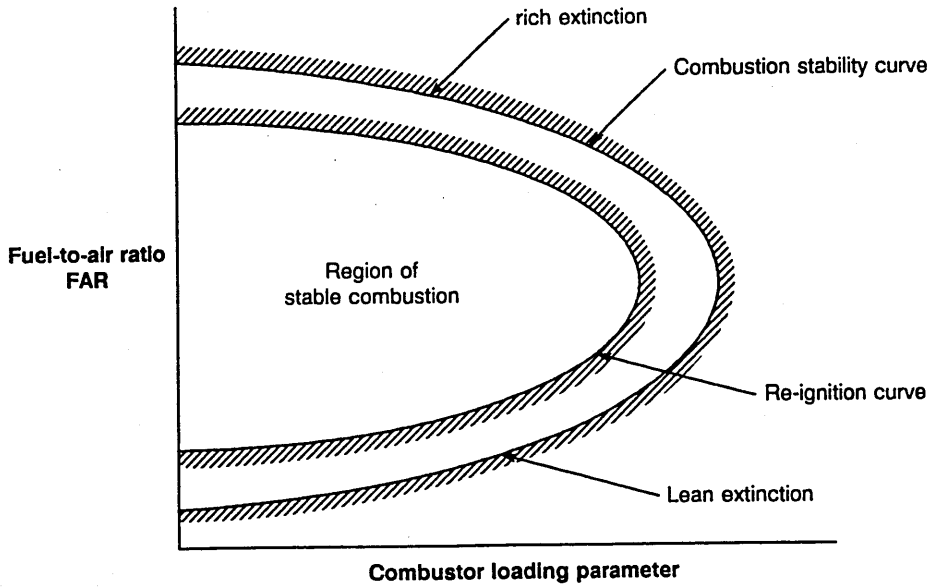

Figure 7.4 Typical combustor stability and re-ignition curves

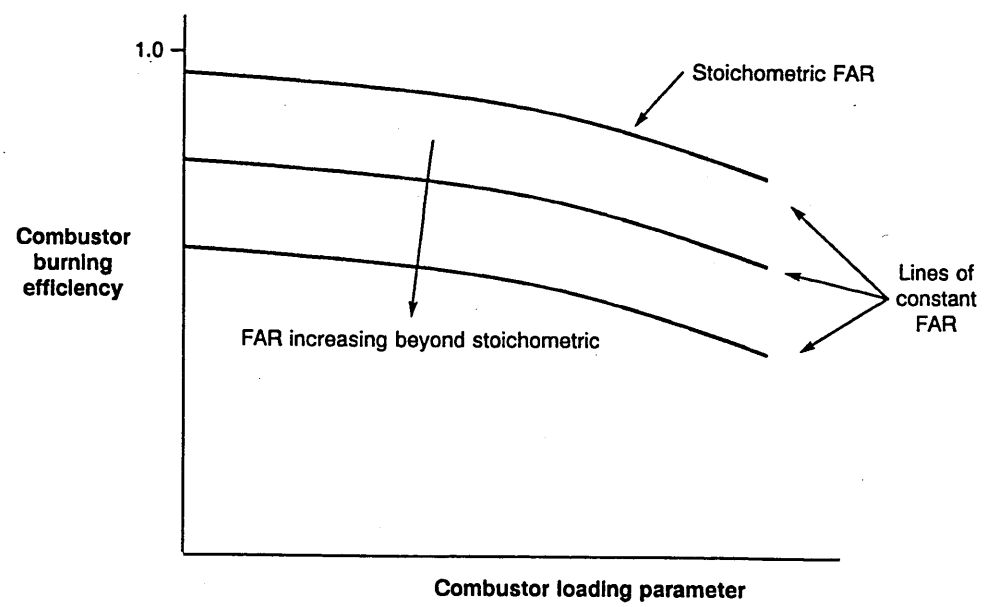

Figure 7.5 Typical variation of combustor efficiency with loading and fuel-to-air ratio

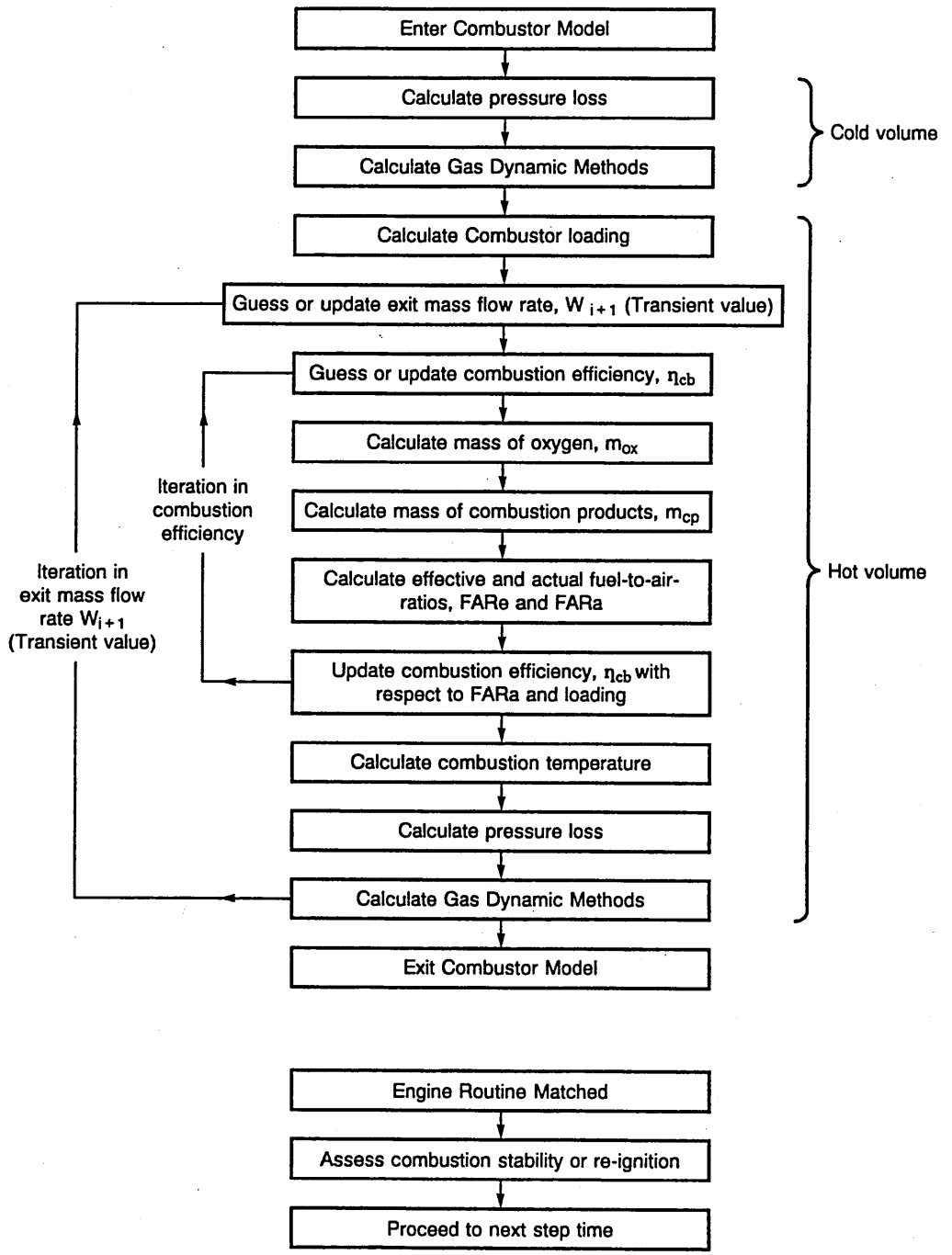

Figure 7.6 Combustor model calculation procedure

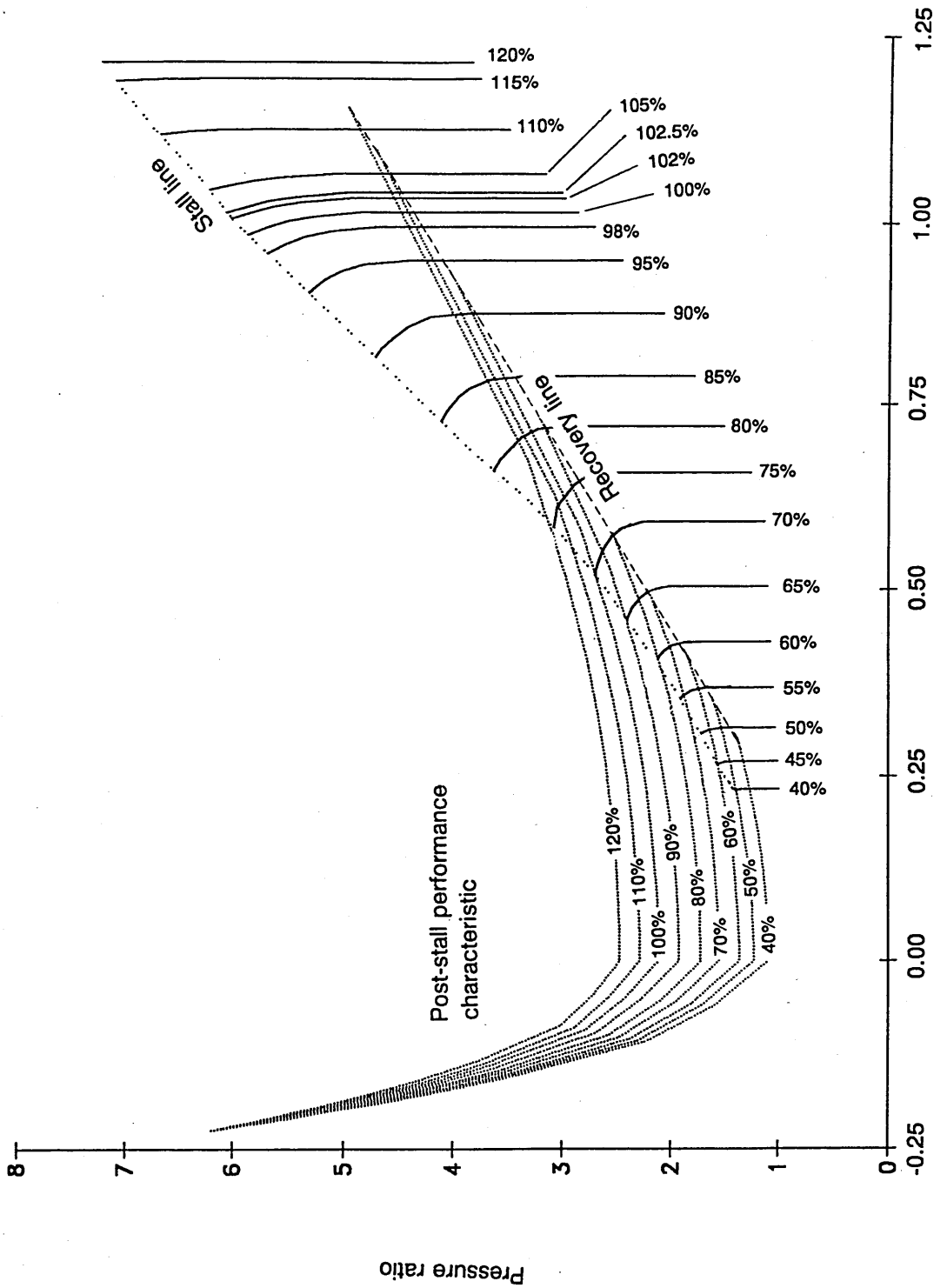

Figure 7.7a Post-stall compressor characteristic

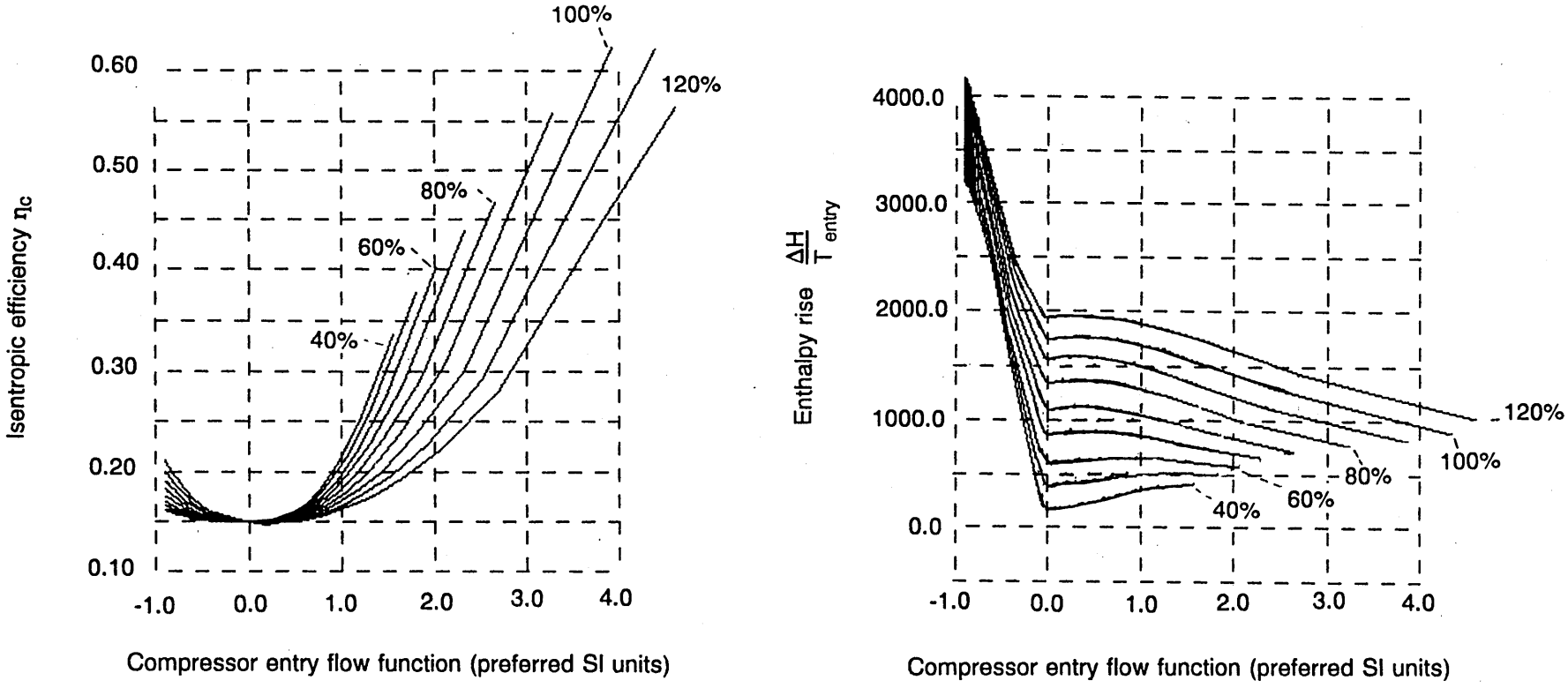

Figure 7.7b Post-stall compressor characteristic

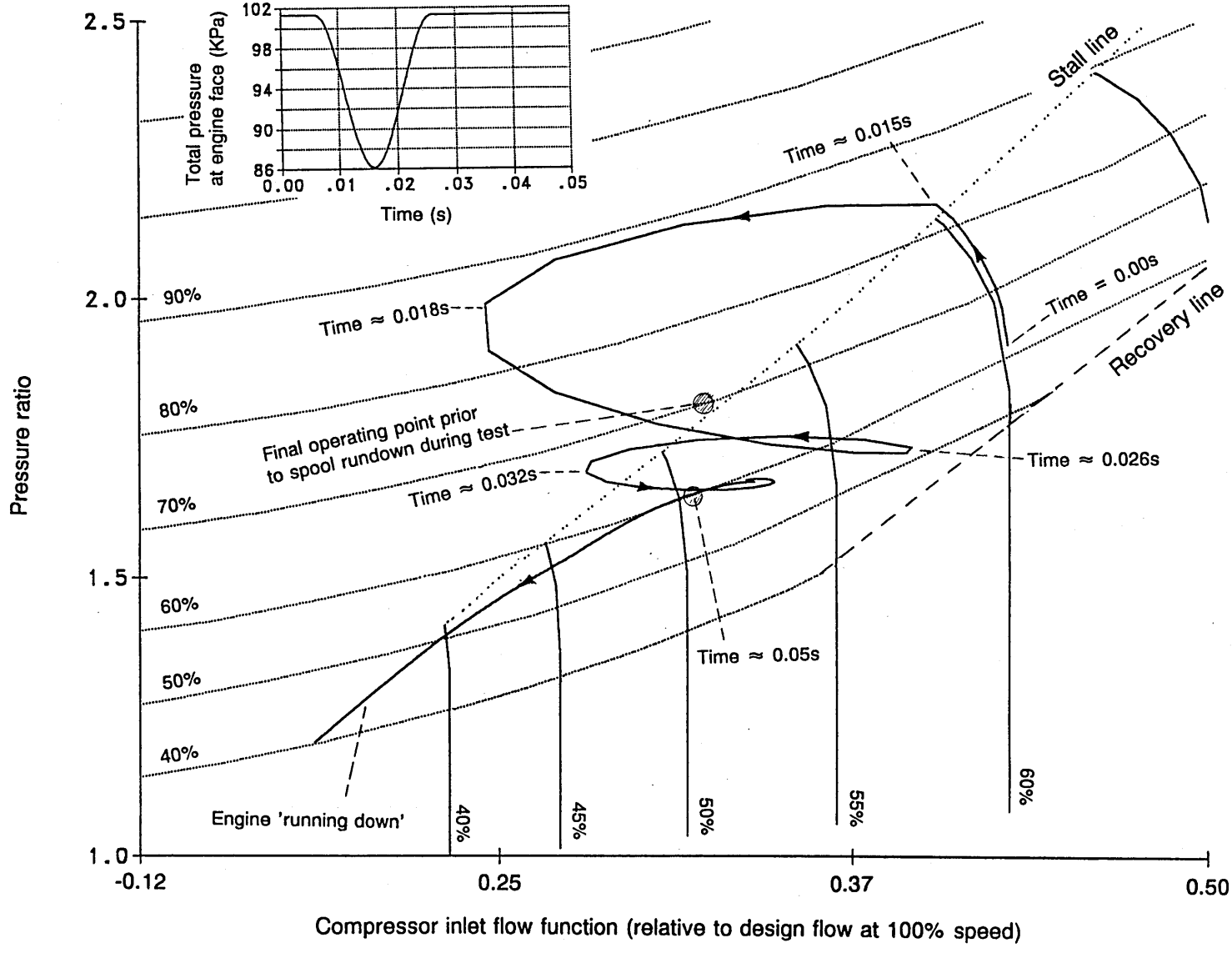

Figure 7.8a Post-stall event at 60% engine speed

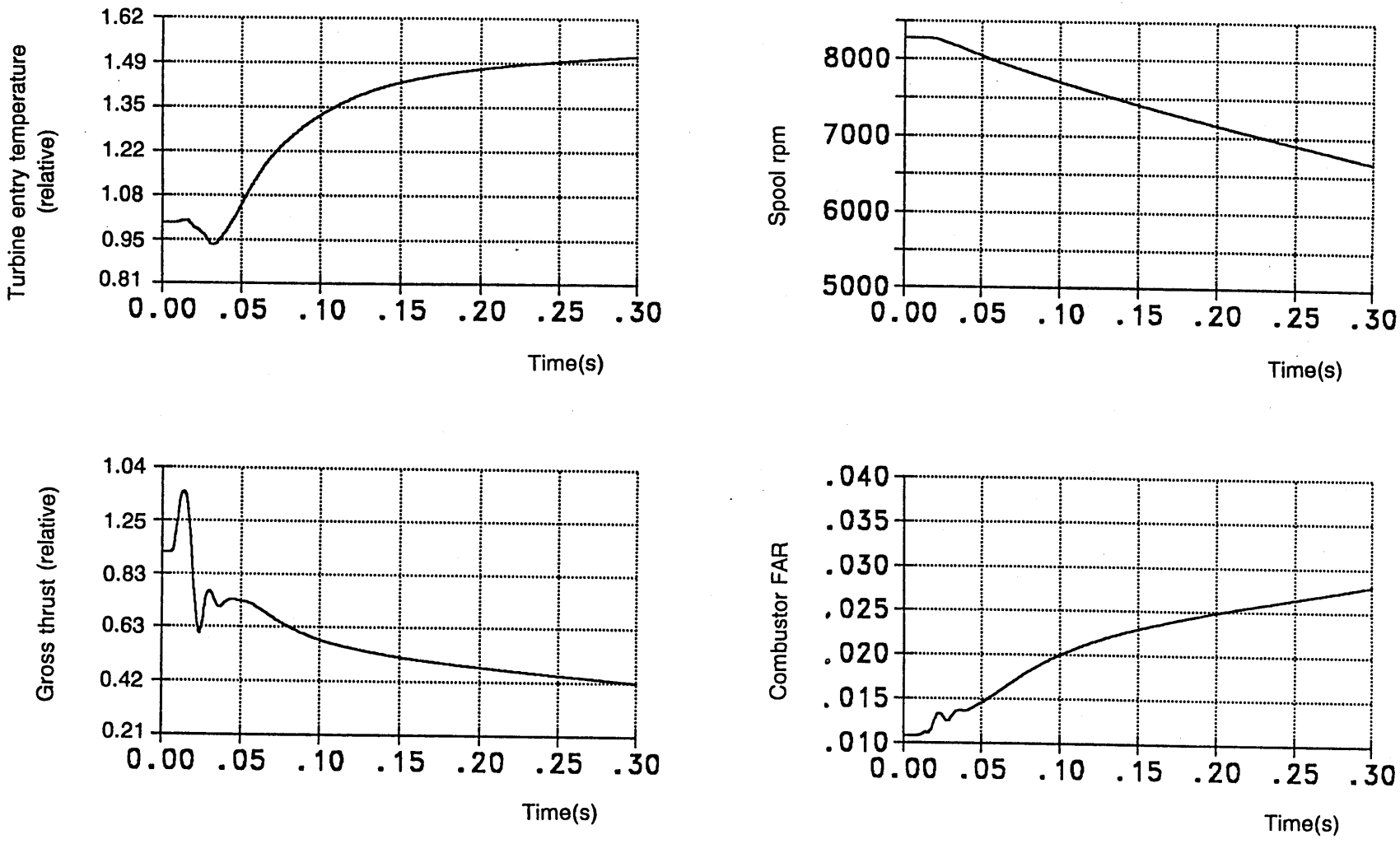

Figure 7.8b Post-stall event at 60% engine speed

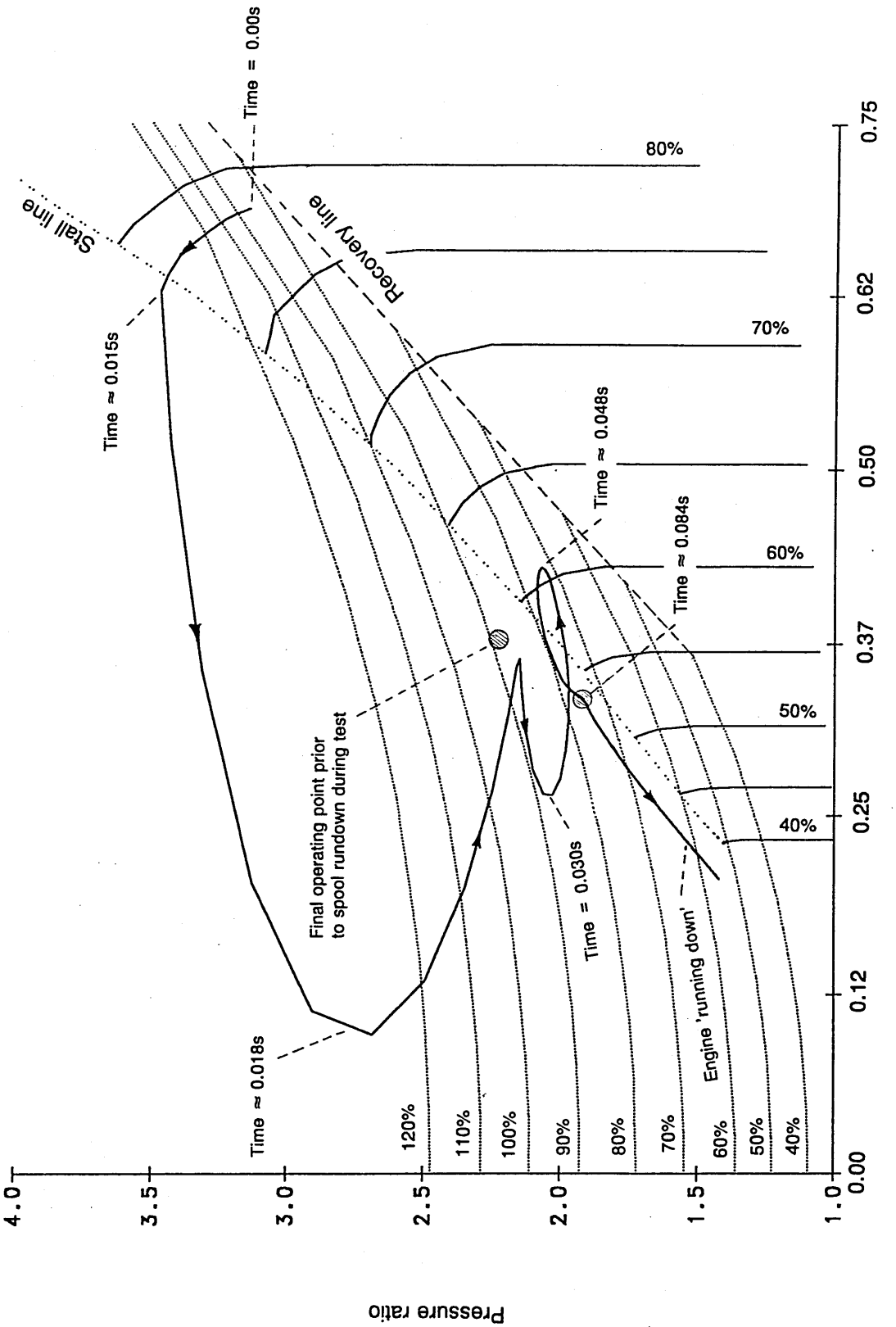

Figure 7.9 Post-stall event at 78% engine speed

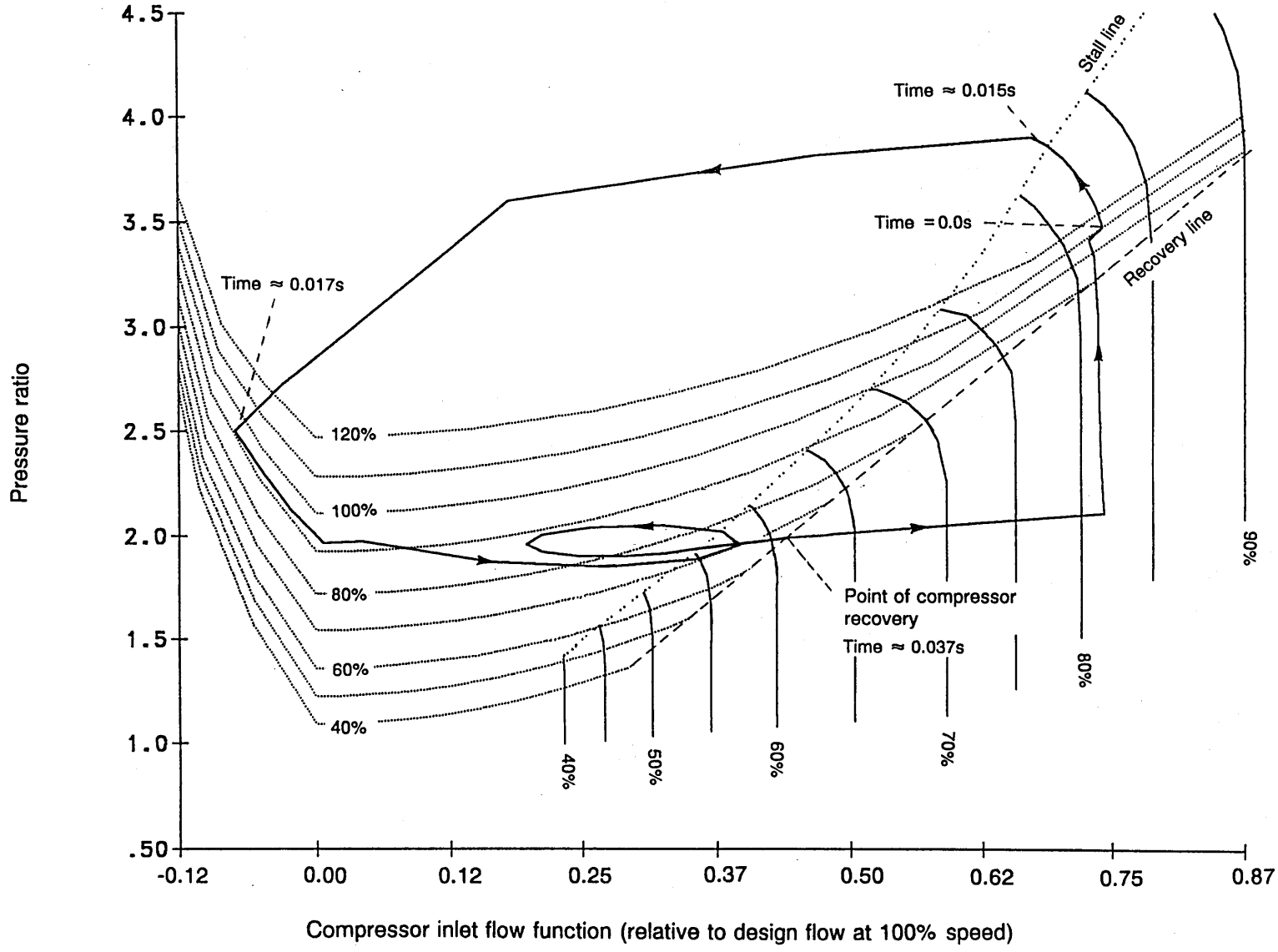

Figure 7.10 Post-stall event at 82% engine speed

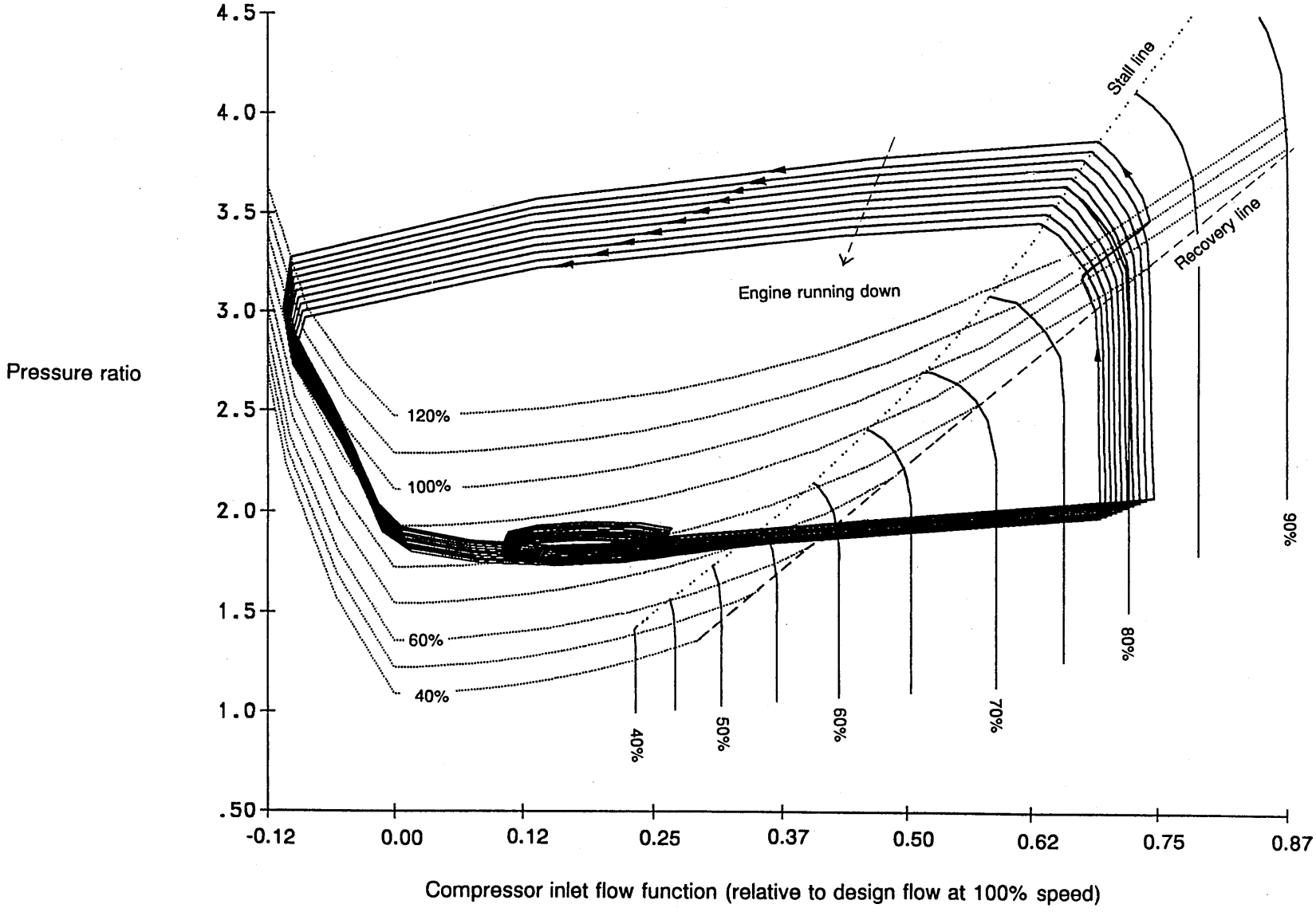

Figure 7.11 Post-stall event at 82% engine speed

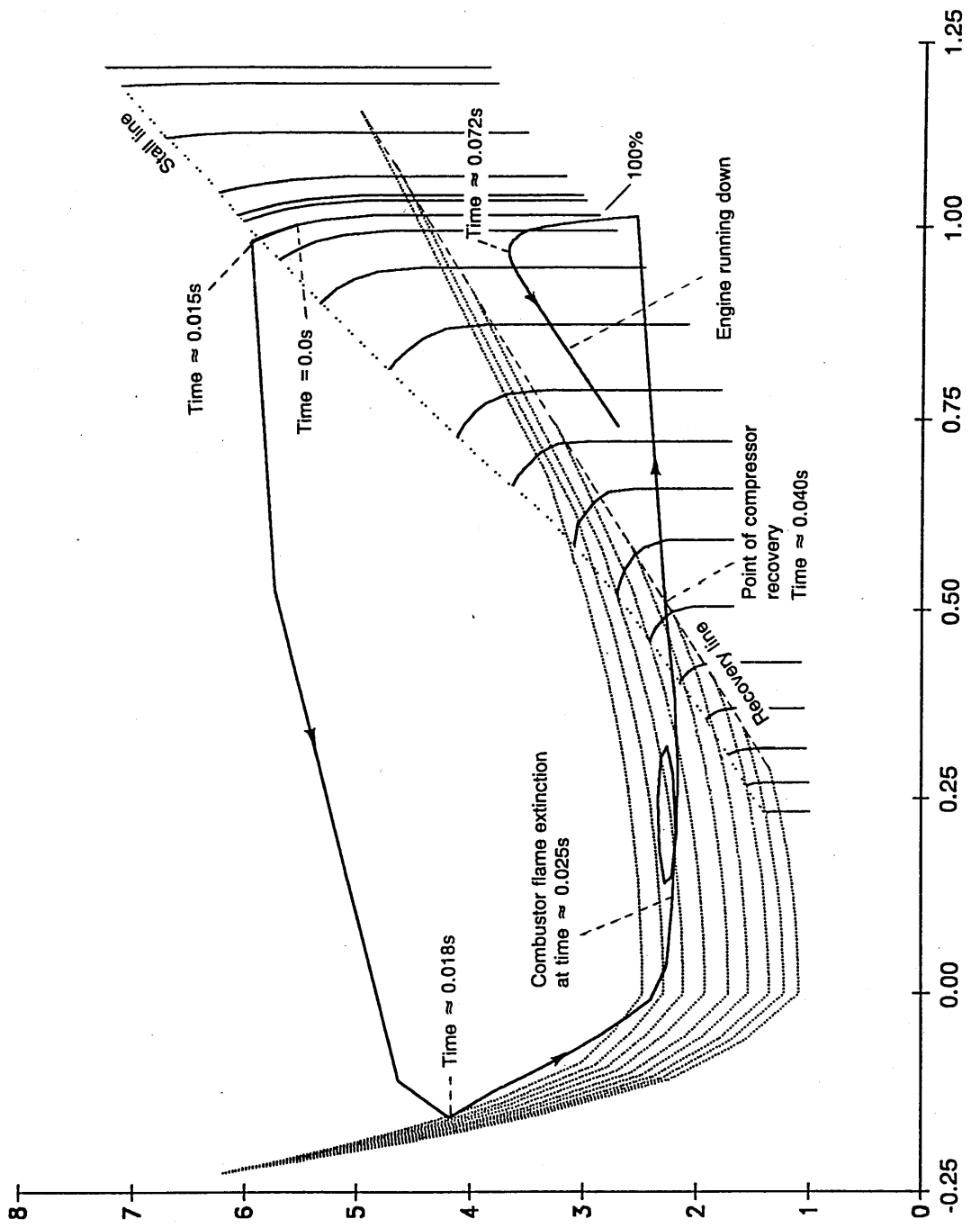

Figure 7.12a Post-stall event at 100% engine speed

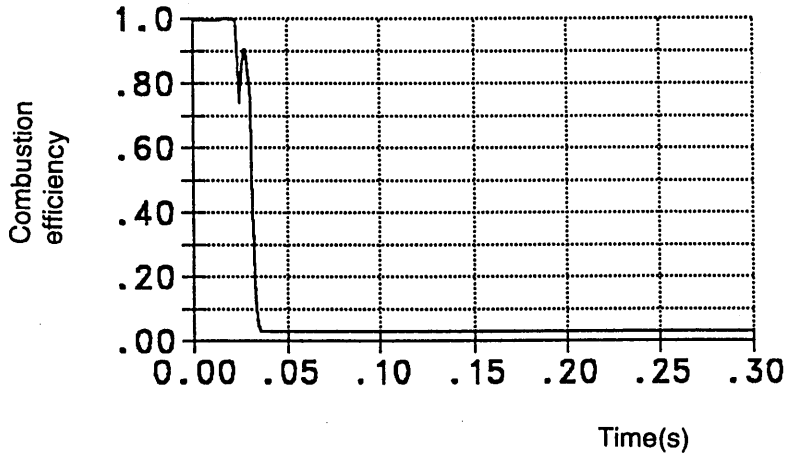

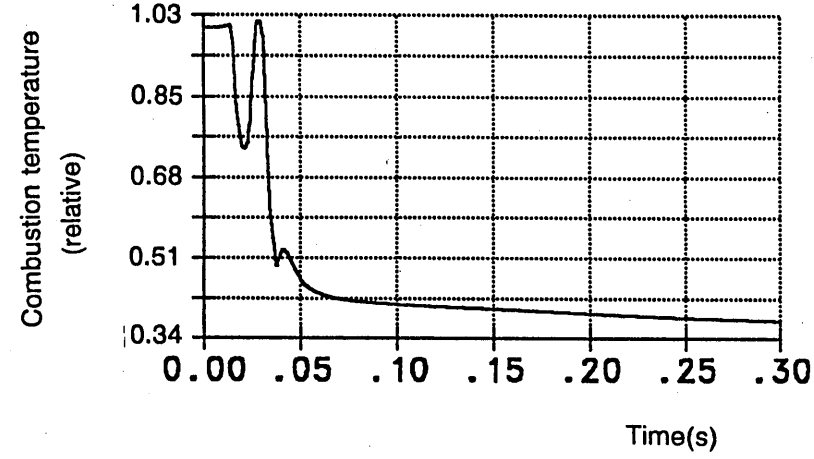

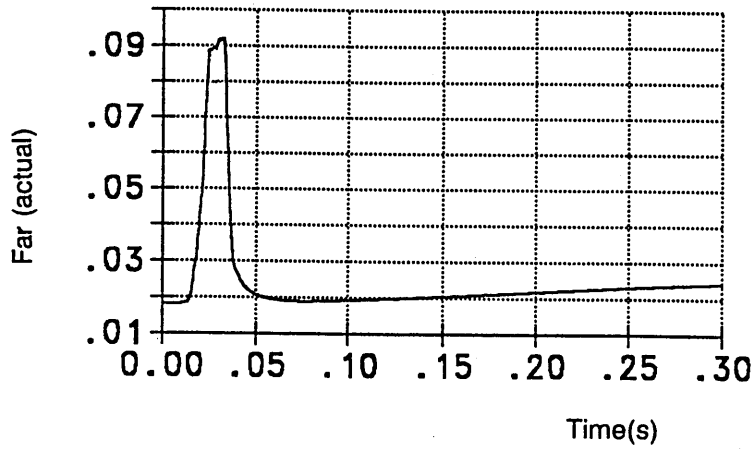

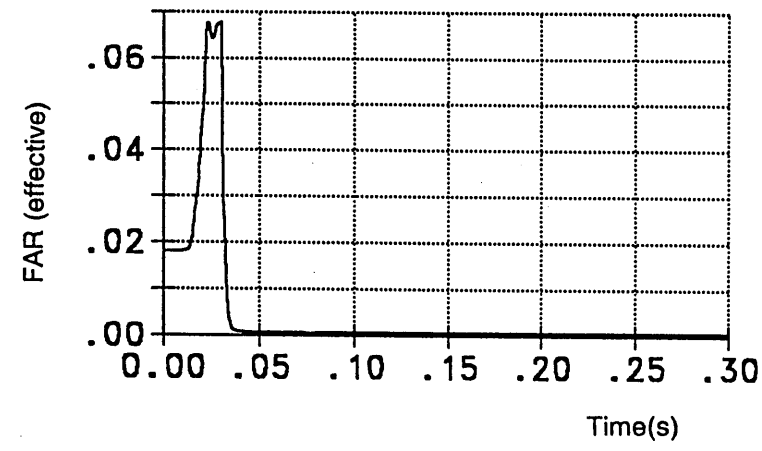

Figure 7.12b Post-stall event at 100% engine speed

Table 3.1 - Degree of contingency with respect to risk

Risk	Identification number	Contingency (%)
Very low risk	1	5
Low risk	2	10
Medium risk	3	15
High risk	4	30
Very high risk	5	40

Table 3.2 - Breakdown of Estimated and Total hours for each Area of Work

Area of Work	Total Contingency (%)	Estimated Hours Own	RR	Total Hours Own	RR
1.1	8.1	515	573	579	619
1.1	8.2		114		123
1.3	5.0	144	136	151	143
1.4	8.3		52		56
1.5	22.0		969		1182
1.6	15.9		748		867
1.7	29.8		462		600
1.8	17.3		936		1098
1.9	20.1		394		473
1.10	29.1		386		498
1.11	13.2		190		215
1.12	13.2		190		215
1.13	13.4		505		573
	Total	659	5655	730	6662

RR - Rolls-Royce

Table 3.3 - Constituent Areas of Work for each Course of Work

Course of Work	Constituent Areas of Work (WBS) Level 2
1	1.1 1.2 1.3 1.4 1.5 1.6 1.9 1.11 1.12 1.13
2	1.1 1.2 1.3 1.4 1.5 1.6 1.10 1.11 1.12 1.13
2	1.1 1.2 1.3 1.4 1.5 1.7 1.8 1.9 1.11 1.12 1.13
3	1.1 1.2 1.3 1.4 1.5 1.7 1.8 1.10 1.11 1.12 1.13

Table 3.4 - Summary of Estimated and Total Hours for each Course of Work

Course of Work	Estimated Hours Own	Estimated Hours RR	Total Hours Own	Total Hours RR
1	659	3871	730	4467
2	659	3477	730	4492
3	659	4521	730	5298
4	659	4127	730	5323

RR - Rolls-Royce

Table 3.5 - Rolls-Royce man hour utilisation rates

Period	Qtr 1	Qtr 2	Qtr 3	Qtr 4
Basic Hours	458.4	458.4	611.2	458.4
Public Holidays	0.0	46.0	15.7	31.4
Planned Hours	458.4	412.4	595.5	427.0
Annual Leave	20.9	41.5	96.3	46.5
Other Lost Time	16.0	11.0	8.0	11.0
Overtime	31.1	29.8	41.9	30.1
Utilisation Rate	452.6	389.7	533.1	399.6
Utilisation Rate per year = 1775 hours Utilisation for course period = 5325 hours				

Table 3.6 - Summary of anticipated modelling capability of each Course of Work

Course of Work	Summary of modelling capability
1	**Model 1** will be a development of the existing Rolls-Royce High Frequency Transient Compression System Model, incorporating, - gas dynamic methods - combustor heat addition - pre- and post-stall modelling - stage compressor performance modelling **Application:** single- and two-spool compression systems **Limitations:** compression system only, no reverse flow capability
2	**Model 2** will be a development of the existing Rolls-Royce High Frequency Transient Compression System Model, incorporating, - gas dynamic methods - combustor heat addition - pre- and post-stall modelling - reverse flow capability **Application:** single- and two-spool compression systems **Limitations:** compression system only, compressor represented by single volume - lower frequency response than Model 1
3	**Model 3** will be developed using the Rolls-Royce Aeroengine Performance computer deck, RRAP, incorporating, - gas dynamic methods - stage compressor performance modelling - pre- and post-stall modelling **Application:** whole engine modelling **Limitations:** no reverse flow capability
4	**Model 4** will be developed using the Rolls-Royce Aeroengine Performance Computer deck, RRAP, incorporating, - gas dynamic methods - pre- and post-stall modelling - reverse flow capability **Application:** whole engine modelling **Limitations:** compressor represented by single volume - lower frequency response than Model 3

Appendix 1.1 Project Specification

The project objective is twofold.

(1) To develop and verify a generic computer based modelling method, capable of simulating the high frequency transient response to one-dimensional flow disturbances in the pre- and post-stall domains of single and multi-spool gas turbine engines. See section 1.3.

(2) The work done must be suitable for a PhD thesis.

The technical and PhD course specification is set out as follows and includes alternative courses of work should problems occur that are either insoluble or impractical to overcome.

Technical Specification

The Technical Specification is split into six sections.

i) High frequency gas dynamic response

Note - For flow disturbances in gas turbines of greater than approximately 5 Hz, the time dependence of flow behaviour, due to temporary accumulation of mass, momentum and energy, becomes significant. The inclusion of what is often referred to as 'high frequency gas dynamic response' is therefore necessary if the simulation of engine response during rapid pre- and post-stall transients is to be representative. For convenience, the method of

predicting 'high frequency gas dynamic response' will from here on be referred to as 'Gas Dynamic Methods' (GDM), and transients greater than 5 Hz as 'high-frequency-transients'.

The GDMs developed must be able to predict the temporary accumulation of fluid mass, momentum and energy and hence the time dependency of fluid mass flow rate, temperature and pressure, up to a frequency response of approximately 40 Hz.

Application of GDMs to a whole gas turbine engine model will be achieved by splitting an engine into component volumes and solving one-dimensional, time dependent equations conserving mass, momentum and energy across each. The GDMs must be extended to cater for variation in by-pass ratio in multi-spool engines. Circumferential variation in flow properties will not be predicted. The GDMs will apply to inviscid, non heat conducting and compressible flow. The flow process will be adiabatic.

The GDMs will be compatible with, and developed using the Rolls-Royce Aero Engine Performance computer deck, RRAP. Inherent in this requisite is the suitability of the methods with one, two or three spool engine models of civil, military or industrial application.

ii) Whole engine modelling using the Rolls-Royce Aero Engine Performance computer deck, RRAP

Engine models will operate at International Standard Atmosphere (ISA), Sea Level Static conditions with a bell mouth intake. Engine installation or application effects will not be modelled.

Compressor and turbine performance will be represented by an overall characteristic. Fan performance will be represented by an inner and outer characteristic. Inter-stage characteristics will not be used.

Combustor performance will take into account pressure loss loss due to viscous drag and the fundamental pressure loss due to combustion.

Compressor, combustor and turbine characteristics must be taken straight from the existing Rolls-Royce data base and not require any alteration.

Engine spool speed must be predicted as a function of time by taking into account turbine excess power and spool inertia.

Engine control schedules will not be modelled.

iii) Pre-stall whole engine high-frequency-transient modelling

It must be possible to predict the propagation of disturbances in pressure, temperature and mass flow rate along the working fluid flow paths of the engine when it is subjected to time dependent perturbations in,

- inlet planar pressure and/or temperature waves
- fuel flow rate
- final nozzle area

It must also be possible to predict the variation in spool speed and compressor operating point when the engine is subjected to the above perturbations.

iv) Post-stall whole engine high-frequency-transient modelling

Inception of compressor instability will be determined by a stall line superimposed on a compressor characteristic and not predicted theoretically. Similarly, the point of compressor recovery from stall will be represented by a recovery line.

It must be possible to predict the propagation of disturbances in pressure, temperature and mass flow rate along the working fluid flow paths of the engine, during cyclic surge and the 'descent' into rotating-stall.

It must also be possible to predict the engine spool speed and compressor operating point during cyclic surge and the descent into rotating-stall.

The possible occurrence of flow reversal in the compressor and combustor during surge must be catered for.

Compressor rotating-stall and reverse flow characteristics will be empirical or based on rig tests and not theoretically derived. The format of the characteristic data must be compatible with the existing RRAP computer data base.

The occurrence of combustor blow-out and possible re-light must be catered for, and when lit, burning efficiency must be predicted as a function of combustor loading and fuel-to-air ratio.

Turbine characteristics must be extended to cater for the low flows that may occur during surge.

v) Methods Verification

The GDMs will be verified against experimental measurements taken of pressure waves, at varying frequencies and amplitudes, within a plane open ended duct.

Prediction of pre- and post-stall compressor high-frequency-transient behaviour will be verified using compressor test rig data.

Prediction of single spool gas turbine pre- and post-stall high-frequency-transient behaviour will be verified using engine test data.

Prediction of multi-spool gas turbine pre- and post-stall high-frequency-transient behaviour will be verified using engine test data.

Generation of the above experimental data will not be a part of this project.

The extent of method verification will depend on the amount of the above test data made available within the project time scale.

vi) Alternative Courses of Work

Should inclusion of the GDMs into RRAP prove to be impossible, or impractical, with the resources provided, the existing Rolls-Royce Transient Compression System Model must be developed. This will result in a two spool compression system and combustor, exhausting through choked nozzles. Mechanical spool speed will be held constant. The

above specification will still apply save for turbine and varying mechanical spool speed modelling capability.

Should the modelling of reverse flow in the combustor and compressor during a strong surge prove to be impossible, or impractical with the resources provided, work will concentrate on the further development and refinement of the post-stall modelling capability by introducing stage compressor performance calculations.

Course Specification

The objective is set to be achieved to the above technical specification within a three year period. The technical work must be done whilst based in industry, be project managed and written up in a format suitable for presentation as a PhD thesis. The thesis must also include a description and an appraisal of the Project management techniques used.

Both Technical and Project Progress must be presented to a Supervisory Panel and discussed at least three times per year. The Panel will consist of four members - the Chairman, and Academic, Industrial and Project Management Supervisors. Individual meetings will also be held with the Academic, Industrial and Project Management Supervisors on a regular basis.

Progress Reports detailing both technical and project progress must be submitted to the Panel after the first nine and eighteen months of the course.

Technical courses both directly applicable and complementary to the project work must be completed within the three year period. Similarly non-technical courses including project management courses, are to be attended. Course attendance can amount to three weeks per year.

Level 1 - **PhD Thesis** 'Simulation of Aeroengine Pre- and Post-Stall Transient Behaviour'		Estimated Hours Own	RR
Level 2 - Areas of Work			
1.1	PhD course requirements	515	573
1.2	Project Management		114
1.3	Literature Search	144	136
1.4	Computing Resource		52
1.5	Technology Acquisition		969
1.6	Pre- and post-stall development of existing Rolls-Royce High Frequency Transient Compression System Model		748
1.7	Introduction of Gas Dynamic Methods into the Rolls-Royce Aeroengine Performance computing deck, RRAP		462
1.8	Pre- and post-stall whole engine high frequency transient modelling methods development using RRAP		936
1.9	Development of stage-by-stage compressor model		394
1.10	Development of reverse flow capability		386
1.11	Dedicated single spool turbojet pre- and post-stall high frequency transient model development		190
1.12	Dedicated two spool turbofan pre- and post-stall high frequency transient Model development		190
1.13	Methods Verification		505

APPENDIX 3.1 - THE WORK BREAKDOWN STRUCTURE (WBS)

RR - Rolls-Royce

Levels 3 and 4 of Level 1.1 - PhD course requisites	Risk	Estimated Hours Own	RR
1.1.1 Progress Reports 1 and 2	1	85	
1.1.2 Periodic presentations to supervisory panel on technical and project progress	2		64
1.1.3 Course attendance and Paper authourship			
1.1.3.1 Technical courses	1		102
1.1.3.2 Project Management courses	1		103
1.1.3.3 Paper authourship	3		68
1.1.4 Supervision Meetings			
1.1.4.1 Academic	1		68
1.1.4.2 Project Management	1		12
1.1.4.3 Industrial	2		156
1.1.5 Thesis			
1.1.5.1 Preparation	3	350	
1.1.5.2 Final presentation	2	60	
1.1.5.3 Oral preparation	1	20	
Level 3 of Level 1.2 - Project Management			
1.2.1 Project Justification	1		20
1.2.2 Project Specification	1		20
1.2.3 Project Organisation	2		50
1.2.4 Project Control and Progress Assessment	2		24
Level 3 of Level 1.3 - Literature Search			
1.3.1 Preliminary search and overview	1		136
1.3.2 Ongoing literature search	1	144	

Work Breakdown Structure cont'd

	Risk	Estimated Hours	
Level 3 of Level 1.4 - Computing Resource			
1.4.1 Attend training courses on relevant Rolls-Royce computing methods and facilities	2		34
1.4.2 Attend RRAP 'User' and 'Programer' course	1		18
Levels 3 and 4 of Level 1.5 - Technology Acquisition			
1.5.1 Development of Gas Dynamic Methods			
1.5.1.1 Alternative equation sets	2		34
1.5.1.2 Boundary conditions	3		34
1.5.1.3 Reverse flow capability	3		34
1.5.1.4 Solution methods	3		34
1.5.2 Post-Stall Combustion Methods			
1.5.2.1 Prediction of burning efficiency and combustor loading	3		20
1.5.2.2 Inclusion of 'blow out' and re-light capability	3		34
1.5.2.3 Reverse flow capability	5		102
1.5.3 Post-Stall Compressor Modelling Methods			
1.5.3.1 Response lag laws	2		136
1.5.3.2 Rotating-stall and reverse flow characteristics	4		273
1.5.3.3 Characteristic interrogation methods	3		68
1.5.4 Core and Bypass Flow Mixing Methods	4		100
1.5.5 Low Flow Turbine Characteristics	2		100

Work Breakdown Structure cont'd

Level 3 of Level 1.6 - Pre- and post-stall development of existing Rolls-Royce High Frequency Transient Compression System Model	Risk	Estimated Hours Own	RR
1.6.1 Generate simple duct models	2		68
1.6.2 Compression System Model pre-stall development	2		136
1.6.3 Implementation of Post-Stall Combustion Methods	4		136
1.6.4 Feasibility study of reverse flow modelling	5		34
1.6.5 Implementation of Post-Stall Compressor Modelling Methods	3		136
1.6.6 Pre- and post-stall Compression System Model development	2		238
Level 3 of Level 1.7 - Introduction of Gas Dynamic Methods into the Rolls-Royce Aeroengine Performance computing deck, RRAP			
1.7.1 Generate simple duct models	2		68
1.7.2 Introduce Gas Dynamic Methods	4		180
1.7.3 Assess and remove any numerical instability	5		180
1.7.4 Develop duct models	3		34

Work Breakdown Structure cont'd

Levels 3 and 4 of Level 1.8 - Pre- and post-stall whole engine high frequency transient modelling methods development using RRAP	Risk	Estimated Hours Own	RR
1.8.1 Compressor Rig Model			
1.8.1.1 Generate compressor rig model	2		34
1.8.1.2 Implement Gas Dynamic Methods	3		34
1.8.1.3 Implement Post-Stall Compressor Modelling Methods	3		34
1.8.2 Single Spool Turbojet Model			
1.8.2.1 Generate single spool turbojet model	1		51
1.8.2.2 Implement Gas Dynamic Methods	3		34
1.8.2.3 Implement Post-Stall Compressor Modelling Methods	4		103
1.8.2.4 Implement Post-Stall Combustion Methods	4		103
1.8.2.5 Introduce Low Flow Turbine Characteristics	2		20
1.8.2.6 Feasibility study of reverse flow modelling	5		34
1.8.3 Two Spool Turbofan Model			
1.8.3.1 Generate two spool turbofan model	1		60
1.8.3.2 Implement Gas Dynamic Methods	3		137
1.8.3.3 Implement Post-Stall Compressor Modelling Methods	3		34
1.8.3.4 Implement Post-Stall Combustion Methods	4		34
1.8.3.5 Introduce Low Flow Turbine Characteristics	2		20
1.8.3.6 Implement Core and Bypass Flow Mixing Methods	3		34
1.8.4 Development of Compressor Rig Model	2		34
1.8.5 Development of Single Spool Turbojet Model	2		68
1.8.6 Development of Two Spool Turbofan Model	2		68

Work Breakdown Structure cont'd

Level 3 of Level 1.9 - Development of stage-by-stage compressor model	Risk	Estimated hours Own	RR
1.9.1 Introduction of compressor inter-stage performance calculations	3		102
1.9.2 Prediction and introduction of inter-stage pre-stall characteristics	2		68
1.9.3 Prediction and introduction of inter-stage rotating-stall characteristics	4		78
1.9.4 Prediction and introduction of inter-stage reverse flow characteristics	4		78
1.9.5 Introduction of inter-stage instability line	3		34
1.9.6 Compressor inter-stage model development	3		34
Level 3 of Level 1.10 - Development of reverse flow capability			
1.10.1 Implement reverse flow boundary conditions	4		68
1.10.2 Implement reverse flow combustor modelling methods	4		68
1.10.3 Implement reverse flow compressor modelling methods	4		80
1.10.4 Introduce reverse flow compressor characteristics	2		68
1.10.5 Development of reverse flow modelling methods	5		102

Work Breakdown Structure cont'd

Level 3 of Level 1.11 - Dedicated single spool turbojet pre- and post-stall high frequency transient model development	Risk	Estimated hours Own	RR
1.11.1 Engine baseline performance and geometric data acquisition	1		34
1.11.2 Generate and introduce Rotating-Stall and Reverse Flow Characteristics	3		68
1.11.3 Develop dedicated engine model	3		88
Level 3 of Level 1.12 - Dedicated two spool turbofan pre- and post-stall high frequency transient model development			
1.12.1 Engine baseline performance and geometric data acquisition	1		34
1.12.2 Generate and introduce Rotating-Stall and Reverse Flow Characteristics	3		68
1.12.3 Develop dedicated engine model	3		88

Work Breakdown Structure cont'd

Levels 3 and 4 of Level 1.13 - Methods Verification	Risk	Estimated hours Own	RR
1.13.1 One-dimensional Duct Model			
1.13.1.1 Experimental data acquisition and analysis	2		55
1.13.1.2 Method Verification	3		68
1.13.2 Compression System			
1.13.2.1 Pre-stall experimental data and analysis	2		55
1.13.2.2 Post-stall experimental data acquisition and analysis	3		68
1.13.2.3 Method Verification	3		68
1.13.3 Whole Engine			
1.13.3.1 Pre-stall experimental data acquisition and analysis	2		55
1.13.3.2 Post-stall experimental data acquisition and analysis	3		68
1.13.3.3 Method Verification	3		68

Work Breakdown Structure cont'd

Appendix 3.2 The Work Plan and Strategy

The plan is idealised and does not represent the required cross fertilisation of ideas between items of work; but it does show the predicted direction of the research work and the four possible Alternative Courses of Work.

The Work Plan and Strategy is split into three phases. Phase 1 leads to Decision Point 1, Phase 2 to Decision Point 2 and Phase 3 to the Project End, figure 3.3. The Decision Points are positioned at the points of greatest technical risk. The phases include all the WBS Areas of Work except levels 1.1 to 1.4 - the PhD Course Requisites, Project Management, Literature Search and Computing Resource. These are not dependent on any other items of work, and so can be completed as necessary between the Project Beginning and the Project End.

Phase 1

The objective of phase 1 is to develop the Gas Dynamic Methods (GDM), WBS Level 1.5, and introduce them into the Rolls-Royce Aero Engine Performance computer deck, RRAP, WBS Level 1.7. Phase 1 will conclude with Decision Point 1, which will depend on the successful inclusion of the GDMs into RRAP.

Phase 2

A 'yes' to Decision Point 1 will mean that all subsequent development can be done using the RRAP system. This is the desired course as it will ultimately lead to a generic modelling capability. The GDMs will then be verified against existing experimental data of pressure waves, at

varying frequencies and amplitudes, measured in a plane open ended pipe, WBS Level 1.13. With verification complete Phase 2 will conclude with pre- and post-stall whole engine high-frequency-transient modelling methods development, WBS Level 1.8.

If the response to Decision Point 1 is 'no' then the existing Rolls-Royce High Frequency Transient Compression System Modelling Model, WBS Level 1.6, will be developed further. Verification will follow using the experimental duct data, WBS Level 1.13.

Phase 2 will conclude by conducting a study into the feasibility of modelling reverse flow according to the Project Specification, appendix 1.1 part iv).

Phase 3

The desired route will lead to the development of reverse flow capability using a whole engine RRAP model of a single spool turbojet, WBS 1.10. This will enable the simulation of deep surge at high engine speeds according to the Project Specification, appendix 1.1 part iv).

If it is concluded that modelling reverse flow is possible, then all methods developed will be applied to a whole engine model of the Rolls-Royce Viper Mk 522, WBS Level 1.11. This is the desired route as it will enable the simulation of deep surge at high engine speeds. Subsequent verification of the pre- and post-stall modelling methods will follow using existing Viper test data, WBS 1.13.

If the response to Decision Point 2 is 'no' then a more detailed approach to compressor modelling will be developed by introducing stage performance characteristics, WBS 1.9.

Phase 3 will conclude by assessing the compatibility of the pre- and post-stall modelling methods with multi-spool engines, WBS Level 1.12. Subsequent verification will depend upon the availability of suitable test data over the three year project period.

Table 3.6 summarises the four Alternative Courses of Work. Note that Course of Work No. 4 is the most desirous as it completely satisfies the Specification.

Appendix 3.3 Course Details

Course commencement date	-	1 January 1991
Course completion date	-	31 December 1993

Supervising Panel

1 **Academic Supervisor**
Professor Robin Elder
Head of Department of Turbo Machinery and Engineering Mechanics
School of Mechanical Engineering
Cranfield University

2 **Industrial Supervisor** (Jan 92 - Jan 94)
Dr David Lambie
Principal Technology Engineer
Compressor Technology Dept.
Rolls-Royce plc, Bristol

3 **Panel Chairman**
Mr Ken Ramsden
Senior Lecturer
School of Mechanical Engineering
Cranfield University

4 **Project Management Supervisor**
Mr Garth Ward
Director of MSc in Project Management
Cranfield School of Management
Cranfield University

5 **Industrial Supervisor** (Jan 91 - Sept 91)
Mr Darrell Williams (Retd. Sept 91)
Chief of Powerplant Technology (Military)
Rolls-Royce, Bristol

6 **Student**
Mr Nicholas Merriman
Senior Technology Engineer
Powerplant Technology (Military)
Rolls-Royce, Bristol

Cont'd

Supervisory Panel Meetings		
Date	**Location**	**Present**
12-04-91	Rolls-Royce, Bristol	1,3,4,5,6
07-01-92	Cranfield University	1,2,3,4,6
29-04-92	Rolls-Royce, Bristol	1,2,3,6
27-08-92	Cranfield University	1,2,3,4,6
17-11-92	Cranfield University	1,2,3,4,6
08-02-93	Rolls-Royce, Derby	1,2,3,6
02-08-93	Rolls-Royce, Bristol	1,2,3,4,6
03-12-93	Cranfield University	1,2,3,6

Academic and Project Management Supervision Meetings			
Date	**Location**	**Academic**	**Project Management**
01-11-90	Rolls-Royce, Bristol	1,5,6	
09-01-91	Cranfield University	1,5,6	
22-03-91	Rolls-Royce, Bristol	1,5,6	
26-04-91	Cranfield University	1,6	4,6
10-07-91	Rolls-Royce, Bristol	1,6	
11-09-91	Rolls-Royce, Bristol	1,6	
18-09-91	Rolls-Royce, Bristol	1,6	
07-01-92	Cranfield University	1,6	
13-02-92	Cranfield University	1,6	
16-04-92	Rolls-Royce, Bristol	1,6	
21-07-92	Cranfield University	1,6	
27-08-92	Cranfield University	1,6	
17-11-92	Cranfield University	1,6	
01-12-92	Rolls-Royce, Bristol	1,6	
08-01-93	Cranfield University		4,6
07-05-93	Rolls-Royce, Bristol	1,6	
02-08-93	Rolls-Royce, Bristol		4,6
19-10-93	Rolls-Royce, Bristol	1,6	

Cont'd

Courses and Conferences Attended, and Papers Presented	
Courses Attended	
30-07-90 03-08-90	Computational Fluid Dynamics
08-10-90 28-10-90	Gas Turbine Theory and Design
17-02-92 21-02-92	Developing Project Management - Techniques
11-05-92 15-05-92	Fan and Compressor Theory
04-01-93 18-01-93	Management for Technology
12-07-93 16-07-93	Gas Turbine Transient Performance
Conferences Attended	
09-06-92 10-06-92	AGARD Lecture Series 183 - Steady and Transient Performance Prediction of Gas Turbine Engines
Papers Presented	
08-04-94	Simulation of aeroengine transient behaviour including the effects of volume dynamics IMechE, Birdcage Walk, London Seminar in Turbo Compressor and Fan Stability

Further Presentations		
Date	**Location**	**Present**
18-11-91	Cranfield University	Professor Robin Elder - Head of Department of Turbo Machinery and Engineering Mechanics, Cranfield University Christopher Freeman - Chief Propulsion Systems Specialist, Rolls-Royce, Derby Dr Alex Cargill - Theoretical Science Group, Rolls-Royce, Derby 3 Cranfield PhD Students
11-12-92	Rolls-Royce Bristol	Powerplant Technology Departmental Technical Forum

Appendix 4.1a Radial flow definition

The diagram below is a side view of the two volume component geometry shown in figure 4.3. The radial mass flow rate at the inter volume plane k, and the inner and outer volume mean temperature and pressure are defined.

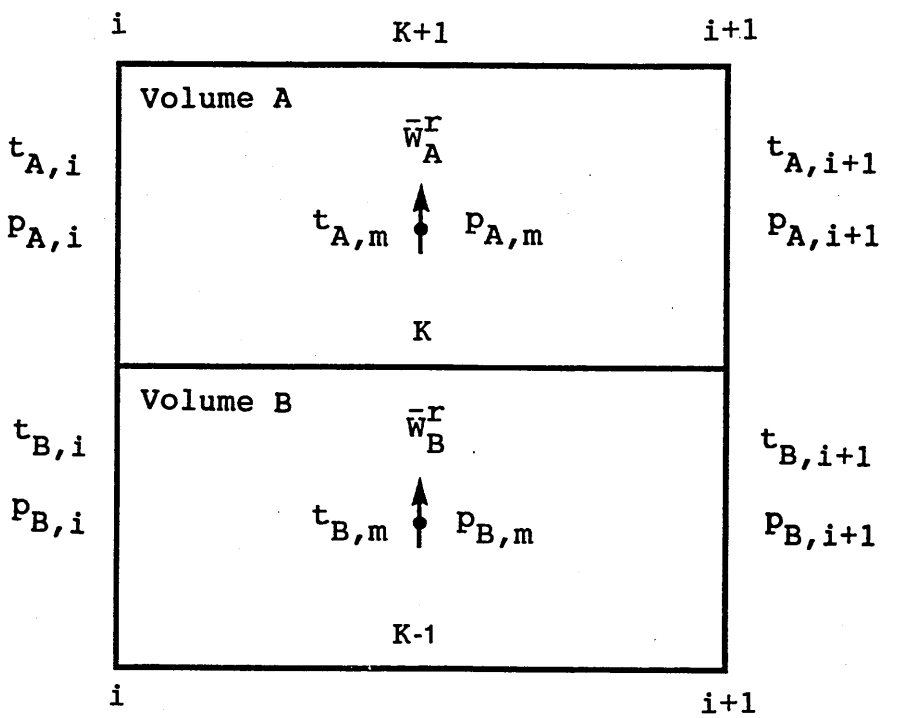

Radial mass flow rate at the k plane (linear interpolation)

$$W_K = \frac{1}{2} (\bar{w}^r_A + \bar{w}^r_B)$$

$$W_{K+1} = 0 \qquad W_{K-1} = 0$$

Mean temperature, volume A (linear interpolation)

$$t_{A,m} = \frac{1}{2} (t_{A,i} + t_{A,i+1})$$

Mean temperature, volume B (linear interpolation)

$$t_{B,m} = \frac{1}{2} (t_{B,i} + t_{B,i+1})$$

Temperature at k plane (bi-linear interpolation)

$$t_K = \frac{1}{4} (t_{A,i} + t_{A,i+1} + t_{B,i} + t_{B,i+1})$$

Mean pressure, volume A (linear interpolation)

$$p_{A,m} = \frac{1}{2} (p_{A,i} + p_{A,i+1})$$

Mean pressure, volume B (linear interpolation)

$$p_{B,m} = \frac{1}{2} (p_{B,i} + p_{B,i+1})$$

Pressure at k plane (bi-linear interpolation)

$$p_K = \frac{1}{4} (p_{A,i} + p_{A,i+1} + p_{B,i} + p_{B,i+1})$$

Pressure at k-1 and k+1 plane (linear extrapolation)

$$p_K + p_{K+1} = p_{A,i} + p_{A,i+1}$$

$$p_K + p_{K-1} = p_{B,i} + p_{B,i+1}$$

Appendix 4.1b Radial flow definition

The diagram below is a side view of the two volume component geometry shown in figure 4.3. The axial and radial flow velocities are defined.

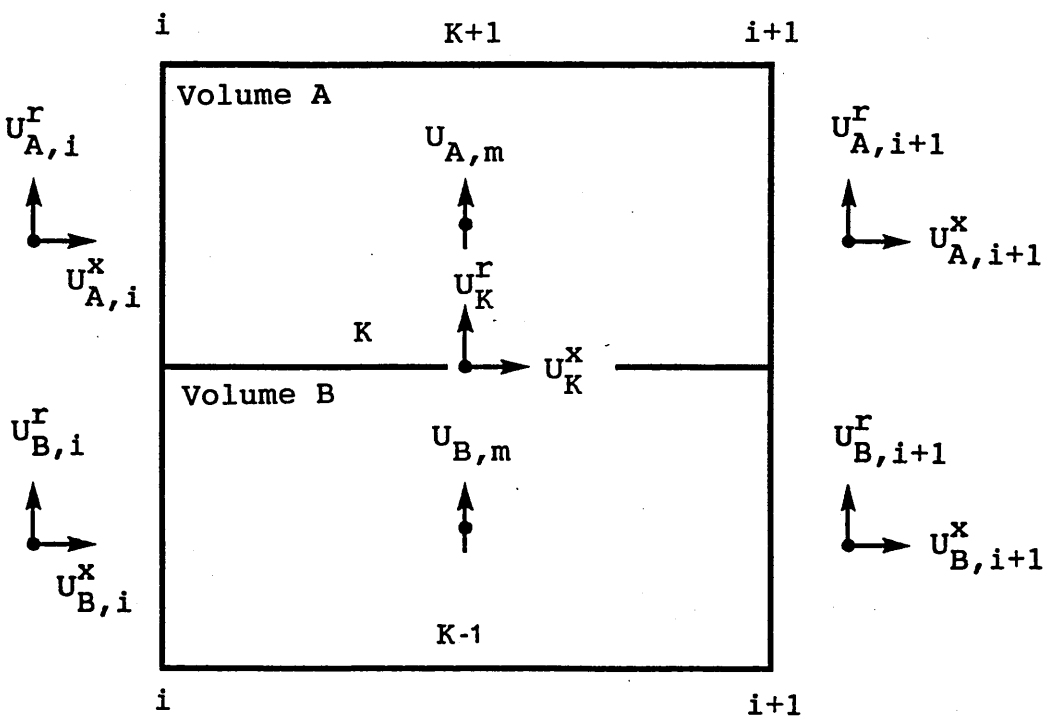

Mean radial flow velocity, volume A

$$U_{A,m} = \left[\frac{\bar{W}^r_A \, Rt_{A,m}}{p_{A,m} \, A_{K+\frac{1}{2}}} \right]$$

Mean radial flow velocity, volume B

$$U_{B,m} = \left[\frac{\bar{W}^r_B \, Rt_{B,m}}{p_{B,m} \, A_{K-\frac{1}{2}}} \right]$$

Axial flow velocity at k plane (bi-linear interpolation)

$$U_K^x = \frac{1}{4} \left(U_{A,i}^x + U_{A,i+1}^x + U_{B,i}^x + U_{B,i+1}^x\right)$$

Radial flow velocity at k plane (linear interpolation)

$$U_K^r = \frac{1}{2} \left(U_{A,m} + U_{B,m}\right)$$

Radial flow velocity, volume A (linear extrapolation)

$$U_{A,i+1}^r = 2U_{A,m} - U_{A,i}^K$$

Radial flow velocity, volume B (linear extrapolation)

$$U_{B,i+1}^r = 2U_{B,m} - U_{B,i}^K$$

Appendix 5.1. The RRAP Implicit Matching Method

The Implicit Matching Method is a damped Newton-Raphson numerical scheme capable of solving up to ninety-eight non-linear simultaneous equations.

A system of simultaneous equations is represented in the Engine Routine in the following format.

$$MQ_{A_1} = f_1(V_1, V_2, V_3, \ldots\ldots V_n)$$

$$MQ_{A_2} = y_1$$

$$MQ_{B_1} = f_2(V_1, V_2, V_3, \ldots\ldots V_n)$$

$$MQ_{B_2} = y_2$$

$$MQ_{C_1} = f_3(V_1, V_2, V_3, \ldots\ldots V_n)$$

$$MQ_{C_2} = y_3$$

$$=$$
$$=$$
$$=$$
$$=$$

$$MQ_{n_1} = f_n(V_1, V_2, V_3, \ldots\ldots Vn)$$

$$MQ_{n_2} = y_n$$

The unknowns denoted by V are called the **Variables**. The value of each function and its respective y value are assigned to what are called **Matching Quantities**. Solution is achieved when, for a given set of Variables, each Matching Quantity of a pair are equal to within a defined tolerance, for all Matching Quantity Pairs. When a solution is found the Engine Routine is said to be **'Matched'**.

Predicted values of the Variables are calculated by matrix inversion of the governing influence matrix. The influence matrix relates the change in each Matching Quantity with respect to a defined **Increment** in each of the Variables.

$$\delta MQ_A = (MQ_{A_1} - MQ_{A_2}) = \frac{\partial MQ_A}{\partial V_1} \delta V_1 + \frac{\partial MQ_A}{\partial V_2} \delta V_2 + \frac{\partial MQ_A}{\partial V_3} \delta V_3 + \ldots$$

$$\delta MQ_B = (MQ_{B_1} - MQ_{B_2}) = \frac{\partial MQ_B}{\partial V_1} \delta V_1 + \frac{\partial MQ_B}{\partial V_2} \delta V_2 + \frac{\partial MQ_B}{\partial V_3} \delta V_3 + \ldots$$

$$\delta MQ_C = (MQ_{C_1} - MQ_{C_2}) = \frac{\partial MQ_C}{\partial V_1} \delta V_1 + \frac{\partial MQ_C}{\partial V_2} \delta V_2 + \frac{\partial MQ_C}{\partial V_3} \delta V_3 + \ldots$$

The predicted change in the solution Variables is given by

$$\delta \underline{V} = A^{-1} \delta \underline{MQ}$$

where the matrix A is the above influence matrix.

The scheme has three alternative methods of predicting a better solution. The least complex method, and therefore computationally 'cheapest', is used by default. However, should solution prove evasive, the second, and if necessary, the third and most computationally expensive method, is invoked.

For ease of explanation each of the three methods are described below with respect to a single function problem, $y = f(x)$.

Solution of a single valued function y = f(x)

The Newton-Raphson method:

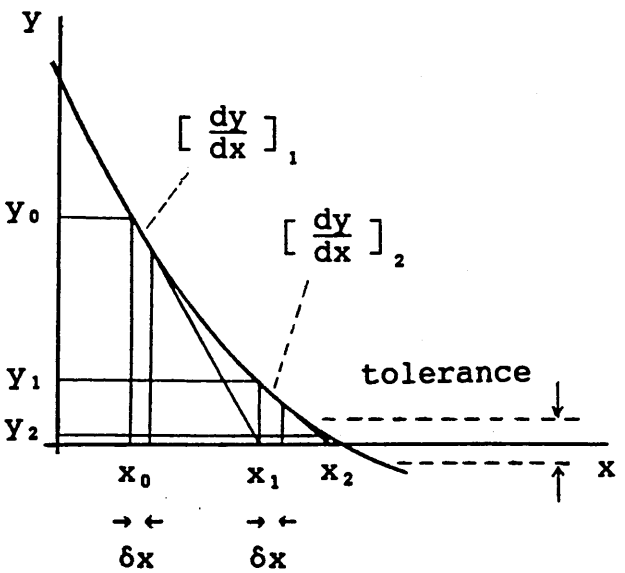

From the approximation

$$\left[\frac{dy}{dx}\right]_1 = \frac{y_0 - y_1}{x_0 - x_1}$$

an improved estimate of the root can be calculated.

$$x_1 = x_0 - \left[\frac{y_0 - y_1}{\left[\frac{dy}{dx}\right]_1}\right]$$

$$\text{and } x_2 = x_1 - \left[\frac{y_1 - y_2}{\left[\frac{dy}{dx}\right]_2}\right] \text{ etc}$$

The solution is found when the error ie, $|(y-0)|$, is to within a chosen tolerance.

The three solution methods differ only in the calculation of the derivative (dy/dx) or in the size of step predicted. With respect to the above diagram the predicted step is defined as $(x_1 - x_0)$ and $(x_2 - x_1)$.

Method 1 is called the **Prediction Mode.** It is identical to the scheme described above except that, provided the error does not increase with each predicted step made, the value of the derivative is not re-calculated. Using the same value of derivative for as many consecutive predictions as possible obviously reduces computing time.

Method 2 - The Bisection Mode

If the first prediction made using a newly calculated derivative results in an increase in the error, then the predicted step is bisected. This can occur within a function of the following form.

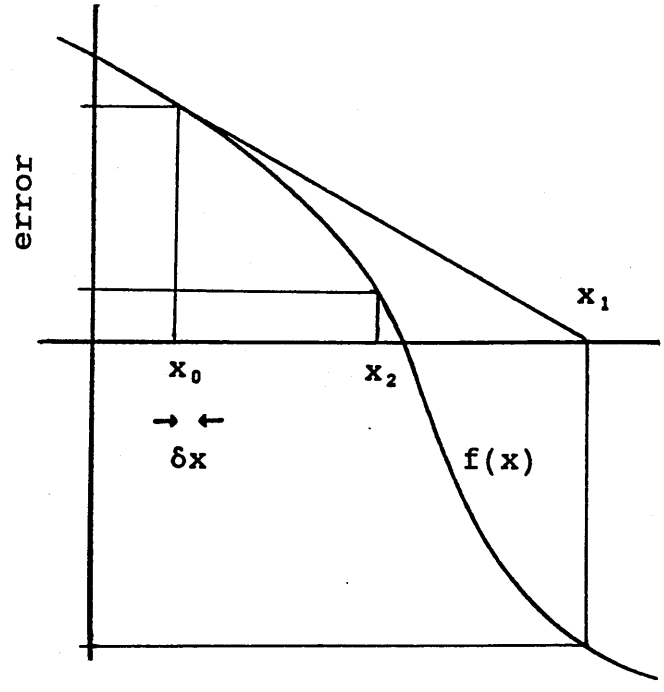

Here the predicted solution x_1 results in a larger error. The predicted step is halved, x_2, and the error recalculated. If the error is reduced by bisecting then the Prediction Mode will take over, otherwise the predicted step is halved again. A maximum of ten bisections are allowed.

Method 3 - The Central Differencing Mode

If a function has a rapidly changing gradient and the increment δx, is relatively large, then it is possible for ten bisections to fail in producing a smaller error.

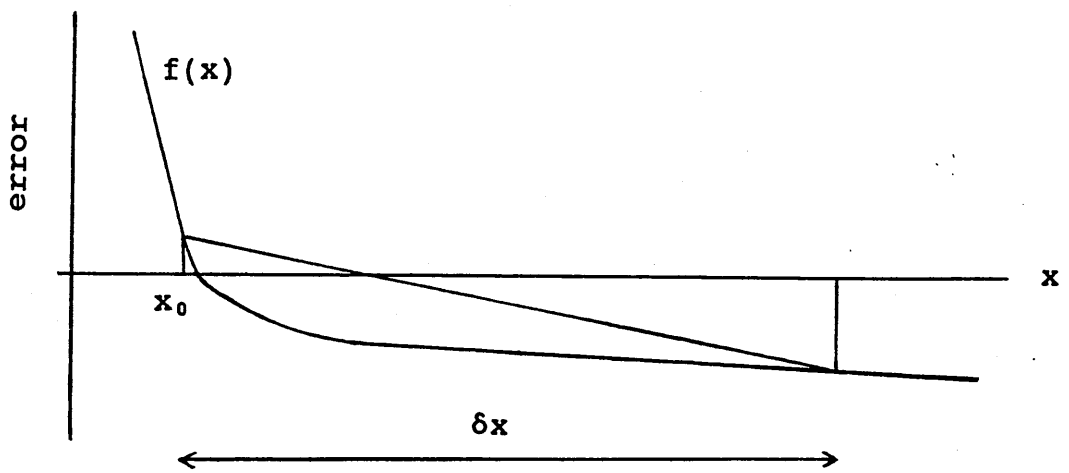

If this occurs a more representative gradient is calculated by central differencing.

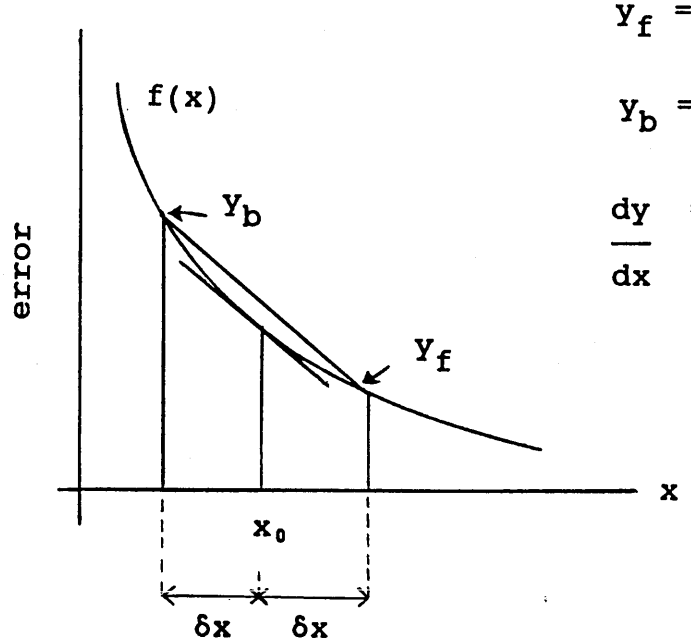

$$y_f = f(x + \delta x)$$

$$y_b = f(x - \delta x)$$

$$\frac{dy}{dx} = \frac{y_f - y_b}{2\delta x}$$

If a predicted solution calculated from the new derivative results in a smaller error, then the Prediction Mode will take over. If, however, the error is greater, then the Bisection mode will take over. Again a maximum of ten bisections are allowed and if the error does not improve the calculation is stopped. Figure 5.3 illustrates the internal logic used by the Implicit Matching Method in using its Prediction, Bisection and Central Differencing modes; and the lines of communication with the RRAP system shown in figure 5.2 are also shown.

Appendix 5.2 The gas dynamic equation set solution variables

Set out below is the one dimensional gas dynamic equation set, expressed in the RRAP compatible form (ie. Component Performance Terms expressed with respect to steady state exit flow variables) and in terms of the solution variables adopted by the Successive Back Substitution iterative method.

Conservation of mass

$$\frac{d\bar{\rho}}{dt} = \frac{1}{V}\left[W^{*}_{i+1} - W_{i+1} \right]$$

Conservation of momentum

$$\frac{d\bar{W}^{x}}{dt} = \frac{1}{L_x}\left[(WU + pA)^{*}_{i+1} - \left(\frac{W^2Rt}{pA} + pA\right)_{i+1}\right]$$

Conservation of energy

$$\frac{d\overline{\rho s}}{dt} = \frac{1}{V}\left[(Ws)^{*}_{i+1} - (Ws)_{i+1} \right]$$

$$S_{i+1} - S_o = Cpln\left[\frac{t_{i+1}}{T_o}\right] - Rln\left[\frac{p_{i+1}}{p_o}\right]$$

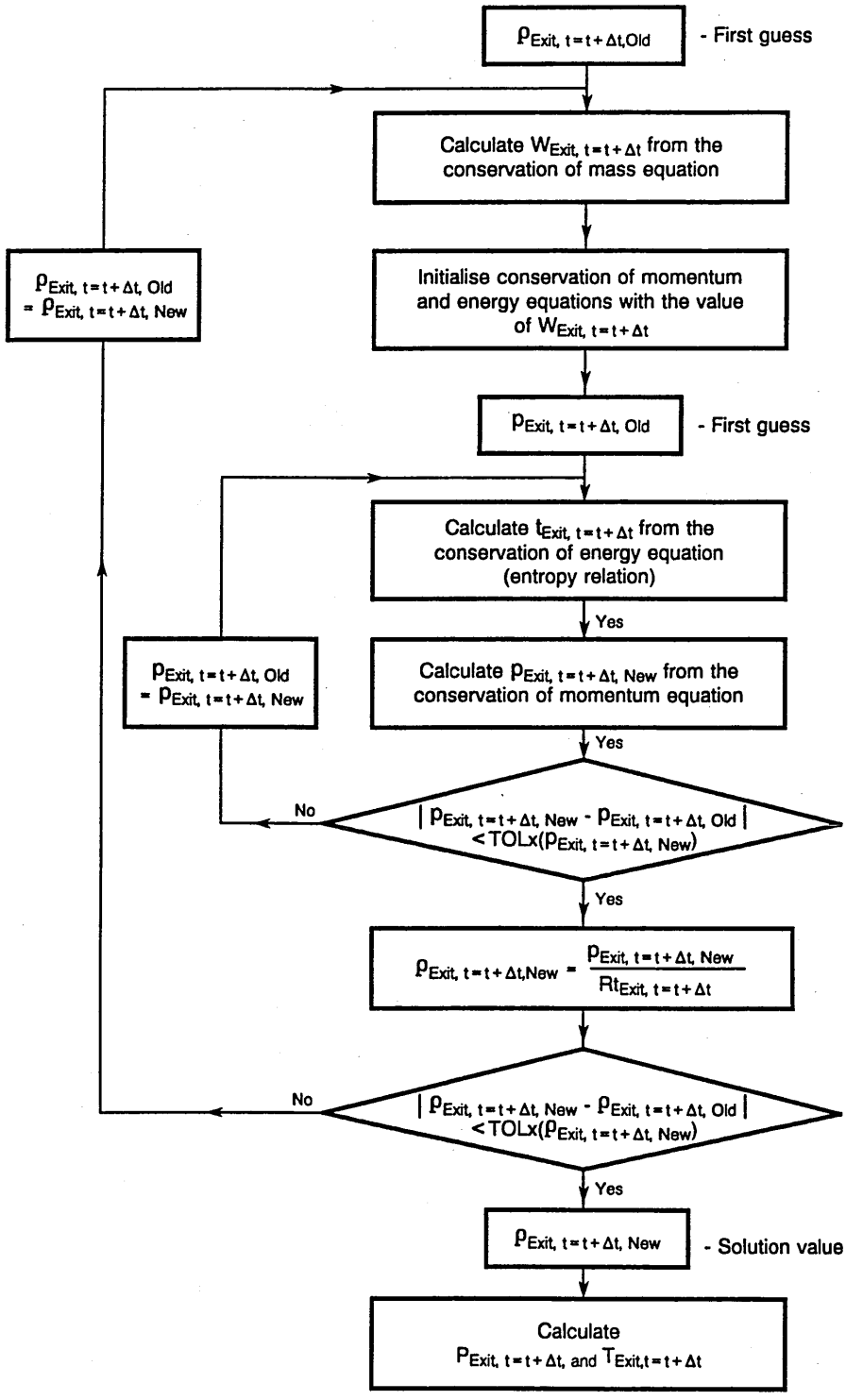

TOL = Numerical tolerance

Appendix 5.3 The Successive Back Substitution iteration procedure

Appendix 6.1a RRAP spool speed prediction

An engine match at time t=t defines the excess power generated by the turbine, $EP_{t=t}$.

The torque exerted by the turbine is then given by

$$\frac{EP_{t=t}}{\left[\frac{2\pi}{60} \cdot N_{t=t}\right]}$$

and if the rotational acceleration of the spool is approximated by

$$\frac{\Delta N}{\Delta t}$$

then the change in rotational speed can be predicted from,

$$\frac{EP_{t=t}}{\left[\frac{2\pi}{60} \cdot N_{t=t}\right]} = I \cdot \frac{2\pi}{60} \cdot \frac{\Delta N}{\Delta t}$$

or $$\Delta N = EP_{t=t} \left[\frac{60}{2\pi}\right]^2 \cdot \frac{1}{I} \cdot \frac{\Delta t}{N_{t=t}}$$

The spool speed at time t=t+Δt is then given by

$$N_{t=t+\Delta t} = N_{t=t} + \Delta N$$

Appendix 6.1b RRAP compressor forward flow steady-state performance calculation

The compressor performance subroutine calculates the exit temperature and pressure and the mass flow rate from the upstream temperature and pressure and a definition of its operating point. The operating point is defined by the corrected speed $N/\sqrt{T_1}$, and the value of ß, see figure 6.1.

The compressor

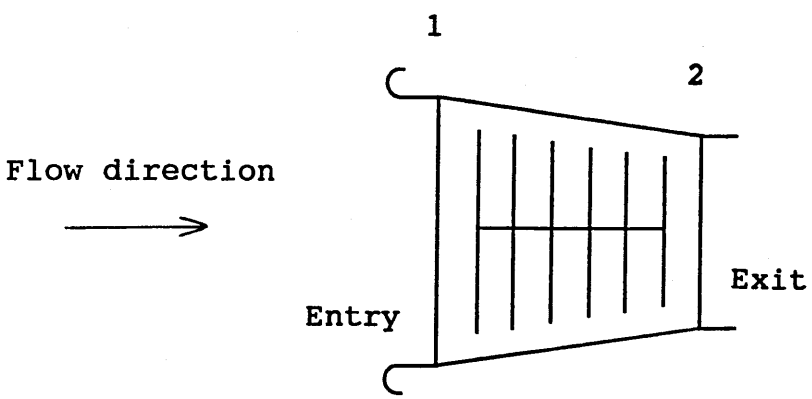

Compressor performance enthalpy/entropy diagram

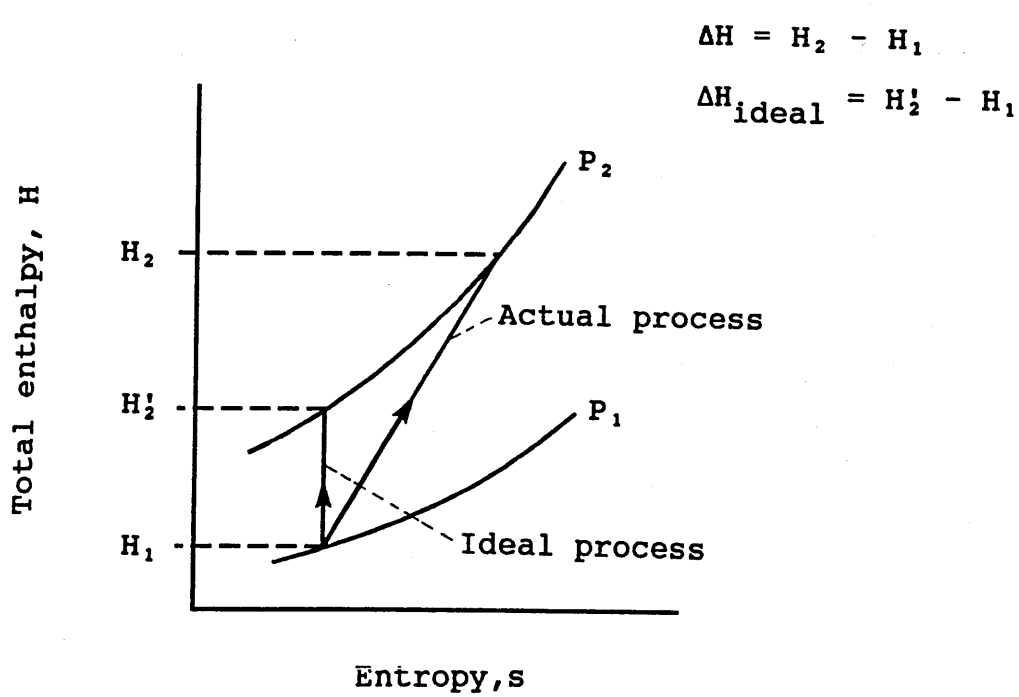

From the corrected speed $N/\sqrt{T_1}$ and the value of ß, the performance subroutine accesses the compressor performance characteristics and determines a value of,

$$\left[\frac{W\sqrt{T}}{P}\right]_1 , \left[\frac{\Delta H}{T_1}\right] \text{ and } \left[\frac{\Delta H}{T_1}\right]_{ideal}$$

Compressor performance is then calculated based on the above enthalpy/entropy diagram and the upstream temperature and pressure.

Compressor exit temperature T_2

Total enthalpy at compressor entry $H_1 = CpT_1$
where $Cp = f(T_1)$

Total enthalpy at exit $H_2 = H_1 + \Delta H$

The exit temperature T_2 is calculated from the enthalpy H_2 using an iterative procedure.

Compressor exit pressure P_2

Ideal total enthalpy at compressor exit

$$H_2' = H_1 + \Delta H_{ideal}$$

The ideal exit temperature T_2' is calculated from the enthalpy H_2' using an iterative procedure.

From the entropy relation

$$s - s_o = Cp\ln\left[\frac{T}{T_o}\right] - R\ln\left[\frac{P}{P_o}\right]$$

the ideal, or isentropic process illustrated in the above diagram, is represented by,

$$Cpln\left[\frac{T_1}{T_o}\right] - Rln\left[\frac{P_1}{P_o}\right] = Cpln\left[\frac{T_2'}{T_o}\right] - Rln\left[\frac{P_2}{P_o}\right]$$

The compressor pressure ratio is therefore given by,

$$\frac{P_2}{P_1} = e^A \quad \text{where} \quad A = \frac{1}{R}\left[Cpln\left[\frac{T_2'}{T_o}\right] - Cpln\left[\frac{T_1}{T_o}\right]\right]$$

Compressor mass flow rate

$$W_c = \left[\frac{W\sqrt{T}}{P}\right]_1 \sqrt{\frac{P_1}{T_1}}$$

Compressor power

$$P_c = W_c\left[\frac{\Delta H}{T}\right] T_1$$

Appendix 6.1c RRAP steady-state combustor performance calculation

The inner and outer or 'hot' and 'cold' combustor volumes are represented by a single volume. Across the volume an energy balance is used to calculate the exit temperature, and momentum is conserved to calculate the pressure loss due to heating. The pressure loss due to viscous drag, or the 'cold loss', is calculated from a user defined factor.

The combustion chamber

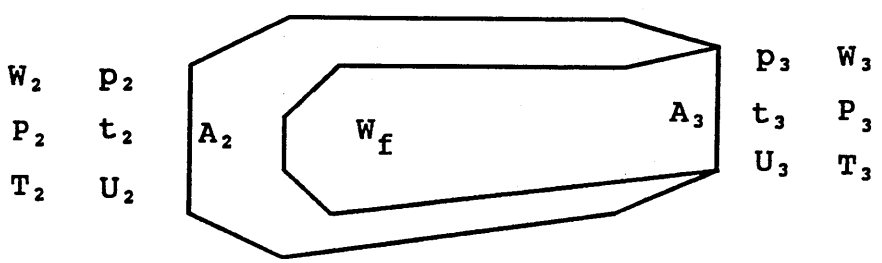

where W_2, P_2, T_2, p_2, t_2 and U_2 are all known and calculated from the compressor exit flow variables and flow area.

Combustor exit temperature

An enthalpy balance across the combustor gives

$$H_3(W_2 + W_f) = H_2W_2 + W_f\eta_{cb}H_f$$

or

$$H_3\left[\frac{1 + FAR}{FAR}\right] = \frac{H_2}{FAR} + \eta_{cb} H_f$$

where the fuel-to-air ratio, FAR is given by $\frac{W_f}{W_2}$ and the burning efficiency η_{cb} by,

$$\eta_{cb} = \frac{\text{Effective fuel mass flow rate}}{\text{Actual fuel mass flow rate}}$$

Unless defined as constant, the burning efficiency η_{cb} can be specified as a function of the fuel-to-air ratio and the combustor loading. The loading is defined by

$$\frac{W_2 \ 10^9}{P_2^{1.8} \ e^{\left[\frac{T_{i-1}}{300}\right]} \ V_{cb}}$$

and its relationship to the burning efficiency and fuel-to-air ratio is defined graphically and typically takes the form illustrated in figure 7.5. The specific heat of combustion of fuel H_f, is also modified at higher temperatures to account for the heat absorbed during the dissociation of combustion products. The threshold temperature is typically 1300K and the loss in heating value taken from a graph.

The above calculation is not explicit and is solved by an iterative procedure.

Combustor pressure loss

The fundamental pressure loss due to heating is calculated by conserving momentum.

$$p_2A_2 + W_2U_2 = p_3A_3 + W_3U_3$$

By conserving mass $W_3 = W_2 + W_f$ and assuming $A_2 = A_3$, two unknowns remain, U_3 and p_3.

Again by conserving mass at the combustor exit

$$p_3 A_3 = \frac{W_3 R t_3}{U_3}$$

and combined with the momentum equation above, a quadratic in U_3 is generated.

TOTAL

$$U_3^2 - \left[\frac{P_2 A_2 + W_2 U_2}{W_3} \right] U_3 + R t_3 = 0 \qquad (1)$$

A further equation can be derived by conserving energy at the combustor exit.

$$\frac{T_3}{t_3} = 1 + \frac{U_3^2}{2 C p_3 t_3} \qquad (2)$$

Simultaneous solution of equations (1) and (2) result in values of U_3 and t_3, from which the remaining flow variables are calculated.

The pressure loss due to viscous drag, or the 'cold loss' is calculated by specifying a dynamic head loss factor

$$\text{factor} = \frac{\Delta P_{2,3}}{P_2 - p_2}$$

Appendix 6.1d RRAP turbine steady-state performance calculation

The turbine performance subroutine calculates the exit temperature and pressure from the excess power EP, the corrected speed and the upstream temperature and pressure. The excess power is always specified as a Variable by the Implicit Matching Method. The subroutine also provides a Matching Quantity in turbine inlet flow function.

The turbine

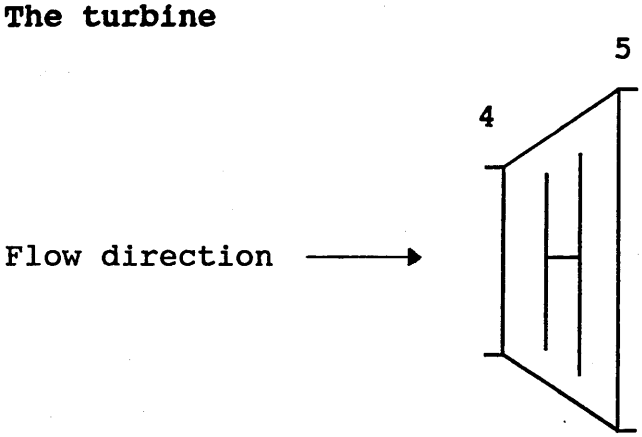

Turbine performance enthalpy/entropy diagram

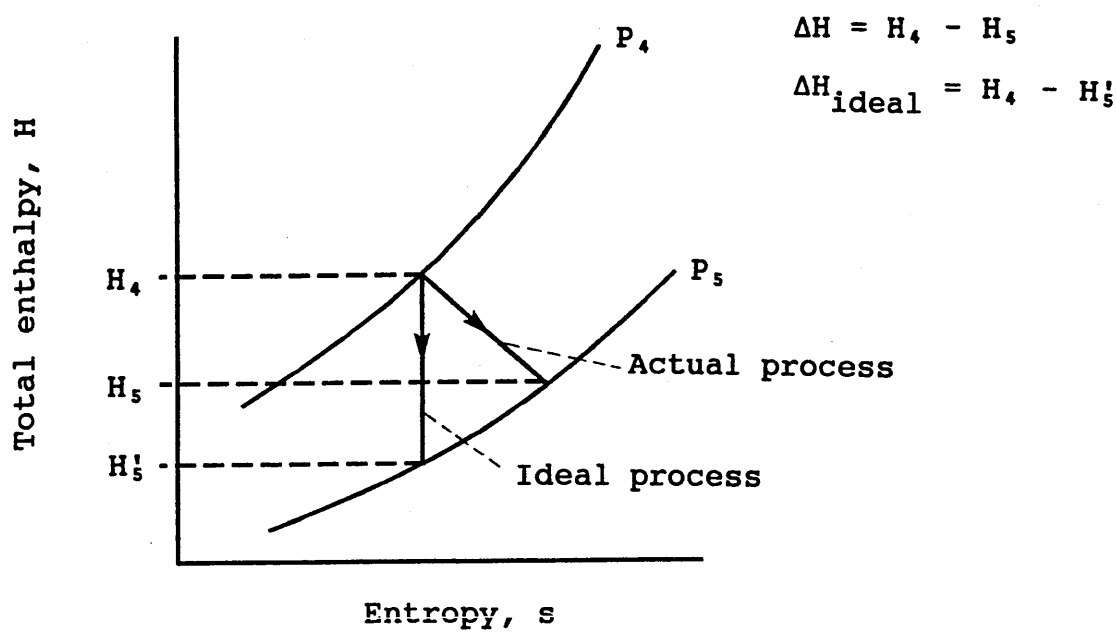

Turbine exit temperature T_5

The enthalpy drop across the turbine ΔH is calculated from a spool power balance equation.

$$P_{c,t=t+\Delta t} = (W_4 \Delta H)_{t=t+\Delta t} + EP_{t=t+\Delta t}$$

Total enthalpy at turbine entry $H_4 = CpT_4$
where $Cp = f(T_4)$

Total enthalpy at exit $H_5 = H_4 - \Delta H$

The exit temperature T_5, is calculated from the enthalpy H_5 using an iterative procedure.

Turbine exit pressure, P_5

The turbine efficiency is read from a performance characteristic using values of the corrected speed and enthalpy drop.

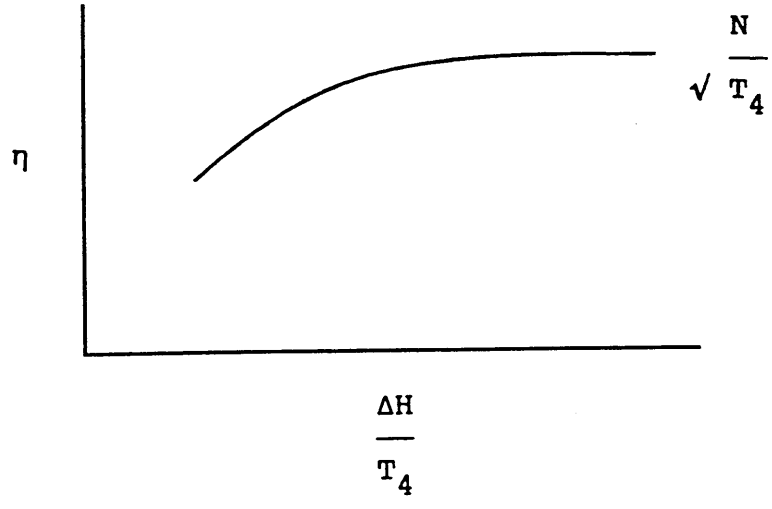

The ideal enthalpy drop is calculated from,

$$\eta = \frac{\Delta H}{\Delta H_{ideal}}$$

The ideal total enthalpy a turbine exit $H_5' = H_4 - \Delta H_{ideal}$
The ideal temperature T_5' is calculated from the enthalpy H_5' using an iterative procedure.

From the entropy relation

$$s - s_o = Cpln\left[\frac{T}{T_o}\right] - Rln\left[\frac{P}{P_o}\right]$$

the ideal, or isentropic process, is represented by,

$$Cpln\left[\frac{T_4}{T_o}\right] - Rln\left[\frac{P_4}{P_o}\right] = Cpln\left[\frac{T_5'}{T_o}\right] - Rln\left[\frac{P_5}{P_o}\right]$$

The turbine pressure ratio is therefore given by,

$$\frac{P_5}{P_4} = e^A \quad \text{where} \quad A = \frac{1}{R}\left[Cpln\left[\frac{T_5'}{T_o}\right] - Cpln\left[\frac{T_4}{T_o}\right]\right]$$

The turbine flow function is read from a performance characteristic using values of corrected speed and enthalpy drop.

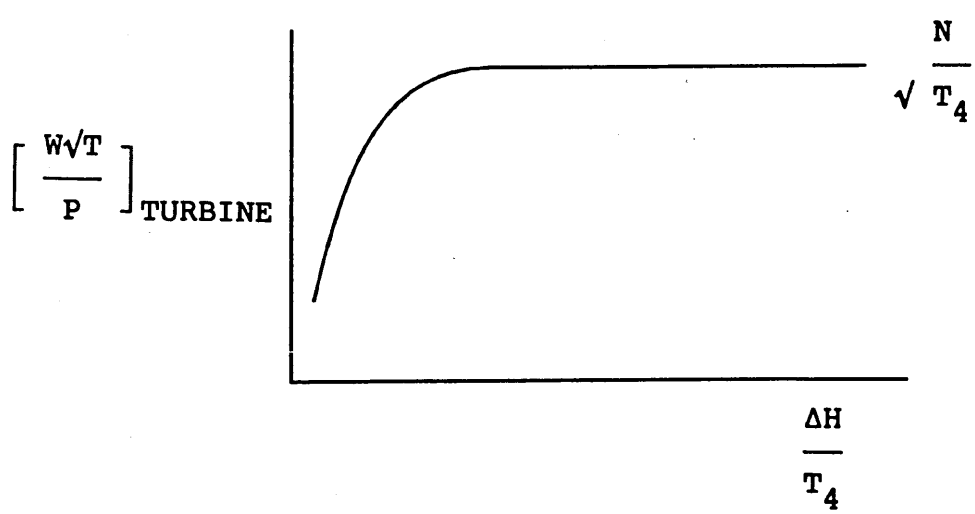

At a Matched performance point the turbine flow function must equal the flow function at exit from the combustor. These two flow functions are used as a Matching Quantity Pair by the Implicit Matching Method.

Appendix 6.1e RRAP nozzle performance calculation

The nozzle

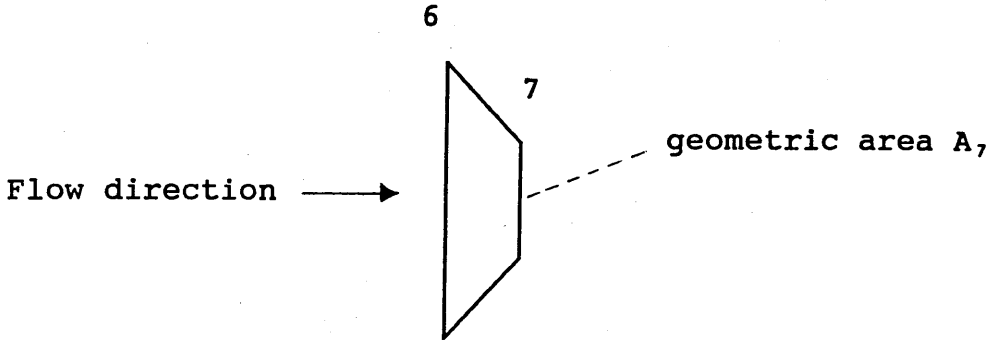

Choked nozzle condition

The nozzle is represented by a actuator disc. The throat area is specified as a boundary condition and so only another two flow parameters are required to completely specify the flow. The chosen two are mass flow rate and temperature at nozzle entry. Together these are used to calculate what should be the pressure at entry to the nozzle, which for a choked nozzle is calculated from,

$$P_6 = \frac{W_6\sqrt{T_6}}{A_7 Q^*}$$

At a Matched performance point the pressure at exit from the jet pipe must equal the pressure calculated at entry to the nozzle, and are therefore used as a Matching Quantity Pair by the Implicit Matching Method.

If the nozzle is not choked an iterative procedure is used to first calculate the throat static temperature.

Guess static temperature t_7

Calculate flow velocity $U_7 = \dfrac{W_6 R t_7}{p_7 A_7}$ where p_7 is the ambient static pressure.

Calculate first value of specific enthalpy $h_a = Cpt_7$

Calculate second value of specific enthalpy

$$h_b = CpT_6 + \frac{U_7^2}{2}$$

Iterate on static temperature till the difference in h_a and h_b are to within a set tolerance.

Total pressure at entry to nozzle is then given by

$$P_6 = p_7 e^{A} \quad \text{where} \quad A = \left[\frac{Cp}{R}\right] \ln\left[\frac{T_6}{t_7}\right]$$

Appendix 7.1 Compressor reverse flow performance analysis

Relationships which link the pressure ratio and temperature to the enthalpy and ideal enthalpy (isentropic) changes for a compressor operating in steady-state reverse flow are derived below. A reverse flow performance parameter θ, is also defined which replaces the conventional forward flow efficiency.

The compressor

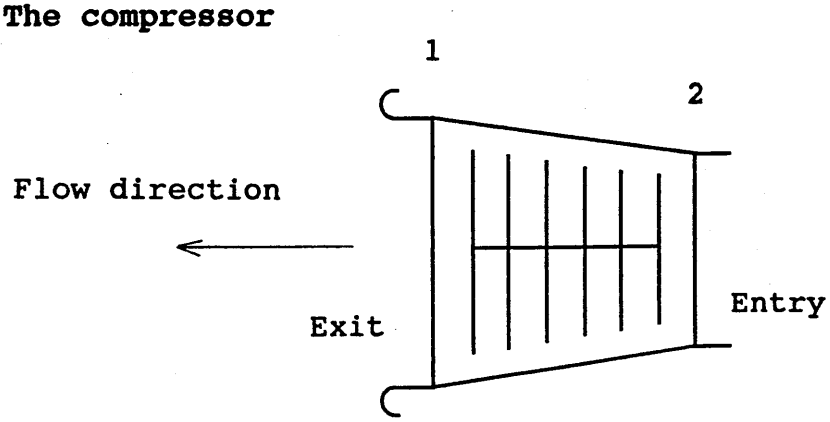

Compressor performance enthalpy/entropy diagram

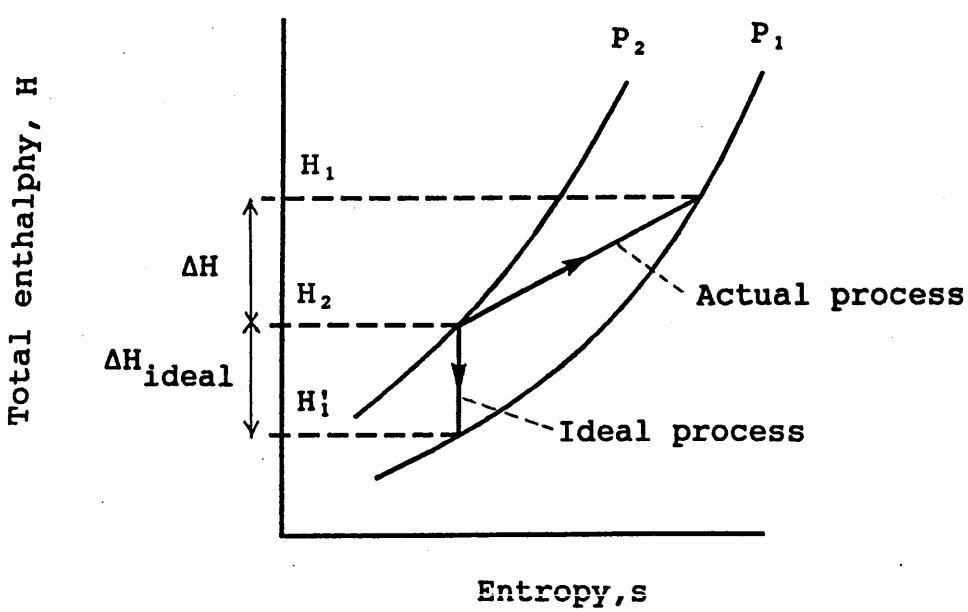

The change in enthalpy is given by $\Delta H = Cp\ [T_1 - T_2]$

$$\text{or} \quad \frac{\Delta H}{T_1} = Cp \left[1 - \frac{T_2}{T_1}\right]$$

Note that here the specific heat Cp is assumed constant.

The ideal change in enthalpy is given by

$$\Delta H_{ideal} = Cp\ [T_2 - T_1']$$

and by noting that $\left[\frac{T_1'}{T_2}\right] = \left[\frac{P_1}{P_2}\right]^{\left[\frac{R}{Cp}\right]}$

$$\frac{\Delta H_{ideal}}{T_2} = Cp \left[1 - \left[\frac{P_1}{P_2}\right]^{\left[\frac{R}{Cp}\right]}\right]$$

$$\text{or} \quad \frac{\Delta H_{ideal}}{T_1} = Cp \left[\frac{T_2}{T_1}\right] \left[1 - \left[\frac{P_1}{P_2}\right]^{\left[\frac{R}{Cp}\right]}\right]$$

The reverse flow performance parameter θ, was defined as

$$\theta = \frac{\Delta H_{ideal}}{\Delta H} = \left[\frac{T_2 - T_1'}{T_1 - T_2}\right]$$

again it is assumed that the specific heat Cp is constant. Note that it is possible for its value to exceed unity.

$$\theta = \frac{T_2 \left[1 - \left[\frac{P_1}{P_2}\right]^{\left[\frac{R}{Cp}\right]}\right]}{[\,T_1 - T_2\,]}$$

Summary of reverse flow performance

Actual enthalpy rise

$$\frac{\Delta H}{T_1} = Cp \left[1 - \frac{T_2}{T_1}\right]$$

Ideal enthalpy rise

$$\frac{\Delta H_{ideal}}{T_1} = Cp \left[\frac{T_2}{T_1}\right] \left[1 - \left[\frac{P_1}{P_2}\right]^{\left[\frac{R}{Cp}\right]}\right]$$

Performance parameter

$$\theta = \frac{T_2 \left[1 - \left[\frac{P_1}{P_2}\right]^{\left[\frac{R}{Cp}\right]}\right]}{[T_1 - T_2]}$$

Appendix 7.2 Compressor steady-state performance calculation - Reverse Flow

Like the forward flow calculation (appendix 6.1b), the reverse flow compressor performance subroutine calculates the exit temperature and pressure and the mass flow rate from the upstream temperature and pressure and a definition of the compressor operating point. Again the operating point is defined by the corrected speed $N/\sqrt{T_1}$, and the value of ß, see figure 6.1.

The compressor

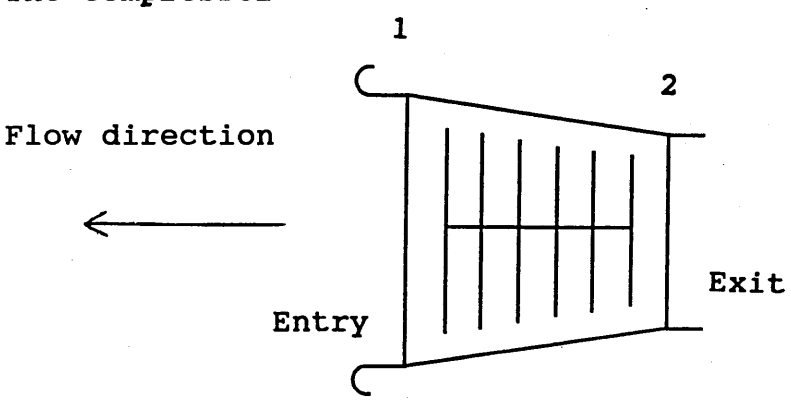

Compressor performance enthalpy/entropy diagram

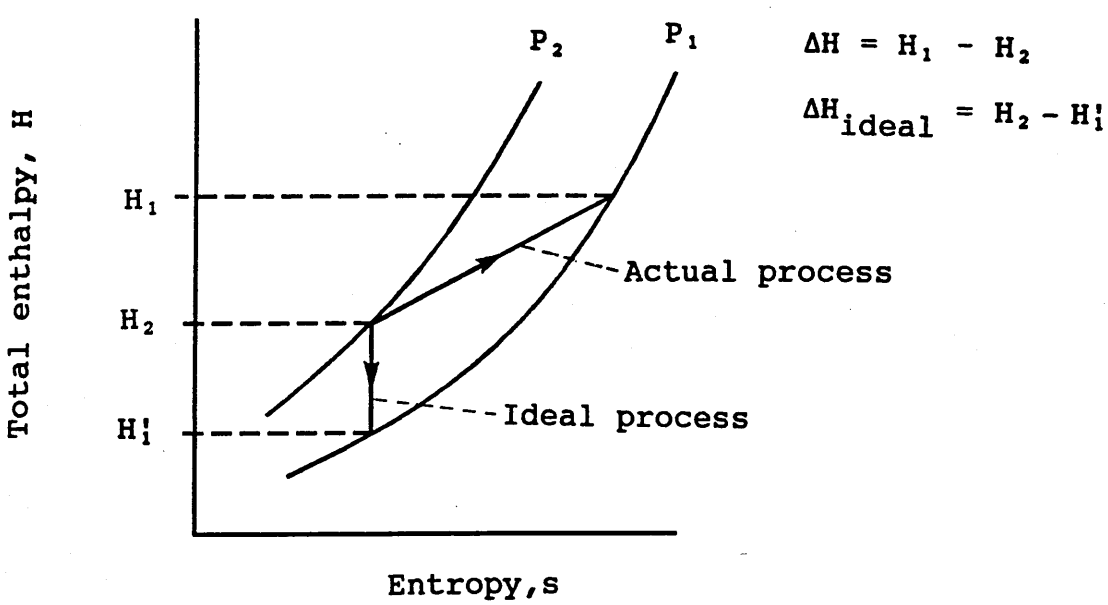

From the corrected speed $N/\sqrt{T_1}$ and the value of ß, the performance subroutine accesses the compressor performance characteristics and determines a value of,

$$\left[\frac{W\sqrt{T}}{P}\right]_1 , \left[\frac{\Delta H}{T_1}\right] \text{ and } \left[\frac{\Delta H}{T_1}\right]_{ideal}$$

Compressor performance is then calculated based on the above enthalpy/entropy diagram and the upstream temperature and pressure.

Compressor exit temperature T_2

Total enthalpy at compressor entry $H_1 = CpT_1$
where $Cp = f(T_1)$

Total enthalpy at exit $H_2 = H_1 - \Delta H$

The exit temperature T_2 is calculated from the enthalpy H_2 using an iterative procedure.

Compressor exit pressure P_2

Ideal total enthalpy at compressor exit

$$H_i' = H_1 - \Delta H - \Delta H_{ideal}$$

The ideal exit temperature T_i' is calculated from the enthalpy H_i' using an iterative procedure.

From the entropy relation

$$s - s_o = Cp\ln\left[\frac{T}{T_o}\right] - R\ln\left[\frac{P}{P_o}\right]$$

the ideal, or isentropic process illustrated in the above diagram, is represented by,

$$Cpln\left[\frac{T_i'}{T_o}\right] - Rln\left[\frac{P_1}{P_o}\right] = Cpln\left[\frac{T_2}{T_o}\right] - Rln\left[\frac{P_2}{P_o}\right]$$

The compressor pressure ratio in reverse flow is therefore given by,

$$\frac{P_2}{P_1} = e^A \quad \text{where} \quad A = \frac{1}{R}\left[Cpln\left[\frac{T_2}{T_o}\right] - Cpln\left[\frac{T_i'}{T_o}\right]\right]$$

Compressor mass flow rate

$$W_c = \left[\frac{W\sqrt{T}}{P}\right]_1 \sqrt{\frac{P_1}{T_1}}$$

Compressor power

$$P_c = |\, W_c \,| \left[\frac{\Delta H}{T}\right] T_1$$

Appendix 7.3 The ideal chemical combustion process

The combustion reaction was assumed to be the complete oxidation of kerosene fuel to carbon dioxide and water. The chemical reaction is given by,

$$C_{12}H_{24} + 18O_2 \rightarrow 12CO_2 + 12H_2O$$

The relative atomic mass of each element is,

Carbon - C = 12
Oxygen - O = 16
Hydrogen - H = 1

By mass the chemical reaction takes the form,

$$[12x12 + 24x1] + 18x[2x16] \rightarrow 12x[12 + 2x16] + 12x[2x1 + 16]$$

$$168 + 576 \rightarrow 528 + 216$$

$$744 \rightarrow 744$$

The relative proportions by mass, used in the combustor model were as follows.

K_1 = mass fraction of oxygen gas consumed per unit mass of combusted fuel

K_2 = mass fraction of fuel per unit mass of combustion products

K_3 = mass fraction of oxygen gas consumed per unit mass of combustion products

$$K_1 = \frac{576}{168} = 3.429$$

$$K_2 = \frac{168}{744} = 0.2258$$

$$K_3 = \frac{576}{744} = 0.7742$$

Appendix 7.4 Mass fraction of oxygen in 'Standard Air'

The composition by volume of standard air was taken to be that of ISO 2533.

Nitrogen	0.78084
Oxygen	0.20948
Carbon dioxide	0.00031
Water	0.0
Argon	0.00934
Neon	0.00003

Noting Avogadro's Law - Equal volumes of all gases contain equal numbers of particles under the same conditions of temperature and pressure - the mass fraction of oxygen in standard air is thus 0.20948. This fraction was denoted by K_4.

K_4 = mass fraction of oxygen in Standard Air

Appendix 7.5 Calculation of mass of combustion products

The gases contained by the combustor hot volume were divided into three categories,

i) the mass of combustion products which comprise carbon dioxide and gaseous water and is denoted by m_{cp}

ii) the mass of 'unburnt' air which was standard air as described by appendix 7.4, and is given by

$$\frac{m_{ox}}{K_4}$$

iii) the mass of 'burnt' air which was standard air, but without the oxygen that was consumed to form the combustion products, and is denoted by m_b

By conservation of mass each were related to the total mass of gas contained in the hot volume.

$$m_v = m_{cp} + \frac{m_{ox}}{K_4} + m_b \qquad (1)$$

Where m_v was the total mass of gas.

The mass of oxygen consumed in generating the combustion products was given by,

$$K_3 m_{cp}$$

where K_3 was the mass of oxygen consumed per unit mass of combustion products.

The mass of 'burnt' air, m_b, was therefore given by,

$$\frac{[1-K_4]}{K_4} K_3 m_{cp} \qquad (2)$$

where K_4 is the mass fraction of oxygen in standard air.

By substituting equation (2) into (1) and rearranging, the mass of combustion products was given by,

$$m_{cp} = \frac{m_v - \left[\frac{m_{ox}}{K_4}\right]}{\left[\frac{K_3(1-K_4) + 1}{K_4}\right]}$$

Appendix 7.6 Calculation of combustor pressure loss

The overall pressure loss of a combustor is conventionally expressed in the following form,

$$\frac{\Delta P}{P_{ENTRY}} = \frac{R}{2A}\left[\frac{W\sqrt{T}}{P}\right]_{ENTRY}\left[K_C + K_H\left[\frac{T_{EXIT}}{T_{ENTRY}} - 1\right]\right]$$

where K_H and K_C are the 'hot' and 'cold' loss factors respectively, and A is a representative flame tube cross section area. The pressure loss factors are difficult to predict and are usually determined experimentally.

Because the combustor model was split into separate cold and hot volumes the pressure loss was correspondingly split.

The cold loss was calculated from,

$$\frac{\Delta P}{P_{i-1}} = \frac{R}{2A}\left[\frac{W\sqrt{T}}{P}\right]_{i-1} K_C$$

Note - the subscript 'i' refers to the combustor station numbers given in figure 7.3b.

and the hot loss calculated from,

$$\frac{\Delta P}{P_i} = \frac{R}{2A} \left[\frac{W\sqrt{T}}{P} \right]_i K_H \left[\frac{T_{i+1}}{T_i} - 1 \right]$$

Both the the loss factors K_H and K_C were evaluated by calibration against the steady flow combustor model described in section 6.2.1.4. Each factor was then then held constant during transient simulations.